

https://dspace.org/

Ultrastructure of cell death in Prorocentrum redfieldii, a bloom-forming dinoflagellate

Xuma-Toni, Tutuzwa

2024-11

University of the Witwatersrand, Johannesburg

https://hdl.handle.net/10539/48061

Xuma-Toni, Tutuzwa. (2024). Ultrastructure of cell death in Prorocentrum redfieldii, a bloom-forming dinoflagellate. [PhD thesis, University of the Witwatersrand, Johannesburg]. WIReDSpace. https://hdl.handle.net/10539/48061

Downloaded from a DSpace repository. https://dspace.org/



UNIVERSITY OF THE
WITWATERSRAND,
JOHANNESBURG

Ultrastructure of cell death in *Prorocentrum redfieldii*, a bloom-forming dinoflagellate

By

TUTUZWA XUMA-TONI

A thesis Submitted to the Faculty of Science, University of the Witwatersrand, in fulfilment of the requirements for the degree of Doctor of Philosophy

School of Animal, Plant and Environmental Sciences University of the Witwatersrand Johannesburg, South Africa

NOVEMBER 2024

DECLARATION

I declare that this thesis is my own original work. It is being submitted for the Degree of Doctor of Philosophy to the University of Witwatersrand, Johannesburg. It has not been submitted for any other higher degree or examination in any other university. The experimental work described in this thesis was carried out in the School of Animal, Plant and Environmental Sciences, University of the Witwatersrand, Johannesburg, South Africa, under the supervision of Professor Stuart Sym (School of Animal, Plant and Environmental Sciences, University of the Witwatersrand) and Professor Pierre Durand (Evolutionary Studies Institute. University of the Witwatersrand).

(Signature of candidate)



Signed at the University of the Witwatersrand, Johannesburg, South Africa on the 11 November 2024.

DEDICATION

I dedicate this thesis to my husband Athi, “enkosi Ntlane”, and my children Olo and Nande, for all their love, support and understanding during this challenging period of my life.

It is also dedicated to my late father who instilled the importance of education to me.

“Ndiyabulela Ndila no Mamthembu ngento yonke”

ACKNOWLEDGEMENTS

This work is the outcome of many people who contributed and supported me in various ways. I would like to express my sincere gratitude to the following:

The Almighty God, for wisdom, strength and ability to endure during this journey. I give Him the glory. My sincere gratitude goes to Prof. Stuart Sym and Prof. Pierre Duran for their invaluable guidance. Thank you, Stuart and Pierre, for your immense contribution to this research project and for your encouragement and commitment in the duration of this PhD journey. I would also like to thank my manager Prof. Alexander Ziegler, thanks Prof. for your support and encouragement. A great appreciation goes to my colleagues at the WITS MMU, thank you guys for words of encouragement .and support. Thank you, “Dr Deran”, for donating all your EM consumables to me.

I extend my thanks to the University of Witwatersrand for funding this PhD and granting me the opportunity to embark on this work.

Lastly, but not least, my greatest appreciation and thanks to my family and friends for your love and support. “Enkosi Maskhonza” for words of encouragement. Special thanks to my siblings, Feziwe and Luthando, and all my cousins, nieces and nephews.

ABSTRACT

Phytoplankton are primary producers in oceanic food chains and are very important in the ocean's biogeochemical cycles (Azam, 1998; Falkowski, 1994; Wilken *et al.*, 2018). During nutrient replete conditions, population growth in phytoplankton communities can surpass external loss factors (e.g. grazing, sinking and lysis) leading to bloom formation (Brussaard *et al.*, 1995; Choi *et al*., 2017). In recent years there has been an increase in the occurrence of HABs, which are exacerbated by anthropogenic inputs. The involvement of programmed cell death (PCD) as a loss factor in collapsing blooms has become an area of interest in phytoplankton ecology.

The study examined, for the first time, the ultrastructure of cell mortality in a collapsing anaerobic HAB of *Prorocentrum redfieldii,* an armoured dinoflagellate and ascertain whether there was structural evidence of PCD as a driver of the bloom collapse. These ultrastructural responses were compared with those of replete cultures subjected to stressors known to induce PCD, i.e., macronutrient deprivation nitrogen (NO^{3-}) and phosphorus (PO_4^{3-}) and heat stress. Biochemical assays associated with PCD, such as caspase-like activity, ROS and cell viability staining as well as DNA laddering, were carried out.

The findings of this study established that cells dying from a collapsing bloom exhibited morphological characteristics like extensive vacuolation, ER derived double membrane structures and lytic vacuoles, which resemble the process of autophagy. There was an upregulation of the endomembrane system, and interaction between the endomembrane and autophagic systems. Structural alterations were observed in organelles known to be sources of ROS like the mitochondria and chloroplasts. Similar changes in ultrastructure were observed in the nutrient deprived and mild heat-shocked cells (32 ºC). Biochemical activity further revealed an overproduction of ROS, loss of cell viability and no caspase activity in the dying cells. The study concluded that *P. redfieldii cells* in a collapsing bloom were dying a caspase independent autophagic cell death mediated by oxidative stress.

TABLE OF CONTENTS

1 INTRODUCTION & LITERATURE REVIEW 1

1.1 Introduction 1

1.1.1 The concepts of cell death 3

1.1.2. Nomenclature 4

1.1.3 Background to the study 5

1.1.4 Study organism 7

1.1.5 Study site 8

1.1.6 Overview of past research on the role of programmed cell death in phytoplankton ecology 10

1.2 LITERATURE REVIEW 13

1.2.1 Harmful algal blooms 13

1.2.2 Dynamics of dinoflagellate blooms in upwelling regions 14

1.2.3 Impact of harmful algal blooms in the Benguela region 15

1.2.4 Cell Death 16

1.2.5 Phenotypes of programmed cell death 18

1.2.6 Structural markers of PCD in phytoplankton 20

1.2.7 Cell ultrastructural changes in the SAR clade (former Chromalveolata) following stress induced PCD 23

1.2.8 The relevance of programmed cell death for unicellular organisms 25

1.3. Aim and Objectives 29

1.4 Importance of the study 31

1.5 Structure of Thesis 31

2: COMPARATIVE ULTRASTRUCTURES OF A REPLETE CULTURE AND DYING *P. REDFIELDII* CELLS FROM A HAB 33

2.1 INTRODUCTION 33

2.1.1 Background 33

2.1.2 Glossary 33

2.1.3 Dinoflagellates 35

2.1.4 Structural markers of programmed cell death 39

2.1.5 Autophagy 40

2.1.6 Multivesicular bodies 43

2.1.7 Vacuolation 43

2.1.8 Ultrastructural changes in phytoplankton during PCD 44

2.1.9 Aim and objectives 45

2.2 METHODS 47

2.2.1 Growth dynamics of laboratory cultures 47

2.2.2 Sampling of field organisms 48

2.2.3 Transmission electron microscopy 48

2.2.4 Statistical analysis 49

2.3 RESULTS 50

2.3.1 Growth dynamics of laboratory cultures 50

2.3.2 Ultrastructure of nutrient replete cells 51

2.3.3 Ultrastructure of field-sampled organisms 57

2.4 DISCUSSION 70

2.5 CONCLUDING REMARKS 76

3 THE ULTRASTRUCTURE AND. BIOCHEMICAL ACTIVITY OF *PROROCENTRUM REDFIELDII* CELLS DEPRIVED OF ESSENTIAL MACRO-NUTRIENTS (NITRATES & INORGANIC PHOSPHATES). ... 79

3.1 Introduction 79

3.1.1 Nitrogen as a limiting macro-nutrient 79

3.1.2 Phosphorus as a limiting macro-nutrient 81

3.1.3 Caspase or caspase-like protease activity in PCD of unicellular organisms 82

3.1.4 Reactive oxygen species (ROS) 85

3.1.5 Nuclear DNA oligo-nucleosomal fragmentation 86

3.1.6 Aims and objectives 87

3.2 METHODS 89

3.2.1 Growth conditions 89

3.2.2 Growth studies: cultures 89

3.2.3 Transmission electron microscopy 90

3.2.4 Caspase-like analysis assay 90

3.2.5 Reactive oxygen species assay 92

3.2.6 DNA Laddering assay 93

3.3 RESULTS 96

3.3.1 Growth studies 96

3.3.2 Cell Ultrastructure 99

3.3.3 Morphometric measurements of ultrastructure 137

3.3.4 Caspase-like activity assay 139

3.3.5 Reactive Oxygen Species (ROS) 140

3.3.6 DNA Laddering assay in N- and P-deplete cells 148

3.4 DISCUSSION 150

3.4.1 Growth dynamics 150

3.4.2 Ultrastructure 151

3.4.3 Biochemical activity 155

3.4.4 Is there any evidence that PCD was induced by nutrient deprivation in 157

3.4.5Similarities in structural elements of the laboratory nutrient deplete cells with those from a collapsing bloom 159

3.5 CONCLUDING REMARKS 159

4- THE ULTRASTRUCTURE AND BIOCHEMICAL ACTIVITY OF *PROROCENTRUM REDFIELDII* CELLS SUBJECTED TO HEAT-SHOCK STRESS TO INDUCE CELL DEATH 163

4.1 INTRODUCTION 163

4.1.1 Background 163

4.1.2 Heat shock proteins 164

4.1.3 Heat stress as an inducer of programmed cell death in unicellular organisms 165

4.2 METHODS: 167

4.2.1 Growth conditions 167

4.2.2 Transmission electron microscopy 169

4.2.3 Caspase assay 169

4.2.4 Reactive oxygen species assay 169

4.2.5 Gating strategies 169

4.2.6 DNA Laddering assay 169

4.3 RESULTS 170

4.3.1 Cell ultrastructure 170

4.3.2 Caspase-like analysis assay 184

4.3.3 Reactive Oxygen Species (ROS) 185

4.4 DISCUSSION 190

4.4.1 Ultrastructural morphology 190

4.4.2 Biochemical activity 193

4.4.3 Is there any evidence that PCD was induced by heat-shock in 193

4.5 CONCLUDING REMARKS 194

5- GENERAL DISCUSSION & CONCLUDING REMARKS 196

REFERENCES…… .199

SYMBOLS AND ABBERVIATIONS

PCD	Programmed cell death
MPT	mitochondrial membrane transition
TUNEL	terminal deoxynucleotidyl transferase-mediated dUTP nick end labeling
PS	Phosphatidylserine
MMP	mitochondrial membrane potential
HAB	Harmful algal bloom
DO	dissolved oxygen
DOP	Dissolved organic phosphorus
DIP	Dissolved inorganic phosphorus
NCCD	Nomenclature committee on cell death
AIF-	Apoptosis-inducing facto
DHR 123	Dihydrorhodamine 123
PI	Propidium Iodide
TEM	Transmission electron microscopy
EM	Electron microscopy
CAT	Catalase
SOD	Superoxide dismutase
APX	Ascorbate peroxidase
PS II	Photosystem II
MVB	Multivesicular bodies
ATG	Autophagy-related genes
TOR	Target of rapamaycin
ER	Endoplasmic reticulum

LIST OF FIGURES

Figure 1.1	Generalized drawings of *Prorocentrum redfieldii.*	8
Figure 1.2	The location of St Helena Bay on the South African west coast.	9
Figure 1. 3	Eukaryotic tree of life showing the SAR.	24
Figure 2.1	Schematic diagram of the amphiesma.	36
Figure 2.2	A schematic representation of different types of autophagy.	42
Figure 2.3	Stages of the growth curve of replete cells of *P. redfieldii.*	50
Figure 2.4	Ultrastructure of nutrient replete cells of *P. redfieldii.*	52
Figure 2.5	Ultrastructure of the nucleus, endomembrane system and pusule in nutrient replete cells.	54
Figure 2.6	Ultrastructure of mitochondria and chloroplast in nutrient replete cultures.	56
Figure 2.7	Overview of cells in early and late bloom stages.	58
Figure 2.8	Ultrastructure of nuclei from cells sampled during the early and the late stages of the bloom.	60
Figure 2.9	The endomembrane system in cells sampled during the early and late stages of the bloom.	62
Figure. 2.10	Macro-and micro-autophagy in cells sampled in the early and late stages of the bloom.	64

Figure 2.11 Different mitochondria profiles of cells sampled during the early and late stages of the bloom. 66

Figure 2.12 Damage to the chloroplast structure in cells during the early and late stages of downwelling. 68

Figure 3. 1 Gating strategies used during flow-cytometer measurements. 94

Figure 3.2 Macroscopic observation of replete versus N- & P- deplete. 97

Figure 3.3 Cell densities of replete vs N- and P-deplete cells. 99

Figure 3.4 Accumulation of reserves and increased vacuolation in replete and -nutrient deplete cells. 101

Figure 3.5 Vacuolation in N- and P-deplete cells. 103

Fig. 3.6 Damage to the amphiesmal membranes and other organelles. 104

Figure 3.7 The pusule in Replete and nutrient -deplete cells. 106

Figure 3.8 Nuclei of replete and N- deplete cells. 108

Figure 3.9 Nuclei of P-deplete cells and alterations to the chromosome. 110

Figure 3.10 The endomembrane system in replete cells. 112

Figure 3.11 The endomembrane system in N-deplete cells. 114

Figure 3.12 The endomembrane system in P-deplete cells. 115

Figure 3.13 Multivesicular bodies (MVBs) in replete cells. 116

Figure 3.14 Multivesicular bodies (MVBs) in N-deplete cells. 118

Figure 3.15 Multivesicular bodies (MVBs) in P-deplete cells. 120

Figure 3.16 Macro-autophagy in N-deplete cells. 122

Fig. 3.17 Macro-autophagy in P-deplete cells. 123

Figure 3.18 Multilamellar bodies in N-deplete. 125

Figure **3.19** Membranous clumps in N-deplete over 14 days, 127

Figure 3.20 Multilamellar bodies in P-deplete cells. 128

Figure 3.21 Alterations to the mitochondria structure in N -deplete cells. 130

Figure 3.22 Alterations to the mitochondria structure in P-deplete cells over 14 days of treatment. 132

Figure 3.23 Single membraned structures in nutrient deplete cells. 133

Figure 3. 24 **C**hloroplast structure in replete and N-deplete cells. 135

Figure 3.25 **C**hloroplast structure in P-deplete cells. 137

Figure 3.26 Caspase activity following N starvation. 140

Figure 3.27 Caspase activity following P starvation. 141

Figure 3.28 DHR 123 green fluorescence probe in N-deplete and-replete cells . 144

Figure 3.29 Propidium Iodide red fluorescence probe in N-deplete and-replete cells. 146

Figure 3.30 DHR 123 green fluorescence probe in P-deplete and -replete cells. 146

Figure 3.31 Propidium Iodide red fluorescence probe in P-deplete and -replete cells. 148

Figure 3.32 Agarose gel electrophoresis of N- and P -deplete samples. 149

Figure 4.1 Overview of *P redfieldii* cells before and after exposure to heat-shock at 32 ºC. 171

Figure 4.2 Overview of *P redfieldii* cells before and after exposure to heat-shock at 37 ºC. 172

Figure 4.3 Nuclei of control and heat-shocked cells at 32º C after 1 & 48-HRS. 173

Figure 4.4 The Golgi cisternae and ER in control and cells after 1 and 48 HRS heat-shock at 32º C. 175

Figure 4. 5 Multivesicular bodies and lytic vacuoles in 32º C heat –shocked cells at 1 HR after treatment. 176

Figure 4.6 Multilamellar bodies in heat-shocked cells at 32º C after 1 HR of treatment. 177

Figure 4.7 Evidence for microautophagy in heat-shocked cells at 32º C after 1 and 48 HRS of treatment. 178

Figure 4.8 Alterations to mitochondria of heat shocked cells at 32º C after 1 and 48 HRS of treatment. 180

Figure 4.9 Chloroplasts in control cells and those heat-shocked at 32 and 37 ºC. 182

Figure 4.10 DEVdase activity in heat-shocked cells at 32º C, 1- and 48- HRS post-treatment. 184

Figure 4.11 DHR 123 green fluorescence probe in control and 32º C heat-shocked cells, after 1 and 48 HRS of heat stress 186

Figure 4.12 DHR 123 green fluorescence probe in control and 37º C heat-shocked cells, after 1HR of heat stress 187

Figure 4.13 . Propidium Iodide red fluorescence probe in heat-shocked cells at 32º C 1- and 48- HRS after treatment. 188

Figure 4.14 Propidium Iodide red fluorescence probe in heat-shocked cells at 37º C 1- HR after treatment 189

LIST OF TABLES

Table 1.1	Terminology used in current study vs alternative terms.	4
Table 1.2	A summary of the different cell death phenotypes.	19
Table 1.3	A summary of PCD - associated ultrastructural changes exhibited by various members of the SAR group.	24
Table 2.1	Definitions of terms used in this chapter and in others	33
Table 2.2	A summary of ultrastructural observations following induced PCD in microalga.	45
Table 3.1	Proportion of vacuolated cell surface**.**	138
Table 3.2	Measurements of endomembrane organelles in Replete, N-& P-deplete cells.	138
Table 3.3	Structures associated with autophagy in cells after 14 days of nutrient depletion.	138
Table 3.4	Thylakoid width after 7 days of nutrient depletion.	139
Table 3.5	Quantification of extracted DNA in Replete, N-and P-deplete samples	149
Table 3.6	Summary of TEM and biochemical results as evidence for PCD	150
Table 4.1	A summary of HSPs identified in bloom forming and symbiotic dinoflagellates.	165
Table 4.2	A summary of heat-shock induced programmed cell death in microalgae.	166

INTRODUCTION & LITERATURE REVIEW

1.1 Introduction

Phytoplankton are primary producers in oceanic food chains and are very important in the ocean's biogeochemical cycles (Azam, 1998; Falkowski, 1994; Orellana *et al*., 2013; Wilken *et al.*, 2018). Globally, their carbon-based primary productivity is almost half of the overall yearly productivity although their biomass constitutes a low percentage of the total plant carbon (Bidle and Falkowski, 2004; Falkowski, 1994). Studies trace the importance of phytoplankton back to the oxygenation of Earth's atmosphere ~2.3 billion years ago (Bidle, 2016).

During nutrient replete conditions, population growth in phytoplankton communities can surpass external loss factors (e.g. grazing, sinking and lysis) leading to bloom formation (Boss and Behrenfeld, 2010; Brussaard *et al.*, 1995; Choi *et al*., 2017; Walsh, 1983). An algal bloom is defined as a rapid increase in cell abundance up to million cells per millilitre (Hallegraeff, 1993). Harmful or toxic blooms with detrimental effects on other organisms are given the term harmful algal blooms (HABs; Smayda, 1997a). Researchers in this field agree that in recent years there has been an increase in the occurrence of HABs, which are exacerbated by anthropogenic inputs.

Some HABs are not toxic but form a threat to other organisms, because when they collapse, the decaying concentrated biomass supports a bloom of aerobic decomposing microbes. Consequently, the massive bloom decay causes anoxia in the surrounding water because of increased respiration that exceeds the dissolved oxygen DO resupply (Diaz 2016; Pitcher and Probyn, 2016). The anoxic conditions result in massive kills of other organisms in the surrounding water (Backer and Mcgillicuddy, 2006; Pitcher and Calder, 2000). The HAB that is the focus for the current study falls under the latter category.

For a long time, studies on phytoplankton populations attributed biomass losses to grazing by zooplankton and/or vertical sinking (Berges and Falkowski, 1998; Walsh, 1983). It has since been established that other forms of losses exist, including, cell lysis because of viral infections, bacterial attack, parasitism and programmed cell death (PCD) (Brussaard *et al.*, 1995; Kirchman, 1999; Veldhuis and Brussaard, 2006). Massive losses incurred by cell lysis explain abrupt collapses of blooms in the field and in laboratory cultures (Franklin *et al.,* 2006). The involvement of PCD as a loss factor in collapsing blooms has become an area of interest in phytoplankton ecology (Bar-Zeev *et al.,* 2013; Berman-Frank *et al.,* 2004; Kay D. Bidle *et al.,* 2007; Choi *et al.*, 2017; Vardi *et al.,* 2009). Various definitions are given to PCD, however the current study adopts the definition by Berman -Frank *et. a.l.* (2004) whereby PCD is defined as an "active, genetically controlled, cellular self-destruction driven by a series of complex biochemical events and specialized cellular machinery". This definition has also been adopted by others (Durand and Ramsey, 2023).

Programmed cell death has long been established in multicellular organisms as it is a very important phenomenon in their development and for the maintenance of tissue homeostasis in adults (Fuchs and Steller, 2011; Glücksmann, 1951; Lockshin and Williams, 1964; Shen and Tower, 2009). These organisms also use it as a defence mechanism to guard against a host of infections (viral, bacterial and those that are parasitic) by swift elimination of the infected cells (Debrabant *et al.*, 2003).

Rather surprisingly, it has been found that PCD also exists in unicellular organisms (Ameisen, 1996; Ameisen *et al*., 1995 Deponte, 2008; Bidle, 2016; Nedelcu *et al*., 2011). Unicellular PCD is counterintuitive because the benefits are not immediately clear if the cell kills itself. However, research shows that PCD in unicellular organisms does not only exist, but its existence has an ancient evolutionary origin, because it occurs in diverse lineages in both prokaryotes and eukaryotes (bacteria, archae, protozoa, fungi, and algae) (Debrabant *et al.*, 2003; La *et al.*, 2022). The existence of PCD genes in unicellular organisms is of great interest to evolutionary biologist and various suggestions have been postulated for their retention (Ameisen,

2009; Bidle, 2016; Bidle and Falkowski, 2004; Durand *et al.*, 2016, 2011; Nedelcu *et al.*, 2011; Vostinar *et al.*, 2019). Some of the suggestions that are given for the retention of PCD genes by unicellular organisms are that it benefits their conspecifics (Bidle, 2016; Bidle and Falkowski, 2004; Durand *et al.*, 2016) and ecological communities (Ndhlovu *et al.,* 2020). The retention and suggested role of unicellular PCD is discussed further in section 1.2.8.

The potential role that PCD plays in ecological communities of unicellular organisms has triggered a growing interest in microalgal death. Elucidating the role of PCD in the collapse of HABs is an active research area (Vardi *et al*., 1999; Burson *et al.*, 2014; Zhou *et al*., 2018; Bar-Zeev *et al.*, 2013; Berman-Frank *et al*., 2004; Vardi *et al.*, 2007). A broader overview of such research is provided in section 1.1.5.

The aim of this study was to examine the ultrastructure of cell mortality in a collapsing anaerobic HAB of *Prorocentrum redfieldii* Bursa (1959)*,* an armoured dinoflagellate. The detailed aim and objectives for the study are provided in section 1.3.

1.1.1 The concept of cell death

When the concept of PCD was first adopted in multicellular and later unicellular organisms it was regarded in mechanistic terms. The discovery of PCD in unicellular organisms however created more questions, for example, around its evolutionary and ecological significance. Recently, PCD has been conceptualized in five different ways, namely, the mechanistic, evolutionary, developmental, ecological and immunological concepts (Durand and Ramsey, 2023). From the five, three are relevant for the current study and will be defined further. The mechanistic concept is useful because it gives insight of the structural and biochemical pathway in a cell undergoing PCD. Various mechanistic definitions exist but this study

adopts the definition that PCD is "active, genetically controlled, cellular self-destruction driven by a series of complex biochemical events and specialized cellular machinery" (Berman-Frank *et al.,* 2004). The evolutionary and the ecological concepts are also important because they give insight about the behaviour of organism in relation to its population and environment. The evolutionary concept defines PCD as either and adaptation or non-adaptation (Durand and Ramsey, 2018), while the ecological concept defines PCD based on environmental factors like stress and nutrient cycling in phytoplankton communities (Franklin *et al.,* 2006).

1.1.2. Nomenclature

To standardise the criteria by which different cell death types are classified the nomenclature committee on cell death (NCCD) was established (Kroemer *et al*., 2009, 2005; Kroemer and Levine, 2008). However, research in this area is broad, involving divergent forms of life and cellular death and terminology is not standard. Sometimes different terms are used in literature to explain the same phenomenon. To obviate confusion, the current study will restrict use to the terms listed in Table 1.1.

Table 1.1. Terminology used in current study vs alternative terms

TERMS IN CURRENT STUDY	ALTERNATIVE TERMS
APOPTOSIS	Apoptosis-like cell death
AUTOPHAGIC CELL DEATH	Vacuolar cell death Death with autophagy
NECROTIC CELL DEATH	Necrosis

	Necroptosis
	Accidental cell death
	Incidental cell death
PROGRAMMED CELL DEATH (PCD)	Regulated cell death (RCD)
	Active cell death (ACD)
	PCD-like cell death
	Endogenous cell mortality

1.1.3 Background to the study

A HAB erupted in St Helena Bay on the South African west coast from January to February 2015. When the bloom collapsed, the dying concentrated biomass of the causative organism attracted microbes. The over-consumption of dissolved oxygen caused by the high respiration rates of the bacteria resulted in anoxia in the surrounding waters. Large numbers of rock lobster *Jasus lalandii,* H. Milne Edwards (1837), white mussel *Donax sera* Röding (1798) and various fish (approximately 415, 21, and 7 tons, respectively) suffocated and were washed out of the water onto the beach (Pitcher and Louw, 2021; Ndhlovu *et al.*, 2017). The culprit was identified by morphological, ultrastructural and molecular phylogenetic techniques as the dinoflagellate, *Prorocentrum triestinum* Schiller (Ndhlovu *et al.*, 2017). The author of this thesis was part of this research group.

For a long time, *P. redfieldii* described by Bursa (1959) was erroneously relegated to synonymity (Dodge, 1975) with *P. triestinum*, a species originally described much earlier by Schiller (1918). In a recent in-depth investigation (Tillman *et al*., 2021) have unambiguously shown that these two species can be discriminated both morphologically and molecularly. Most referrals of organisms to *P. triestinum*, including the current isolate, transpire in fact to be *P. redfieldii* (Tillman *et al*., 2021).

The collapse of a previous concentrated biomass HAB in St Helena in 2013 was verified to be triggered by nutrient limitation (starvation) and a decrease in DO, which is caused by high night-time respiration (Pitcher and Probyn, 2016a). The 2013 HAB was made up by various dinoflagellate species, namely, *Ceratium furca*, *P. minimum* and *Alexandrium catenella.* The collapse of the 2015 *P. redfieldii* HAB was also assumed to be triggered by nutrient limitation and a decrease in DO (Ndhlovu *et al.*, 2017). The mode of death, during the demise of HABs in the Benguela has not been investigated. As primary producers, phytoplankton has a direct influence on its environments (Bidle and Falkowski, 2004) and the way its constituents die has great impact on other marine organisms (Kirchman, 1999). Thus, determining the cell death pathways involved in a collapsing HAB of *P. redfieldii* will contribute to our understanding of the process of bloom collapse. The collapse of high biomass HABs in the Benguela region also negatively impacts both the aquaculture and commercial fishing in this region (Pitcher and Calder, 2000).

The 2015 *P. redfieldii* HAB was investigated further in the current study, with a particular emphasis on the ultrastructural changes that occurred in the causative organism. To corroborate interpretation of structural features found in cells sampled during the collapse of the bloom in the field study, clonal cultures of this organism established from this bloom were grown and subjected to different stresses known to induce PCD in other unicellular organisms (nitrogen and phosphorus deprivation and heat-shock; Jimenez *et al*., 2009; Sathe *et al.*, 2019; Wang *et al*., 2014; Zuppini *et al.*, 2007). Ultrastructural changes were monitored and known biochemical markers for PCD were simultaneously applied to these cultures to determine whether this organism underwent a mode of death that can be unambiguously interpreted as PCD.

PCD detection is filled with problems (Barreto Filho *et al*., 2022a) and requires a multifaceted approach to diagnose it. Electron microscopy (EM) has been a valuable tool in the morphological characterisation of PCD from as far back as the original coining of the term “apoptosis” by a research group of pathologists who used ultrastructure observations to describe active, inherent cell death in animal

tissue (Kerr *et al.*, 1972). It still continues to be viewed as the best standard in the characterisation of PCD (Barreto Filho *et al*., 2022a; Durand, 2020; Hasanzadeh *et al.*, 2017; Zhao *et al.*, 2006). The biochemical/molecular assays that are utilised to detect PCD are quick and less labour intensive in comparison with EM but they are not always appropriate as they are sometimes not specific to PCD (Allen *et al*., 1997; Barreto Filho *et al*., 2022a; Durand, 2020). Nevertheless, they still have relevance when used in conjunction with EM.

The outcomes of the current study will contribute to management strategies to deter the development of concentrated blooms in their early stages in this region and elsewhere. Early management of HABs can minimize the catastrophic events that impact the ecosystem (and any commercial enterprise dependent thereon) when the high biomass blooms collapse. The importance of mitigating HABs has been highlighted by others (Burson *et al.,* 2014; Choi *et al*., 2017; Erdner *et al.*, 2016; Smayda, 2002).

1.1.4 Study organism

Species in the genus *Prorocentrum* are known to be major contributors to HABs (Dou-ding and Goebel, 2001; Heil *et al*., 2005; Ndhlovu *et al*., 2017; Pitcher *et al.*, 2005). There is a lack of literature records that denote *P. redfieldii* as a causative organism and references are given to its epithet *P. triestinum* (Dou-ding & Goebel, 2001). It is a planktonic dinoflagellate characterised by two thecal plates and an apical spine/tooth which is 3 to 5 µm (Fig. 1.1). The cell is about 18-32 µm in length and 6-10 µm in width (Bursa, 1959). This organism is non-toxic but the decay of its high biomass during bloom collapse is known to cause massive fish kills because of the anoxic conditions in the surrounding waters (Ndhlovu *et al.*, 2017; Pitcher and Probyn, 2011, 2016). Only two recorded events in South Africa implicated this species, one in 2002 (Stephen and Hockey, 2007) and the other in 2015, which is the subject of this study. Both events resulted in massive rock-lobster walkouts.

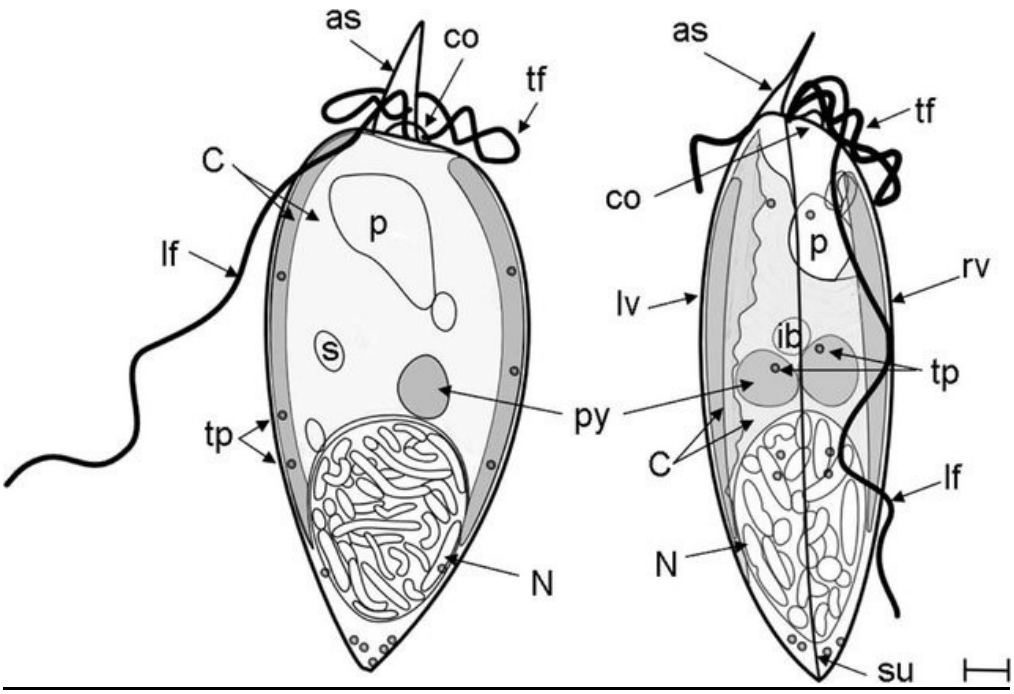


Figure 1.1 Generalized drawings of *Prorocentrum redfieldii* at the light microscope level by Ndhlovu *et al*., 2017 © **copyright [2017]**, reused by permission of Informa UK Limited, trading as Taylor & Taylor & Francis Group. LEFT, valve view; RIGHT, lateral view, Scale bar =2µm. Abbreviations: as, anterior spine; c, chloroplast; co, collar (anterior protuberance); ib, inclusion body; lf, longitudinal flagellum; lv, left valve; N, nucleus; p, pusule; py, pyrenoid; rv, right valve; s, starch; su, suture; tf, transverse flagellum; tp, trichocyst pore.

1.1.5 Study site

The HAB covered an extensive area over the Cape west coast from St Helena Bay to just north of the mouth of the Olifants river. The collection sites used in this study are in St Helena Bay (Fig. 1.2). Algal cell samples were collected by Dr G C Pitcher (Department of Forestry, Fisheries and Environment; Marine and Coastal Management, Cape Town) from the affected area during the onset of an algal bloom in February 2015 and during the decline phase in March and April 2015. St Helena Bay falls within the Benguela region which is characterised by the cold, upwelled

Benguela current (Pitcher, 1988). These wind-driven upwelling-downwelling cycles in the southern Benguela play an important role in the dynamics of algal populations in this region (Pitcher & Calder, 2000). Upwelling occurs in areas where water currents diverge and it results in nutrient enriched waters while downwelling occurs in areas where currents converge and results in nutrient poor water (Hutchings *et al.*, 1995). Detailed descriptions of upwelling and downwelling events are in section 1.2.1.

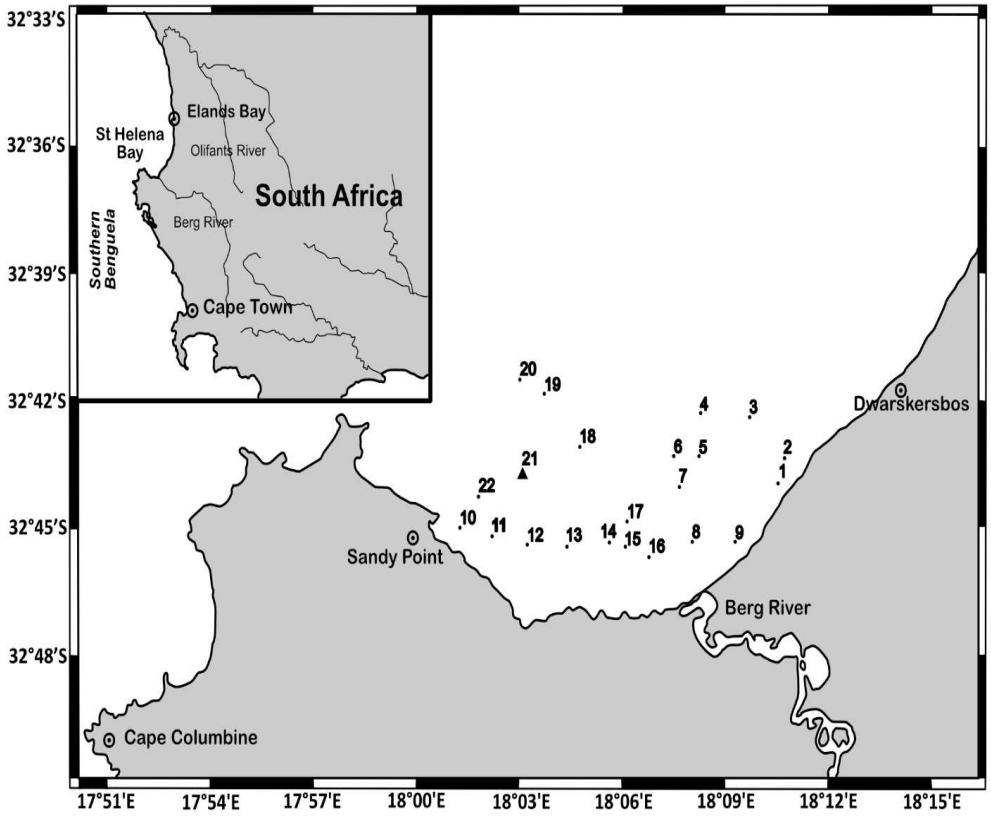


Figure 1.2 The location of St Helena Bay on the South African west coast and of the 22 stations that were sampled during the HAB outbreak (February 2015). *Prorocentrum redfieldii* samples used for field characterisation experiments and as a source of the isolate used in this study were collected from station 21 (after Ndhlovu *et al,* 2017) © **copyright [2017]**, reused by permission of Informa UK Limited, trading as Taylor & Taylor & Francis Group.

1.1.6 Overview of past research on the role of programmed cell death in phytoplankton ecology

Towards the end of the twentieth century it was discovered that PCD occurs in phytoplankton and there has been an ongoing research interest on its role in phytoplankton ecology (Barreto Filho *et al.*, 2022b; Bar-Zeev *et al.*, 2013; Berges and Falkowski, 1998; Berman-Frank *et al.*, 2004; K. D. Bidle et al., 2007; Bidle, 2016; Bidle and Falkowski, 2004; Bramucci and Case, 2019; Darehshouri *et al.,* 2008; Durand *et al.*, 2014, 2016; Franklin *et al*., 2004a; Yida Gao and Erdner, 2022; Ndhlovu *et al.*, 2017; Orellana *et al.,* 2013; Sathe *et al.*, 2019; Segovia, 2003).

There is evidence that PCD as a cell death pathway exists in dinoflagellate bloom forming species when subjected to stressful conditions and some of this research is summarised below.

1.1.6.1 PCD in *Peridinium gatunense* Nygaard (Vardi *et al.,* 1999)

The work on *P. gatunense* is one of the pioneering research works showing PCD in a HAB species. *Peridinium gatunense* forms blooms on lake Kinneret (Israel) during spring which terminate suddenly in summer. This study was conducted on cultures and live cells from the bloom. This study revealed that at the peak of the bloom the water pH rose above 8 which led to a limitation in dissolved CO_2. The CO_2 limitation increased the intracellular reactive oxygen species (ROS) and culminated in an oxidative stress that induced a cell death. The addition of a catalase (i.e., an enzyme that breaks down hydrogen peroxide to water and oxygen) and a cysteine protease inhibitor (E-64) decreased ROS and inhibited cell death, respectively.

These observations led to the conclusion that hydrogen peroxide (H_2O_2) was the ROS species responsible for the oxidative stress and that the cell death was programmed. Observations of these cells under the light microscope revealed protoplast shrinkage, a morphological characteristic associated with apoptotic cell death (Kerr *et al.*, 1972). The chromatin of the nuclei of these cells were

fragmented, this was revealed by **T**erminal-transferase-mediated d**U**TP [deoxy-uridine triphosphate] **n**ick-**e**nd **l**abelling (TUNEL) assay. The TUNEL assay is one of the biochemical essays that detects damage in the nuclei of cells undergoing cell death. This assay has a downside because it only shows that nuclear DNA is fragmented but it is not specific to PCD as cells undergoing necrosis can also be positive for this assay (Barreto Filho *et al.*, 2022a).

The highlights of this study are that apoptotic-like cell death was detected in a bloom forming dinoflagellate both from cultures and bloom cells from the lake. The cell death was induced by an increase in ROS. Cell death in these cells was successfully inhibited by the addition of a catalase and a cysteine protease inhibitor, the latter also stimulated the formation of cysts.

1.1.6.2 PCD in *Prorocentrum donghaiense* Lu (Huang *et al.*, 2016)

Prorocentrum donghaiense forms frequent HABs in the East China Sea. In this study *P. donghaiense* cultures in logarithm stage were exposed to a phosphate limitation. The physiological response of the phosphate limited cultures to stress was recorded using biochemical assays that are associated with PCD. These include the detection of ROS, caspase-like activity assay and the detection of metacaspase genes. ROS, caspase-like activity and the expression of the metacaspase gene was higher in the phosphate depleted cultures compared to the replete cultures. However, the observed increases in biochemical activity did not correspond to increases in cell death as the number of dead cells was low. This study concluded that the PCD biochemical markers in this organism were not only involved in the cell death process but were also associated with stress acclimation to the phosphate limitation.

1.1.6.3 PCD in *Prorocentrum donghaiense* (Ji *et al.*, 2021)

Cultures of an isolate of *P. donghaiense* from Changjiang Estuary in China were grown up to the exponential stage. Some were treated with varying concentrations of modified clay (MC) by the flocculation technique. The top liquid with cells not

trapped by the flocculant was removed and inoculated in fresh medium. Cells were sampled at different time-points and analysed over a 96-hour period using biochemical assays associated with PCD. These included, ROS, caspase-like activity, externalization of phosphatidylserine (PS, a phospholipid located on the interior of cell membranes that becomes externalized in cells undergoing PCD), the TUNEL assay and the mitochondrial membrane potential (MMP). Cell viability was assessed using Sytox-Green a nuclear stain that can only permeate membranes of non-viable cells. The ultrastructure was characterised with the transmission electron microscope (TEM) at the same time points. When the treated cells were compared to the controls, the MC treated cells displayed a significant increase ($P < 0.05$) in ROS, caspase-like activity and the number of Sytox-Green stained cells. The MMP decreased and the TUNEL and PS externalization assays were positive. The ultrastructural changes observed were protoplast shrinkage, amorphous chloroplasts (i.e., disorganization of the regular thylakoid membranes stacking), the nuclei decreased in size and there was increased vacuolation. There was an increase in the number and size of starch grains. These changes worsened with time and at 96 hours the nuclear membranes were ruptured.

1.2 LITERATURE REVIEW

1.2.1 Harmful algal blooms

The occurrence of algal blooms is a frequent phenomenon in coastal regions, more so when the water is enriched by events such as upwelling or cultural eutrophication (Hallegraeff, 1993).

Initially, it had been argued that the observed increase in HABs is artificial and is due to awareness of bloom increases because of improved monitoring systems and more collaborative global research (Anderson, 1989; Hallegraeff, 1993). Subsequent studies dispute that argument and the consensus is that the occurrence of HABs has increased (Anderson *et al*., 2012; Pitcher and Calder, 2000; Skarlato *et al*., 2018; Stephen and Hockey, 2007). The observed increase in HABs has been attributed to man-made organic nutrient increase in coastal regions (cultural eutrophication) as a result of sewage treatment plants, agricultural and aquacultural run-offs (Anderson *et al.*, 2002). Other contributors to the increased occurrence of HABs are the wind-driven upwelling and downwelling events (Bakun and Agostini, 2001; Kudela *et al*., 2010; Pitcher *et al*., 2005; Send *et al*., 1987). The wind-driven upwelling-downwelling events have a great influence on the incidence of HABs in the Benguela region (Pitcher *et al.*, 2005; section 1.2.2). Upwelling occurs when currents diverge while downwelling occurs when currents converge (Hutchings *et al.*, 1995).

The upwelling-downwelling events can occur in the open ocean and in coastal areas, the latter being applicable to the current study. In the southern hemisphere, coastal upwelling occurs when prolonged northward winds blowing parallel to the coast create friction on the water surface. The top layers of water are dragged by the frictional force of the wind and because of the effect of the Coriolis force the mass of water is deflected to the left of the wind direction (i.e., Ekman transport) creating an area of divergence. As a result, the body of warm surface water that is

deplete of nutrients is then replaced from below by the cold nutrient rich water that stimulates phytoplankton productivity (Pitcher and Calder, 2000; Sellner *et al.*, 2003; Wells *et al.*, 2015).

During coastal downwelling when the direction of the wind changes to a southerly direction, surface water is moved by Ekman transport towards the coast (Csanady, 1982; Send *et al*., 1987). The surface water piles up near the coast and eventually is forced to sink to the bottom. This increases the stratification in the water column and since this water is limited in nutrients it increases the depth of the nutrient limited zone and results in decreased productivity levels (Bakun and Agostini, 2001). There is also a period when the upwelling winds subside and there is no upwelling of new nutrients and this period is referred as relaxation (Smayda and Trainer, 2010), a term that will be adopted in the current study. This period is also nutrient limited because nutrients are not replenished.

The downwelling and the upwelling-relaxation periods favour dinoflagellate abundance. The stratified water favours their dominance in the water column (Margalef, 1978) because of their ability to migrate considerable vertical distances, i.e., they are able to periodically migrate downwards to lower levels or upwards to the euphotic zone, to take on nutrients and to obtain light respectively, outcompeting the non-motile diatoms (Pitcher *et al*., 2010). Nutrient exhaustion resulting from the persistent downwelling and long periods relaxation is one of the factors that initiate the decay of the dinoflagellate blooms (Pitcher *et al.*, 2014).

1.2.2 Dynamics of dinoflagellate blooms in upwelling regions

Understanding the phytoplankton bloom patterns in upwelling regions might provide insights about the behaviour of *P. redfieldii* as one of the causative species of HABs in the Benguela upwelling region. In this region the blooms are a function of the growth dynamics between two role players the flagellates

and the diatoms (Trainer *et al*., 2010). During the wind-driven upwelling stage, the water is mostly turbulent, well mixed and high in nutrients. These conditions favour the diatoms, because their hard silica-based cell wall (Crawford, 1981) provides protection against shear stress on the cell membrane as they get tossed about in the turbulent waters (Pitcher *et al*., 1991). Even though some dinoflagellates like the study organism also possess protective coverings (i.e., are thecate) their fragile flagella are not suited to withstand turbulent waters. Thus, diatom blooms dominating recently-upwelled waters are intermittently replaced by dinoflagellate blooms during the relaxation or downwelling periods (Bakun and Agostini, 2001; Smayda and Trainer, 2010).

While dinoflagellate blooms supersede those of diatoms, their success and species composition is not always predictable (Smayda and Trainer, 2010). Accordingly, their occurrence is more irregular/erratic when compared with that of the diatom blooms (Smayda and Trainer, 2010). However when they occur as blooms, they are harmful or detrimental to the health of other organisms because of their concentrated biomass that cause anoxic conditions when their populations collapse (Stephen and Hockey, 2007; Trainer *et al*., 2010; section 1.1).

1.2.3 Impact of harmful algal blooms in the Benguela region

HABs directly impact human beings both socially and economically (Anderson, 1989; Anderson *et al.*, 2002; Pitcher and Calder, 2000). The Benguela region experiences problems with HABs that have a negative influence on the livelihood of people in the region (Fawcett *et al.*, 2006). Aquaculture, commercial and recreational fishing are greatly affected when the high biomass blooms collapse resulting in anoxic waters and massive deaths of other organisms in the surrounding waters (Pitcher and Calder, 2000). Shellfish poisoning is one major HAB impact that affects human beings indirectly. Filter-feeding shellfish ingesting toxic phytoplankton accumulate their toxins inside their meat and can be lethal to humans especially when consumed in large quantities (Pitcher and Calder, 2000). The

resulting illnesses have been described as Paralytic (PSP), Diarrhetic (DSP), Neurotoxic (NSP) and Amnesic (ASP) shellfish poisoning (Hallegraeff., 1993). Dinoflagellates are responsible for all the above disorders except ASP which is caused by a genus of diatoms *Pseudo-nitzschia* spp. (Pitcher & Calder, 2000).

The collapse of blooms has always been linked to external loss factors like grazing, sinking, viral infection and nutrient exhaustion, but there is increasing evidence that a collapse may be brought about by programmed cell death which is a genetically controlled process as a response to either biotic or abiotic stress signals (Vardi *et al*., 1999; Burson *et al.*, 2014; Zhou *et al*., 2018; Bar-Zeev *et al.*, 2013; Berman-Frank *et al*., 2004; Vardi *et al.*, 2007).

1.2.4 Cell Death

Cell demise can be active (i.e., require energy) and genetically controlled as a response to stress signals or inherent factors, like cell development (programmed cell death) or it can occur with minimal energy and without the expression of genes, as a response to only stress signals and not inherent factors (necrotic cell death; Kroemer *et al.,* 2005).

Reports on cell death during embryogenesis date back to the nineteenth century, when Vogt (1842) reported the disappearance of cells in the notochord during the regression of the larval tail of toads undergoing metamorphosis (Clarke and Clarke, 1996). Other reports in the nineteenth century on cell death in lower vertebrates during embryo development are reviewed in Clarke and Clarke (1996), however, up to this point cell death was merely observed as a loss or disappearance of cells but it was not the focus of the research and its role in tissue and organ development was not appreciated.

1.2.4.1 Programmed cell death

It was much later that attention was given to the morphology of the dying cells and

to link the elimination of redundant cells to tissue and organ development (Glücksmann, 1951). These observations were made in higher vertebrate embryogenesis and organogenesis and examples include the loss of cells observed during the blastula, notochord and neural tube formation stages. The author observed changes in the nuclear material where firstly, the chromatin material formed clumps and separated from the non-chromatin material and he referred to this stage as chromatopycnosis. Further clumping occurred followed by the shrinkage of the nucleus and cytoplasm and he referred to this stage as hyperchromatosis. In the final stage which he referred to as chromatolysis the cell disintegrated into smaller pieces and disappeared. The name "programmed cell death" was coined by Lockshin and William (1964) when they reported cell death in the intersegmental muscles during the metamorphosis of a silk moth. The dying cells had a reduction in the size of mitochondria, increased vacuolation and lysosome-like structures. Changes to the nuclei of dying cells occurred later than the changes in the cytoplasm which contrasted with the observation by Glücksmann, (1951).

The term "apoptosis" was coined by a research group of pathologists who used ultrastructural observations to describe "an active, inherent cell death in animal tissue" (Kerr *et al.*, 1972). The ultrastructure of the dying cells revealed a reduced cytoplasmic volume accompanied by condensed chromatin in their nuclei. This was followed by the formation of plasma membrane blebs and the migration of the clumped chromatin to the nuclear envelop. Subsequently the nucleus disintegrated to smaller fragments. The nuclear fragments together with other organelles were enveloped by the membrane blebs and the cells eventually disintegrated into small membrane bound bodies termed apoptotic bodies. The apoptotic bodies were later taken up by phagosomes of surrounding cells and degraded in the lysosomes of adjacent healthy cells. The study by Kerr and others (1972) marked the turning point in the research of programmed cell death and for many years was used as a blueprint to define PCD (Tinari *et al.*, 2008). Programmed cell death and apoptosis were previously used interchangeably but it was later established that apoptosis is only one of the many phenotypes of PCD (Kroemer *et al*., 2009).

Cells that undergo programmed cell death die prematurely and spontaneously before reaching the stationary phase of the growth cycle and their death is actively controlled and gene expression is involved (Nedelcu *et al.*, 2011). However, other forms of cell death like the "autophagic cell death", as described below do not meet the first requirement because cell death in this phenotype is prolonged.

1.2.5 Phenotypes of programmed cell death

The types of programmed cell death are differentiated from each other based on the structural and biochemical changes observed in the cells undergoing PCD (Allen *et al.*, 1997; Durand, 2020; Kroemer *et al*., 2005, van Doorn *et al*., 2011). The resultant PCD phenotypes can be influenced by many factors, including the type, magnitude and duration of the stressor that induces PCD. For example, the same organism has been shown to exhibit different morphologies when subjected to different stimuli /stressors (Jimenez *et al.*, 2009; Moharikar *et al*., 2006; Sathe *et al*., 2019).

There are three main (most common across all phyla in both unicellular and multicellular organisms) phenotypes of cell death namely, apoptosis referred to as "type 1 cell death", autophagic cell death "type 2 cell death" and necrotic cell death "type 3 cell death" (Kroemer *et al*., 2009, 2005). Type 1 and 2 are programmed forms of cell death but type 3 was previously regarded as accidental cell death but there is consensus that some forms of necrotic cell death involve gene expression (Kroemer *et al*., 2009). Apoptosis is the most researched phenotype. It is important to note that these phenotypes can also overlap. For example, aponecrosis has a phenotype that combines those of apoptosis and necrotic cell death (Jimenez *et al.*, 2009). Other "atypical" phenotypes exist, mostly exhibited by the metozoa, are not relevant to this study, with the possible exception of paraptosis because it was observed in a dinoflagellate (Franklin and Berges, 2004). The different cell death phenotypes are summarised in Table 1.2.

Table 1.2. A summary of the different cell death phenotypes

PCD phenotype	protease activity dependent/ independent	structural features	biochemical activity	references
APOPTOSIS/APOPTOSIS-LIKE	caspase/ metacaspase dependent	Reduced cytoplasm early stage nuclear pyknosis karyorrhexis organelle membranes remain intact, plasma membrane blebbing and formation of apoptotic bodies	Loss of MMP, release of apoptotic factors from mitochondria to the cytosol (cytochrome c, AIF), increase in ROS, Internucleosomal	Kerr *et al*., 1972; Kroemer *et al*., 2009; Saraste and Pulkki, 2000)
AUTOPHAGIC/ VACUOLAR-LIKE PCD	caspase/metacaspase independent	Excessive autophagic vacuolation (characterised by double membraned vacuoles) accompanied by lysosomal/ vacuolar degradation, nuclear degradation is absent or can occur at the late stage of cell death	Increase in ROS	Kroemer *et al*., 2009
PARAPTOSIS	Caspase/metacaspase independent	extensive vacuolation by single-membrane vesicles derived from dilated ER and mitochondria, mitochondrial swelling; there is no nuclear pyknosis and karyorrhexis, the nucleus and plasma membrane remain intact.	Increase in ROS	(Sperandio *et al*., 2004; Yan *et al*., 2020a)
NECROTIC	Caspase/metacaspase independent	Increase in cell size, damage/rapture of the cell membrane, nuclear pyknosis and karyorrhexis, organelle swelling and damage to their membranes. vacuolation.	Increase in ROS	Kroemer *et al*., 2009

1.2.6 Structural markers of PCD in phytoplankton

This section elaborates on the structural markers of PCD phenotypes that are listed in table 1.1 above. These observations are achieved using microscopy (both light and electron microscopy).

- Cell / cytoplasmic / protoplast shrinkage (Bidle, 2016; Deponte, 2008; Moharikar *et al.*, 2006; Vardi *et al.*, 1999; Zuppini *et al.*, 2010). It is attributed to the movement of ions particularly K^+ and Cl^- out of the cell resulting in an ion imbalance inside the cell that can further trigger the activation of the cell death process (Bortner and Cidlowski; 2002).
- Plasma membrane blebbing (H. Wang et al., 2020) due to loss of structural integrity in actin filaments from increased hydrostatic pressure within the cell supersedes AVD and leads to the formation of apoptotic bodies (Aoki *et al*., 2020).
- Nuclear degradation observed as chromatin condensation / clumping (this phenomenon is termed pyknosis; Jimenez *et al*., 2009; Moharikar *et al.*, 2006; Sathe *et al.*, 2019; Segovia, 2003) and forms distinct electron dense clumps that migrate to the nuclear envelope (Prokhorova *et al.,* 2015). (see biochemical / molecular markers below; Kroemer *et al.,* 1995). Chromatin condensation occurs when proteases and endonucleases enter the nucleus and alter the structure of chromatin by cleaving proteins in the nuclear matrix and lamina and cause irreversible condensation.

  Chromatin pyknosis is followed by the break-down of the structural integrity of the nuclear envelope which results in membrane bound fragments that bud off the nucleus (this is termed karyorrhexis). In animal cells the fragments which are unevenly scattered throughout the cytoplasm are pocketed either individually or with other organelles by the plasma membrane blebs which then close-up and are pinched off the cell as membrane bodies termed apoptotic bodies (Kerr *et al.*, 1972), the entire cell is eventually dismantled into these apoptotic

bodies which are later taken up by phagocytic cells. By disintegrating in this manner, the toxic substances from the dying cells do not trigger an inflammatory response that might affect those cells that are not undergoing PCD. Nuclear pyknosis and karyorrhexis can occur in cells dying from either apoptosis or necrosis, but for the latter the cell disintegrates without the formation of apoptotic bodies and often results in an inflammatory response (Elmore, 2007).

- Excessive development of vacuoles has been reported as a marker of PCD (Barreto Filho *et al.*, 2022b; Franklin *et al.*, 2004b; Franklin and Berges, 2004; Jimenez *et al.*, 2009; Sathe *et al.,* 2019; Sperandio *et al*., 2000). This process is referred to as vacuolation or vacuolization, the first term will be used in the current study. The term vacuolation is used broadly in literature and can refer to different processes that culminate in the formation of vacuoles, for example, the upregulation of single or double membraned vesicles associated with cellular degradation (Affenzeller *et al*., 2009; Darehshouri *et al.,* 2008), self-consumption of the cytoplasm by micro-autophagy (Minina *et al.,* 2014), it has also been reported as the development of numerous lytic vacuoles on the cytoplasm of the cell or areas that have lost electron density when viewed with an electron microscope (Barreto Filho *et al.*, 2022b; Bidle and Bender, 2008). This PCD marker is associated with various phenotypes of PCD including that of autophagic cell death, paraptosis and necrotic cell death.
- Alterations to the structure of other cell organelles:
  - (i) mitochondria:

    The mitochondria play a central role in the intrinsic pathway of PCD as they are the primary targets of the stress signals in the initial stages of the PCD pathway. In the early stages of PCD the alterations that occur to the mitochondria are at a biochemical/molecular level and are discussed below in section 1.2.7. It was initially assumed that no structural changes occurred to mitochondria as Kerr *et al*. (1972) reported that organelles (including mitochondria) were still

intact when observed inside the apoptotic bodies. However, swelling of mitochondria has been reported in cells dying via the paraptosis phenotype (Franklin and Berges, 2004; Sperandio *et al*., 2000). The swelling results from excess calcium ions (a calcium ion imbalance inside the endoplasmic reticulum [ER] can occur because of misfolded proteins response to stress) transferred from the ER into the matrix of mitochondria at contact sites between the two organelles. The excess calcium exerts an osmotic pressure resulting in the dilation of the mitochondrial matrix and the ER lumen (Yoon *et al.*, 2014).

The swollen mitochondria and the dilated ER form single membraned vacuoles that are later used for degradation (Sperandio *et al.*, 2000; Yan *et al.*, 2020b).

(ii) chloroplasts:

Chloroplast like the mitochondria are targets of Structural alterations to the chloroplast include damage to the chloroplast envelope, disorganization of the orderly thylakoid stacking, resulting from an increase in the inter-and intra-thylakoidal space (Zuppini *et al.*, 2007; Pokrzywinski, 2014; Simeonova *et al.*, 2000) and the chloroplasts do not have a defined structure. (Jing *et al.*, 2017).

(iii) ribosomes: Ribosome clumping and reduction has also been reported (Pokrzywinski, 2014)

(iv) endomembrane system: Dilated ER can be used in the formation of lytic vacuoles (Sperandio *et al.*, 2000).

1.2.6.1 Cell biochemical/molecular hallmarks of PCD

PCD is noted to be accompanied by:

- A decrease in the mitochondrial membrane potential (MMP) that leads to the release of mitochondrial proteins located in the mitochondrial intermembrane space to the cytosol, e.g., cytochrome c, endonuclease G

and apoptosis inducing factor (AIF). When translocated to the cytosol these mitochondrial proteins initiate a cascade of events that initiate the PCD process. For example, cytochrome c mediates the activation of cysteine proteases (caspases) which initiate the cell death pathway.

- Oxidative stress, observed as an increase in reactive oxygen species
- The externalisation of phosphatidylserine (PS) to the outside of the plasma membrane. This amino-phospholipid is normally restricted to the protoplasmic face of the plasma membrane (van den Eijnde *et al*., 1998).

The laddering of DNA - this occurs when the nuclear chromatin is digested by nucleases and fragmented into oligo-nucleosomal size fragments, which can be seen as ladders in an agarose electrophoresis gel.

1.2.7 Cell ultrastructural changes in the SAR clade (former Chromalveolata) following stress induced PCD

The focus in this section is to report on ultrastructural and biochemical changes observed during successful induction of PCD in two groups, namely, the Stramenopila and Alveolata represented in the Stramenolina, Alveolata, Rhizaria (SAR) clade, the lineage to which the current study organism belongs (Table 1.2; Fig.1.3). The groups were formerly classified under the supergroup Chromalveolata but have recently been classified in the SAR clade that includes, Stramenopiles, Alveolates, Rhizaria (Torruella *et al.*, 2024). This lineage is well removed from the classical groups used to typify PCD (Opisthokonta and Archaeplastida; Fig. 1.3), so focusing on members of the SAR should provide a better baseline against which to compare the study organism. The summary of ultrastructural changes in Table 1.3 is restricted to algal representatives of the SAR clade.

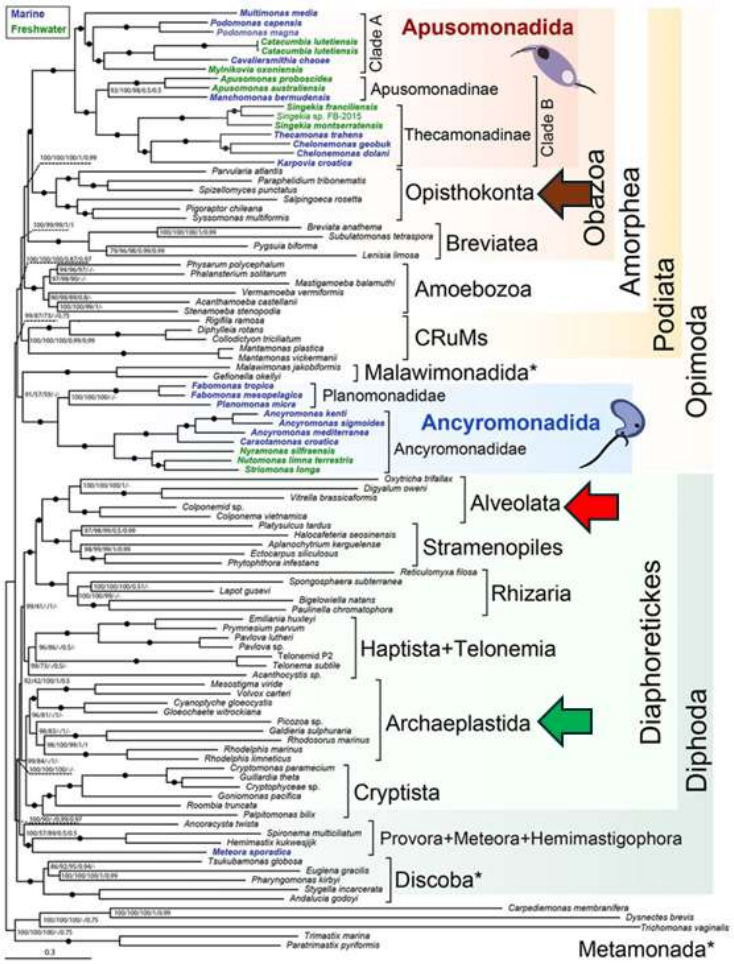


Figure 1.3 Eukaryotic tree of life showing the Alveolata (red arrow), Archaeplastida (green arrow) and the Opisthokonta (within the Amorphea, brown arrow) by Torruella *et al.*(2024) licenced under CC BY-NC 4.0.

Table 1.3. A summary of PCD - associated ultrastructural changes exhibited by various members of the SAR group.

Species name	Stressor	Ultrastructural changes	PCD phenotype	Refs
Prorocentrum donghainse	Modified clay	Cell shrinkage, amorphous chloroplast	Not specified	(Jing *et al.*, 2017)

(Alveolata, Miozoa, dinoflagellates		structure, nucleus decreased in size, chromosomes appeared darker and condensed, excessive vacuolation, increase in starch grains		
***Karlodinium veneficum* (Alveolata, Miozoa, dinoflagellates)**	Exposure to cytotoxic activity of exudates of the	Organelle loss, extensive vacuolation leading to only cell outlines (ghost cells) being observed in some cell in later stages, amorphous intracellular material	Paraptosis	(Franklin and Berges, 2004)
***Amphidinium carterae* (Alveolata, Miozoa, dinoflagellates)**	Darkness & Senescence	Excessive vacuolation, organelle (nuclei, chloroplasts, and mitochondria) degradation but the plasma membranes remained intact	Paraptosis	(Franklin and Berges, 2004)
***Thalassiosira pseudonana* (Stramenopiles, Bacillariophyta, diatom)**	Fe Starvation	Excessive vacuolation, swollen mitochondrial and intact plasma membrane	Not specified	(Bidle and Bender, 2008)

1.2.8 The relevance of programmed cell death for unicellular organisms

The discovery of PCD in unicellular organisms has triggered interest and questions about its ecological relevance and evolutionary role. It was initially believed that PCD and the "death genes" evolved with the development of multicellular organisms. However, its existence in pro- and eukaryotic unicellular organisms makes it apparent that its evolutionary origin predates multicellularity (La *et al.*, 2022; Nedelcu, 2009).

The existence of PCD in unicellular organisms is not easily justifiable because in a unicellular system there is no benefit for the eliminated individual and thus

maintenance of complex PCD genes is counterintuitive (Welburn *et al.,* 1997). However, PCD is maintained in bacteria, archaea, protozoa, fungi, and algae which are diverse groups of unicellular lineages (Debrabant *et al.,* 2003). The question that arises is how can a process that eliminates the cell allow for adaptation because for a trait to be adaptive it must confer a benefit. In multicellular organisms the maintenance of PCD as an adaptation and its benefits are easily understood.

In a multicellular system there is clonality and a mutual dependency between the cells (Fisher *et al.,* 2013). If some of the cells in a multicellular system are programmed to die the remainder of cells that are not affected (i.e., the whole organism) receive the benefits. In terms of evolution, the sacrificial behaviour by the cells that commit themselves to die to benefit others in a multicellular system can be explained by the kin and group selection theories (Bidle and Falkowski, 2004). In the kin selection theory, an individual can carry a negative trait (e.g., a behaviour that is negative to its reproductive fitness) if it benefits those individuals that are genetically related to it (Simon *et al.*, 2013). In multicellular organisms PCD has important biological functions, e.g., in cell differentiation and when eliminating rogue cells and their genetic mutations that are detrimental to the organism (Debrabant *et al.*, 2003), this again shows that in these organisms PCD is selected for because it contributes to their fitness. Since unicellular organisms reproduce asexually under favourable conditions and are thus considered to be clonal, the kin and group selection theories have also been used to explain the maintenance of unicellular PCD (Bidle and Falkowski, 2004). It is considered, however, that under stress conditions cells might change to sexual reproduction and this can result in genetically modified cells that enter a resting stage. Their expression as new clonal populations, each new zygote potentially with variable receptivity to the benefits of PCD (or the ability to perpetuate, diminish or enhance PCD), would only be expressed at the termination of the next favourable growth period.

It has been argued that the benefits of programmed death would be for the conspecifics (Barreto Filho *et al.*, 2022b; Durand and Ramsey, 2018), an argument

that has been supported by the following example, cells of a *Chlamydomonas sp*. were killed by two different stressors, one that induced PCD (heat stress) and one that was non-PCD (i.e., cells were lysed). When the supernatants of dead cultures were added to consecutive cultures, their presence promoted growth more when cells were harvested from PCD-induced cultures than non-PCD induced cultures or even controls. It was interpreted that the cells dying by PCD released beneficiary biomolecules to the media (Durand *et al.*, 2011). In another experiment, involving a population of *Heterosigma akashiwo,* PCD was shown to be selectively induced in virally infected cells resulting in the complete elimination from the population before it could be replicated (Bidle and Falkowski, 2004; Lawrence *et al.*, 2001).

More experimental evidence exists that has been interpreted to suggest that unicellular PCD benefits the kin in a population. Some of the PCD benefits that have been suggested, include the maintenance of clonality (Welburn *et al.*, 1997), for example in a population of trypanosomatids (protozoan parasites) an *in vivo* study showed that when inside the gut of the insect vector, not all cells differentiate to become infectious and those cells that were not infectious died by PCD. It was suggested that this ensured the preservation of the genome because only those individuals that were fit (i.e., the infectious type) continued the life cycle and are transferred to the mammalian host (Debrabant and Nakhasi, 2003; Welburn *et al.*, 1997).

Notwithstanding the benefits that are offered by PCD genes to unicellular organisms, some researchers caution about the general assumption that unicellular PCD is an adaptation and maintained by kin and group selection as is the case in multicellular organisms (Nedelcu *et al.*, 2011). They argue that although unicellular organisms are clonal and have high relatedness some populations can be heterogenous. For an example, a study showed that the genetic makeup of a diatom bloom population was heterogenous (Nedelcu *et al.,* 2011; Rynearson *et al.*, 2006), indicating that although the population is made up of unicellular organisms in this instance PCD cannot be justified by the kin selection theory because the benefit of PCD can be received by a random member in the population who is not genetically

related to the dying cell. These authors suggest that PCD in unicellular organisms is a maladaptive trait that has not been purged because it is linked to adaptive pro-survival traits (i.e., it is a by-product) at the level of the individual. However, this maladaptive trait could be re-purposed under certain conditions that favour kin/group selection (e.g., the examples of *Chlamydomonas sp.*, *Heterosigma sp.* and the trypanosomatids above).

There is an ongoing debate about unicellular PCD being an adaptation or not and this creates uncertainties when establishing the evolutionary interpretations of unicellular PCD. To address this, Durand and Ramsey (2018) have suggested an approach that looks at the evolutionary histories of the mechanisms that bring about the PCD. If it is established that the "function of causing death is selected for", they refer to it as true PCD. They have recommended two definitions for PCD, either as an adaptation or a maladaptation and have coined two names. The first name, "True PCD" refers to PCD where it has been proved that it is selected for and the second name, "Ersatz PCD" refers to PCD that is a result of pleiotropy (Durand, 2020; Durand and Ramsey, 2018). Pleiotropy occurs when a single gene is responsible for the expression of two or more unrelated traits (Stearns, 2010). In "Ersatz PCD" the genes have been retained because they serve another purpose other than PCD and the latter occurs as a by-product.

1.3. Aim and Objectives

There has been little research done on how populations of phytoplankton collapse and consequently not much is known about the biological mechanisms that play out in the abrupt termination of algal blooms (Bidle and Falkowski, 2004). The current study investigates the cell death pathway in an algal bloom focused on detailed ultrastructural changes within the causative organism, from the development through to the final collapse of the bloom. Substantial research has been done in upwelling regions worldwide including the Benguela region, South Africa on the monitoring, characterisation and classification of HABs (Fawcett *et al*., 2006; Pitcher, 1988; Pitcher *et al.*, 2010; Pitcher & Calder, 2000; Probyn *et al.*, 2000), but an in depth study using electron microscopy to investigate PCD as a death pathway in a collapsing bloom would add a novel perspective into the existing research.

This study aimed to determine, for the first time, ultrastructural changes that occur in cells sampled from a collapsing harmful algal bloom of *P. redfieldii* and ascertain whether there was structural evidence of PCD as a driver of the bloom collapse. Further, these ultrastructural responses were compared with those of cultures grown in replete conditions established from a cell isolated from this very bloom and subjected to stressors known to induce PCD, i.e., macronutrient deprivation nitrogen (NO^{3-}) and phosphorus (PO_4^{3-}) and heat stress.

For each stressor tested, biochemical assays known to associate with PCD, such as the expression of caspase-like activity and of ROS as well as DNA laddering, were used to corroborate that the ultrastructural responses were linked with the induction of PCD.

The individual objectives to meet this aim were:

1). To collect, preserve and establish a unialgal culture of *P. redfieldii:*

This was achieved by collection of samples of the study organisms from St Helena Bay at the onset of and late into the harmful bloom event. Unialgal cultures were maintained in the laboratory throughout the experimental period and the growth dynamics of the study organism were established.

2). To characterise the ultrastructure of nutrient replete cells of *P. redfieldii:*

This was achieved by a detailed analysis of the ultrastructure of replete cells by transmission electron microscopy and the focus was on alterations to the nucleus, endomembrane system (Golgi bodies, endoplasmic reticulum and associated vesicles); mitochondria; chloroplasts; vacuolation and amphiesmal membranes.

3). To characterise the ultrastructure of field samples collected at the onset and late into the bloom:

This objective was achieved as in (2) above

4). To induce PCD using a macro-nutrient stress:

This was achieved by depriving the cultures of two macro-nutrients (nitrogen as NO_3^{--}- and phosphorus as PO_4^{3-}). Samples were characterised as in (2) above. Concurrent measurements of PCD associated biochemical assays were performed including:

i) DEVDase activity assay:

ii) DNA laddering assay

iii) ROS assay:

5). To induce PCD using heat-shock:

This was achieved by exposing the cultures to a heat-shock at different temperatures. Cells were subjected to similar analysis as those in (2, & 4) above.

1.4 Importance of the study

The frequent occurrence and subsequent collapse of anaerobic HABs caused by dinoflagellates greatly affects the population dynamics in upwelling regions like the Benguela. The impact is experienced in various trophic levels, changing the species diversity in the affected areas. The study of the cell death pathway in a causative organism will contribute to the fundamental knowledge that is required to alleviate the problem.

An ultrastructural study of *P. redfieldii* detailing its mortality at the inception of a bloom until its collapse has not been done and the current study will close this gap in the existing knowledge about this species and give insight about its behaviour during the bloom. It is acknowledged that documenting PCD is difficult, because of the problems with detection (Barreto Filho *et al.,* 2022a). Ultrastructural changes are the gold standard (Barreto Filho *et al*., 2022a; Durand, 2020; Hasanzadeh *et al.*, 2017; Zhao *et al.*, 2006) because "seeing is believing" and there is a need to have ultrastructure before having confidence in the biochemical and cell biology essays. This gold standard assessment is crucial for future interpretations of this organisms in HABs, since transmission electron microscopy is laborious what is observed in this study can be used as a baseline to correlate with the PCD molecular biomarkers.

1.5 Structure of Thesis

This section gives an overview of the thesis and the objectives that will be achieved in each research chapter. Each chapter from 2-4 is divided into an introduction and literature review, material and methods, discussion and conclusion relevant to that chapter. All the references were compiled at the end of the thesis.

Chapter 2

This chapter will address objectives 1, 2 and 3.

Chapter 3

This chapter will address objective 4

Chapter 4

This chapter will address objective 5

Chapter 5

This is the general discussion chapter and will also include the overall conclusion, limitations of the study and future work

2: COMPARATIVE ULTRASTRUCTURES OF A REPLETE CULTURE AND DYING *P. REDFIELDII* CELLS FROM A HAB

2.1 INTRODUCTION

2.1.1 Background

Dinoflagellates are frequent causative organisms of blooms in upwelling systems like the Benguela (Ndhlovu *et al.*, 2017; Pitcher *et al.*, 2010; Probyn *et al.*, 2000; Stephen and Hockey, 2007). When the relaxation and downwelling conditions persist, nutrients become depleted leading to the decay of these blooms, often resulting in anoxia and massive deaths of other organisms (Pitcher *et al*., 2014). Species of *Prorocentrum* are frequent contributors to these anaerobic blooms (Pitcher and Louw, 2021). How these organisms, and others during the bloom decay, die is a relatively unexplored phenomenon, and there is a growing interest in linking the collapse of these blooms to causes of cell death like programmed cell death (Segovia, 2003; Franklin *et al*., 2006; Bidle, 2016).

This chapter gives insight on the growth dynamics of *P. redfieldii* cells grown in the laboratory in nutrient replete conditions. It will also reveal the ultrastructure of the nutrient replete cells and those sampled from a collapsing bloom. The observed ultrastructure of the replete cells was used as a standard against which to compare those sampled from the bloom and to determine whether they were dying in a regulated manner, namely by PCD.

2.1.2 Glossary

Table 2.1. Definitions of various terms used in this chapter and beyond.

Accumulation bodies-	Spherical bodies with electron dense and fibrous material found in the cytoplasm of dinoflagellates. They exhibit acid phosphate activity and are suspected to have an autodigestive function.

Amphiesma-	A complex structure making up the cell covering of dinoflagellates. It is made up of vesicles that are flattened, known as the alveoli, and may contain thecal plates. An additional sub thecal layer of microtubules or an amorphous pellicle can be present.
Autophagosomes-	Double-membraned structures that enclose intracellular cargo to be recycled in autophagic vacuoles.
Autophagy-	A catabolic process found in eukaryotes involves the engulfment of degenerated organelles by vesicles known as autophagosomes and their subsequent transportation to vacuoles, where the contents are recycled.
ATG genes-	Autophagy related genes encoding proteins required for autophagy.
Dinokaryon-	Dinoflagellate nucleus characterized by the presence of permanently condensed chromosomes which lack histones.
Pusule-	Membranous subcellular organ found in dinoflagellates that opens to the cell exterior via a duct in the region of the cingulum/sulcus junction close to where the flagella arise. It has been suggested to have an osmoregulatory role.
Vacuolation-	Consumption of the cell cytoplasm by the formation and coalescence of vacuoles
Axoneme-	The central part of a flagellum that contains microtubules and other proteinaceous structures e.g., the cytoskeletal motor protein dynein.
Cingulum-	A transverse groove that divides the dinoflagellate cell into the upper epicone and lower hypocone and which houses the transverse flagellum.
Sulcus-	A groove on the ventral side of the cell that is predominantly on the hypocone and that lies perpendicular to the cingulum. It houses the proximal portion of the longitudinal flagellum.

2.1.3 Dinoflagellates

Dinoflagellates possess some distinct characteristics that differentiate them from other eukaryotes and this section provides an overview of their morphology, ultrastructure and other characteristics. A detailed background of their ultrastructure is required if meaningful distinctions are to be made between healthy (early cultured) and stressed (late bloom) cells of *P. redfieldii*. A study of the ultrastructure is also essential if PCD interpretations are to be made (Barreto Filho *et al*., 2022).

Dinoflagellates are generally unicellular eukaryotes that are documented as one of the dominant obvious primary producers in both oceans and fresh water (Spector, 1984). They are classified under the Alveolate group (see below) and form part of the TSAR superclade (Burki *et al.*, 2020). They are a diverse group of eukaryotic organisms and employ various feeding strategies including autotrophy, heterotrophy, mixotrophy, parasitism and/or symbiosis (Janouškovec *et al*., 2017). Notwithstanding the important role in CO_2 fixation and primary production of some, their abundance can result in concentrated HABs that often cause mass mortality of other organisms in those environments when their populations collapse (Ndhlovu *et al*., 2017; Pitcher and Calder, 2000; Sellner *et al*., 2003; Soyer-Gobillard, 2017).

2.1.3.1 The cell covering

Dinoflagellates are covered by an amphiesma (Box 2.1), a membranous complex structure made of flattened vesicles known as alveoli (Loeblich, 1970; Fig. 2.1), a characteristic that groups them together with ciliates and apicomplexans in the taxonomic group, the Alveolata (Segovia, 2008a; Sogin, 1991). Thecal plates are formed within the alveoli vesicles by secretion of cellulose or other polysaccharides (Lau *et al*., 2007; Segovia, 2008b) and form a protective structure often perforated by pores which are used for ejecting trichocysts (described below). Dinoflagellates can be classified as armoured when they possess thick and obvious plates or unarmoured when these plates are thin or negligible (Taylor, 1987). In the species of *Prorocentrum* the amphiesma consists of an outer membrane (i.e., the plasma membrane), beneath this membrane are the alveoli vesicles which constitute an

outer and inner alveoli membrane (the vesicles are continuous and house the two major thecal plates). A single membrane (i.e., the inner membrane) underlies the vesicles and separates the amphiesma from the cytoplasm (Dodge, 1973).

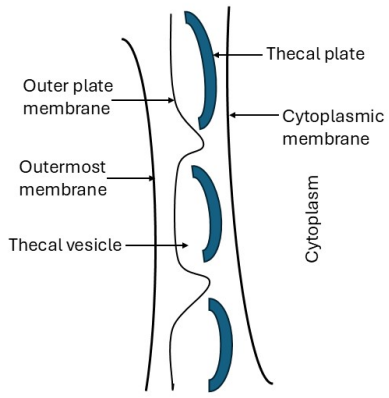


Figure 2.1 Schematic diagram of the amphiesma of a thecate dinoflagellate.

In *P. redfieldii* there are only two major (alveoli) thecal plates or valves that cover most of the cell and that are joined by sutures. The eight plates of the periflagellar region are smaller in size and are referred to as thecal platelets (Faust and Gulledge, 2002; Ndhlovu *et al*., 2017).

2.1.3.2 Trichocysts

Trichocyts are ejectile, defence structures that are synthesized in the Golgi region in enclosed membranes or sacs and migrate towards the periphery of the cell as they mature (Barsanti and Gualtieri, 2005).

2.1.3.3 Flagella

In most dinoflagellates, the flagella arrangement is termed the dikokont whereby the two flagella axonemes are inserted into the cell perpendicular to one another and result in a longitudinal and transverse orientation (Taylor, 1987). The transverse

flagellum, situated in the cingulum, wraps around the cell in a wavy ribbon-like manner and facilitates much of the forward movement and spin of the organism during swimming. The proximal end of the longitudinal uncoiled flagellum lies inside the sulcus and trails behind the organism, acting like a propeller (Gagat *et al*., 2014). In *P redfieldii*, the cingulum and sulcus are absent and both flagella extend from the same flagella pore (Loeblich *et al.*, 1979) in the apical region of the cell (Dodge and Bibby, 1973; Ndhlovu *et al*., 2017), this flagella arrangement is termed the desmokont arrangement (Taylor, 1987). Dinoflagellates are fast swimmers and their movement is accompanied by a spiral motion of the cell (Soyer-Gobillard, 2017). Many are rapid swimmers, and this allows them to traverse relatively great distances in the water column, which can be important if they are to obtain nutrients in the lower depths of the column during periods of relaxation and downwelling when nutrients are not replenished in the euphotic zone.

2.1.3.4 The Nucleus

Dinoflagellates possess a mesokaryotic nucleus, which is unique to them, also known as the dinokaryon (Soyer-Gobillard, 2017; Talbert and Henikoff, 2012). Some of the differences between the dinokaryon and most other eukaryote nuclei include:

- A very low protein to DNA ratio (1:10) compared with that of other eukaryotes where the ratio approaches equity (1:1).
- Large nuclear DNA per cell (starting from 3 up to 250 picograms of DNA per cell ; Spector, 1984; Wang *et al.*, 2014).
- The chromatin possesses specific DNA-binding proteins (which are non-histones) and it lacks nucleosomes (Mínguez and Franca, 1994; Soyer-Gobillard, 2017). These non-histone proteins are homologues of the dinoflagellate / viral nucleo proteins (DVNP's) and histone-like proteins (HLPs), which originate from viruses and bacteria, respectively (Chan and Wong, 2007; Janouškovec *et al*., 2017; Riaz *et al.*, 2018).
- Chromosomes remain permanently condensed throughout the cell cycle (Dodge, 1965; Gornik *et al.,* 2012; Pokrzywinski, 2014). This is attributed to

a highly ordered structure of their cholesteric liquid crystalline chromosomes (LCCs). At high concentrations DNA molecules can be condensed by self-assembly to various forms of liquid crystalline phases. Essentially LCCs are a form of DNA packaging for highly dense DNA molecules in the absence of histones, they are different from the histone and nucleosome facilitated packaging of chromosomes found in other eukaryotes (Chow *et al*., 2010; Gornik *et al.*, 2019).

- Another unique feature of the dinokaryon is the presence of metal ions like calcium and magnesium in high proportions in relation to DNA base pairs, almost in a (1:1) ratio. These divalent cations could serve to neutralise the negative charge of DNA in the absence of histones which normally provide the positive charge to neutralize the DNA of other eukaryotes (Pokrzywinski, 2014).
- There is also a difference in the DNA base pairs in that the thymine bases are replaced by 5-hydroxymethyluracil (HOMeU), which is also found in the DNA of some bacteria (Ohtsuka *et al.*, 2015).

2.1.3.5 The Pusule

The pusule, a subcellular membranous organelle situated at the anterior end of the cell, is another unique structure found in dinoflagellates. There are two main types, those that contain vesicles and those that are tubular or sac-like. Other types have been described, but they are variations of these two fundamental types (Dodge, 1972). The function of the pusule in dinoflagellates is unclear but it has been suggested to play an osmoregulatory or secretory role (Dodge, 1972; Klut *et al.*, 1987).

2.1.3.6 Plastids (Chloroplasts)

In those groups of dinoflagellates that possess plastids their acquisition occurred through multiple events of endosymbiosis. In a simplified occurrence of events, the primary endosymbiotic event occurred when an ancestral eukaryotic cell ingested and enslaved a photosynthetic cyanobacterium, resulting in a primary plastid with a two-membrane envelope. A secondary endosymbiotic event occurred by the

enslavement of a eukaryote that already had a primary plastid (e.g., a red algae) by a protist resulting in a secondary plastid with three or four enveloping membranes. A secondary endosymbiosis is the common pattern in autotrophic dinoflagellates and results in the peridinin containing species like the study organism, *P. redfieldii*.

The peridinin plastid is bounded by a three-membrane envelope and it is not connected to the endoplasmic reticulum as observed in some groups of micro-algae (Dodge, 1968; Solymosi, 2012). The plastid contains pigments like chlorophylls a and c as well as its accessory pigment, the carotenoid peridinin (Zhang *et al*., 1999). The thylakoid membranes are appressed, mostly arranged in stacks of three and each of these units forms a lamella. The orientation of the lamellae is parallel to the longitudinal axis of the chloroplast (Dodge, 1968). Pyrenoids are often present (Hoppenrath and Leander, 2008).

2.1.3.7 Accumulation bodies

Accumulation bodies are electron dense bodies that might contain fibrous or membranous and granular material when viewed using TEM (Dodge and Bibby, 1973; Siano and Montresor, 2005). The presence of accumulation bodies has been reported in dinoflagellates (Taylor, 1968; Zhou J and Fritz L, 1994). Their function is suggested to be that of an autodigestive organelle, and it was discovered that they become larger in starved cells (Taylor, 1968).

2.1.3.8 Other organelles

Other organelles like the Golgi bodies, endoplasmic reticulum, ribosomes and mitochondria resemble the ones found in other eukaryotic lineages. The shape and size of mitochondria vary but they all possess tubular cristae (Taylor, 1991).

2.1.4 Structural markers of programmed cell death

The existing empirical research on microalgal PCD has mostly been measured / detected using markers that have been adopted from the long established PCD research on Metazoans and Fungi (Opisthokonta; Barreto Filho *et al.*, 2023). The problem with this is, firstly, that some microalgae possess chloroplasts and cell

walls, which are lacking in opisthokonts. Secondly the ecological niches occupied by opisthokonts and microalgae are diverse. In a recent study, Barreto Filho *et al*., (2023) have recommended structural and biochemical markers that can be used for detecting PCD in phytoplankton based on their high correlation with this phenomenon across highly divergent taxa. The PCD structural markers will be used as a guide in the current study and will be correlated with ultrastructural alterations to the nucleus, chloroplasts, mitochondria, endomembrane system (endoplasmic reticulum, Golgi bodies and associated vesicles), plasma membrane and vacuolation of the cells sampled from a HAB to detect if the cells are dying in an ordered manner. These structural markers have been detailed in in Chapter 1, section 1.2.6.

2.1.5 Autophagy

Nutrient availability plays an important role in the dynamics of phytoplankton blooms. When nutrients become limiting, bloom organisms adopt strategies to alleviate the resultant stress. Autophagy, a catabolic process found in most eukaryotes (Shemi *et al.*, 2015), is used as a stress response to temporally cope with nutrient limitations and oxidative stress (Yang and Klionsky, 2009). It is also observed during cellular differentiation, regular organelle recycling and protein turnover (i.e., it creates an equilibrium within the cell by degrading damaged / aging organelles and proteins allowing for the synthesis of new constituents), elimination of invasive pathogens, e.g., viruses (Yang and Klionsky, 2009) and cell death (Mizushima, 2004).

There are two main types of autophagy, namely, macro-autophagy and micro-autophagy (Ohsumi 2013). The former is the most common form and is generally referred to as autophagy. Autophagy is divided into distinct steps. The material destined for disposal (e.g., degenerated organelles, protein aggregates, lipid droplets and membranes) is first isolated by an engulfing double membrane termed a phagophore to form a vesicle known as an autophagosome. The autophagosome with its cargo is then transported to lytic vacuoles where the entire autophagosomes and contents are engulfed, degraded and recycled (Fig. 2.2; Bassham and Crespo,

2014; Kourtis and Tavernarakis, 2009; Kwon and Park, 2008; Rabinowitz and White, 2010).

Early studies on autophagy relied on electron microscopy and were on animal cells (the rat liver; Ashford and Porter, 1962; Duve, 1959; Mizushima, 2004). The isolation of autophagy–related genes (ATGs) in the yeast *Saccharomyces cerevisiae* by Tsukada and Ohsumi in the 1990's gave insight into the molecular aspects of this phenomenon (Tsukada and Ohsumi, 1993). The ATGs are kinases involved in various stages of the autophagy process. In a simplified description of the autophagy process in yeasts, the ATG 1 complex composed of ATG 1, 13 and 17 (the numbering denotes the sequence of their discovery) together with the target of rapamycin (TOR) are involved in the induction of autophagy. TOR is also a kinase protein and is a signaling molecule that monitors and regulates cell growth as a response to the availability of nutrients (Kiel, 2010a) and it is evolutionary conserved in eukaryotes.

In non-stressed conditions TOR is activated and phosphorylates the ATG 13 protein and by doing that the ATG 13 protein loses the affinity to bind with the other two proteins to form the ATG 1 complex, and consequently autophagy remains at low levels. In stressed conditions TOR is deactivated and ATG 13 is dephosphorylated allowing it to bind to ATG 1 and 17 to form the ATG 1 complex and this upregulates autophagy. Other ATGs (either individually or in groups like the ATG 1 complex) are involved in various stages of the autophagy process, including the nucleation, expansion and fusion of membranes to form the autophagosomes. For example, another complex, the ATG 8 + Phosphatidylethanolamine (PE) lipids and ATG 9 are involved in the formation of the autophagosome), the expansion of the membrane of the autophagosome, the sequestering and transportation of the cargo to the vacuole (Yang and Klionsky, 2009). The PE phospholipids are the major lipids found in biological membranes (Patel and Witt, 2017). At the vacuole **interface** the fusion of the outer membrane of the autophagosome to the vacuolar membrane is facilitated by a group of membrane fusion proteins, namely, the soluble N-ethylmaleimide-sensitive-factor attachment protein receptor (SNARE) (Kiel, 2010).

Knowledge about the source of the phagophore membrane is elusive, with some researchers identifying the endomembrane system (endoplasmic reticulum, Golgi bodies and associated vesicles) and the outer membrane of the mitochondria as the donors for it (Morel, 2020).

Micro-autophagy is a second, less-reported type of "autophagy" and occurs at the vacuolar membrane site by direct engulfment of the cytoplasm and organelles through the formation of an autophagic tube which is an extension of the vacuolar membrane (Kiel, 2010; Li *et al*., 2012). Therefore, this pathway does not require specialized vesicles like the autophagosome to transport the cargo to the vacuole.

Both types of autophagy can be selective or non-selective, for example, in selective autophagy, only specific organelles like the mitochondria, ER, peroxisomes, ribosomes and some components of the nucleus (this process is termed piecemeal autophagy of the nucleus) would be targeted and degraded in the vacuole.

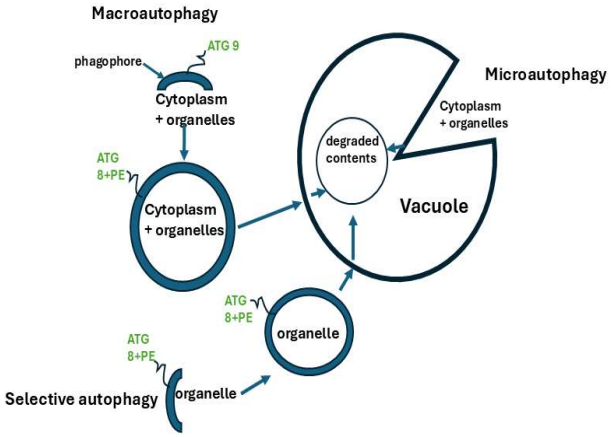


Figure 2.2 A schematic representation of the different types of autophagy. The ATG 9 and the ATG 8-PE complex are involved in the expansion of the autophagosome membrane and the transportation of the cargo to the vacuole.

Although autophagy is regarded as a survival process adopted by organisms to alleviate stressful conditions it can lead to cell death viz., type 2 autophagic cell death (see Chapter 1, section 1.2.5). This type of cell death is defined as a caspase-independent cell death. Cell death occurs when a certain threshold (of autophagic vacuoles occupying a greater volume of the cytosol than the functioning organelles) is exceeded (Li *et al.,* 2012).

2.1.6 Multivesicular bodies

Multivesicular bodies (MVBs; also referred to as endosomes or prevacuolar compartments) are single-membraned vesicles which traffic proteins and lipids packaged in intraluminal vesicles (ILVs; Viotti, 2014; Vitale and Denecke, 1999). The packaging of proteins into ILVs facilitated by ESCRT- machinery (Scheuring *et al.*, 2011), occurs at the *trans*-Golgi network (TNG). The protein cargo inside MVBs is then dispatched either to the plasma-membrane via the endocytic pathway or to the vacuoles for degradation (Le Borgne and Hoflack, 1998).

Studies in animal and plant cells demonstrate a relationship between MVBs and autophagy (Fader and Colombo, 2009). An association between MVBs and autophagy occurred in the unicellular green alga *Micrasterias denticulata* while undergoing autophagic PCD (Darehshouri *et al*., 2008).

2.1.7 Vacuolation

Extensive vacuolation is a structural marker that is common to the phenotypes of different types of cell death (both programmed and incidental); viz., autophagic death, paraptosis, necrosis, plant vacuolar cell death and hypersensitive response (this list is not exhaustive and the last two only occur in plants). The biogenesis of the vacuolation in the various phenotypes of cell death differs and will be discussed in this section.

In autophagic cell death, vacuolation results from extreme sequestering of cytoplasm and organelles by autophagosomes and the subsequent degradation of their contents in lytic vacuoles (Bassham and Crespo, 2014). It can also occur by the direct sequestering of the adjacent cytoplasm and organelles by the lytic

vacuoles (microautophagy) (Li *et al.*, 2012). The two pathways are not exclusive and can occur at the same time, working in synergy (Li *et al.*, 2012).

In paraptosis, vacuoles are derived from ER and mitochondrial dilations (Khalili and Radosevich, 2018; Sperandio *et al.,* 2000). In animal cells, vacuoles are derived only from the dilated ER but in plants vacuoles can be derived from the ER and mitochondria (Li *et al.*, 2017). Biogenesis of vacuoles from ER can occur in various ways (the pathways are not exclusive to paraptosis but refer to other processes in the cell where vacuoles are derived from ER). They can form when small vacuoles originating from dilated Golgi or ER cisternae coalesce to form a large vacuole, or the ER can sequester / enclose parts of the cytoplasm, these areas are digested to form a vacuole (Pacini *et al.*, 2011).

During necrosis, excessive vacuoles are formed through the rupture of cell membranes and acidification of the cytoplasm (this is caused by leaks in the lytic vacuoles),and leads to the dilation and rupture of other organelles (McCall, 2010).

2.1.8 Ultrastructural changes in phytoplankton during PCD

Ultrastructural changes that have been observed in microalgae when undergoing PCD are summarised in Table 2.2.

Table 2.2. A summary of ultrastructural observations following induced PCD in microalgae

Organism	**PCD inducer**	**Ultrastructural response**	**References**
***Amphidinium carterae* Dinoflagellate**	Light deprivation	-Vacuolization which increased with time (from day3-8) -Amorphous intracellular contents -Cell membranes remained intact	Franklin & Berges (2004)

Prorocentrum minimum **Dinoflagellate**	*Shewanella sp* (Algicide-IRI-160AA	Increased vacuolization; Electron dense aggregates in vacuoles -Increase in inter-thylakoid space in chloroplast -Mucilage vesicles degraded -Change in chromosome structure, fibrils protruding from chromosomes	Prokrzywinski (2014)
Karlodinium veneficum **Dinoflagellate**	*Shewanella sp* (Algicide-IRI-160AA)	-Amphiesmal and nuclear blebbing -Mitochondria increase in size -Migration of nucleus and chloroplasts to opposite ends of cell -Large cytoplasmic vacuole-Alteration in the compaction of chromosome structure	Prokrzywinski (2014)
Thalassiosina pseudonana **(Diatom)**	Iron starvation	Vacuolation. -amorphous organelles -Intact cell membranes	Bidle & Bender (2007)

2.1.9 Aim and objectives

The aim of this chapter was to determine whether *P. redfieldii* cells in a collapsing harmful bloom in St Helena Bay exhibited morphological markers of PCD that were not reflected in nutrient replete cultures. The findings would thus establish whether the collapse of the bloom was caused by PCD.

This aim was addressed by the following objectives:

1). To collect, establish and maintain a unialgal culture of *P. redfieldii:*

This was achieved by collection of samples of the study organisms from St Helena Bay at the onset and late into the harmful bloom event. A unialgal culture was established and maintained in the laboratory throughout the experimental period and the growth dynamics of nutrient replete cells of the study organism were established.

2). To characterise the ultrastructure of nutrient replete cells of *P. redfieldii:*

This was achieved by a detailed analysis of the ultrastructure of nutrient replete cells by transmission electron microscopy and the focus was on the ultrastructure of the nucleus, endomembrane system; mitochondria; chloroplasts; vacuolation and amphiesmal membranes. The observed ultrastructure of replete cells was used as a benchmark against which to compare ultrastructural alterations with those cells sampled from a collapsing bloom.

3). To characterise the ultrastructure of field samples collected at the early and late stages of the bloom and do a comparative analysis of their ultrastructure with that of samples grown in nutrient replete conditions to establish whether the cells from the collapsing bloom die by PCD.

This objective was achieved by a detailed analysis of the ultrastructure of the bloom samples by TEM and the focus was on the alterations to the ultrastructure of the nucleus, endomembrane system; mitochondria; chloroplasts; amphiesmal membranes and vacuolation to compare with nutrient replete cells.

2.2 METHODS

2.2.1 Growth dynamics of laboratory cultures

Prorocentrum redfieldii was isolated and a clonal culture successfully established from a sample taken from the HAB at station 21 of the map in Chapter 1 section 1.1.5. The nutrient composition of the bloom water was not analyzed in the current study, however, a previous study (Pitcher & Probyn, 2016) on a bloom in the same study region revealed that the nutrient composition of the bloom consists of nitrates (NO_3^-), Ammonium ions (NH_4^+), Nitrites ($N0_2^-$), phosphates (PO_4^3-) and Silicates (SiO_4^{2-}). The Daigo IMK growth medium (Nihon Pharmaceutical Co., Ltd.) that was used to grow nutrient replete cultures had a similar composition of macro-nutrients excluding the silicates. Isolation was accomplished by micro-pipetting individual cells from a natural sample and then culturing each cell in individual wells of a multi-well dish. This resulted in a clonal culture (number DID1, SANPCC) that was maintained in filtered, autoclaved sea water supplemented with Daigo IMK growth medium. Cultures were grown in 250 ml Erlenmeyer flasks in a growth chamber set at a temperature of 20 ºC and with a 16:8 h light-dark photoperiod at a white fluorescent light intensity of 13 µmol m^{-2} s^{-1}. To maintain a stock culture, sub-culturing into fresh medium was carried out every third week.

A growth curve was determined in batch cultures of *P. redfieldii* grown in IMK enriched seawater. Eight replicate flasks of inoculum made up of 30 x 10^4 cells ml^{-1} (from a dense, actively growing stock culture) and 130 ml IMK media were set up and the growth monitored until the stationary phase was reached. Daily monitoring was achieved by determining the cell density, using a haemocytometer, in samples harvested from each replicate. An aliquot of 500 µl of culture was collected in a 1.5 ml Eppendorf tube and the cells were immobilised by adding 5 µl of 2 % Lugol's iodine (I_3 K) solution (Lugol, 1829).

A 5 µl aliquot of this was mounted onto a haemocytometer and viewed using a 10x objective of a Zeiss trinocular standard light microscope (Zeiss, West Germany) at a total magnification of 100x. Six readings were taken from each replicate and

averaged. The cell concentration was calculated using the following formula:

$$\text{Total cells/ml} = \text{Total cells counted} \times \frac{\text{dilution factor}}{\text{\# of Squares}} \times 10{,}000 \text{ cells/ml}$$

# of squares = the number of haemocytometer squares used

Dilution factor= the dilution by the amount of Lugol's I_3 K stain used (=1.01).

2.2.2 Sampling of field organisms

Sampling from station 21 (Chapter 1, section 1.1.3, Fig. 1.2) was done on two occasions, three weeks apart, during a coastal downwelling period in the Benguela upwelling system. The later sampling event incurred heightened stress regarding available dissolved oxygen and nutrients (Ndhlovu *et al.,* 2017; Pitcher and Probyn, 2016a).

2.2.3 Transmission electron microscopy

2.2.3.1 Fixation and embedding

Non-axenic nutrient replete cultures in the exponential phase and samples of field bloom organisms were fixed in 5 % glutaraldehyde (GTA) in 0.1 M sodium cacodylate buffer, made up in 0.5 M Sucrose. This fixative was added 1:1 with the culture /samples in centrifuge tubes, mixed by inversion and allowed to fix for 1 hour at room temperature. After fixing, the cells were centrifuged at 1400 *g* (5 minutes), this was then increased to 4000 *g* (10 minutes) to form a pellet. The supernatant was gently removed by Pasteur pipette, and the pellet was washed four times in 0.1 M Na cacodylate buffer with a decreasing molarity of sucrose (from 0.5, 0.4, 0.2, 0.1 to 0 M sucrose). In the last wash the pellets from the centrifuge tubes were all combined and centrifuged again. The cells were then post-fixed in 2 % osmium tetroxide (1 hour), washed twice in 0.1 M Na cacodylate buffer and dehydrated through an increasing series of ethanol concentrations (10, 30, 50, 75 and 90 %; 20 minutes in each concentration) and then twice in 100 % ethanol (30 minutes) each. This was followed by a gradual infiltration by Spurr's resin (Spurr,

1969) starting with a 3:1 ratio of ethanol: resin, followed by a 1:1 ration ethanol: resin, each for 1 hour) each, then left overnight in a 1:3 ratio and finally in 100 % resin (1 hour). The pellet was broken up into smaller pieces and deposited in fresh resin in a small tin foil dish. Once the fragments sank to the bottom of the dish, the resin was cured in an oven at 60 ºC for 16 hours.

2.2.3.2 Microtomy and Viewing

Resin blocks of the nutrient replete cells and field samples were cut into ultrathin sections averaging 60 nm using an RMC Boeckler Cryo-microtome (RMC Boeckler CR-X, PT-PC, PowerTome; Arizona, USA). Sections were collected on 100 mesh copper grids and stained with 2 % uranyl acetate and Reynold's (1963) lead citrate for a period of five minutes with each stain to enhance contrast. The stained sections were viewed on the FEI Tecnai T12 120 KV transmission electron microscope (FEI Tecnai T12 Spirit 120 KV; Oregon, USA). The viewing was done at 80 KV. The ultrastructure from encountered cells in linear, non-overlapping transects was captured and analysed until a total of 50 cells were viewed. Viewing focus was on alterations to organelles as mentioned in section 2.1.9, changes in the integrity of the amphiesmal membranes, vacuolation, subcellular structures and vesicles not observed in replete cells. Changes in abundance and size of organelles relative to those of replete cells was noted.

2.2.4 Statistical analysis

All reported measurements are presented as means ± standard error (SE), sample size was (n = 50). Statistical differences between variously sampled cells were identified using a one-way ANOVA ($P \leq 0.05$), with a Tukey's *post-hoc* test to determine which groups were involved. Both were accomplished using Origin Pro 8.0 software (Origin lab, Northampton, Massachusetts, USA).

2.3 RESULTS

2.3.1 Growth dynamics of laboratory cultures

Nutrient replete cells revealed a short lag phase that did not last longer than two days. After day two the growth curve revealed a linear growth trend, i.e., the cells did not exhibit a sharp increase in cell abundance. Cells entered a short stationary phase around the 10th day. The stationary phase is characterized by limited nutrients and no further increment in cell abundance. A steady decline in cell abundance was observed on day 14. Nutrient replete cells that were used for this study were sampled towards the end of the linear phase (around day six).

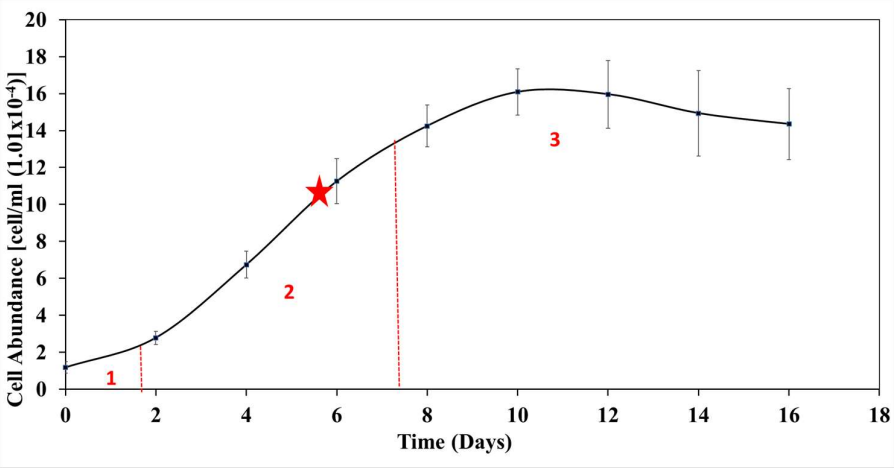


Figure 2.3 Stages of the growth curve of *P. redfieldii* over a 16 - day period.

The numbers 1, 2 & 3 indicate the Lag phase, linear phase & stationary phase, respectively. The icon (★) denotes the sampling time for all laboratory experiments.

2.3.2 Ultrastructure of nutrient replete cells

Transmission electron microscopy of *P. redfieldii* cultures revealed features of an armoured dinoflagellate. The cells have a slightly oval anterior with an apical spine and a pointed posterior (e.g., Figs 2.4 A, C & D). The cells are covered by a three-membraned amphiesma which consists of the outermost membrane (i.e., the plasma membrane), the two alveolar membranes (outer and inner alveoli membranes). The plasma membrane and the outer alveoli membrane were not evidenced in cells where the cell covering was being shed (e.g., Figs 2.4 A &B). In some of the cells juvenile alveoli vesicles were observed beneath the mature alveoli vesicles. The main vacuolar network with crystalline inclusions underlies the chloroplasts (e.g., Fig. 2.4 B). The alveolar membranes are continuous around the thecal plates (e.g., Fig. 2.4 B) and this conforms to the illustration by Morrill and Loeblich (1984; Fig. 2.1). The two lateral thecal plates cover most of the cell except for the anterior periflagellar area and are joined together by sutures (e.g., Fig. 2.4 B). The pellicle and microtubule layers are absent (e.g., Fig. 2.4 B). The periflagellar area is made up of 8 platelets and this conforms to the illustration by Ndhlovu *et al* (2017), four of which are visible in Figure 2.4 C (numbering after Hoppenrath *et al.* 2013).

Inside the cell, the dinokaryon is located at the posterior end of the cell (e.g., Fig. 2.5 A). The nucleus has permanently condensed chromosomes enclosed by a double membraned nuclear envelope with nuclear pores (e.g., Figs 2.5 A & B). The anterior end of the cell is occupied by a sac-like pusule with vesicles (e.g., Fig. 2.5 D). The pusule which comprises of vesicles is vacuolated and bound by a double membrane. Organelles that make up the endomembrane system like Golgi bodies, smooth endoplasmic reticulum (ER) and endomembrane vesicles are also present on the cytoplasm (e.g., Fig. 2.5 C). Golgi cisternae are stacked in four or five systems forming Golgi bodies, which are grouped together to form the centrally located Golgi complex. The ER is represented by a network of membranous tubules and sheets (e.g., Fig. 2.5 C) and is sometimes associated with ribosomes to form the rough ER (e.g., Fig. 2.5 C). The ER lumen is granular and resembles the cytoplasm. Trichocysts (e.g., Fig. 2.5 C) and ribosomes (Fig. 2.5 C) were seen throughout the cytoplasm. An accumulation body containing electron dense material is present in

the cytoplasm (e.g., Fig. 2.5 A).

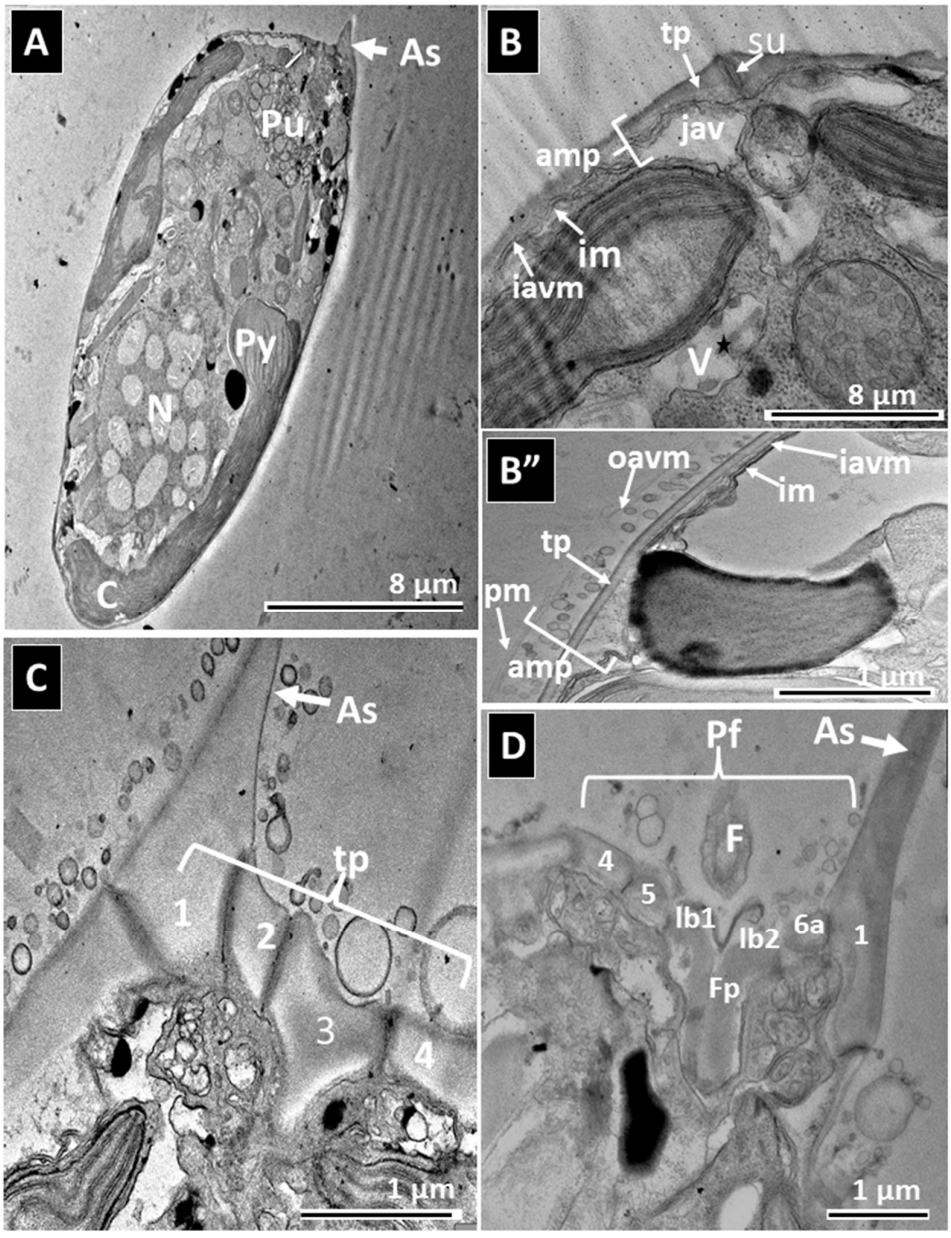


Figure 2.4 Ultrastructure of nutrient replete cultured cells of *P. redfieldii*.

(A) Longitudinal section of a cell of *P. redfieldii*; showing the apical spine, location of the pusule, nucleus, chloroplasts and pyrenoids

(B) Transverse section showing the amphiesma and a suture between the two thecal plates, the inner alveoli membrane and the inner membrane are visible, but

the outer alveoli membrane and the plasma membrane are absent. Juvenile alveoli vesicles are present beneath the amphiesma, note the vacuolar network with crystalline inclusions inside the (black asterisk).

(B") Section of a complete amphiesma revealing the plasma and outer alveoli vesicles.

(C) Section through the periflagellar region showing arrangement of 4 thecal platelets (from left to right; platelets 1, 2, 3 and 4; numbering after Hoppenrath *et al* 2013).

(D) A different view of the periflagellar region showing the apical spine, longitudinal flagellum, flagellar pore and a few thecal platelets (from left to right; plate 4, 5, the two labial plates, plate 6a and plate 1) *Abbrev: av = alveolar vesicles, amp = amphiesma, As= apical spine; C = chloroplast; F = flagella; Fp= flagella pore; L = lipid; lb=labial plate; N=nucleus; ; oavm = outer alveolar vesicle membrane; im = inner membrane; iavm = inner alveolar vesicle membrane; jav= juvenile alveoli vesicles, Pf = periflagellar region; pm = plasma membrane Pu = pusule; Py1 = lobed pyrenoid; th = thylakoids; tp = thecal plates; Su = suture; V = vacuole.*

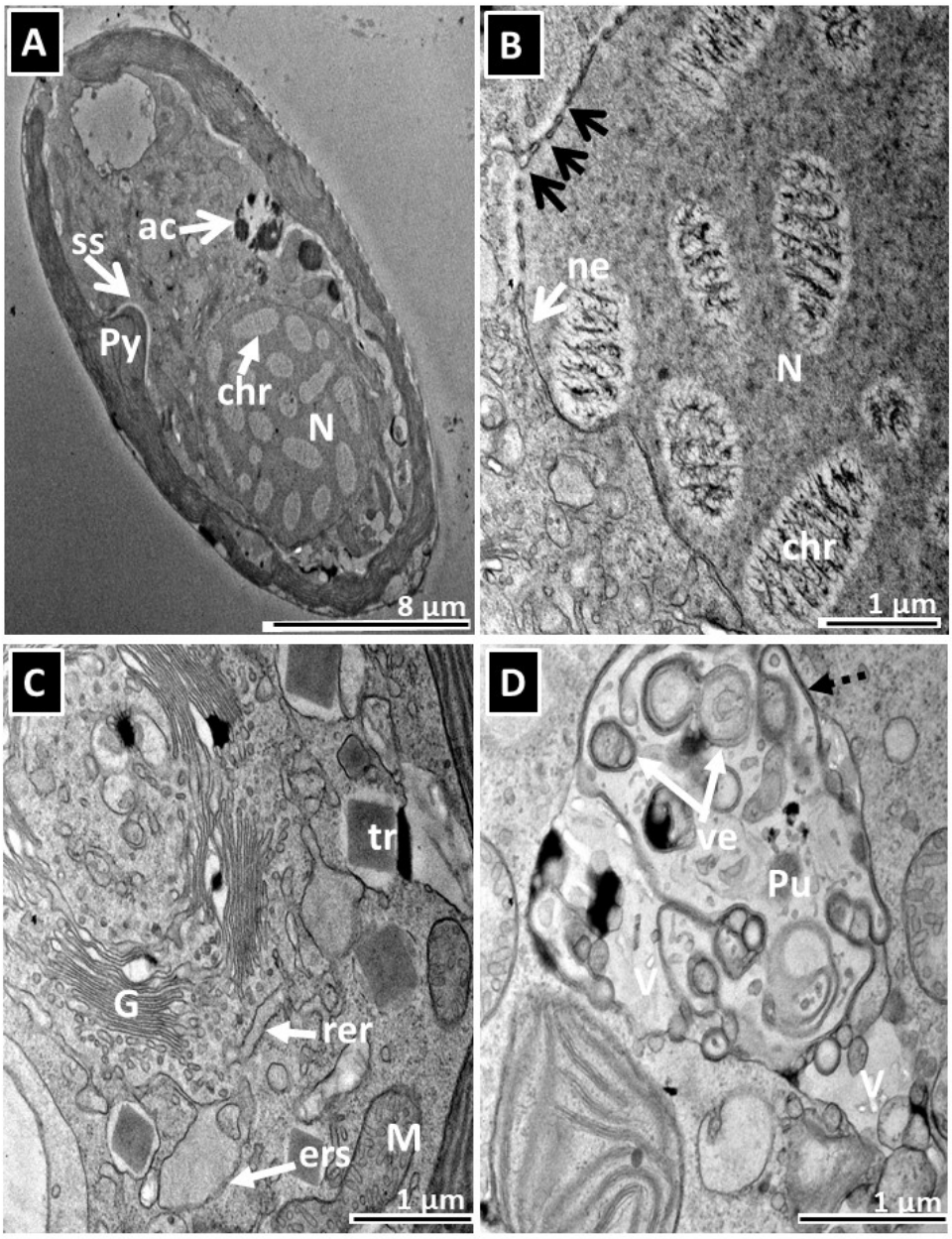


Figure 2.5 Ultrastructure of the nucleus, endomembrane system and pusule in nutrient replete cells.

(A) Detail of posterior end of cell showing the dinokaryon nucleus with condensed chromosomes, two pyrenoids and an accumulation body.

(B) A higher magnification of the nucleus showing the nuclear envelope (white arrow) with nuclear pores (black arrow) and condensed chromosomes.

(C) The endomembrane system showing the Golgi complex comprising up to four dictyosomes arranged in a sphere, with their trans cisternae facing the interior, ER and vesicles. Also included are cross-sectional profiles of trichocysts, mitochondria.

(D) The pusule with vesicles is bound by a double membrane (broken black arrow). *Abbrev.: ac = accumulation body; chr = chromosomes; er = endoplasmic reticulum; ers=endoplasmic reticulum sheet G = Golgi complex; M = mitochondrion N = nucleus; ne = nuclear envelope; Pu = pusule; Py = pyrenoid; rer = rough endoplasmic reticulum; ss= starch sheath; tr = trichocyst; v = vacuole; ve= vesicle.*

Mitochondria with varying shapes are found throughout the cytoplasm. They are bound by a double membrane. Anastomosing tubular cristae which are of uniform size fill up most of the mitochondrial matrix, which is granular and has the same electron density as the cytoplasm. Mitochondrial DNA was not evidenced in those areas that lacked cristae. (e.g., Figs 2.6 A & B). The peridinin chloroplasts are bounded by a three-membrane envelope which has no connections to ER and are often associated with pyrenoids (e.g., Figs 2.6 C & D). They are found on the periphery of the cell underlying the amphiesma in the longitudinal axis of the cell (e.g., Fig. 2.5 A). The thylakoid membranes of uniform width are appressed and arranged in stacks of three to form the lamellae. The lamellae run parallel to the longitudinal axis of the chloroplast with uniform spacing between them with no connections between them. Those areas devoid of the lamellae (i.e., the stroma) have a granular appearance. (e.g., Figs 2.6 C- E). A bulging pyrenoid bound by the chloroplast envelope is capped by a starch sheath and is traversed in a random manner by lamellae made up of two and sometimes three thylakoid membranes (e.g., Figs 2.6 F). As expected, plastoglobuli (lipid droplets) are found inside the chloroplasts. Photosynthetic reserves like starch and lipid are extraplastidial. When starch grains and lipid droplets were evidenced, they were small, and sparsely distributed in the cytoplasm.

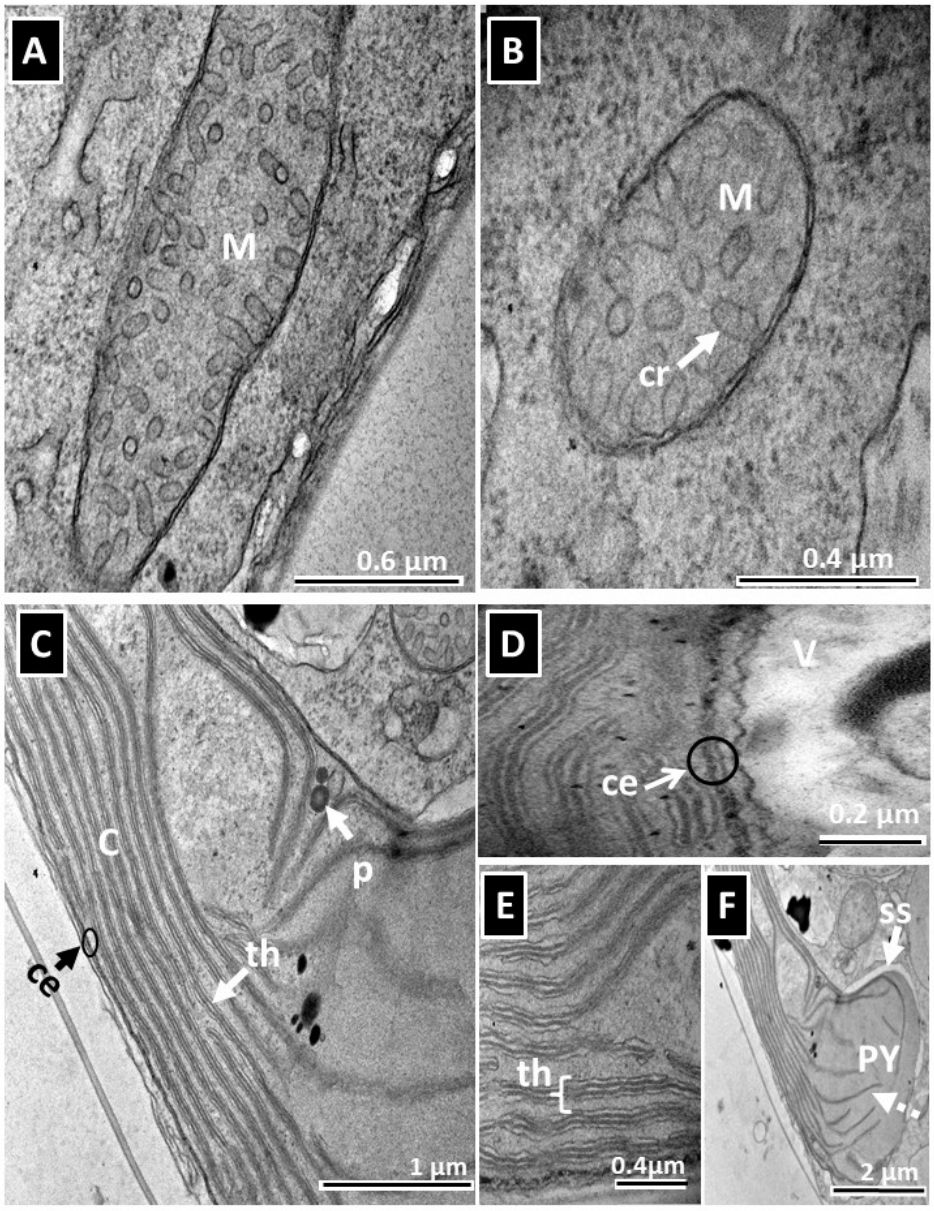


Figure 2.6 Ultrastructure of mitochondria and chloroplast in nutrient replete cultures

(A&B) Longitudinal and transverse profiles of mitochondria, showing mitochondrial outer and inner membranes and tubular anastomosing cristae.

(C) Section through a chloroplast showing a chloroplast envelope, an immersed pyrenoid, thylakoid membranes and plastoglobuli.

(D & E) High magnifications of the chloroplast showing the chloroplast envelope consisting of three parallel membranes (the two inner membranes were often observed lying close together appearing as a double membrane, while the outer membrane could be easily detected) and grouped thylakoids, respectively.

(F) A pyrenoid randomly traversed by thylakoids in stacks of two (broken arrow). *Abbrev.: C=chloroplast; ce = chloroplast envelope; cr = cristae; M=mitochondria; p = plastoglobulus; th = thylakoids.*

2.3.3 Ultrastructure of field-sampled organisms

2.3.3.1 Vacuolation of cells and accumulation of reserves

In the early stage of the bloom in 90 % of cells (n = 50) there was no excessive vacuolation and these cells had a greater accumulation of starch and lipid reserves when compared with those cells grown in replete conditions (e.g., Figs 2.7 A & B & *cf* Fig. 2.4 A). In most cells the inner amphiesmal membranes were beneath the thecal plates as observed in the replete cells. The chloroplasts in these cells were peripheral underlying the amphiesma, retaining the position that was observed in the replete cells (e.g., Fig. 2.7 B *cf* Fig., 2.5 A).

In the late stage of the bloom, 73 % of cells (n = 50) showed expansion of the vacuolar spaces further into the cytoplasm reducing the total space occupied by the cytoplasm and this resulted in the displacement of some organelles like the peripheral chloroplasts (e.g., Figs 2.7 C & E).

About 55 % of the cells were excessively vacuolated and had lost most of their cytoplasmic contents, but the amphiesmal membranes were preserved and still retained the position beneath the thecal plates (e.g., Fig. 2.7 E). In 45 % of cells the amphiesmal membranes were retracted from the thecal plates (e.g., Fig. 2.7 F & G).

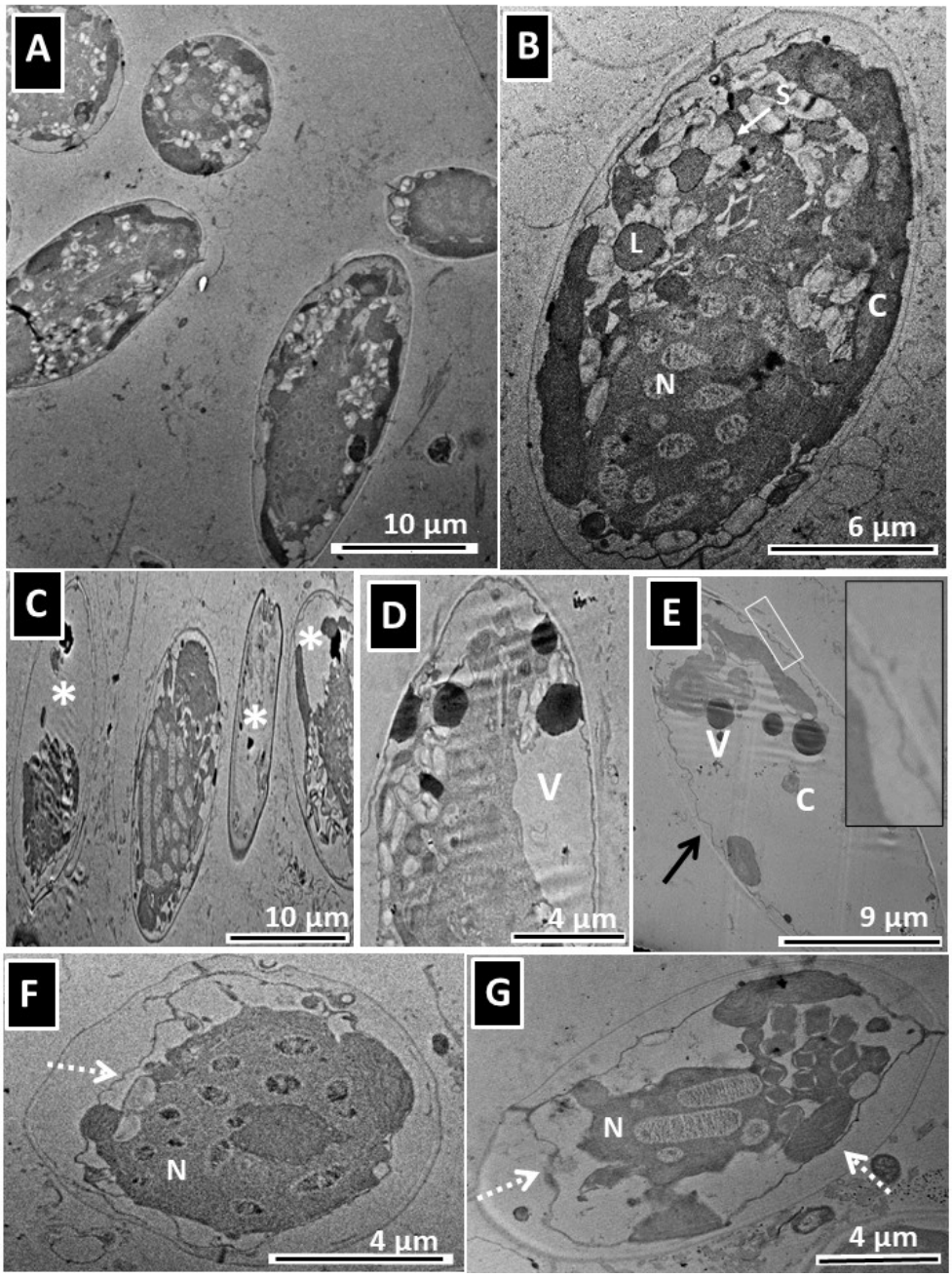


Figure 2.7 Overview of cells in early and late bloom stages.

(A) An overview of cells sampled during the early stage of the bloom, note the accumulation of reserves.

(B) A representative cell collected in the early stage of the bloom with no excessive vacuolation.

(C) An overview of cells sampled during the late stage of the bloom, note the vacuolation of the cells (asterisks).

(D & E) Different levels of vacuolation in late bloom cells, note that the inner amphiesmal membranes are not retracted from the thecal plates (black arrows). Insert is an enlarged area showing that amphiesmal membranes are preserved.

(F & G) A cell with retracted inner amphiesmal membranes from the thecal plates during the late stage of the bloom.

Abbrev. C= chloroplast; L= lipid bodies; N=nucleus; S=starch; V = vacuole.

2.3.3.2 The nucleus

In about 92 % of cells sampled during the early stage of the bloom when the nucleus was evidenced (n=50), the nucleus and its envelope were structurally intact (e.g., Fig. 2.8 A). However, it was observed in the remainder of cells there were protrusions on the nuclear envelope that formed contact sites with adjacent lytic vacuoles (e.g., Fig. 2.8 B).

In cells sampled during the late stage of the bloom; the nucleus structure was preserved in 76 % of cells and in some nuclei the contact sites between the nuclear envelope and lytic vacuoles were present (e.g., Fig. 2.8 C). In the remainder of cells that were excessively vacuolated and compromised the chromosomes were more electron dense than those of other nuclei that were less vacuolated cells (e.g., Fig. 2.8 D *cf* Fig. 2.8 D).

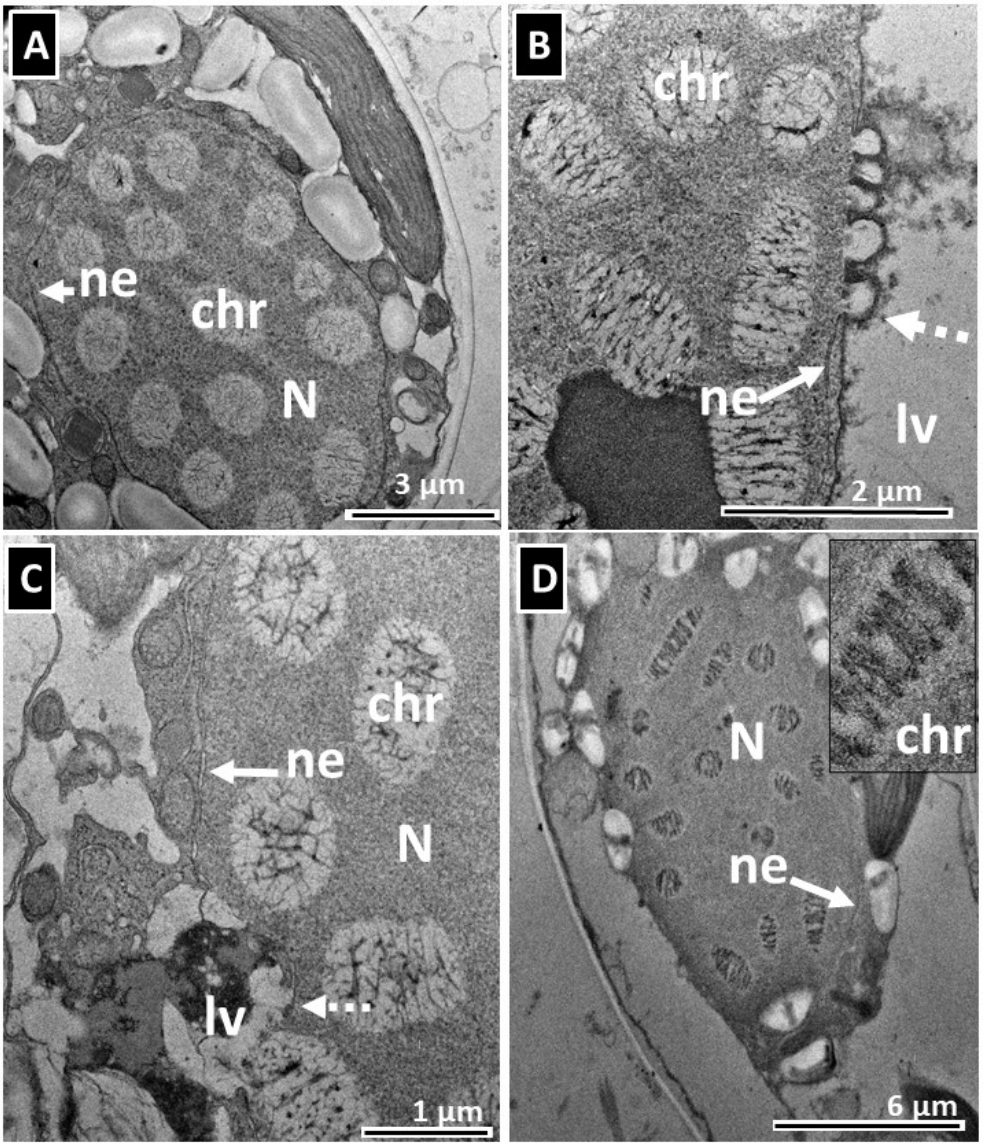


Figure 2.8 Ultrastructure of nuclei from cells sampled during the early and the late stages of the bloom.

(A) A nucleus showing an intact nuclear membrane in the early stage of the bloom.

(B) A nucleus with nuclear envelope protrusions forming contact sites with adjacent vacuoles in the early stage of the bloom (broken white arrow).

(C) A nucleus showing nuclear envelope and lytic vacuole contact sites in the late stage of the bloom.

(D) A compromised cell showing electron dense chromosomes in the late stage of the bloom. *Abbrev: chr = chromosome; N = nucleus; ne = nuclear*

envelope; lv=lytic vacuole

2.3.3.4 The endomembrane system

Dilation of ER cisternae was prevalent in cells sampled in the early and late stages of the bloom compared with those grown in replete nutrient conditions (e.g., Figs 2.9 A-F *cf* Fig. 2.5 C). The dilated ER cisternae had the same electron translucent appearance as vacuoles when viewed using the electron microscope (e.g., Fig. 2.9 A). Occasionally, the electron transparent ER cisternae were observed sequestering parts of the cytoplasm / organelles like the mitochondria in a way that resembled phagophores during autophagy (e.g., Figs 2.9 A, B, D & F). In cells collected during both stages of the bloom, there was an increase in the number and size of single-membraned endosomal vesicles that resemble multivesicular bodies (MVBs) (e.g., Figs 2.9 B, C, E & G). The MVBs contained smaller vesicles that resemble intraluminal vesicles (ILVs) (e.g., Figs. 2. 9 C, E, & G). In cells from both sampling times there were also large single membraned vesicles which contained ILVs and partially degraded organelles including membranous material which will be referred to as lytic vacuoles (e.g., Figs 2.9 B, C, E & G). Hemi-fusion between the limiting membranes of MVBs and lytic vacuoles was observed and this was evidence for the process of coalescence to form bigger structures (e.g., Figs C, E & G). At times contact between the lytic vacuoles and the dilated ER were observed (e.g., Figs 2.9 C).

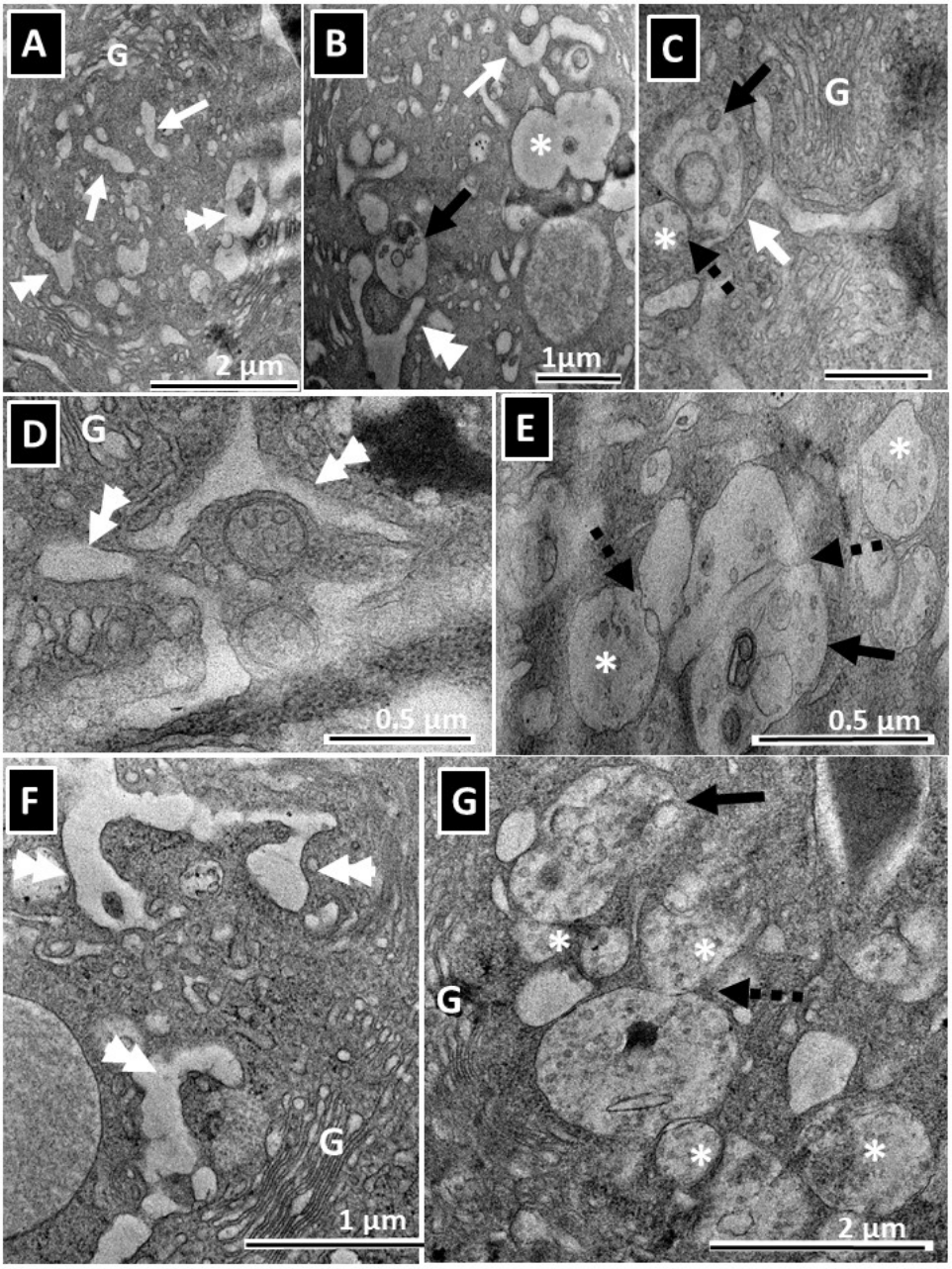


Figure 2.9 The endomembrane system in cells sampled during the early and late stages of the bloom.

(A, B & D) Dilated translucent ER cisternae in cells sampled during the early stage of bloom (white arrows). Note dilated ER sequestering parts of the cytoplasm (double arrow heads).

(C) Contact sites between a MVB (white asterisk), a lytic vacuole (black arrow) and dilated ER (white arrow), during the early stage of bloom.

(E) Coalescence between MVBs (white asterisks) and lytic vacuoles (black arrows). Note hemi-fusion of membranes (broken black arrows).

(F) Dilated translucent ER cisternae (white arrows) sequestering the cytoplasm / organelles (double arrow heads) during the late stage of bloom.

(G) Coalescence between MVBs (white asterisks) and lytic vacuoles (black arrows) during the late stage of bloom. *Abbrev. G=Golgi bodies; V=vacuole.*

2.3.3.6 Macro- and Micro-autophagy

Double-membraned structures were observed in the cytoplasm and surrounding mitochondrial profiles in cells sampled at both stages of the bloom (Figs 2.10 A-C). The double-membraned structures were derived from ER but those that were formed from the dilated electron-translucent ER cisternae were the prevalent type at both sampling times (Fig. 2.10 B). Often, organelles and parts of the cytoplasm were internalized by the vacuoles (Figs. 2.10 D-F). The vacuolar membrane was often observed wrapping around organelles (Fig. 2.10 F). The excessive consumption of the cytoplasm by vacuoles resembled micro-autophagy.

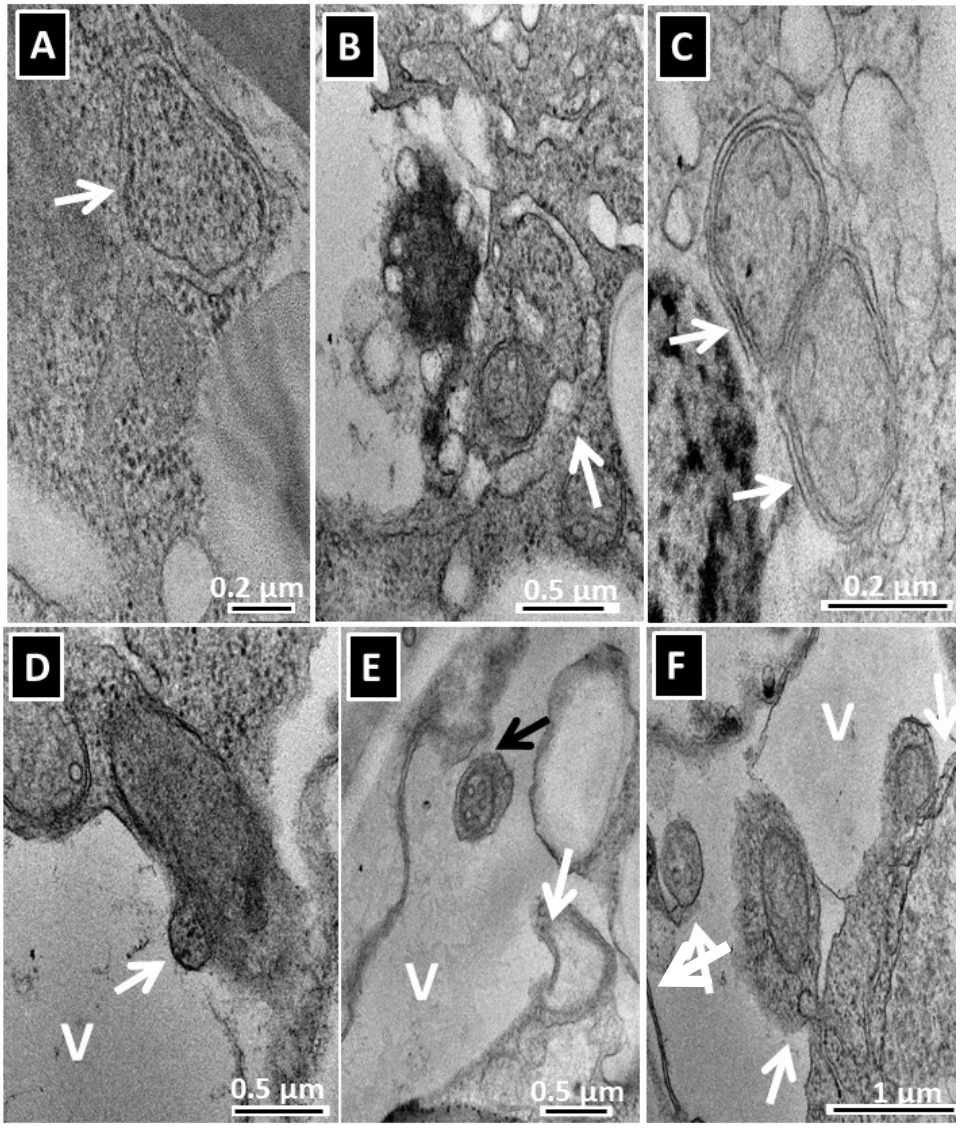


Figure. 2.10 Macro-and micro-autophagy in cells sampled at both times of the bloom

(A-C) Double membrane structures on the cytoplasm and around mitochondria.

(D-F) Micro-autophagy, the vacuolar membrane engulfs parts of the cytoplasm and organelles at the vacuole interface (white arrows).

2.3.3.5 Mitochondria

The outer and inner membranes remained intact in 35 % of sectioned mitochondrial profiles from subset of cells (n = 20) sampled from the early stages of the bloom

(e.g., Figs 2.11 A). In the remainder of mitochondria profiles there was damage to the mitochondrial membranes. The damage was localized in parts of the outer membrane resulting in the herniation of the inner membrane (e.g., Figs 2.11 B -D). In some mitochondrial profiles there was a complete loss of the outer membrane (e.g., Fig. 2.11 D). Similar alterations were observed in 72 % of mitochondria in the late stages of the bloom.

Partially degraded mitochondrial profiles in field bloom cells were occasionally observed inside lytic vacuoles at both sampling times (e.g., Fig. 2. 11 E).

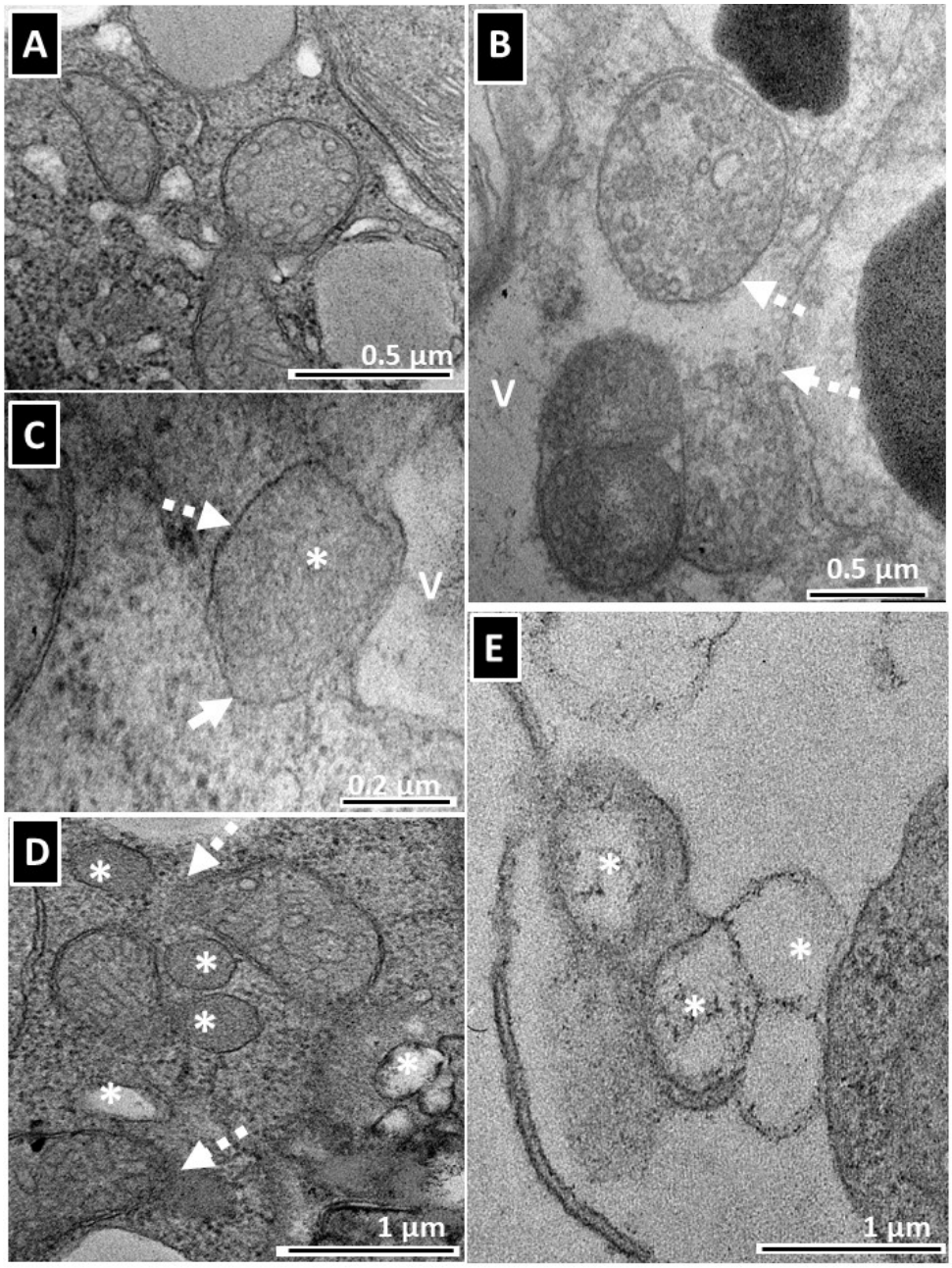


Figure 2.11 Different mitochondria profiles of cells sampled during the early and late stages of the bloom.

(A) Healthy mitochondria showing cristae and inner and outer membrane

(B-D) Herniated mitochondria profiles with partially damaged cristae (white broken arrows)

(D) Mitochondria profiles with a single membrane (asterisks).

(E) Degenerated mitochondria inside a vacuole. *Abbrev. V= vacuole.*

2.3.3.2 Chloroplasts

Chloroplasts were functionally intact in 86 % and 60 % of cells in the early and late stage of the bloom, respectively. The chloroplasts resembled those of cells growing in nutrient replete conditions, with a three membraned envelope, thylakoid membranes arranged in stacks of three running parallel to each other, and plastoglobuli but they lacked pyrenoids. In the remainder of cells sampled at both stages of the bloom there was localized swelling of thylakoid lumina and the parallel array of the lamellae was disrupted and greater inter and intrathylakoidal spacing became apparent in the affected areas of the chloroplasts (Figs 2.12 A-D). In these affected areas thylakoid membrane fragmentation occurred (Figs 2.12 A-D).

At both times the chloroplast envelope was broken in some areas (Figs 2.12 B-D) The damage to the chloroplasts was progressive and in those cells that were highly compromised in the later stage of the bloom, there was extensive disintegration of the thylakoid membranes (Fig. 2.12 E). Chloroplasts which had decreased in size were occasionally observed at the interface of, or inside, vacuoles in the late stage of the bloom (Fig. 2.12 F). Membranous coils or whorls representing thylakoid membranes were observed inside vacuoles that were in proximity with chloroplasts (Fig. 2.12 G).

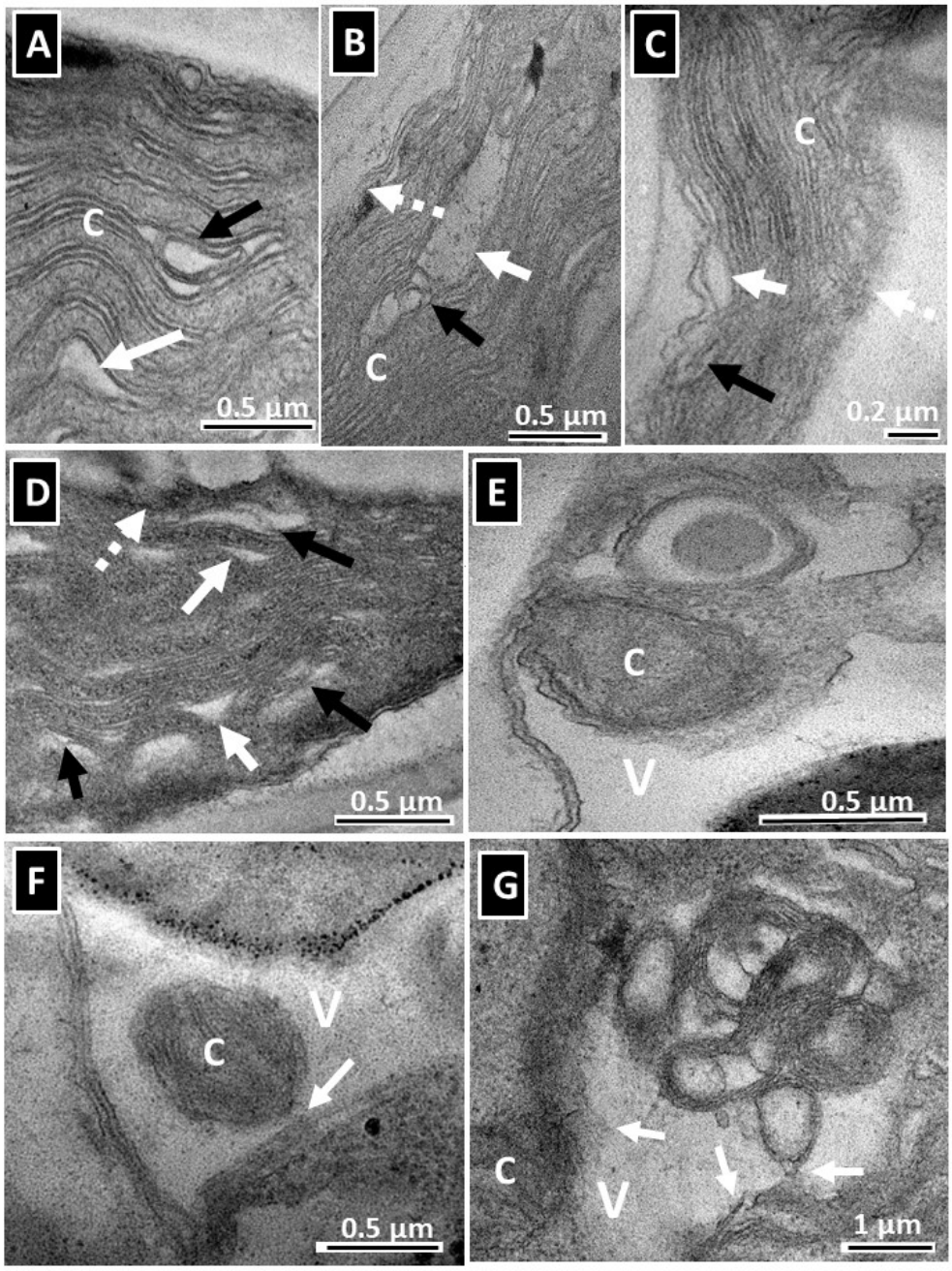


Figure 2.12 Damage to the chloroplast structure in cells during the early and late stages of downwelling

(A -C) Thylakoid lumen swelling (white arrows), membrane fragmentation (black arrows) and damaged chloroplast envelope (broken white arrows) during early bloom stages.

(D) Thylakoid lumen swelling (white arrows), membrane fragmentation (black arrows) and damaged chloroplast envelope (broken white arrows) during late bloom stages.

(E) A chloroplast which is reduced in size at the interface of a vacuole during the early stages of the bloom.

(F) A chloroplast which is reduced in size inside a vacuole during the early stages of the bloom.

(G) Membranous whorls (white arrow) represent thylakoids inside a vacuole during late stages of the bloom. *Abbrev: C = chloroplast, V= vacuole.*

2.4 DISCUSSION

The study established that the ultrastructure of *P. redfieldii* cells grown in nutrient replete conditions conformed to existing dinoflagellate ultrastructure descriptions recorded in the literature (e.g. Dodge and Bibby, 1973). The nutrient replete cultures were thus used as a benchmark against which to compare ultrastructural alterations with those cells sampled from a collapsing bloom in the field. Ultrastructural changes in cells collected from the bloom revealed the occurrence of catabolic processes that led to excessive vacuolization of the cells. Alterations in the structure of nuclei, endomembrane, mitochondria, chloroplasts and cell membranes showed evidence that the cells collected in the early stages of the bloom were dying in a programmed manner. In those cells collected in the later stages of the bloom there was, however, structural evidence for programmed and unprogrammed cell death.

Alterations to the ultrastructure

An increase in reserves in the form of starch and lipid droplets observed in the field cells sampled during the early and late stages of the bloom is a general occurrence in phytoplankton undergoing stress (Jiang *et al*., 2014; Zhu *et al*., 2014; 2018; Sathe *et al*., 2019; Ji *et al.*, 2021). The accumulation of reserves in *P. redfieldii* is not a marker of cell death but shows that the cells were already exposed to an environmental stress even in the early stages of the bloom. This is expected because dinoflagellate blooms are formed when upwelling winds relax or during the persistent downwelling periods when nutrients are no longer replenished (T. J. Smayda and Trainer, 2010).

Vacuolation and autophagy

Moderate to excessive vacuolation of cells was an apparent PCD structural marker in both stages of the bloom. Vacuolation is a widely reported during PCD, however the vacuoles are often derived from different cellular processes (Franklin and Berges, 2004; Pokrzywinski, 2014; Zhang *et al.*, 2017). In *P. redfieldii* the ultrastructural morphology of the bloom cells showed that the excessive vacuolation was an outcome of upregulated catabolic processes, namely the

upregulation of autophagy and endosomal vesicles. This was demonstrated as macro-and microautophagy in *P. redfieldii* bloom cells. The initiation of autophagy in response to stress also occurs in other dinoflagellates (Dunn *et al.,* 2007; Ji *et al.,* 2021; Li *et al*., 2024).

Although autophagy by default is a survival response employed by organisms to counteract a short-term limitation of essential nutrients for the organism's metabolic processes it can be extreme when the stressful conditions are prolonged and can result in cell death (Kourtis and Tavernarakis, 2009). This view is supported by the excessively vacuolated cells that were devoid of most of their organelles during the late stage of the bloom. The cells at the late stage of the bloom could be divided into different profiles those that were excessively vacuolated with intact amphiesmal membranes and those that were excessively vacuolated with retracted and damaged membranes. Intact amphiesmal membrane are indicative of a programmed cell death while those that were damaged and retracted point to an unprogrammed cell death.

The nucleus

In this study the nuclear structure was preserved in most cells during the early and late stages of the bloom. The electron dense chromosomes observed in some excessively vacuolated cells of *P. redfieldii* in the later stages of the bloom were indicative of a degenerating nucleus. Chromatin clumping (pyknosis) and the migration of the clumps to the nuclear envelope is a general occurrence in eukaryotes during early stages of PCD, executed by endonucleases which cleave the phosphodiester bonds of DNA (Kroemer *et al.,* 2009). The type of chromatin clumping observed in other eukaryotes is not expected in dinoflagellates because of their unique nucleus which has permanently condensed liquid crystalline chromosomes, but changes in the appearance of the chromosomes has been reported in in other dinoflagellates during PCD (Ji *et al.*, 2021; Pokrzywinski *et al.,* 2017a).

An uncommon phenomenon which is similar to piecemeal microautophagy of the nucleus (PMN) occurred in a minority of cells and manifested as nuclear projections that were in contact with adjacent lytic vacuoles at both field sampling times during

the downwelling event. This occurrence was different from what was observed in *Prorocentrum minimum* where it was observed that whole or parts of chromosomes were ejected (i.e., by an expulsion force similar to viral DNA) through breaks in the nuclear envelope into adjacent vacuoles in algicide treated cells (Pokrzywinski *et al.,* 2017a). In *P. redfieldii* the pseudopodia-like structures that were extended into the adjacent vacuoles which were sometimes void of chromosomes substantiate the fact that the two mechanisms were not similar. The phenomenon is similar to what occurred in nutrient starved cells of *Saccharomyces cerevisiae* where its function was to recycle non-essential or damaged components in the nucleus (Kiel, 2010b; Kvam and Goldfarb, 2007). It can thus be reasonably assumed that PMN served a similar function in *P. redfieldii* bloom cells. This further demonstrates the involvement of the autophagic processes in these cells.

The endomembrane system

In *P. redfieldii* dilated ER cisternae were observed in cells sampled at both times of the bloom and some of the cisternae were sequestering parts of the cytoplasm / organelles in a way that resembled phagophores during autophagy. It is not clear if the cisternae became dilated because of a change in their functionality since they were co-opted in the process of autophagy. The ER derived double membranes contain hydrolytic enzymes in their lumen which allows for onsite degradation of the sequestered cytoplasm / organelles (van Doorn and Papini, 2013). The dilation of ER and subsequent involvement of autophagy also occurred in *Micrasterias* during autophagic cell death (Affenzeller e*t al.,* 2009). The progressive upregulation of endomembrane derived vesicles which contained degraded membranous materials and damaged mitochondria in *P. redfieldii* was also reported in *Micrasterias* when PCD in this organism was induced by hydrogen peroxide (Darehshouri *et al*., 2008).

The Mitochondria

In the early and late stages of the bloom mitochondria were greatly affected. This is supported by the substantial number of herniated mitochondria and those that were being degraded by autophagy. These mitochondria could have been

experiencing increased levels of ROS that could no longer be counteracted by antioxidants. ROS is a signaling molecule (Ray *et al.*, 2012) and therefore with increased levels of ROS the signal gets amplified and can quickly affect neighboring mitochondria. The mitochondrial herniation observed in *P. redfieldii* is associated with the permeabilization of the inner membrane which opens the mitochondrial permeability transition (MPT) pore (Roy and Hajnóczky, 2008).

High levels of ROS trigger the opening of the MPT pore (Rodriguez-Enriquez *et al.,* 2004) which results in an unregulated influx of ions into the mitochondrial matrix. Subsequently, more water enters from the cytosol resulting in the swelling of the mitochondria and rupture of the outer membrane.

Reports on mitochondrial herniation in phytoplankton were not found during this study. Most reports on mitochondrial alterations during PCD focus on the physiological aspects like the mitochondrial potential (Barreto Filho *et al.*, 2023). It is therefore not known if the herniated mitochondria observed in *P. redfieldii* are species specific or if they occur in other phytoplankton.

In animal cells when the MPT pore opens cells can die either by PCD (Sesso *et al.,* 2012) or die by necrosis (Kinnally *et al.*, 2011), it is the levels of available ATP inside the cells which determine the cell death route.

The chloroplasts

In the current study chloroplast alterations were observed in cells sampled during the early and late stages of the bloom. The chloroplasts in bloom cells could also have been affected by increased levels of ROS because they are also a source of ROS like the mitochondria. The fact that chloroplast structure was more damaged in cells at the later stages of the bloom than those in cells at the early stages, points to a progressive increase in the levels of oxidative stress in the later stage of the bloom. Many studies have reported on the dismantling of the thylakoids in cells that are undergoing PCD (Bidle and Bender, 2008; Ji *et al.*, 2021; Pokrzywinski *et al*., 2017a; Zhang *et al.*, 2017), it is a common PCD marker in chloroplast containing organisms.

Secondly, the membranous coils and chloroplasts that were reduced in size observed in vacuoles at the interface of chloroplasts at both stages of the bloom indicate that the chloroplasts were being recycled and remobilized as intracellular resources. As no double membrane structures were observed, this process must have involved microautophagy as reported in other algae (Gorelova *et al.*, 2019; Solovchenko *et al.*, 2019).

Programmed cell death

Excessive vacuolation by autophagy was prevalent especially in the late stages of the bloom. The PCD phenotype that is associated with excessive vacuolation by autophagy is autophagic cell death (Kroemer *et al*., 2009). Other markers associated with autophagic cell death that were present in *P. redfieldii* bloom cells are the presence of double membraned structures and lytic vacuoles.

Endomembrane organelles in *P. redfieldii* like the ER and MVBs were co-opted into the autophagy process. There is no account in the searched literature which shows a coordination between MVBs and autophagy in dinoflagellates but it occurs in yeasts, plants (including green algae) and animals (Cui *et al., 2018;* Darehshouri *et al.,* 2008; Ebrahimi *et al.*, 2021; Fader and Colombo, 2009; Spitzer *et al*., 2015; Zhuang *et al.*, 2015). The upregulation of MVBs that was observed in *P. redfieldii* bloom cells was regarded to be a marker of PCD in *Micrasterias* (Darehshouri *et al.,* 2008).

The piecemeal microautophagy observed in nuclei of *P. redfieldii* cells in the early stages of the bloom was only in a small number of cells and therefore it cannot be regarded as a marker of PCD in these cells. However, the alterations to chromosomes observed as chromatin clumps in nuclei during the late stages of the bloom conform to what has been reported in chromosomes of other dinoflagellates during PCD (Ji *et al.*, 2021; Pokrzywinski *et al.*, 2017a) and can be regarded to be a marker of PCD. The herniation of mitochondria observed in *P. redfieldii* is associated with permeabilization of the mitochondrial membranes and opening of the MPT pore, which are markers of PCD (Galluzzi *et al*., 2018). The herniation of mitochondria observed in *P. redfieldii* is not a common occurrence in plants and

phytoplankton. It does however occur in animal cells but it is controversial because it is regarded as a marker of both PCD (Feldmann *et al*., 2000; Saunders *et al*., 2024; Sesso *et al*., 2012) and necrosis (Lemasters *et al.,* 1998; Rodriguez-Enriquez *et al.,* 2004). This scenario highlights how structural markers should be looked at collectively to deduce that a cell is dying in a programmed (Barreto Filho *et al*., 2023).

Alterations to the chloroplasts of *P. redfieldii* bloom cells are regarded as structural markers of PCD because they are in accordance with those previously reported in other phytoplankton during cell death (Pokrzywinski *et al*., 2017a; Zuppini *et al.*, 2010). The recycling of chloroplasts that was observed in these cells is also not uncommon in algae especially during stressful conditions (Gorelova *et al.*, 2019).

All the above observations strongly support an autophagic cell death in *P. redfieldii* bloom cells. Autophagic cell death is defined as cell death that occurs with autophagy (Kroemer *et al.*, 2009; Kroemer and Levine, 2008). It is important to highlight that the autophagic cell death in *P. redfieldii* occurs with autophagy but is not autophagy- dependent cell death. Autophagy- dependent cell death can only be established at molecular level when cell death is halted by the knockdown of ATG genes Kroemer and Levine, 2008). Autophagic cell death is characterised by the excessive autophagic vacuolation accompanied by lysosomal/ vacuolar degradation and nuclear degradation is absent or can occur at the late stage of cell death (Kroemer *et al*., 2009). The cells with retracted and damaged amphiesmal membranes indicate an onset of secondary necrosis. In these cells necrosis is regarded as secondary because it is not an initial occurrence in these cells but a switch from an autophagic cell death pathway (Silva, 2010). To support the view of secondary necrosis, organelles like chloroplasts and nuclei were still intact. It is possible that in this group of cells the ATP levels were depleted and these cells could not continue with the autophagic route. With the substantial amount of altered mitochondrial profiles in the late stage of the bloom a drop in the levels of ATP is expected. It is a common occurrence for cells that are undergoing PCD to switch to secondary necrosis (Carmona-Gutierrez *et al*., 2018)

Other PCD phenotypes that have been detected in dinoflagellates are apoptotic-like cell death, paraptosis and necrotic-like cell death (Segovia, 2008a). In other dinoflagellates like *Symbiodinium sp*. cells from the same population subjected to the same stress manifest both PCD and necrosis (Dunn *et al.,* 2004). The apoptotic or apoptotic-like cell death phenotype can be eliminated as a pathway responsible for the demise of the *P. redfieldii* bloom cells because excessive vacuolation is absent in cells that die by apoptosis (Kroemer *et al*., 2009). Paraptotic cell death can also be ruled out as the cell death phenotype in *P. redfieldii* bloom cells, because paraptosis is characterised by extensive vacuolation by single-membrane vesicles derived from dilated ER and mitochondria (Sperandio *et al.*, 2004; Yan *et al.*, 2020a). In *P redfieldii* excessive vacuolation was a result of catabolic processes. A switch from PCD to necrosis is a common occurrence and governed by the energy levels of the stressed cells (Nicotera and Melino, 2004).

2.5 CONCLUDING REMARKS

This study investigated whether the cells of *P. redfieldii* in a collapsing harmful bloom in St Helena Bay exhibited any known morphological markers of PCD that were not reflected in nutrient replete cells grown in the laboratory. The findings were used to establish whether the collapse of the bloom was caused by a genetically controlled death program. Detailed ultrastructure revealed that *P. redfieldii* cells sampled from a natural collapsing bloom were altered compared to those grown in nutrient replete conditions in the laboratory. Some of the alterations observed in the cells included excessive vacuolation by autophagy which was brought about by a combination of catabolic processes. These included the upregulation of multivesicular bodies, macro- and microautophagy and structures associated with autophagy like double membraned structures and lytic vacuoles. Alterations to mitochondria which have been associated with the permeability of the mitochondrial inner membrane (Rodriguez-Enriquez *et al.,* 2004), and altered chloroplast membranes indicate that the cells could have been subjected to an oxidative stress.

Based on the detailed ultrastructural alterations in the *P. redfieldii* cells sampled from the bloom it can be concluded that they are structural markers that conform with the autophagic cell death phenotype (Kroemer *et al.,* 2009). There is also evidence of a switch from autophagic cell death to secondary necrosis which could have been activated by depleted energy levels resulting from the substantial damage to mitochondria in the late stages of the bloom.

In the next chapter the behaviour of these organisms when they are deprived of essential macronutrients like nitrogen and phosphorus is explored. The chapter also gives insight about the biochemical behavior of the stressed *P. redfieldii* cells.

CHAPTER 3 THE ULTRASTRUCTURE AND. BIOCHEMICAL ACTIVITY OF *PROROCENTRUM REDFIELDII* CELLS DEPRIVED OF ESSENTIAL MACRO-NUTRIENTS (NITRATES & INORGANIC PHOSPHATES).

3.1 Introduction

The availability of macro-nutrients like nitrogen and phosphorus in the ocean plays a role in phytoplankton dynamics, namely, their primary production, growth, composition as well as their ecological succession (Salmaso *et al.,* 2012). These macro-nutrients are essential for metabolic processes involved in cellular growth and division of unicellular organisms (Dagenais-Bellefeuille and Morse, 2013; Falkowski, 1994; Kudela *et al*., 2010).

Environmental factors like coastal upwelling increase the available amounts of these macro-nutrients and stimulate population productivity resulting in the formation of blooms (Anderson *et al.*, 2002; Glibert *et al.*, 2016; Kudela *et al*., 2010; Pitcher *et al*., 2005; Winter *et al.,* 2011). A bloom that develops by the means highlighted above would abruptly collapse if these macro-nutrients are lacking. Such a collapse is frequently accompanied by adverse effects, like the development of anoxia in the surrounding water, which negatively affects all aerobic organisms in those environments (Anderson *et al*., 2002; Ndhlovu *et al*., 2017; Pitcher and Probyn, 2016).

Anoxia results from high aerobic respiration which occurs when bacteria decompose the decaying bloom population. The high aerobic respiration rapidly depletes the levels of dissolved oxygen in the water column (Chapter 1, section 1.1). It is understood that the demise of blooms can occur as a result of the depletion of available nutrients, however, there is growing consensus that the resultant stress triggers a programmed intrinsic process involving gene transcription that drives the

bloom demise, namely, programmed cell death (PCD; (Vardi *et al.*, 1999; Burson *et al*., 2014; Bar-Zeev *et al.*, 2013; Berman-Frank *et al.*, 2004; Vardi *et al.,* 2007; Franklin *et al.*, 2006). The potential benefits of such a programme especially in populations of unicellular organisms has already been discussed in Chapter 1 (section 1.2.8).

3.1.1 Nitrogen as a limiting macro-nutrient

Nitrogen (N) as a macro-nutrient plays a very important role in the growth and metabolism of phytoplankton like dinoflagellates. It is a basic structural element used in the synthesis of essential organic compounds like amino acids, enzymes, nucleic acids, and chlorophyll (Dagenais-Bellefeuille and Morse, 2013). Therefore, the concentration of N, as well as its ratio relative to other macro-nutrients like phosphorus, affects the growth of many microalgae.

Even though nitrogen gas is abundantly available as dinitrogen (N_2) in the atmosphere, it is often limiting because it is not available to phytoplankton in its native form but has to be first converted to fixed forms like inorganic ammonium (NH_4^+) and nitrate (NO_3^-) or organic urea ($CO(NH_2)_2$; Jing *et al*., 2017). When environmental conditions are favourable, most phytoplankton including dinoflagellates prefer NH_4^+ compared with other abundant forms of inorganic nitrogen like NO_3^- (Dagenais-Bellefeuille and Morse, 2013; Glibert *et al*.,2006, 2016a) because ammonium ions require less energy to assimilate (Abadie *et al*., 2015).

Microalgae have optimized their ability to take up this macro-nutrient from their surroundings by the use of transporters (Dagenais-Bellefeuille and Morse, 2013). Transporters are protein molecules which use energy to transport the different nitrogen forms across cell membranes, and usually have different preferences for the various forms of N, although some can switch this preference when the source is limited (Forde, 2000). Microalgae are able to adapt and mitigate short-term sporadic N limitations in their environments through the upregulation of physiological and transcriptomic strategies (Abadie *et al*., 2015; Dagenais-Bellefeuille and Morse, 2013). For example, during N limitation some

dinoflagellates like *Prorocentrum minimum* can switch their feeding strategies from taking up only inorganic N sources using transporters to mixotrophy (i.e., use of more than one feeding strategy; Dagenais-Bellefeuille and Morse).

The assimilation of N and carbon (C) are interdependent, such that in alga about 50 % of assimilated carbon is utilized for nitrogen assimilation (Turpin, 1991). The main N assimilation pathway in algae is the GS-GOGAT (glutamine synthetase-glutamine -2- oxoglutarate aminotransferase; Turpin, 1991). During N assimilation, C skeletons (e.g., 2-oxoglutarate) and energy produced during C assimilation are utilised in the synthesis of amino acids and enzymes. Reciprocally, these amino acids (e.g., glutamate) and associated enzymes are precursors required for the synthesis of chlorophyll and other proteins involved in the photosynthetic apparatus (Foyer *et al.*, 2001). When N is limited, the C: N balance is therefore disturbed and assimilated carbon cannot be utilized in the synthesis of organic compounds such as amino acids (Berges and Falkowski, 1998). This is manifested as an increased accumulation of lipid droplets or triacylglycerol (TAG) and starch grains in the affected organisms when observed by microscopy (Goncalves *et al.*, 2016; Jiang *et al*., 2014; Sathe *et al.*, 2019; Weng *et al.*, 2014).

Nitrogen limitation also affects the photosynthetic apparatus because it results in a lack of essential amino acids and enzymes required to synthesize photosynthetic pigments involved in photosystem II (PS II). This photosynthetic unit utilizes pigment molecules and associated proteins for the harvest and transfer of photons, and initiation of the electron transport chain reactions.

Limited N also affects the progression of the cell cycle. During the G1 phase of the cell cycle there is active growth of cells which requires synthesis of new proteins and associated enzymes to support the various metabolic processes in actively growing cells (Olson and Chisholm, 1986). This active growth occurs until a certain "checkpoint" is reached and under nutrient replete conditions cells would move to the next stage, the S stage where DNA synthesis and replication occurs (Bišová and Zachleder, 2014). When nitrogen is limited, the relevant proteins needed for the next step in the cell cycle progression cannot be synthesized and therefore do not pass the "checkpoint" and are thus arrested in the G1 stage of the cycle.

3.1.2 Phosphorus as a limiting macro-nutrient

Phosphorus (P) is the second essential macro-nutrient after N in phytoplankton. It is a building block of nucleic acids and membrane systems (phospholipids), it is used in the activation of many enzymes and proteins, in the formation of energy molecules (ATP & NADP) through phosphorylation. Phosphorylation is an important biological reaction whereby a phosphate group is added to organic molecules by kinases *(*Lin *et al*., 2016), it is also reversible.

The preferred form for assimilation by phytoplankton is as dissolved inorganic phosphate (DIP) or orthophosphate. When conditions are limiting it can also be taken up as hydrolyzed dissolved organic phosphorus (DOP), however this option is costly in terms of energy as it has to be first converted to Pi before it can be used in metabolic processes (Lin *et al*., 2016; Orchard *et al.*, 2009). Phosphorus is important in phytoplankton cell growth and total starvation of this essential macronutrient has similar effects as discussed for nitrogen.

Phosphorus uptake (i.e. in the form of phosphates) in phytoplankton is also facilitated by special P transporters, as with N (Monier *et al.,* 2012). There are two main types of P transporters, namely, low-affinity- Pi and high affinity Pi (L. Wang et al., 2020).

When P limitation studies were conducted on the following dinoflagellates, *Karenia mikimoto* (Lei and Lu, 2011)*, Prorocentrum donghaiense* (Li *et al.*, 2015) *and A. carterae* (Meizhen *et al*., 2016) they resulted in cell cycle arrest at the G1 stage of the dinoflagellate cell cycle. In *P. donghaiense* P limitation also affected the photosynthetic apparatus because it decreased the efficiency of PSII, however the decrease was not significant when it was compared to that of organisms growing in replete conditions (Li *et al.*, 2015). When DIP is limited dinoflagellates may resort to the assimilation of dissolved organic P (Orchard *et al.*, 2009).

The consensus is that N is limiting in marine environments while P is limiting in freshwater (Dyhrman, 2016; Schindler, 1977). However, this view is challenged by some as evidence shows that P can also be limiting in some marine environments

(Benitez-nelson, 1999; Coleman and Chisholm, 2010; Dyhrman, 2016; Karl, 2014). One study showed that growth in *P. triestinum* is limited by P and not by N (Chan *et al.*, 2004). This is because this organism can recycle intracellular pools of N from degraded organelles and macromolecules and thus provide a new source of N to sustain it until external sources are replenished (Chan *et al.*, 2004).

It appears that both N and P transport in dinoflagellates is well developed and that it can be achieved in either organic or inorganic form. The ability to maximise uptake of these essential macro-nutrients makes them frequent causative agents in harmful algal blooms. They cope with short term nutrient limitations, but prolonged stress leads to cell death.

3.1.3 Caspase or caspase-like protease activity in PCD of unicellular organisms

Caspases are a group of cysteine proteases belonging to the C14 family of the CD clan according to the classification system of the MEROPS database of peptidases (Minina *et al.*, 2017; Rawlings *et al.*, 2016), which initiate and effect PCD in metazoans (Cohen, 1997). They exist as zymogens (i.e., inactive structures) activated by proteolysis.

During PCD, initiator caspases which are monomers initiate the proteolytic cascade of reactions which cleave and activate the effector caspases downstream through dimerization (MacKenzie and Clark, 2012). Effector caspases are monomers and once they are activated, execute the cell death process by cleaving the relevant caspase substrate (MacKenzie and Clark, 2012; Shrestha and Clark, 2021). Another structural difference between initiator and effector caspases is their N-terminal amino acid residue referred to as the pro-domain, the initiator caspases have a longer pro-domain (about 100-200 residues) than the effector caspases (about 25 residues; McLuskey and Mottram, 2015). Both initiator and effector caspases are numbered according to the sequence of their discovery, for an example caspase-2, -8,-9, -10, -11 and -12 are initiator caspases, while caspase-3, -6 and -7 are effector caspases (Cohen, 1997).

Caspase structural homologues, the metacaspases, are found in Planta, Chlorophyta, Fungi, Heterokontophyta, Haptophyta and Cryptophyta (Choi and Berges, 2013; Tsiatsiani *et al.*, 2011; Uren *et al*., 2000). Two types of metacaspases were initially discovered viz. metacaspase-I and -II (Vercammen *et al.*, 2004). Metacaspase- I is the most conserved, while metacaspase- II is currently restricted to Chlorophyta and Planta (Choi and Berges, 2013; Klemenčič and Funk, 2018). The two structural differences between metacaspase- I and -II is a large N-terminal pro-domain in metacaspase-I that contains two protein motifs, namely, the zinc-finger and proline-rich motif (Uren *et al*., 2000; Vercammen *et al*., 2004). Secondly, metacaspase- II, possess a long linker region between the p20 and p10 domains (Uren *et al*., 2000).

The similarity between caspases and metacaspases is in their primary structure but their functionality is different (i.e., they are not orthologs). Therefore, the caspase-like activity reported in non-metazoans is not from metacaspases. In Planta and Fungi, it has been discovered that the caspase-like activity is from a different class of cysteine proteases which also cleave their amino residues after aspartic acid. Examples include the vacuolar processing enzymes which are cysteine proteases (Hatsugai *et al.*, 2004) and serine proteases like phytaspases and subtilisins (Johnson *et al*., 2014). In phytoplankton the proteases responsible for caspase-like activity have not yet been determined (Spungin and Berman-Frank, 2019).

Another conundrum is that caspases and their homologues are not specific to cell death but are also involved in other activities inside the cells (Connolly *et al*., 2014; Julien and Wells, 2017; La *et al*., 2022). For example, in *Karenia brevis* a high caspase-like activity was reported although cells were in their exponential stage. It was also reported that during the stationary phase the caspase-like activity was not associated with no cell death. This shows that in these cells the high caspase-like activity was associated with other metabolic activities during the exponential phase and acclimation of cells to stress during the stationary phase (Y Gao and Erdner, 2022).

Structurally, caspases and metacaspases possess a large and small domains the p20 and p10, respectively (Klemenčič and Funk, 2018). The p20 domain is made up of cysteine and histidine (a catalytic pair of amino acid residues) and the amino

residues in p-10 are unspecified but are involved in dimerization (Salvesen *et al*., 2016) and in substrate binding (Pop and Salvesen, 2009). Functionally, caspases and metacaspases differ because they cleave different substrates, the caspases cleaves aspartic acid (acidic amino acid residues) while metacaspases cleave arginine or lysine (basic amino acid residues; Tsiatsiani *et al*., 2011).

The caspase protease activity assay is used in metazoans and non-metazoans. **The term caspase-like activity is used when a positive outcome of the caspase assay is detected in non-metazoans since they lack true caspases** (Rojo *et al.,* 2004). The assay cleaves the substrate after an acidic amino acid residue like aspartate. Synthetic fluorogenic or colorimetric substrates, like the caspase-3 specific Ac-DEVD-AMC {Ac (N-acetyl)-DEVD (Asp-Glu-Val-Asp)-AMC (7-amino-4-methylcoumarin)}, are cleaved to release and activate a fluorogenic component, e.g., AMC. Relevant synthetic substrate inhibitors (these are peptides that act as pseudo substrates which compete with the substrates; Ekert *et al*., 1999) are used in conjunction with the caspase substrate and a successful silencing of the caspase activity proves that the signal is specific to caspase proteases activity (Segovia and Berges, 2009). For example, the synthetic substrate inhibitor Ac-DEVD-CHO is a specific inhibitor for the caspase-3 synthetic fluorogenic substrate Ac-DEVD-AMC (Ekert *et al*., 1999). The addition of a caspase inhibitor to stressed cell cultures of *Thalassiosira pseudonana* prevented PCD (Barreto Filho *et al.*, 2023; Bidle and Bender, 2008), while it resulted in the formation of cysts in *Peridinium gatunense* (Vardi *et al.,* 1999). Synthetic substrates for metacaspases also exist, e.g., Ac-VRPR-(Val-Arg-Pro-Arg)-AMC (Tsiatsiani *et al.*, 2011).

Caspase / DEVDase activation is a requirement for the initiation of some phenotypes of PCD e.g., apoptosis, but other phenotypes can manifest without caspase activation (i.e., caspase-independent PCD). One of the most common types of caspase-independent cell death is the autophagic or type 2 PCD, which is characterised by extensive vacuolation of the cell (Qi and Liu, 2006). Paraptosis, another phenotype for PCD is also characterized by vacuolization, but differs from autophagic cell death in that its vacuoles originate from swollen endoplasmic reticulum or mitochondria (Sperandio *et al.*, 2000), can also be caspase-independent

(Jimenez *et al*., 2009).

3.1.4 Reactive oxygen species (ROS)

Reactive oxygen species are a by-product of aerobic metabolic reactions like the electron transport chain of reactions that occur in mitochondria, chloroplasts and plasma membranes (Sharma *et al*., 2012). They are radical forms of oxygen such as the superoxide anion ($O_2^{\bullet-}$) and hydroxyl radical ($^{\bullet}OH$), as well as non-radical forms such as the singlet oxygen ($^1O_2$) and hydrogen peroxide (H_2O_2). Superoxide and H_2O_2 are the most prevalent forms and the former is the abundant form in mitochondria (Zorov *et al.,* 2014). Superoxide is produced when electrons leaked from redox reactions are added to the oxygen molecule. Hydrogen peroxide forms when superoxide is reduced by the antioxidant, superoxide dismutase (SOD; Patel *et al*., 2017). Hydrogen peroxide is not as reactive and is less damaging than the former two, but it can convert to other more dangerous forms like the $^{\bullet}OH$ radical and $^1O_2$ (Das and Roychoudhury, 2014), the $^1O_2$ is most abundant form produced by redox reactions in the photosystem II reaction centre (Foyer and Hanke, 2022).

Antioxidants can be enzymatic or non-enzymatic. Some examples of enzymatic forms include SOD, catalase (CAT) and ascorbate peroxidases (APX), while non-enzymatic forms include carotenoids, flavonoids and ascorbic acid (Das and Roychoudhury, 2014). The hydroxyl radicals are the most reactive form of ROS and unfortunately do not have antioxidants. The antioxidants for singlet oxygen are β carotene and plastoquinone (Patel *et al*., 2017).

The role of ROS in a cell is two-fold. When their production is balanced with their removal, small amounts of ROS act as signalling molecules sensing changes in environmental stimuli and are involved in processes like cell growth (Das and Roychoudhury, 2014; Mullineaux *et a*l., 2018). Disturbance to this redox balance leads to oxidative stress and can have deleterious effects for the cell causing damage to proteins, pigments, lipids and DNA and can lead to cell death (Das and Roychoudhury, 2014). ROS bursts are thus used as one of the early indicators of programmed cell death (Matthias Josef Affenzeller *et al.*, 2009; Bidle, 2016; Zuppini *et al*., 2010).

The reactive oxygen species assay measures an accumulation of ROS as a response to stress and is thus one of the assays that is used as a biochemical marker of PCD in a cell (Petrov *et al.*, 2015; Zhao *et al*., 2020). Unfortunately, the assay is not specific to PCD as increased ROS levels can also lead to other types of cell death like necrosis (Chapter 1, section 1.2.5, Table 1.2).

3.1.5 Nuclear DNA oligo-nucleosomal fragmentation

Nuclear DNA oligo-nucleosomal fragmentation, activated by endonucleases, is an indicator of programmed cell death (Yoshida *et al*., 2006). The DNA laddering assay using agarose gel electrophoresis is used to investigate DNA fragmentation. Other assays like the TUNEL assay (Terminal deoxynucleotidyl transferase-mediated dUTP nick-end labelling) and the comet assay are also used to investigate DNA damage but are limited as they do not differentiate between DNA damage resulting from necrosis and that from PCD.

The DNA laddering assay detects oligo-nucleosomal fragments using agarose gel electrophoresis, which can be separated into a ladder-like pattern of about 180-200 bp (Bortner *et al.*, 1995) following agarose gel electrophoresis (Iglesias-Guiomarais *et al*., 2012). This assay is specific to PCD as the ordered cleavage of DNA into oligo-nucleosomal fragments (Kuthanova *et al*., 2008) effected by the specific caspase–activated deoxyribonuclease (CAD) can only occur in the nuclei of cells undergoing PCD (Nagata *et al.*, 2003). Unfortunately, it requires a large percentage of cells to be undergoing PCD for it to give positive results, therefore it is not a sensitive assay (Barreto Filho *et al.*, 2023).

In the TUNEL assay the terminal deoxyribonucleotidyl transferase (dUTP) catalyses the addition of tagged deoxynucleotides to the ends of DNA strand breaks (Kyrylkova *et al.,* 2012). The dUTP detects both single and double strand breaks and this makes it a highly sensitive technique, however, it is not specific to PCD (Durand, 2020). It detects damage to DNA but it cannot discriminate whether the damage is as a result of necrosis or PCD, thus having the possibility of giving false positives (Pulkkanen *et al*., 2000).

The comet assay is sometimes referred to as the single cell gel electrophoresis assay (Collins, 2004; Olive and Banáth, 2006), it analyses the migration of fragmented DNA strands from a single cell in electrophoresis gel. The high molecular weight, negatively - charged, undamaged DNA remains inside the cell membrane (comet head) on the negatively charged pole of the electrophoresis gel while the damaged DNA strands migrate out of the cell (the tail) to the positively charged pole. This assay is sensitive and has been declared to be able to distinguish the damaged DNA of cells undergoing PCD from those that are necrotic (Yasuhara *et al*., 2003) even though others caution about assuming that the assay is specific to damaged DNA of cells undergoing PCD (Lorenzo *et al.*, 2013).

In the current study, the DNA laddering assay using agarose gel electrophoresis, will be carried out. It is foreseen that the nuclear structure of the study organism could pose limitations to the successful outcome of the assay as previously reported by others who have carried it out on dinoflagellates (Vardi *et al.,* 1999). In particular, the unique mesokaryotic nucleus of dinoflagellates (described in detail in Chapter 2 section 2.1.3.) possesses permanently condensed chromosomes but lacks true histones. Instead, the chromosomes possess specific DNA binding proteins like the dinoflagellate / viral nucleo proteins (DVNP's) and histone-like proteins (HLPs) and they lack nucleosomes (Chan and Wong, 2007; Janouškovec *et al*., 2017; Riaz *et al.*, 2018). Therefore, because DNA oligonucleosomal ladders occur when DNA is cleaved at linker regions between nucleosomes, the absence of nucleosomes in dinoflagellates might pose a limitation for the assay.

3.1.6 Aims and objectives

The aim of this study was to investigate if depriving *P. redfieldii* cells of two essential macro-nutrients individually, namely, nitrates (N) and organic phosphates (P), would induce a programmed cell death.

The aim was addressed by the following objectives:

1) To determine how the ultrastructure of the cells is modified under nutrient stressed conditions.

This was achieved by depriving the cultures independently of two macro-nutrients (viz., N as NO_3^-- and P as PO_4^{3-}). Samples were characterised by a detailed analysis of the ultrastructure of replete and nutrient deplete cells in culture by transmission electron microscopy. Alterations to the ultrastructure of nutrient deplete cells were compared with those observed in replete cells. The focus was on alterations to the nucleus, endomembrane system (Golgi bodies, endoplasmic reticulum and associated vesicles); mitochondria; chloroplasts; vacuolation and amphiesmal membranes.

2) To carry out concurrent PCD assays on the cultured material including a:

i) DEVDase activity assay,

ii) DNA laddering assay, and

iii) ROS assay

3) To test whether the witnessed elements of cells in a laboratory based nutrient deprivation experiment reflected those of cells sampled during the collapsing HAB:

This was achieved by assessing the impact of nutrient depletion on the ultrastructure and biochemical activity of the laboratory cells to verify the occurrence of programmed cell death.

The ultrastructure of the laboratory cells was then compared with those of a collapsing HAB of the same organisms to detect similarities.

3.2 METHODS

3.2.1 Growth conditions

Prorocentrum redfieldii cultures were grown to the log-linear stage in the F/2 medium (Guillard and Ryther, 1962). To start the nutrient deprivation experiment, an initial concentration of 2 x 10^5 cells ml^{-1} in the log-linear stage was poured into each of 8 centrifuge tubes. These cultures were centrifuged at 500 *g* (Hettich Universal / K2S, Germany) for 10 minutes and the pellet was resuspended in 2 ml seawater. Contents from all the 8 centrifuge tubes were poured into one Erlenmeyer flask and mixed by gently swirling the flask. About 2 ml of this culture was poured into each of three flasks and topped up to 200 ml to a final concentration of approximately 4 x 10^4 cells ml^{-1} with F/2 N-deplete medium. To make up the F/2 nitrogen-deprived medium the $NaNO_3^-$ component was not added to the F/2 medium (Guillard and Ryther, 1962). Another two flasks with 2 ml each of the concentrated culture were topped up with nitrogen-replete F/2 medium and used as controls. Cultures were grown in 250 ml Erlenmeyer flasks in a growth chamber. Cultures were grown at a temperature of 20º C with a 16:8h light-dark photoperiod and a white, fluorescent light intensity of 13 µmol m^{-2} s^{-1}.

Samples for transmission electron microscopy, DEVDase activity analysis, and DNA laddering assays were taken on days 3, 7 and 14 of treatment. The same procedure was repeated for the phosphorus deprivation experiments. To make up the F/2 phosphorus-deprived medium, the $NaH_2PO_4.\ H_2O$ component was omitted from the F/2 medium (Guillard and Ryther, 1962).

3.2.2 Growth studies: cultures

Growth studies were carried out on *P. redfieldii* cultures that were grown in nitrogen- and phosphorus-deprived cultures versus those growing in replete media over 24 days. This was accomplished by measuring the optical density of cultures in the three treatments using a spectrophotometer (Thermo Scientific Helios Gamma spectrophotometer; Massachusetts, USA). The correlation between cell growth and optical density was determined by plotting a standard curve between

the two parameters and establishing the correlation coefficient (R^2) value. Samples were poured into 2 ml cuvettes and the absorbance value was read in a spectrophotometer at 550 nm. Every second day, three replicates were measured from each of the three treatments. The measurements were repeated three times giving nine readings per treatment that were averaged and were used to plot the growth curve.

3.2.3 Transmission electron microscopy

3.2.3.1 Fixation and embedding

Nitrogen- and phosphorus-replete and -deprived cultures were prepared for transmission electron microscopy as detailed in chapter 2 section 2.2.3.

3.2.3.2 Microtomy and Viewing

Resin blocks of Nitrogen- and phosphorus-deprived and -replete samples were cut into ultrathin sections of 60 nm using an ultramicrotome (RMC Boeckler CR-X, PT-PC, PowerTome; Arizona, USA) as explained earlier in chapter 2 section 2.2.3.2.

The ultrastructure from the first 25 cells encountered in linear, non-overlapping transects per treatment was captured and analysed. A sample size higher than 25 cells was difficult to achieve because of the low cell numbers in the nutrient deprived cultures. Viewing focus was on alterations to organelles as mentioned in section 3.1.7, changes in the integrity of the amphiesmal membranes, vacuolation, subcellular structures and vesicles not observed in replete cells. Changes in abundance and size of organelles relative to those of replete cells was noted.

3.2.4 DEVDase analysis assay

3.2.4.1 Preparation of lysates

The DEVDase analysis assay of the N- and P - deplete cultures was carried out at predetermined times over seven days. To remove cells from culture, 5 x 10^5 cells

ml^{-1} from each of the three treatment replicates and two control replicates were poured into glass centrifuge tubes. On days 3 and 7, cultures were concentrated until an approximate concentration of 5 x 10^5 cells ml^{-1} was achieved. The tubes were centrifuged at 600*g* for 5 minutes and 1200 g for another 5 minutes at 4 ºC (Hettich Universal /K2S, Germany). The supernatant was removed by gentle aspiration and the pellet was washed once in 1 ml phosphate-buffered saline (PBS). The cells were centrifuged again, and the supernatant was removed. The cells were resuspended in 1 ml of lysis buffer (250 mM HEPES, 25 mM CHAPS, and 25 mM DTT; **Caspase 3 Assay Fluorimetric Kit, Sigma Aldrich)**, transferred into Eppendorf tubes, and incubated on ice for one hour. The lysed cells were centrifuged at 14000 g (Sigma 201M, Netherlands) for 15 minutes at 4 ºC. The supernatant was transferred into new Eppendorf tubes, frozen immediately in liquid nitrogen, and stored at -20 ºC until they were prepared for reading in a fluorometer (Hoefer DQ300, Massachusetts, USA).

3.2.4.2 Fluorometric analysis

Before the lysates were read in a fluorometer they were thawed to room temperature. A reaction mixture was made up by adding 2 ml assay buffer (200 mM HEPES pH7.4; 1 % CHAPS; 50 mM DTT; 20 mM EDTA; Caspase 3 Assay Fluorimetric Kit, Sigma Aldrich, USA) and 30 µl of caspase 3 substrate (Ac-DEVD-AMC) into cuvettes. These were then stored in the dark until the reactions were started. For the correction of background, a blank was prepared by adding 500 µl of assay buffer into a cuvette and 2 mls of the reaction mixture was added to the blank.

To test for caspase -3 activity, 500 µl of lysates from the stressed samples were poured into 5 ml cuvettes (n=3). The same was done for the control samples (n=2). The reaction was started by adding 2 mls of the reaction mixture to the stressed and control cell lysates.

To test if the caspase- 3 activity reaction is silenced by the caspase- 3 inhibitor, 500 µl of lysates from the stressed samples were poured into cuvettes (n=3) and 20 µl of caspase substrate inhibitor (Ac-DEVD-CHO) were added. The reaction was

started by adding 2 mls of the reaction mixture to the stressed and control cell lysates (n=2).

All the above reactions were incubated at 30 ºC in the dark for one hour. Fluorescence emissions from the samples were measured with a fluorometer using a UV light for excitation.

3.2.5 Reactive oxygen species assay

Flow cytometry analysis of reactive oxygen species (ROS) in N- and P- deplete versus replete cultures was carried out at predetermined times over 14 days. To remove the cells from the growth medium, about 3 x 10^5 cells ml^{-1} from each of the replicates of the starved and replete cells were poured into 50 ml Falcon centrifuge tubes. On day 7 cells were concentrated to obtain the initial concentration of 3 x 10^5 cells ml^{-1} and on day 14 the initial concentration was not achieved, and about 1.7 x 10^5 cells ml^{-1} were used in the experiment. The tubes were centrifuged at 500 g for 10 minutes at 20 ºC (Eppendorf 5702 R, Germany). The supernatant was removed by gentle aspiration and the pellet was washed once in 1 ml seawater. The cells were centrifuged again using the same parameters, the supernatant was removed, and the cells were re-suspended in 1 ml seawater. Cells were assayed following the **manufacturer's protocol (DHR 123 Redox probe, G-Biosciences, USA)**. Briefly, aliquots of 495 µl of cells in seawater were transferred into flow cytometry tubes. Di-hydro-rhodamine 123 (DHR 123) was pipetted into each tube to a final concentration of 10 µM. To check cell viability the procedure was repeated and the DHR 123 stain was replaced with 5 µl propidium iodide (PI). The stained cells were incubated in the dark at room temperature for 20 minutes and assessed using a BD LSR Fortessa TM cell analyzer (Becton-Dickinson, San Jose, CA, USA), interfaced with the BD FACSDiva software. The cells were excited with a blue laser (488 nm) and the emitted green fluorescence was detected using the fluorescent detector channel (FL1) with a (530 / 30 nm) bandpass filter.

All data obtained were analyzed with the FlowJo software (v10.7.1; FlowJo, LCC, Oregon, USA). Data was presented as single-parameter univariate plots (histograms). Various gating strategies were applied to separate / group subsets of

populations of cells that have similar behaviour and to also eliminate doublets (doublets are formed when clumping of cells or particles can result in two cells passing through the laser beam at the same time and therefore being incorrectly registered as a single event), as demonstrated below (Fig. 3.1).

To eliminate debris from live cells, side scatter SSC-Area (i.e., Fluorescence events that are at right angles to the laser beam) was plotted against FSC-Area (i.e., those that are in the plane of the laser) and fluorescence events that were below 50 000 RFU on the X-axis were gated as debris (Fig. 3.1 A). To eliminate doublets, FSC-Height was plotted against FSC-Area, most cells which fall on the diagonal plane are single cells and those outside of the diagonal plane are doublets (Fig. 3.1 B).

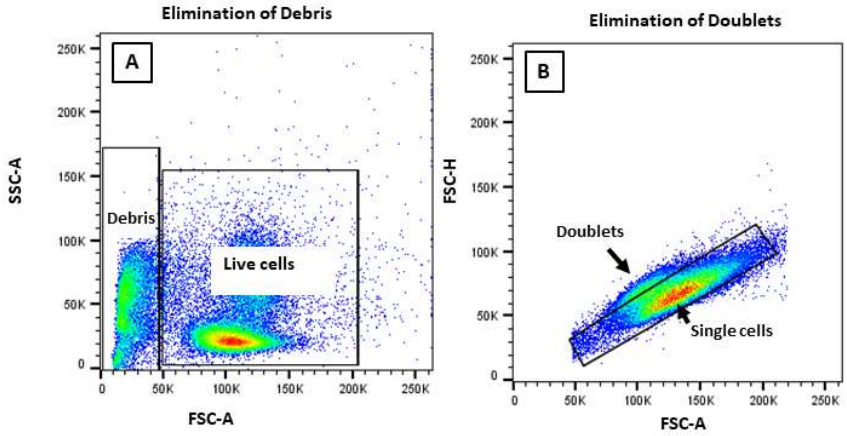


Figure 3. 1 Gating strategies applied to separate, (A) All fluorescence below 50K RFU was regarded to be from debris and those above were live cells (B) Elimination of doublets from single events. X-axis represents relative fluorescence units (RFU) and Y -axis represents cell counts; FSC-A/H (forward scatter -area/height); SSC-A (side scatter-area).

3.2.6 DNA Laddering assay

3.2.6.1 DNA extraction

Cultures grown in N- and P-deplete F/2 medium and those cultures that were grown in the replete medium were sampled on day 7 for DNA extraction following a

revised protocol (Ghatak *et al*, 2013). Approximately 2 x 10^5 cells ml^{-1} N- and P-deplete culture and 3 x 10^5 cells ml^{-1} from the replete culture were centrifuged at 500 *g* (Eppendorf 5702 R, Germany) for 10 minutes at 4 ºC to pellet the cells. The supernatant was removed by gentle aspiration. Cells were lysed by adding 700 µl of lysis buffer (10 mM Tris-HCL (Ph 8); 50 mM EDTA; 0.25 % SDS; Ghatak *et al*, 2013) and incubated for 2 hours at 5 ºC with intermittent mixing. To remove impurities from the lysed cells, Proteinase K was added to a final concentration of 100 ng/ µl, and the lysates incubated further for another 40 minutes. The lysates were spun down at 12 000 g (Eppendorf 5415 R, Germany) at 4 ºC and lysates were transferred to 1.5 ml Eppendorf tubes.

After cooling samples to room temperature, 700 µl of phenol: chloroform: isoamyl alcohol was added and gently mixed with the lysates for five minutes. To separate the aqueous phase, the lysates were centrifuged at 16 000 g for 10 minutes at 20 ºC. The aqueous phase was carefully removed and transferred into a new Eppendorf tube. An equal volume of chloroform: isoamyl alcohol (24:1) was added to the DNA extract, mixed for two minutes, and centrifuged at 12 000 g.

To precipitate the DNA, the aqueous phase was transferred to a new Eppendorf tube, 3 M sodium acetate (1/10 of the volume of aqueous phase; pH 5.2) and 100 % ethanol (twice the volume of the aqueous phase, stored at -20 ºC), were added. The DNA solution was kept at -20 ºC overnight and then centrifuged at 16000 g for 30 minutes at 4 ºC. The supernatant was removed, and the precipitate was rinsed in 70 % ethanol (stored at -20 ºC). The pellet was dried in air and dissolved in 20 µl Tris-EDTA (TE) buffer.

3.2.6.2 Gel electrophoresis

To determine whether the amount of the DNA extracted from the starved and replete samples was sufficient to be visualized on a gel, the DNA from all the samples was measured in a nanodrop spectrophotometer (Thermo Scientific nanodrop 2000c, Massachusetts, USA). A minimum threshold of DNA required to run in ethidium bromide (EtBr) gel is 10 ng/µL, in the current experiment 50 ng/µL DNA in EtBr for each sample was used.

DNA fragmentation in the starved and replete cells was investigated by gel electrophoresis. A 2 % agarose gel in Tris-borate-EDTA was prepared according to the method of Lee *et al* (2012). About 1 µl DNA molecular marker (100bp) was pipetted into the first well (lane) of the gel tray. A loading dye EtBr (0.25 % bromophenol blue, 0.25 % xylene cyanol, 30 % glycerol) was added to the DNA samples in a (1:6) ratio (8 µl loading dye:48 µl DNA). A total of 50 µl of each DNA sample with loading dye was introduced into the remaining wells (lanes). The gel was run at 80 V until the dye had migrated from the cathode to the anode. At the end of the run, the gel was exposed to UV light to detect for DNA fragments or laddering and to capture images.

3.3 RESULTS

3.3.1 Growth studies

Macroscopic observations of cultures displayed that nitrogen-deplete (N-deplete) cells had less pigmentation on all the 14 days of treatment than those deprived of phosphorus and those replete in nitrogen and phosphorus (hereinafter simply referred to as replete; Figs 3.2 A-C). In the phosphorus-deplete (P-deplete) cultures, a decrease in pigmentation relative to that of the replete cultures was noticeable by day 14 of treatment (Fig. 3.2 C).

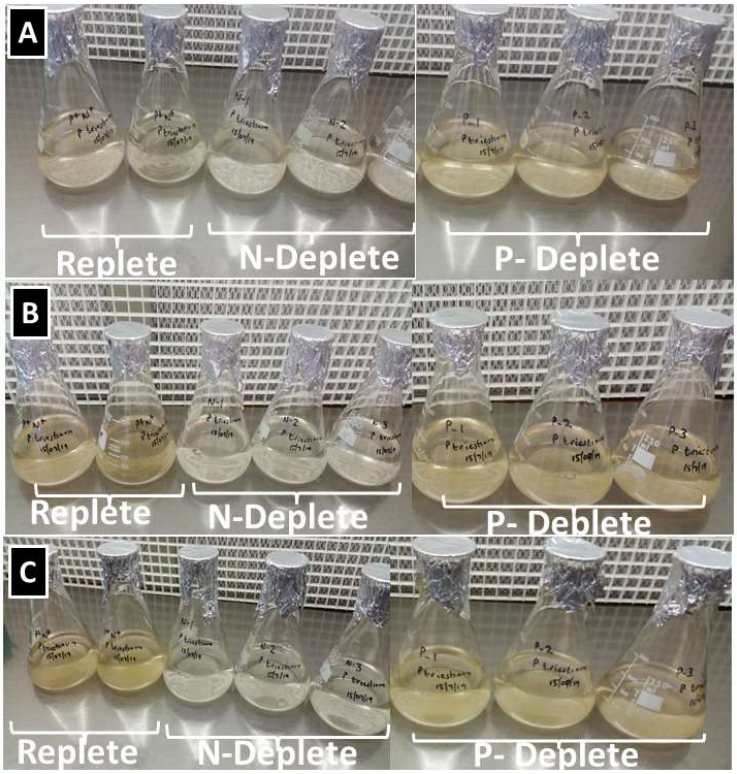
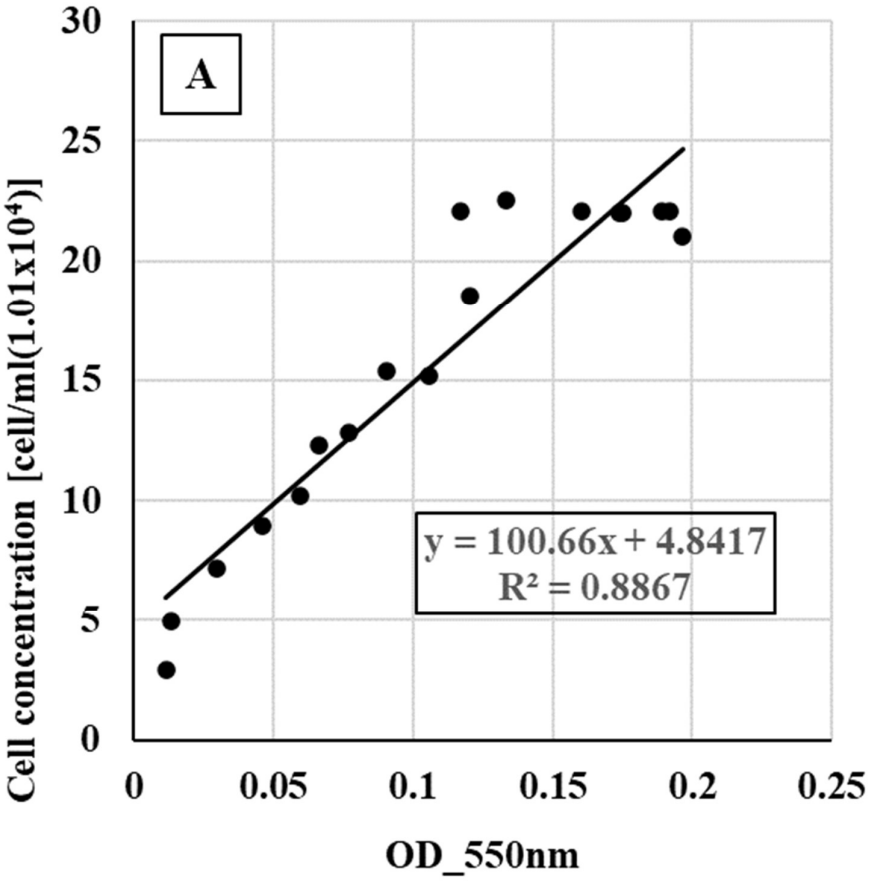


Figure 3.2 Macroscopic observation of replete versus N- & P- deplete cultures during the 14 - day treatment period.

(A) Cultures on day 3, (B) day 7 and (C) day 14 of treatment. Note the lack of pigment in the N-deplete cultures on all days of sampling and the reduced pigment on P-deplete cultures on day 14.

A positive correlation was demonstrated between cell concentration determined by a haemocytometer and optical density (OD) at 550 nm in replete cultures (Fig 3.3 A). This outcome allowed for OD to be subsequently used to measure cell growth in this study (Fig. 3.3 B).

The growth trend observed in replete cultures was different to that observed in the N- and P- deplete cultures (Fig. 3.3 B). The two deplete cultures were similar, but P- deplete cultures outperformed the other (Fig. 3.3 B). The nutrient deplete cultures did not exhibit a logarithmic growth, instead they followed a static trend. On day 12 when maximum cell densities were achieved in the replete cultures, those in deplete cultures were less than half of this value.



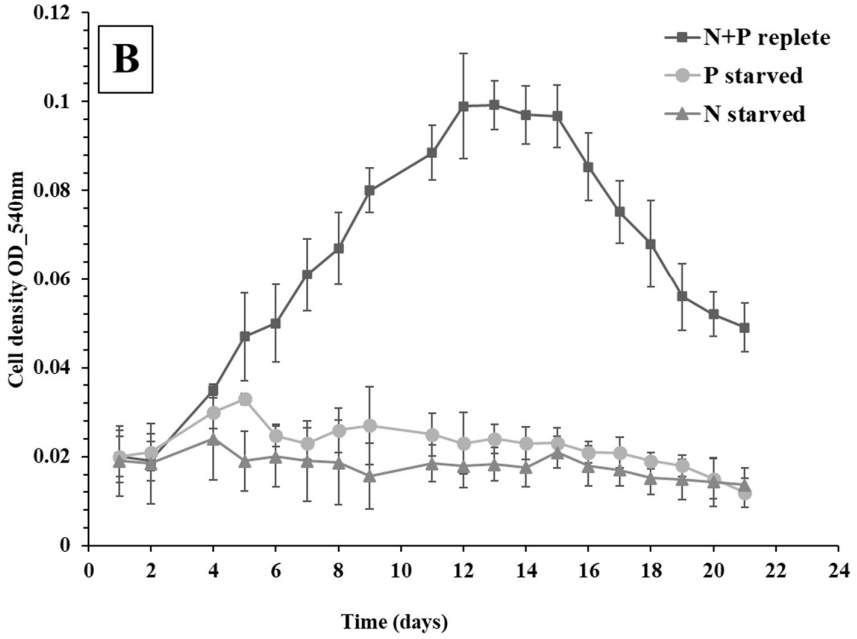


Figure 3.3 Cell densities of replete versus N- and P-deplete cells observed over a 21 day period. The relationship between optical density and cell concentration in nutrient replete cultures.

(A) Relationship between OD measured at 550 nm and cell concentration of N-Replete cells.

(B) Cell densities of replete versus N- and P-deplete cells monitored over a 21-day period

3.3.2 Cell Ultrastructure

3.3.2.1 Accumulation of carbon reserves and vacuolation

Lipid droplets were observed in the nutrient replete and deplete treatments on all days of sampling (e.g., Figs 3.4 A - I). Accumulation of starch grains was observed on days 3, 7 and 14 in the N- and P- deplete cells (e.g., Figs 3.4 D-I) but only on day 14 in the replete cells (e.g., Fig. 3.4 C). On day 7 the N - deplete cells had accumulated more lipid and starch relative to the replete and the P-deplete cells. At this time, 80 % of the N-deplete cells viewed (n = 25) showed obvious accumulation of reserves that occupied most the cell's content and resulted in the obvious compression of other organelles (e.g., Fig. 3.4 E).

Vacuolation increased in the nutrient deplete cells by day 14 of treatment (e.g., Figs 3.4 F & I). The average proportion of cell surface area occupied by vacuoles in the exposed profile of each cell (n=25) was about 27 % in the N-deplete cells while it was 24 % in the P-deplete (Table 3.1). These values were significantly different ($p < 0.05$) to those of replete cells where the average proportion of vacuolated area was 8 % of that of the cell (Table 3.1). In the N-and P- deplete cells vacuolation extended further into the cytoplasm, reducing the total space occupied by the cytoplasm (e.g., Figs 3.4 F & I).

Amphiesmal membrane retraction from thecal plates was observed in 44 % of cells on day14 in the P-deplete cells (Fig. 3.4 I). These cells were also extensively vacuolated.

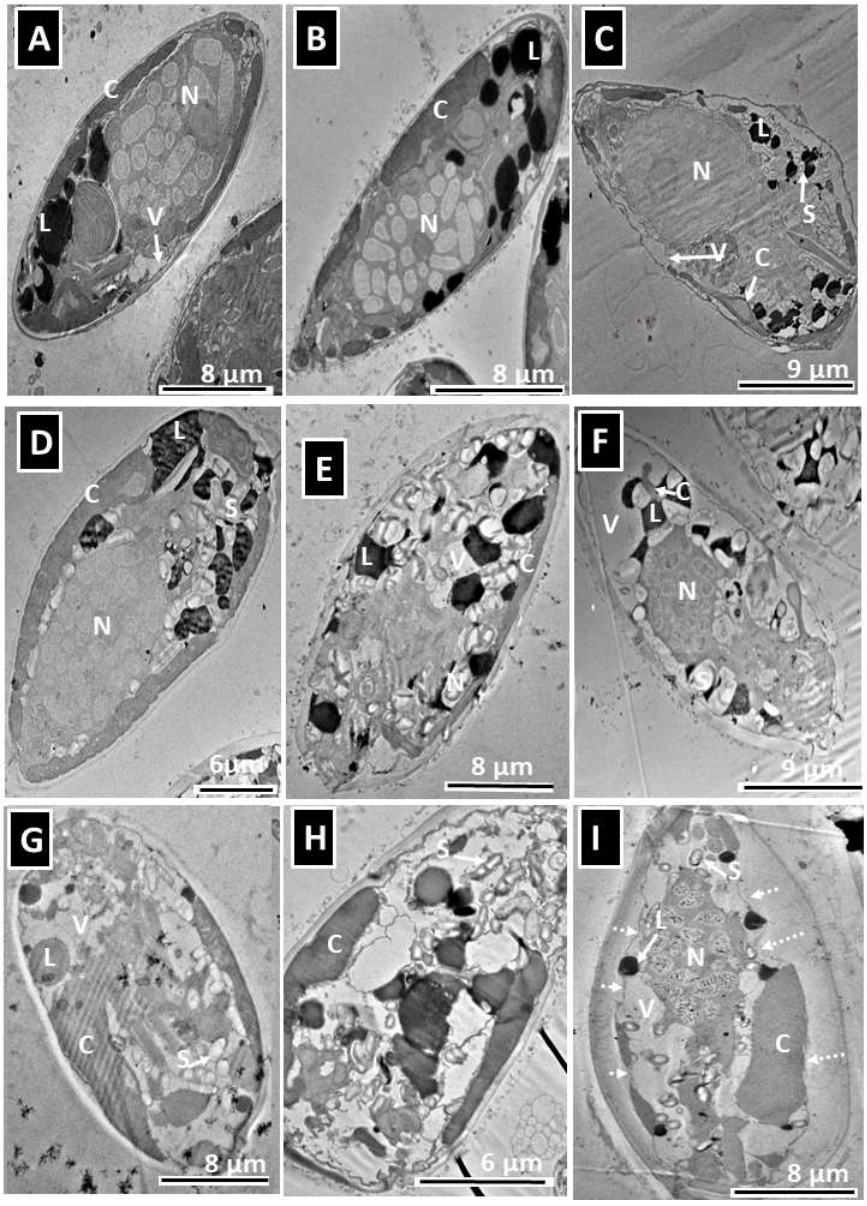


Figure 3.4 Accumulation of reserves and increased vacuolation in replete, N- and P-deplete cells with time.

(A-C) Replete cells on days 3, 7 & 14 of treatment respectively.

(D-F) N-deplete cells on days 3, 7 & 14 of treatment respectively. Note accumulation of starch and lipid bodies in (E) and vacuolation in (E & F).

(G-I) P-deplete cells on days 3, 7 & 14 of treatment 14 respectively. Note vacuolation on all days of treatment (broken arrows) and protoplast shrinkage from

the thecal plates (broken arrows) and vacuolation in (I). *Abbrev: C= chloroplast; L = lipid bodies; N = nucleus; S = starch grains; V = vacuole*

The observed vacuolation observed by day 14 (e.g., Figs 3.5 A-D) some parts of the cytoplasm and its contents (e.g., trichocysts, starch grains) were internalized by the enlarging body in N- and P- deplete cells (e.g., Figs 3.5 A-D). The areas of the cytoplasm that were included within a vacuole were seen to be amorphous, indicating the expected degradation. Inclusions resembling damaged membranes were observed inside the vacuoles (e.g., Figs 3.5 A-D).

None of the N- and P-deplete cells, over the two weeks of treatment monitored, showed the excessive vacuolization exhibited by cells sampled in the collapsing field bloom (chapter 2, section 2.3.3.1), where the cytoplasm, was mostly consumed by vacuoles with only a few organelles remaining.

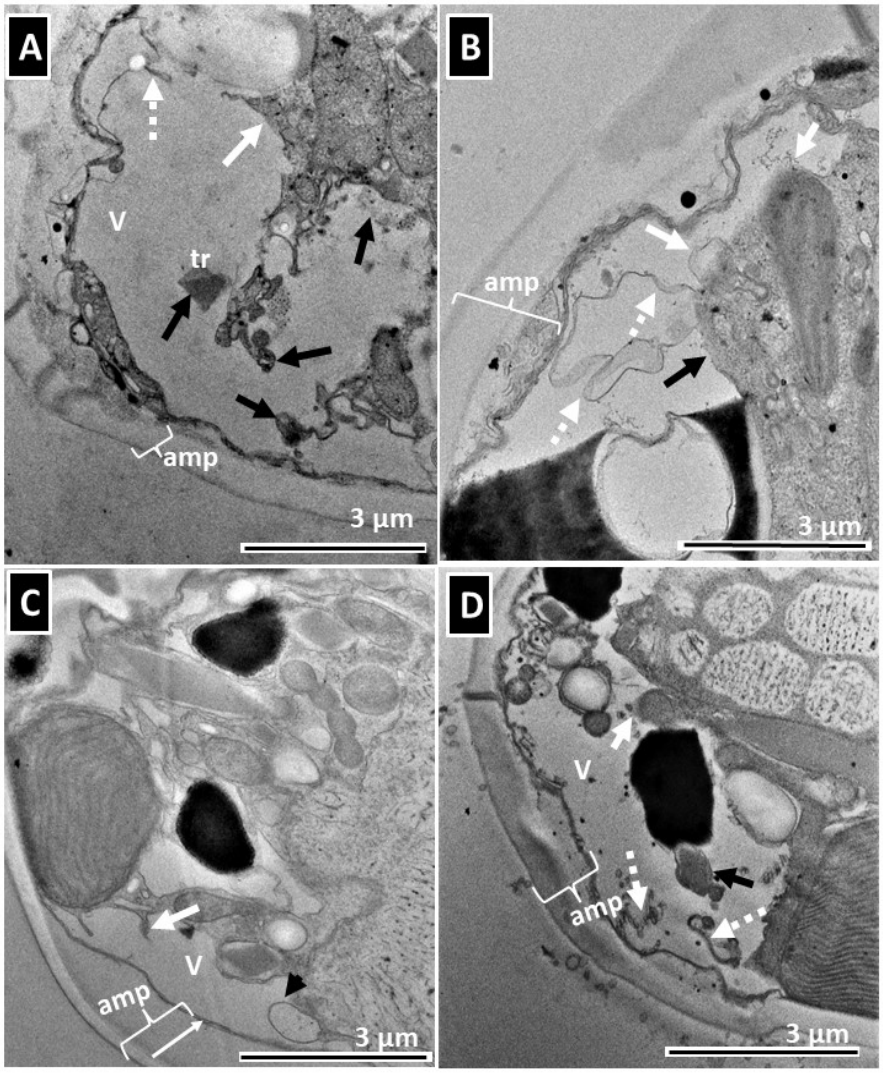


Figure 3.5 Vacuolation in N- and P-deplete cells on day 14 of treatment.

(A & B) Vacuolation in N-deplete cells. Note damage membranes including those of the amphiesma (broken white arrows), cytoplasmic contents and organelles e.g. trichocysts, internalized by the vacuoles (black arrows) and areas of the cytoplasm in direct contact with the vacuole indicating localised collapse of the tonoplast (white arrows).

(C & D) Vacuolation in P- deplete cells. Note damage membranes (broken white arrows) and cytoplasmic contents internalized by the vacuoles (black arrows). Note in (C) retraction of cytoplasmic membrane from the thecal plates (Thin white arrow). *Abbrev: amp=amphiesma; V = vacuole; tr= trichocysts.*

There was also damage to amphiesmal and other limiting membranes of organelles as the expanse of vacuole increased in both N-and P-deplete cells (e.g., Figs 3.6 A, B, C, D & F). Some of the organelles that were damaged as they came into contact with the vacuole were the nucleus and chloroplasts (e.g., Figs 3.6. B, D, E & F).

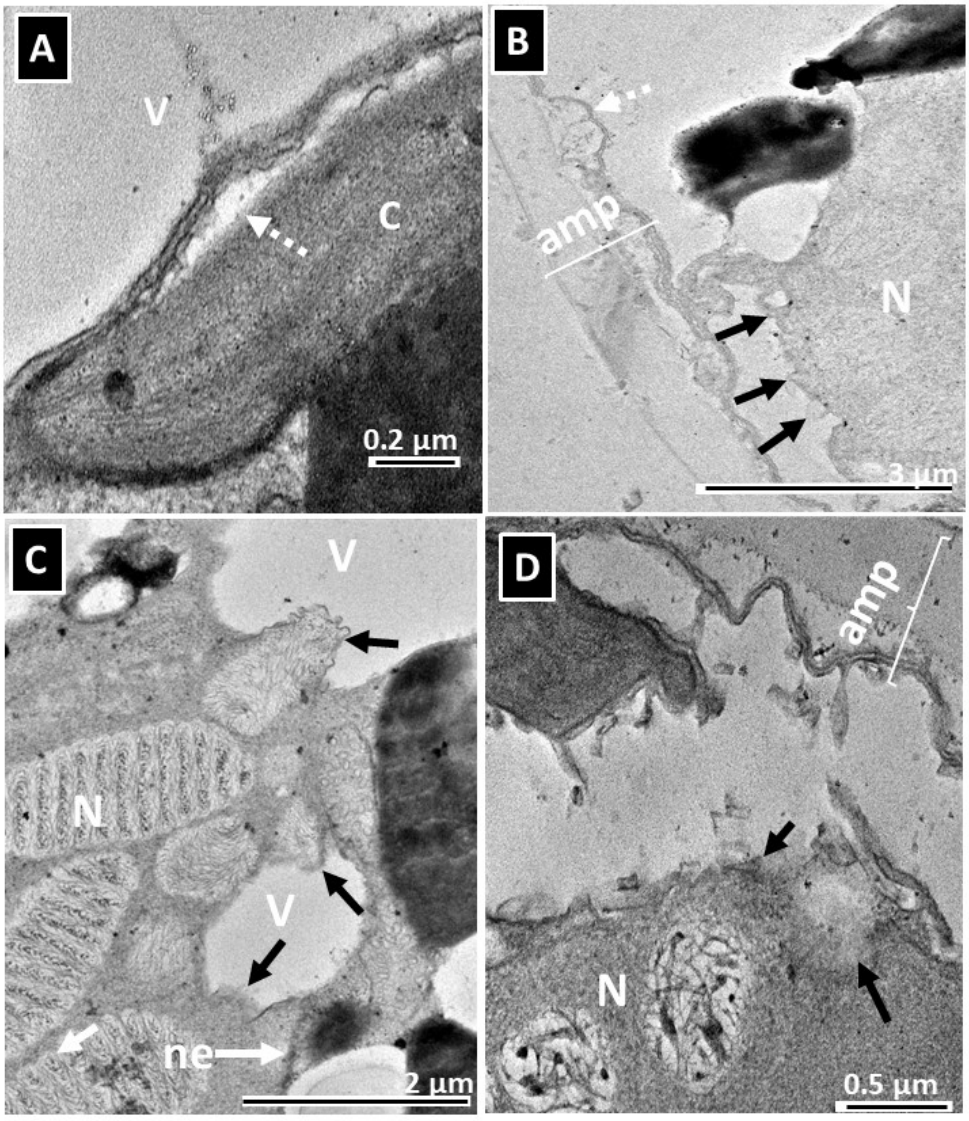


Fig. 3.6 Damage to the amphiesmal membranes and other organelles in N- & P - deplete cells 14 days after treatment.

(A) Damaged chloroplast envelope of N-deplete cells.

(B-C) Damage to amphiesmal membrane (broken arrow) and nuclear envelope (black arrows) in N-deplete cells. Note vacuole inside the nucleus in (C) and damage in parts of nucleus that are in contact (black arrows).
(D) Damage to amphiesmal membrane and nuclear envelope in P-deplete cells. *Abbrev: amp= amphiesma; C=chloroplast; N=nucleus; ne=nuclear envelope; V=vacuole.*

3.3.2.2 The pusule

The pusule in replete cells is bound by a double limiting membrane and inside this chamber there are numerous membranous vesicles also bound by a double membrane and surrounded by a vacuolar reticulum (e.g., Fig. 3.7 A). This condition was altered in N-deplete cells (n=25) cells after 7 days of treatment, there was an increase in the vacuolar space with membranous and amorphous inclusions (e.g., Fig. 3.7 B). After 14 days of treatment the pusule chamber was vacuolated with amorphous remnants of the pusule vesicles in N-deplete cells (e.g., Figs 3.7 C).

The pusule was also altered in P-deplete cells (n=25) after 14 days of treatment (Fig. 3.7 D).

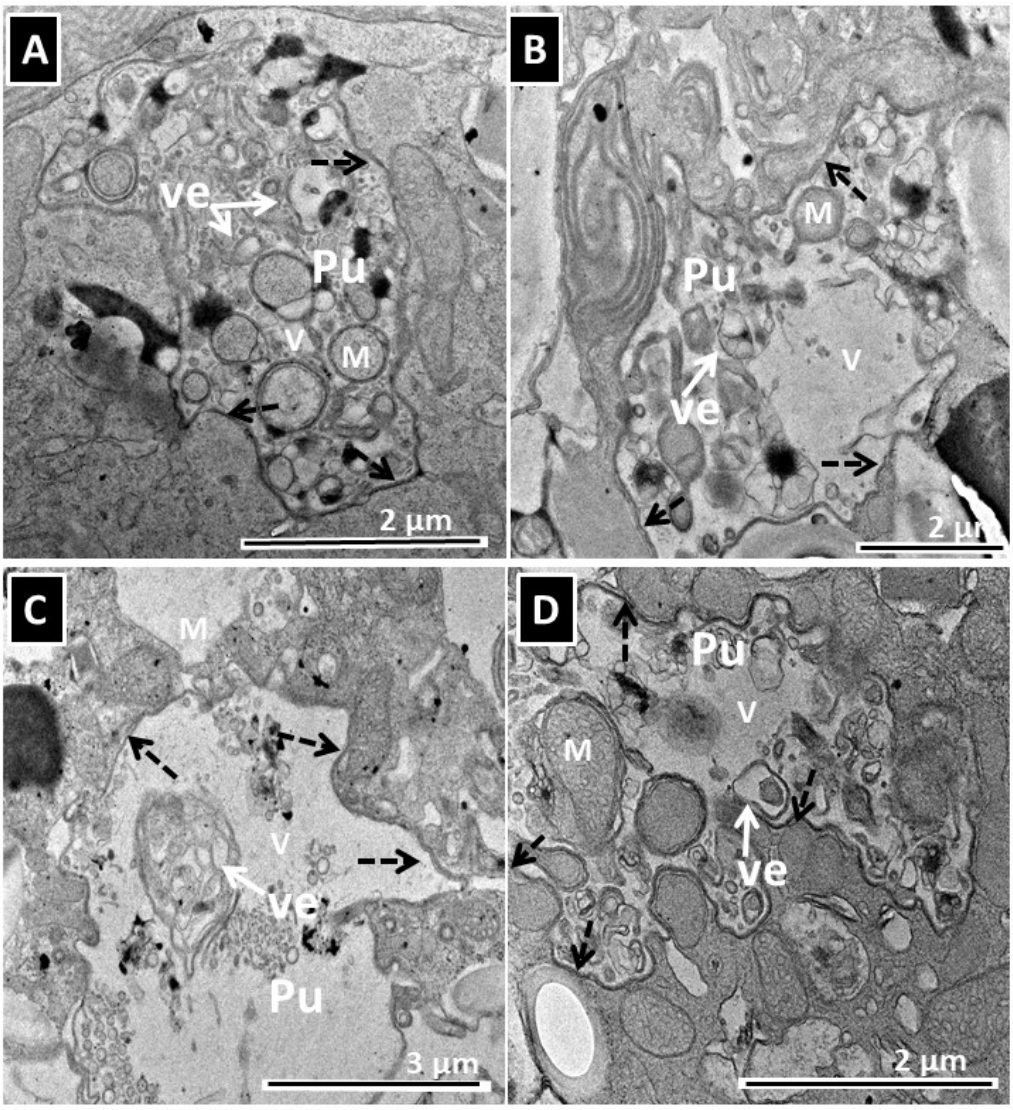


Figure 3.7 The pusule in Replete, N- and P -deplete cells over 14 days of treatment.

(A) Pusule bound by a double limiting membrane (broken black arrows), pusule vesicles (white arrows) and vacuolar reticulum in a replete cell.

(B) Pusule showing vesicles and an increased vacuolated space with membranous and amorphous inclusions (broken wite arrows) of N-deplete cells on day 7 of treatment

(C) Pusule showing an increased vacuolated space with remnants of pusule vesicles and membranous and amorphous inclusions (broken wite arrows) of N-deplete cells on day 14 of treatment, black arrows).

(D) Pusule showing pusule vesicles and an increased vacuolated space with membranous and amorphous inclusions (broken wite arrows) of P-deplete cells on day 14 of treatment. *Abbrev: M=mitochondrion; Pu=pusule; v=vacuole; ve=vesicles*.

3.3.2.3 The nucleus

The structure of the nucleus was intact in 90 % of the N-deplete cells during the two weeks of treatment. So, the nuclear envelope and the chromosome structure remained intact, the chromatin fibrils were tightly packed forming parallel arches (e.g., Fig. 3.8 D), a condition identical to that shown by the replete cells (e.g., Figs 3.8 B *cf* Figs 3.8 A).

Alterations in the remaining 10 % were restricted to breaks in the nuclear envelope (e.g., Fig 3.8 E). Breaks in the nuclear envelope were evidenced from day 3 of the treatment but, throughout the sampling period, they were never found in more than 10 % of the viewed cells (n =25). Such breaks were in the vicinity of nuclear pores, near lytic vacuoles, i.e., vacuoles containing membranous and electron dense material. Commonly, chromosomes abutting such breaks in the nuclear envelope protruded from the nucleus into the adjacent vacuoles. Elsewhere the nuclear envelope remained intact. These junctions between the nucleus and lytic vacuoles also were like that observed in the nuclei of field bloom organisms.

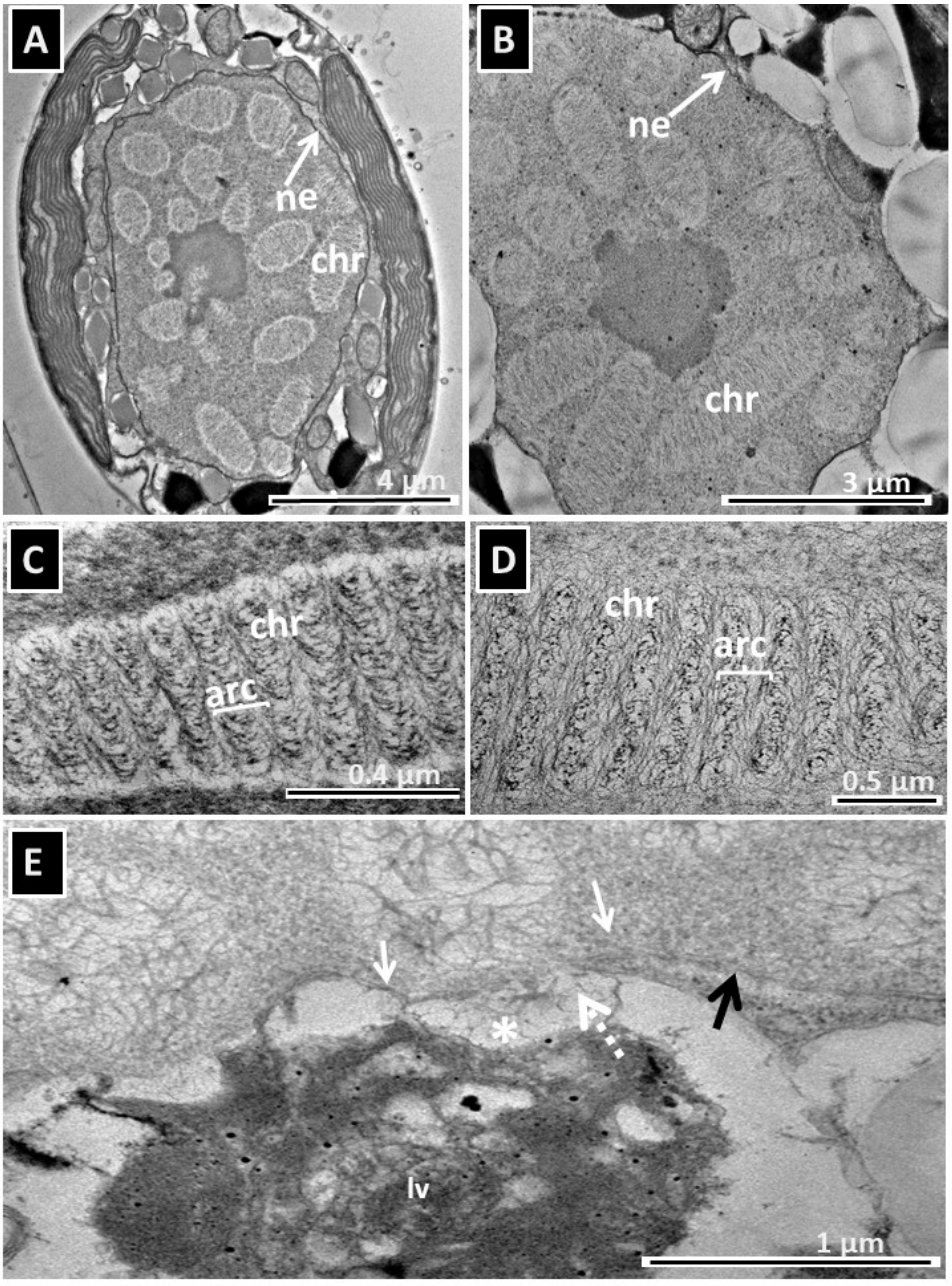


Figure 3.8 Nuclei of replete and N- deplete cells over 14 days of treatment.

(A) Replete cell nucleus showing the nuclear envelope and chromosome structure, on day 14.

(B) Intact nucleus in N-deplete cells on day 14.

(C & D) High magnifications of chromosomes from the nucleus of replete and N-deplete cells, respectively, showing the parallel arches formed by chromatin fibrils.

(E) Breaks in nuclear envelope (broken arrow) and chromosomes protruding into lytic vacuoles in N- deplete cells on day7. Nuclear envelope is visible before and after the break (white arrows). Some of the material inside the vacuoles had the same appearance as the chromosomes (white asterisks). These breaks were in the nuclear pore region (black arrows). *Abbrev: arc = arch*; *N=nucleus; ne=nuclear envelope; lv =lytic vacuole.*

The nuclear envelope remained intact in 98 % of P-deplete cells during the two weeks of treatment (e.g., Figs 3.9 A-C). In the remainder of the cells there was a loss in the integrity of the nuclear envelope as revealed in the N-deplete cells.

The compact structure of chromosomes was altered in more than 96 % of viewed cells (n=25) on all days of treatment in the P-deplete cells (e.g., Figs 3.9 A-C & E-G). Such changes affected all chromosomes within a nucleus. The uniform parallel arches observed in replete chromosomes were absent in P-deplete nuclei (e.g., Fig.3.9 D *cf* Figs 3.9 E-G). The loss of structure was progressive and, by day 7, the arches were not discernible (e.g., Fig. 3.9 G). Chromatin formed clumps in some areas and was observed as electron dense areas (e.g., Figs 3.9 E- G), which were absent in the chromosomes of replete nuclei (e.g., Fig. 3.9 D).

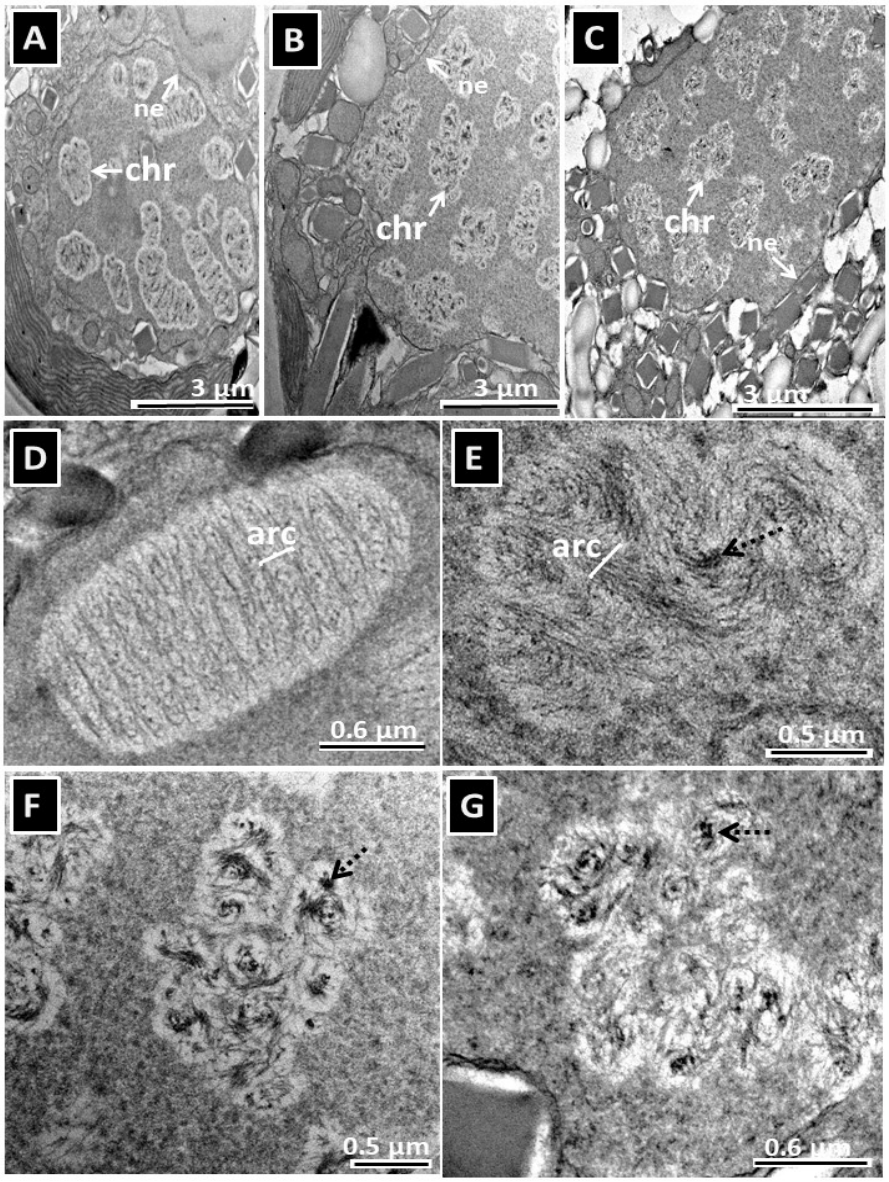


Figure 3.9 Nuclei of P-deplete cells and alterations to the chromosome structure in their nuclei over 14 days of treatment.

(A-C) P- deplete cell nuclei on days 3 to 14 showing an intact nuclear envelope. Note complete unravelling of the chromosome structure within the nucleus while the nuclear envelope remains intact.

(D) Higher magnification of a chromosome in the nuclei of P-replete cells, note the parallel arches and a lack of electron dense areas in the chromatin.

(E-G) Higher magnifications of chromosomes in the nuclei of P-deplete cells on days3, 7 and 14 of treatment. Note the absence of arches and the electron dense areas in the chromatin of P-deplete cells (broken arrows). *Abbrev: arc= arch*; *chr=chromosome; N=nucleus; ne=nuclear envelope.*

3.3.2.4 The endomembrane system

Ribosomes were observed on the cytoplasm and were also attached to ER membranes in replete cells in all days of treatment (e.g., Figs 3.10 A – D). Smooth and rough ER cisternae were also observed throughout the cytoplasm. There were localised dilations of some Golgi cisternae within a stack and these were confined to the trans cisternae (e.g., Figs 3.10 B–D). Multivesicular bodies (MVBs; these are single-membraned vesicles, which traffic proteins and lipids packaged in intraluminal vesicles from the *trans*-Golgi network to either the plasma membrane or the vacuoles; Chapter 2, section 2.1.6) were also present and originated from the trans-Golgi cisternae (e.g., Figs 3.10 B & D).

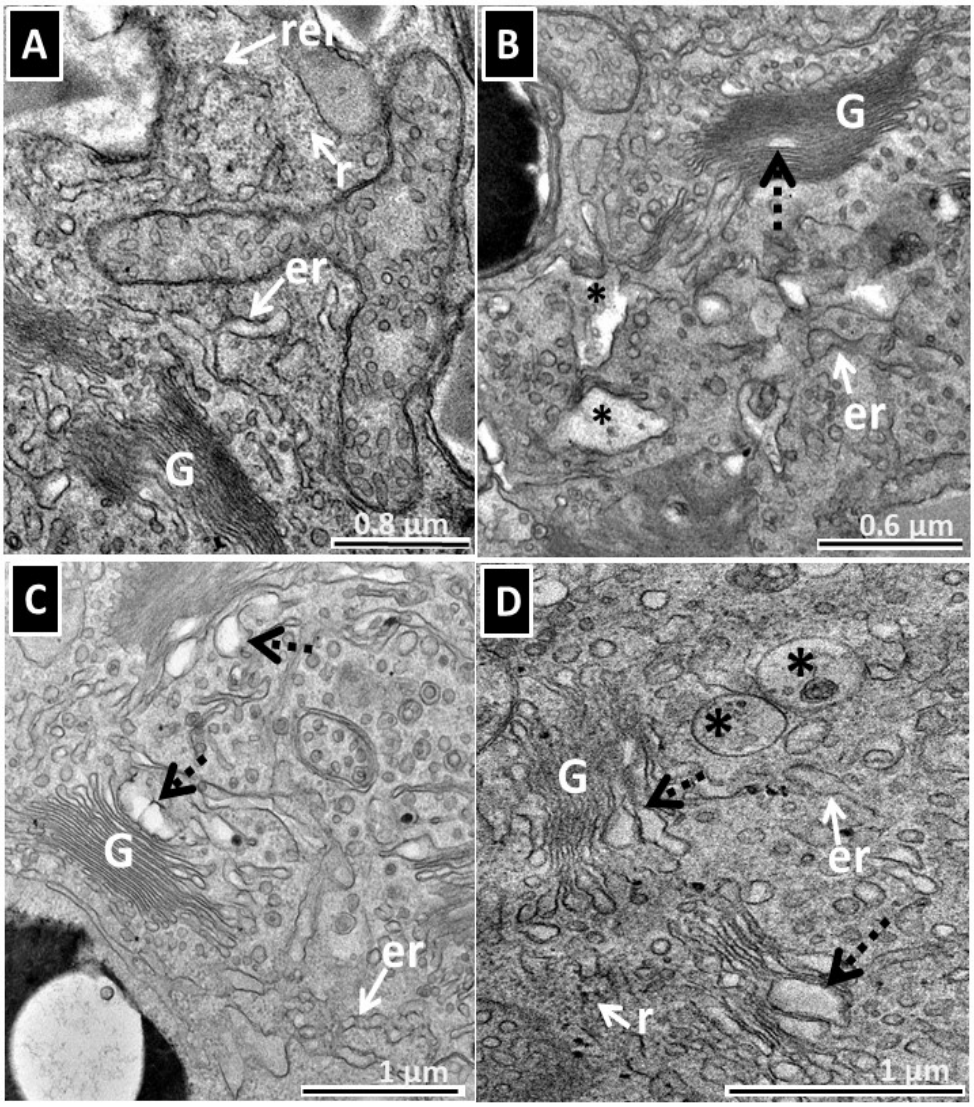


Figure 3.10 The endomembrane system in replete cells observed over 14 days of treatment.

(A-) Smooth and rough ER, ribosomes and Golgi bodies of replete cells on day 3 of treatment.

(B) Multivesicular bodies (black asterisks), swollen Golgi cisternae and ER on day 7 of treatment.

(C-D) Multivesicular bodies (black asterisks), swollen Golgi cisternae, ribosomes and ER on day 14 of treatment. *Abbrev: er=endoplasmic reticulum; rer = rough endoplasmic reticulum; r = ribosomes; G=Golgi bodies.*

Ribosomes were observed in the cytoplasm and were also attached to ER membranes in N-deplete cells in all days of treatment (e.g., Figs 3.11 A, C, D & E). The diameters of ER cisternae in N-deplete cells (n=25) were not significantly different ($p > 0.5$) relative to those of replete cells on all days of treatment (e.g., Fig. 3.11 A; Table 3.2). There were localised dilations of some Golgi cisternae within a stack in all N-deplete treatments (e.g., Figs 3.11 A – D). It was further noticed that in N-deplete cells the dilations affected both the intermediate and trans cisternae, whereas only the trans cisternae of replete cells were affected (e.g., Figs 3.11 A – D *cf* Figs 3.8 C & D). There was an upregulation in the number of MVBs in the Golgi region of N-deplete cells starting on day 3 of treatment (Figs 3.11 C-F; Table 3.2). The MVBs originated from the trans-Golgi region in all treatments.

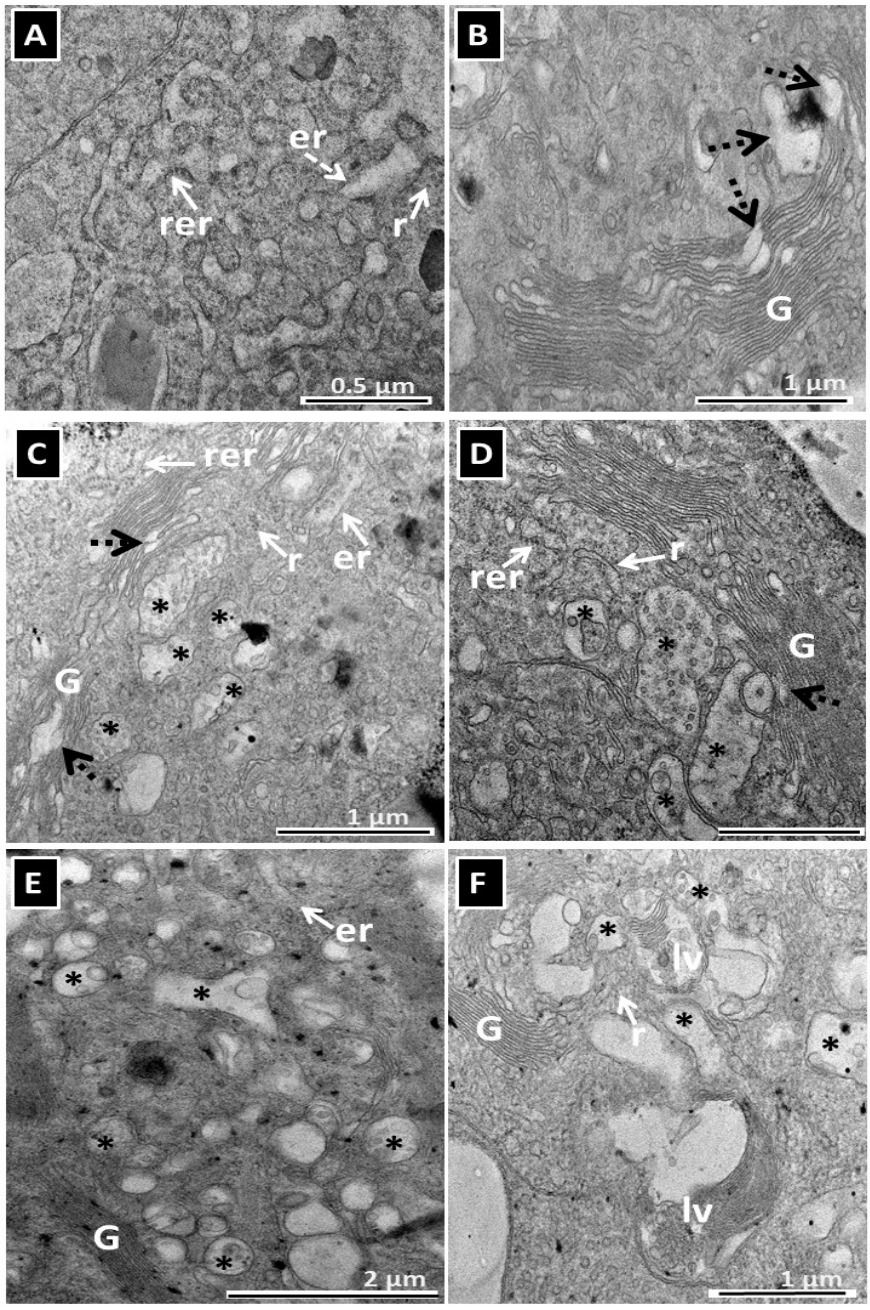


Figure 3.11 The endomembrane system in N-deplete cells observed over 14 days of treatment.

(A & B) Smooth and rough ER, ribosomes, Golgi bodies and MVBs (asterisks) of N-deplete cells on day 3, Note the dilated Golgi cisternae (broken black arrow). (C & D) Multivesicular bodies (black asterisks), swollen Golgi cisternae and ER on day 7 of treatment.

(E & F) Multivesicular bodies (black asterisks), Golgi cisternae, ribosomes and smooth and rough ER on day 14 of treatment *Abbrev: er=endoplasmic reticulum; rer=rough endoplasmic reticulum; r = ribosomes; G=Golgi bodies; MVB=multivesicular bodies.*

Ribosomes were observed in the cytoplasm and were also attached to ER membranes in P-deplete cells in all days of treatment (e.g., Figs 3.12 A, C, & D). The ER cisternae of P-deplete cells were not altered on all days of treatment. Localised dilations were observed in the transient and trans Golgi cisternae in these cells like those of N-deplete cells. (e.g., Figs 3.12 A- D *cf* Figs 3.9- A-C) on all days of treatment. An upregulation of MVBs was observed on days 7 and 14 (e.g., Figs 3.12 B -D).

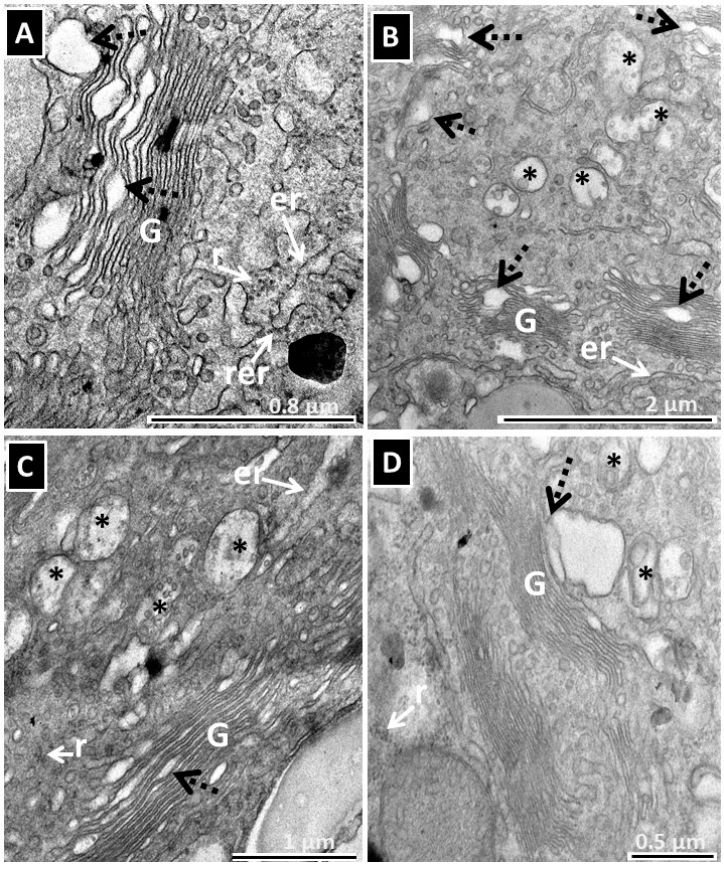


Figure 3.12 The endomembrane system in P-deplete cells observed over 14 days of treatment.

(A) Smooth and rough ER, ribosomes and Golgi bodies of P-deplete cells on day 3, Note the dilated Golgi cisternae (broken black arrow).

(B) Multivesicular bodies (black asterisks), swollen Golgi cisternae and ER on day 7 of treatment.
(C-D) Multivesicular bodies (black asterisks), swollen Golgi cisternae, ribosomes and ER on day 14 of treatment. *Abbrev*: *er=endoplasmic reticulum*; *G=Golgi bodies; rer= rough endoplasmic reticulum; r= ribosomes.*

3.3.2.5 Up-regulation of multivesicular bodies and lytic vacuoles

Multivesicular bodies were present in all treatments including the replete cells, but they were smaller and less abundant than in the nutrient deplete cells on corresponding days of treatment (e.g., Figs 3.13 A & B *cf* Figs 3.14 A-C; Table 3.2).

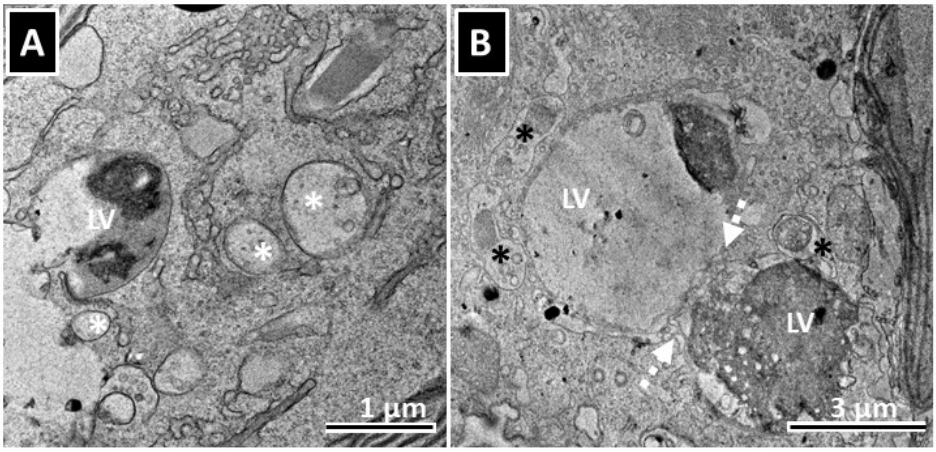


Figure 3.13 Multivesicular bodies (MVBs) in replete cells over a 14-day period.

(A) MVBs (white asterisks) in replete cells on day 3 of treatment containing ILVs.

(B) Lytic vacuoles in replete cells on day 14 of treatment containing electron dense material. Note contact between the membranes of the two lytic vacuoles (broken arrow). *Abbrev*: *LV =lytic vacuole.*

MVBs were present on all days of treatment in N-deplete cells (e.g., Figs. 3.14 A-C). The MVBs originated from the trans- Golgi region. The lytic vacuoles contained double membraned-structures, membranous materials, multilamellar structures and ILVs (e.g., Figs 3.14 B & C). Hemi-fusion between the limiting membranes of lytic vacuoles was observed and the coalescence formed bigger structures (e.g., Figs 3.14 B &C).

The MVBs and lytic vacuoles were like those reported in the cells of the field bloom (section 2.3.3.4). The lytic vacuoles are not part of the pusule and they differ because the pusule has double limiting membranes.

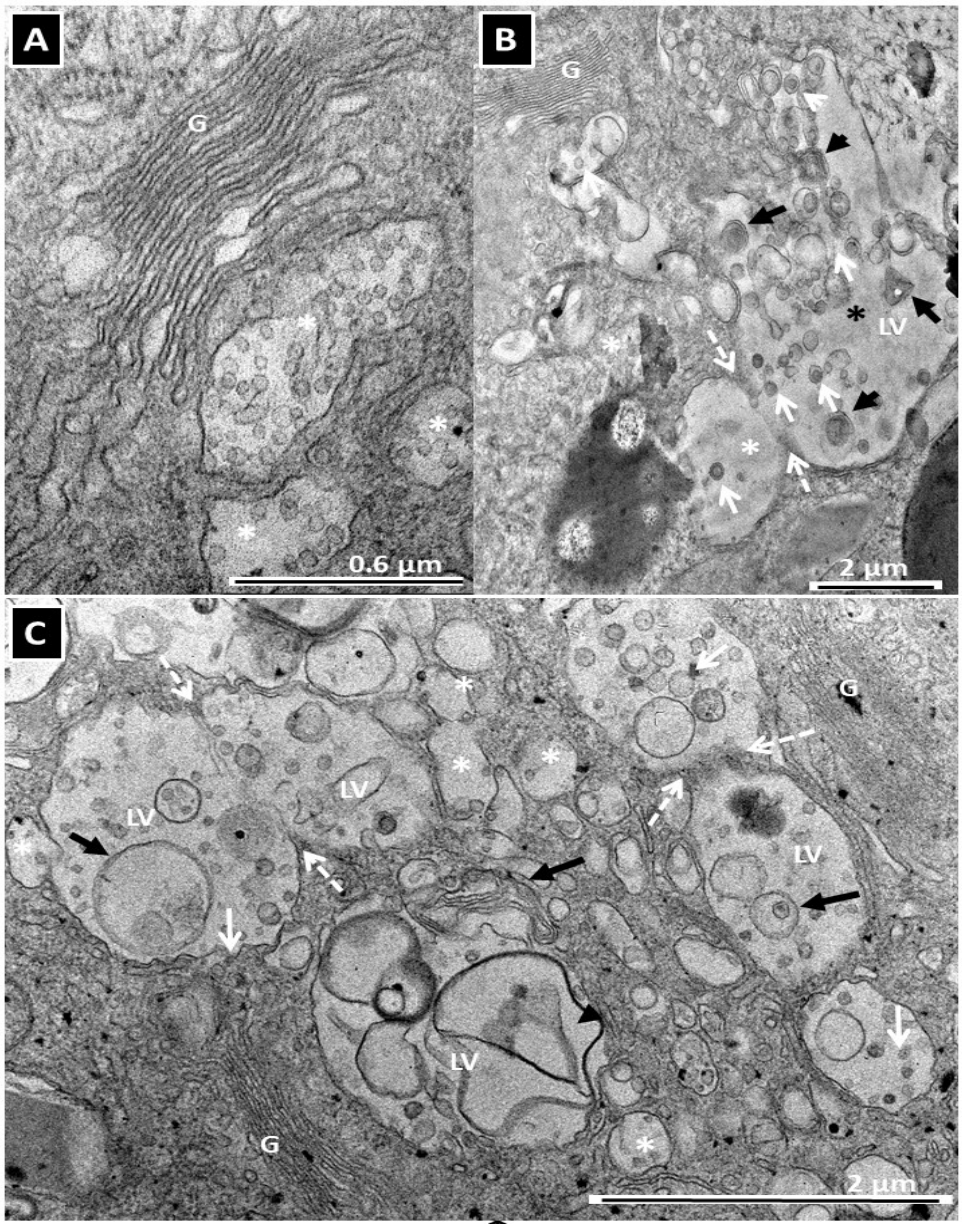


Figure 3.14 Multivesicular bodies (MVBs) in N-deplete cells over a 14-day period.

(A) MVBs (white asterisks) which contain intraluminal vesicles in N-deplete cells on day 3 of treatment.

(B & C) MVBs (white asterisks) on the cytoplasm and at the interface of Lytic vacuoles which contain both degraded materials (black arrows) and ILVs (white

arrows) observed from day 7 to 14 of treatment. Note hemi-fusion of limiting membranes of lytic vacuoles (broken white arrows) which indicates coalescence of the vacuoles. *Abbrev*: *G= Golgi bodies; LV=lytic vacuoles.*

Multivesicular bodies and lytic vacuoles were observed in P-deplete cells on all days of treatment (e.g., Figs 3. 15 A & B). The MVBs in the P-deplete cells were similar to those observed in the N-deplete cells (Figs 3.15 A & B *cf* Figs 3.14 A-D).

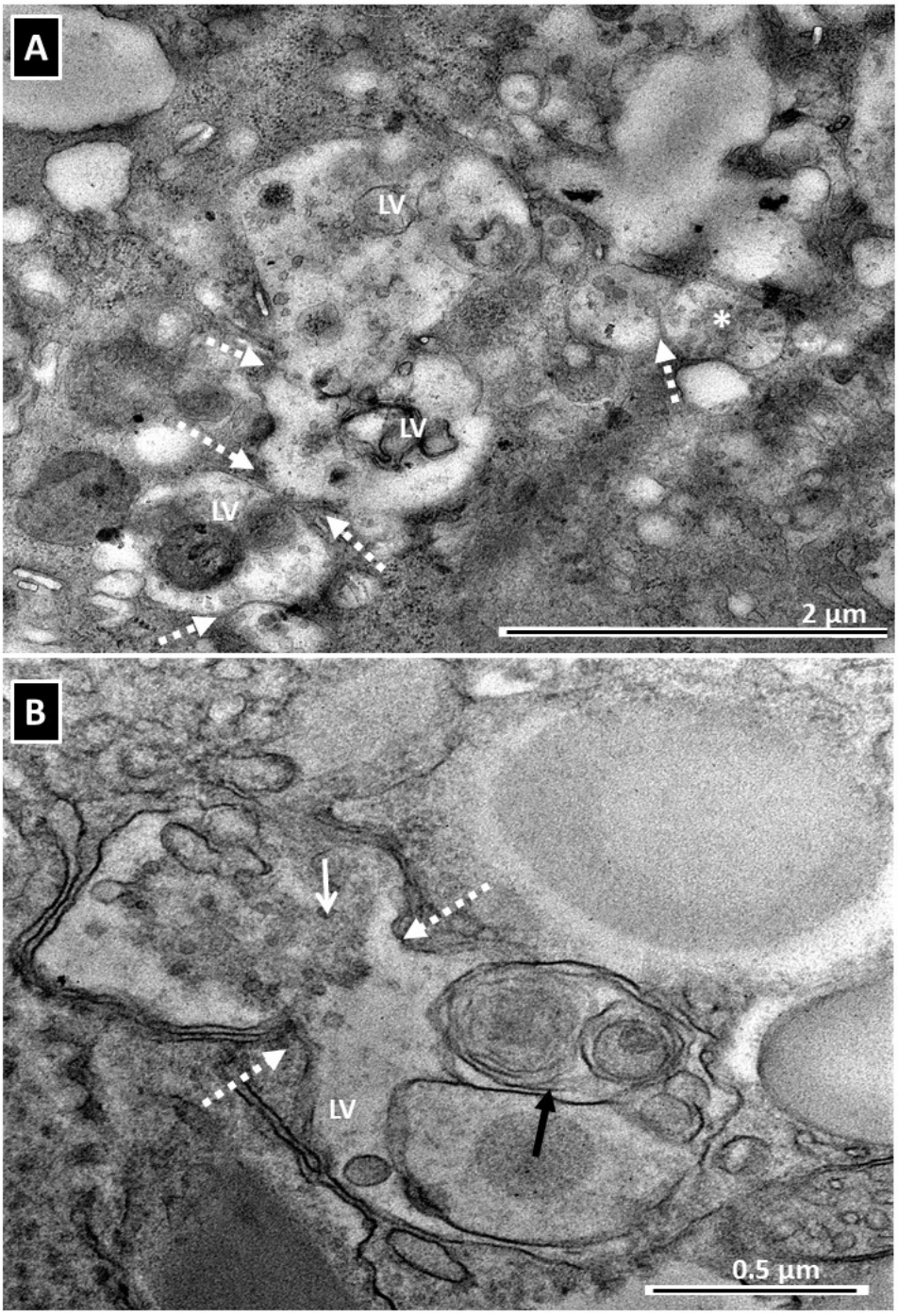


Figure 3.15 Multivesicular bodies (MVBs) in P-deplete cells over a 14-day period

(A) MVBs containing intraluminal vesicles (white asterisks) and lytic vacuoles containing double membraned-structures, membranous materials and ILVs in P-deplete cells on day 14 of treatment. Note hemi-fusion of limiting membranes (broken white arrows) of MVBs and lytic vacuoles.
(C &D) Lytic vacuoles containing partially degraded material and membranous materials and observed on day 14 of treatment. Note hemi-fusion of limiting membranes (broken white arrows) between MVBs. *Abbrev*: *G= Golgi bodies; LV=lytic vacuoles.*

3.3.2.6 Evidence of macro-autophagy

Double membraned structures derived from ER cisternae were observed on the cytoplasm forming cup-shaped and fully closed structures around organelles or parts of the cytoplasm (Figs 3.16 A-D). At times tubular ER derived structures sequestered a portion of the cytoplasm (Figs 3.16 C). Electron translucent regions in the lumen of the double membrane and parts of the cytoplasm and its contents were observed (Figs. 3.16 A-D).

ER derived membraned structures sequestering a portion of the cytoplasm and degraded organelles were also reported in the cells of the field bloom (section 2.3.3.6)

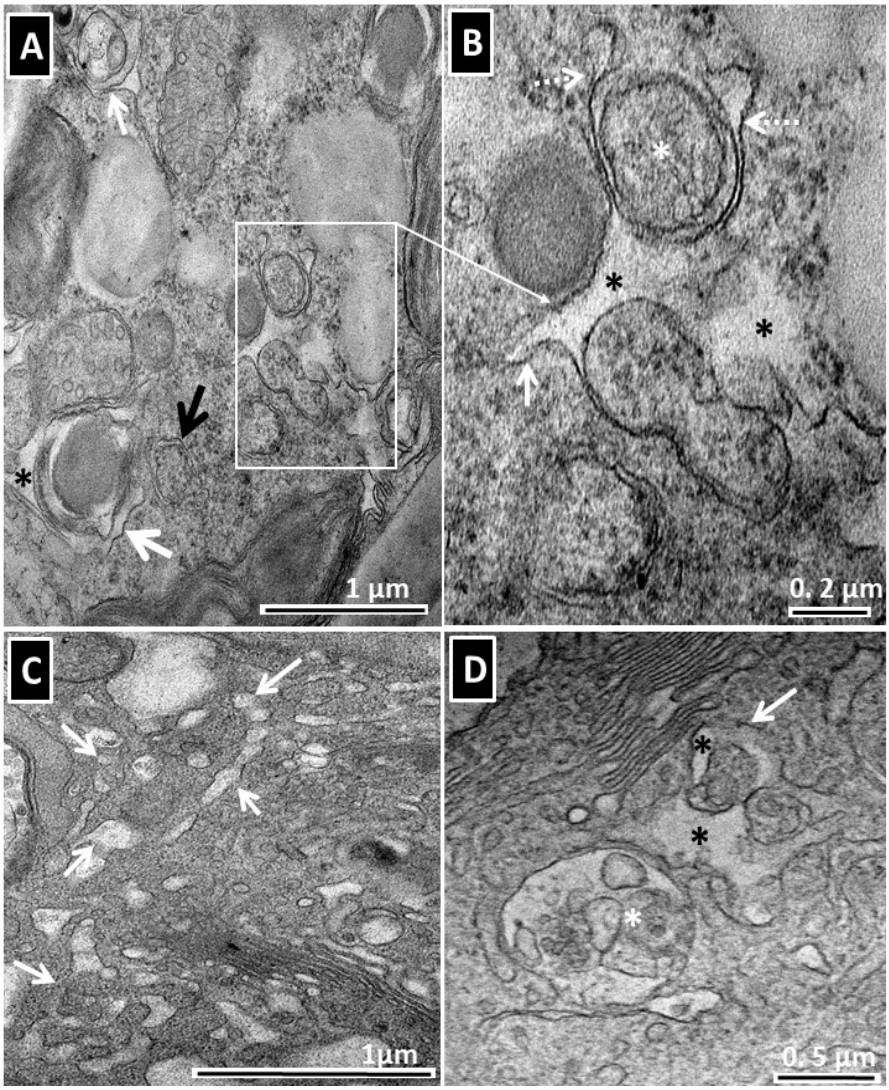


Figure 3.16 Macro-autophagy in N-deplete cells over a 14-day period.

(A & B) Double-membrane structures derived from ER (white arrows), forming a cup-like structure (broken white arrows) around a mitochondrion (white asterisks). Note the electron translucent areas in the lumen of double membranes and parts of the cytoplasm (black asterisks).

(C) ER tubules sequestering parts of the cytoplasm (white arrows).

(D) Double membranes sequestering parts of the cytoplasm and organelles (white arrow). Note electron translucent areas inside the membrane lumen and parts of the cytoplasm (black asterisks). Also, note the single membraned lytic vacuole in the vicinity (white asterisks). *Abbrev: M=mitochondrion.*

Double-membraned structures were observed in P-deplete cells that were like those in N-deplete cells (Figs. 3.17 A-D).

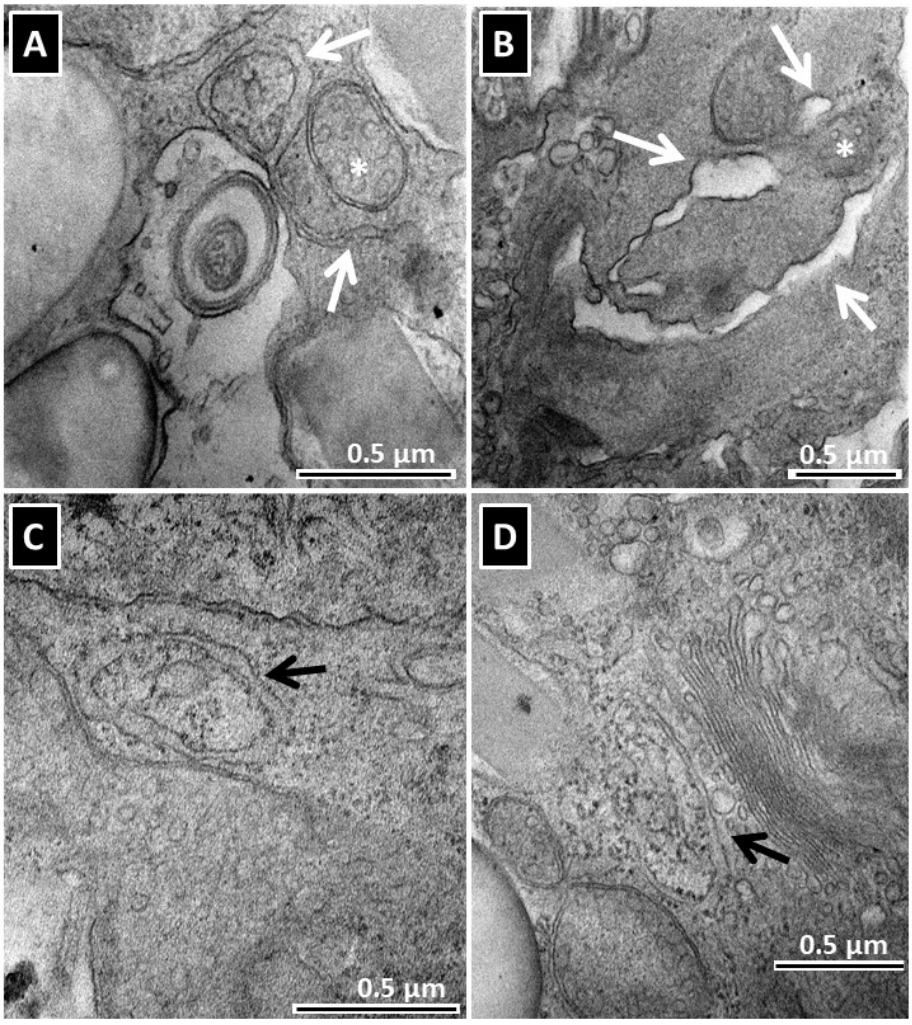


Fig. 3.17 Macro-autophagy in P-deplete cells over a 14-day period

(A) Double-membrane structures derived from ER (white arrows), sequestering parts of the cytoplasm and mitochondrion (white asterisks).

(B) ER tubules sequestering parts of the cytoplasm (white arrows) and a mitochondrion.

(C & D) Rough ER cisternae forming closed double membrane structures (black arrows) engulfing parts of the cytoplasm. *Abbrev: M=mitochondrion.*

3.3.2.7 Multilamellar bodies and membranous structures

Multilamellar bodies formed by concentric membrane whorls were observed in the cytoplasm of N-deplete cells (Fig. 3.18 A). The concentric membranes occasionally surrounded parts of the cytoplasm or degraded organelles which were difficult to discern (e.g., Figs 3.18 A & D). Membrane stacks which also formed whorls were in the cytoplasm in the vicinity of vacuoles (e.g., Figs 3.18 B & C). Multilamellar bodies were also observed at the interface of vacuoles while still in contact with the cytoplasm and inside vacuoles (e.g., Figs 3.18 C & D).

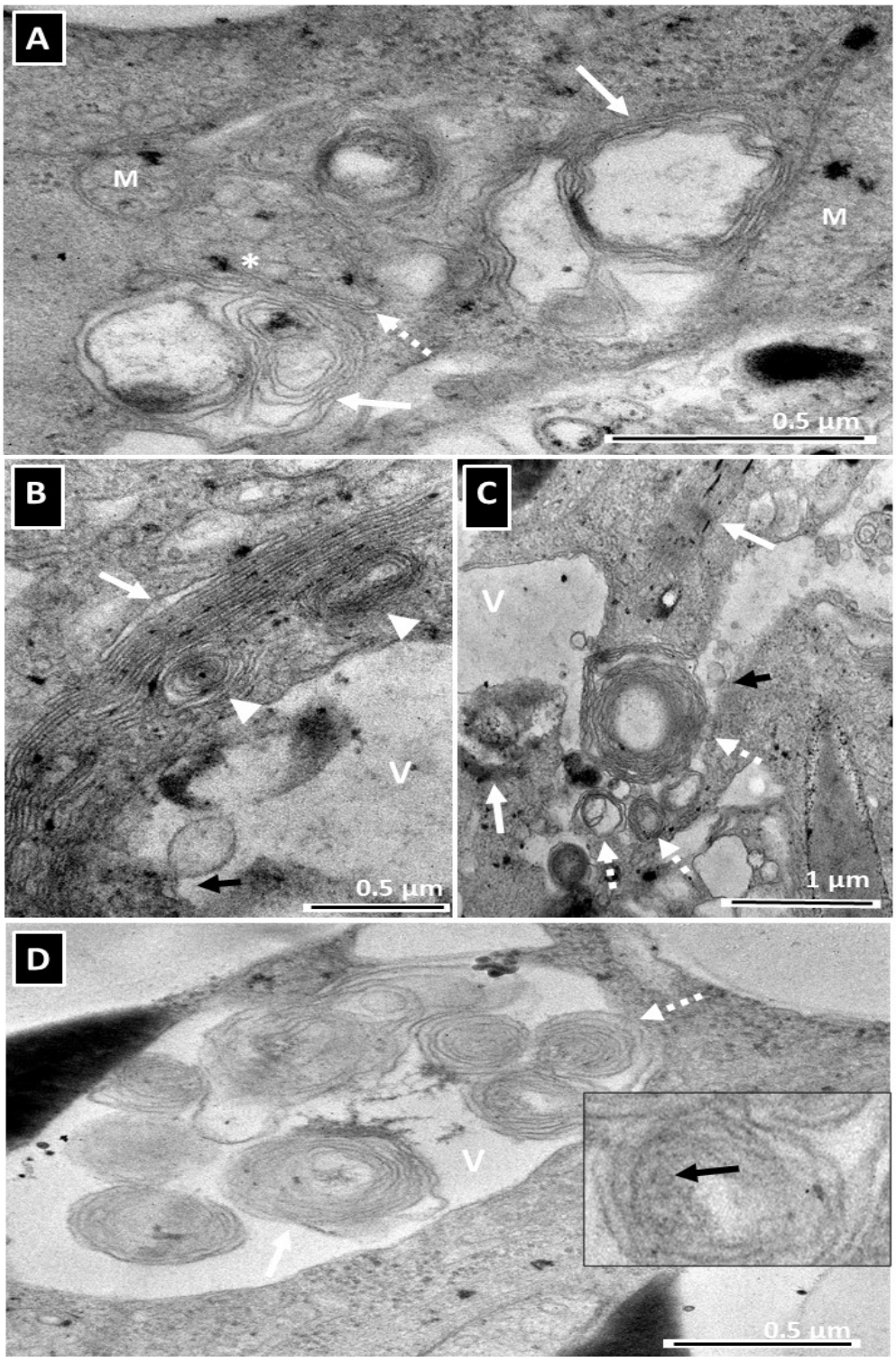


Figure 3.18 Multilamellar bodies in N-deplete over 14 days of N starvation.

(A) Multilamellar bodies inside vacuoles with connections to the cytoplasm (white arrows) in N-deplete cells during the 14 days of treatment. Note concentric membranes (broken white arrow) forming around a mitochondrion with swollen cristae (asterisks).
(B & C) Membrane stacks (white arrows) forming whorls (arrow heads) and multilamellar bodies in the cytoplasm and at the interface of vacuoles while still connected to the cytoplasm.
(D) Multilamellar bodies inside vacuoles (white arrows) while some are still connected to the cytoplasm (broken white arrows) of N-deplete cells. Insert in (E) note what appears to be a degraded mitochondrion surrounded by the concentric whorls. *Abbrev: M=mitochondrion; V= vacuoles.*

Membranous clumps which did not form concentric whorls were observed in the cytoplasm of the N-deplete treatment and were not observed in P-deplete cells (e.g., Fig. 3.19 A). They were also inside vacuoles with fibrillar attachments to the cytoplasm and near lipid bodies (e.g., Fig. 3.19 B & C).

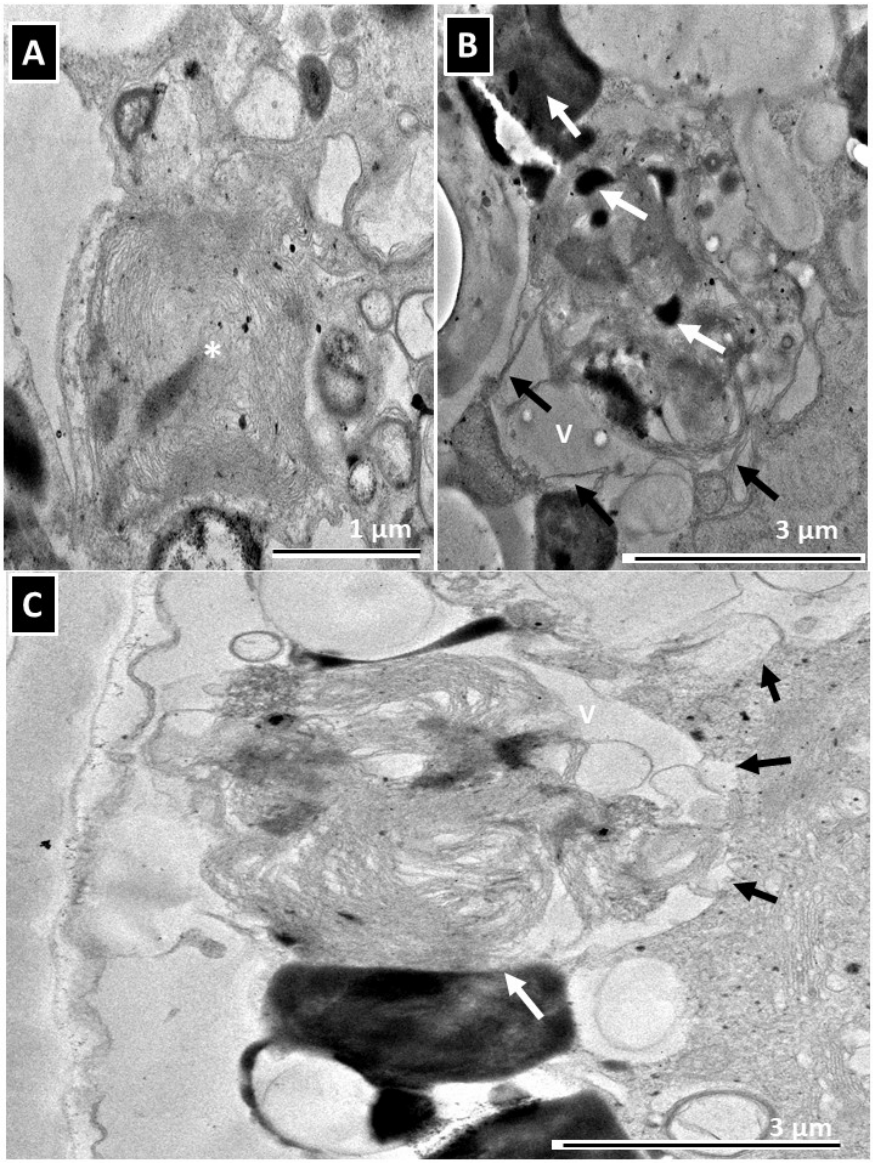


Figure **3.19** Membranous clumps in N-deplete over 14 days N starvation.

(A) Membranous clumps on the cytoplasm
(B &D) Membranous clumps inside vacuoles with attachments to the cytoplasm (black arrows) and lipid bodies (white arrows). *Abbrev: V= vacuoles.*

Multilamellar bodies were also observed in P-deplete cells in the cytoplasm (Fig. 3.20 A). The concentric membranes occasionally surrounding parts of the cytoplasm or degraded organelles which were difficult to discern (Figs. 3.20 A, B

&D). They were also observed at the interface of vacuoles while still in contact with the cytoplasm and inside vacuoles (Figs. 3.20 B-D).

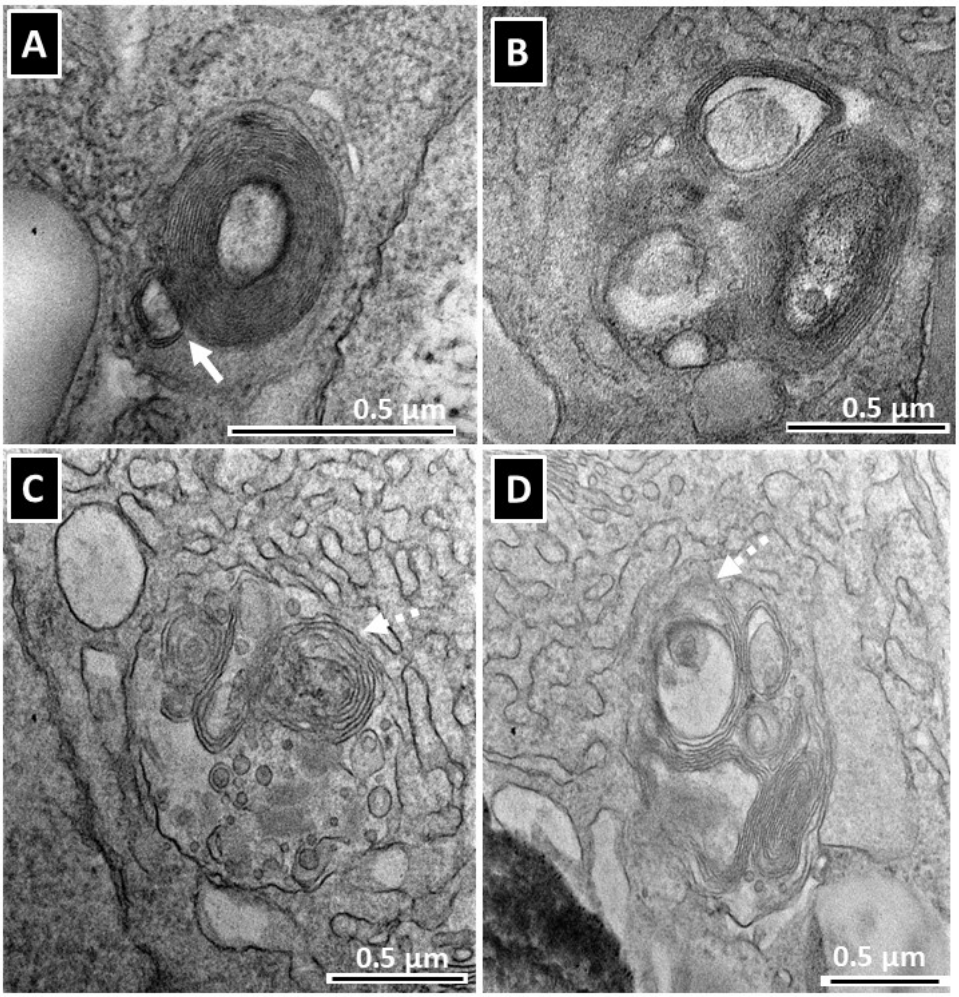


Figure 3.20 Multilamellar bodies in P-deplete cells over 14 days of P starvation.

(A) Multilamellar bodies in the cytoplasm of P-deplete cells during the 14 days of treatment.
(B-D) Multilamellar bodies inside vacuoles (white arrows). Note contact between the membranous coils and the adjacent cytoplasm (broken white arrows).

3.3.2.8 Mitochondria

The outer and inner mitochondrial membranes like those of replete cells, remained intact in 67 % of all observed, sectioned profiles of mitochondria in N-deplete cells

(n = 63), (e.g., Fig. 3.21 A).

Damage to the outer membranes of mitochondria was observed in 27 % sectioned profiles of mitochondria in N-deplete cells on days 3 and 7 of treatment (e.g., Figs 3.21 B-D). The damage which was localized in parts of the outer membrane resulted in the herniation of the inner membrane. Herniated mitochondrial profiles were also observed in cells sampled from the bloom (section 2.3.3.5).

Partially degraded mitochondrial profiles in N-deplete cells were occasionally observed inside lytic vacuoles after 14 days of N starvation (e.g., Figs 3. 21 E).

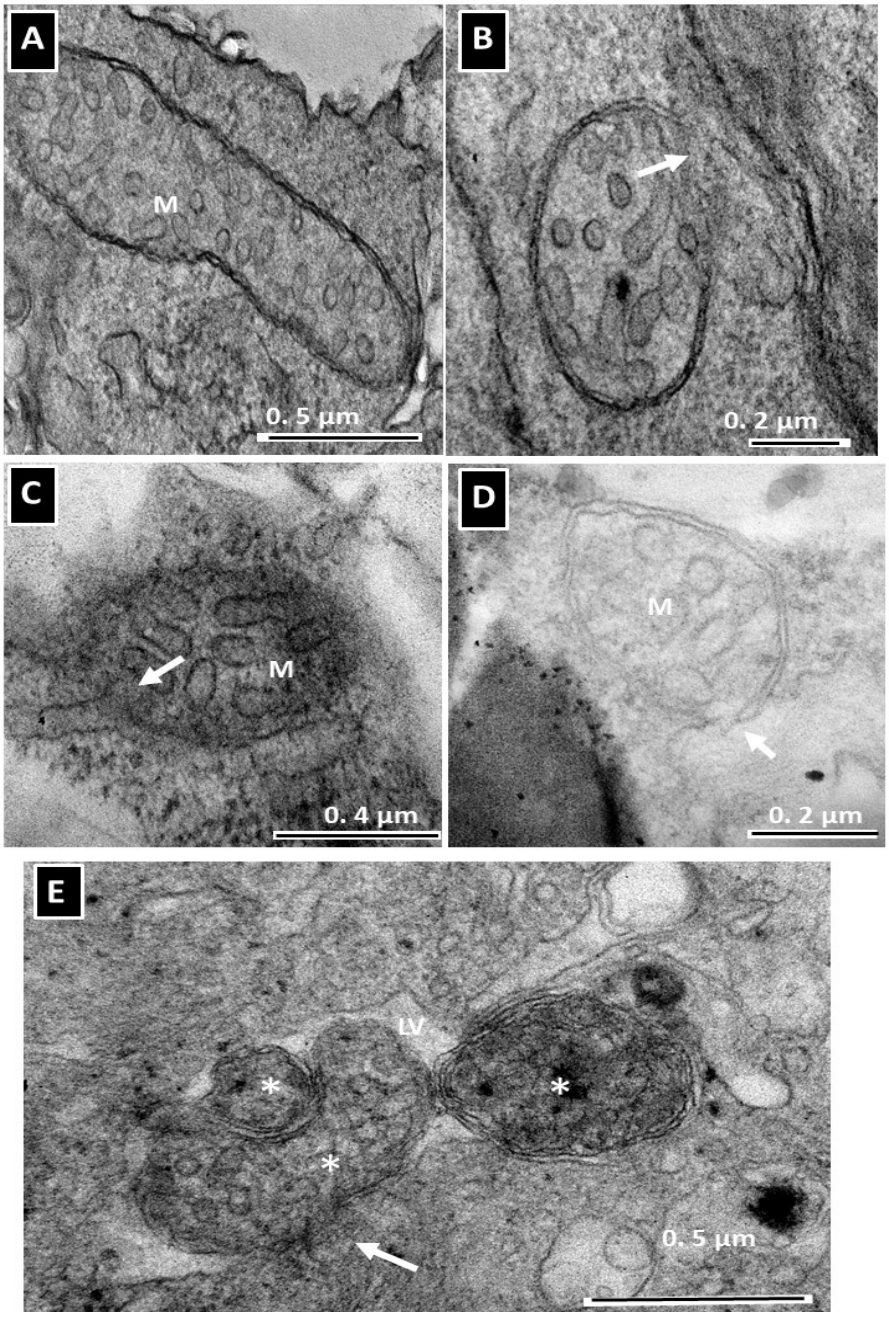


Figure 3.21 Alterations to the mitochondria structure in N -deplete cells over 14 days of treatment.

(A) Intact mitochondrion from a replete cell.

(B-D) Mitochondria in N-deplete cells with breaks in the outer membrane resulting in herniation of the inner membranes (white arrows).

(E) Partial degraded mitochondrial profiles (asterisks) were inside lytic vacuoles. Note the herniation of the inner membrane of a mitochondrion that is inside the vacuole (white arrow). *Abbrev: M=mitochondrion; LV= lytic vacuoles.*

The outer and inner mitochondrial membranes like those of replete cells, remained intact in 47 % of all observed, sectioned profiles of mitochondria in P-deplete cells (n = 57; e.g., Fig. 3.21 A). Alterations to the outer and inner membranes of profiles in 23 % mitochondria of P-deplete cells were observed on day 3 of treatment and was like what was observed in the N-deplete cells (e.g., Figs 3.22 A & B *cf* Figs 3.21 B-D).

In addition, swelling of the cristae of mitochondrial profiles while the outer membrane remained intact was observed in 30 % of sectioned profiles on day 14 of treatment (e.g., Figs 3.22 C & D). Partially degraded mitochondrial profiles were observed inside lytic vacuoles on days 7 and 14 of treatment. (e.g., Figs 3.22 E & F).

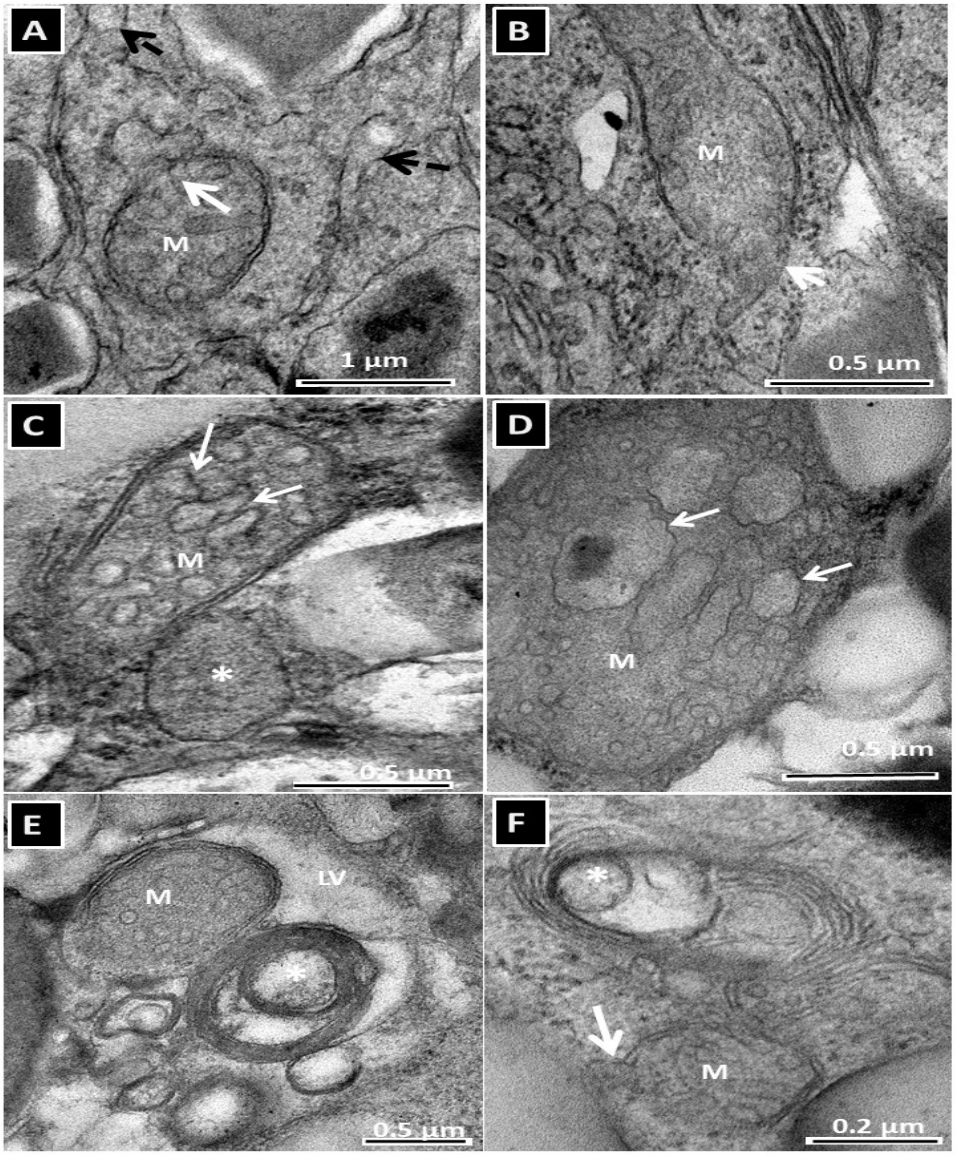


Figure 3.22 Alterations to the structure of mitochondria in P-deplete cells over 14 days of treatment.

(A & B) Mitochondria in P-deplete cells with breaks in the outer membrane (white arrows) resulting in herniation of inner membranes. In (B) note double membrane structure forming around mitochondrion (black broken arrows).

(C & D) Swollen mitochondrial cristae (white arrow) while the outer membrane remains intact. In (C) note the single membrane structure which could be a degenerating mitochondrion (asterisk).

(E & F) Partial degraded mitochondrial inside lytic vacuoles. Note mitochondria surrounded by multilamellar structures inside lytic vacuoles (asterisks). In (D) note mitochondrion surrounded by multilamellar structures inside lytic vacuole (asterisk) and another with herniated inner membrane (white arrow). *Abbrev: M=mitochondrion; LV=Lytic vacuoles.*

3.3.2.9 Single membraned structures

Single- membrane organelles which could be altered mitochondrial profiles were present in N-deplete P- deplete cells (e.g., Figs 3.23 A-D). What appears to be remnants of cristae were visible on the surface (e.g., Figs 3.23 A-D). A similar structure is observed in Fig. 3.22 (C).

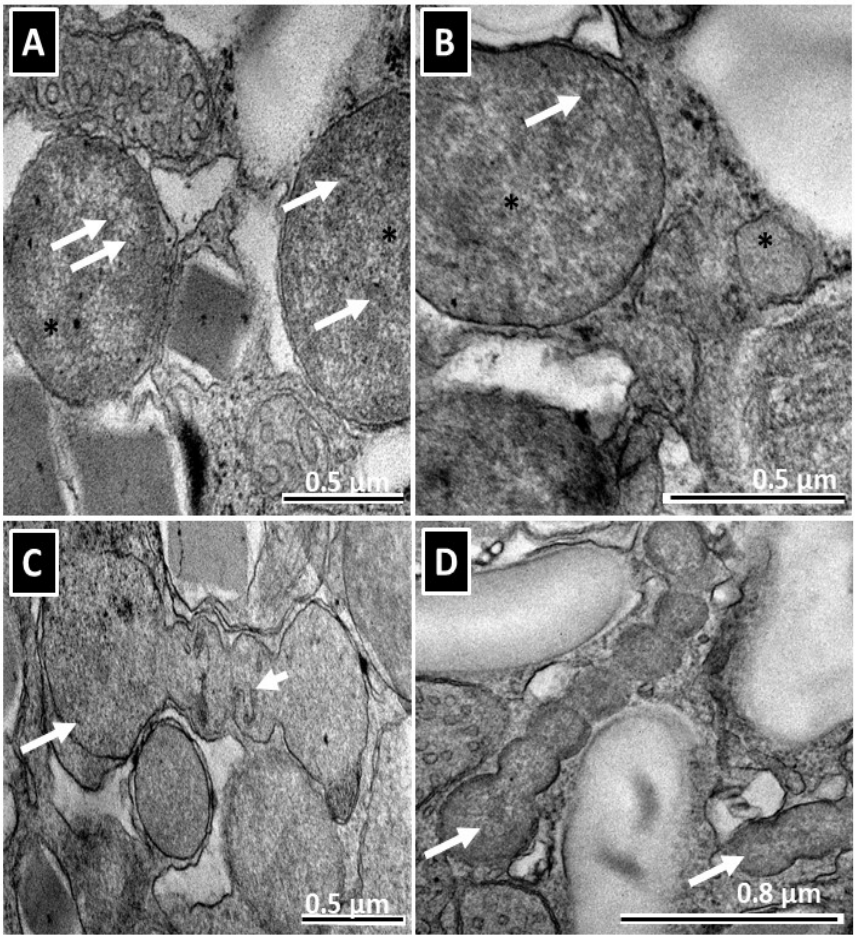


Figure 3.23 Single membraned structures in N-and P- deplete cell over 14 days of treatment.

(A&B) Single-membraned organelles in N-deplete cells. Note what appears to be cristae (white arrows).
(C & D) Single-membraned organelles in P-deplete cells. Note what appears to be cristae (white arrows)

3.3.2.10 Chloroplasts

The structure of chloroplast in replete cells was intact on all days of treatment (e.g., Fig. 3.24 A). Likewise, there were no changes in chloroplasts of N-deplete cells relative to those of replete cells on day 3 of treatment, however sites of contact between the chloroplast envelope and lipid bodies were observed on days 3 and 7 (e.g., Fig. 3.24 B).

Thylakoid membranes in 97 % of all observed, sectioned chloroplasts in N-deplete cells were compressed because of the accumulated starch grains and lipid droplets in the cytoplasm on day 7 (e.g., Figs 3.24 C). The width of thylakoid membrane lumen decreased significantly ($p < 0.01$) relative to that of replete chloroplasts on day 7 (Table 3.4).

By day 14 all chloroplasts were altered, this was observed as breaks in the envelope (e.g., Figs 3.24 D & E). Occasionally the affected chloroplasts were devoid of thylakoid membranes, or they were fragmented and the chloroplasts were left with a few thylakoid membranes (e.g., Figs 3.24 D & E).

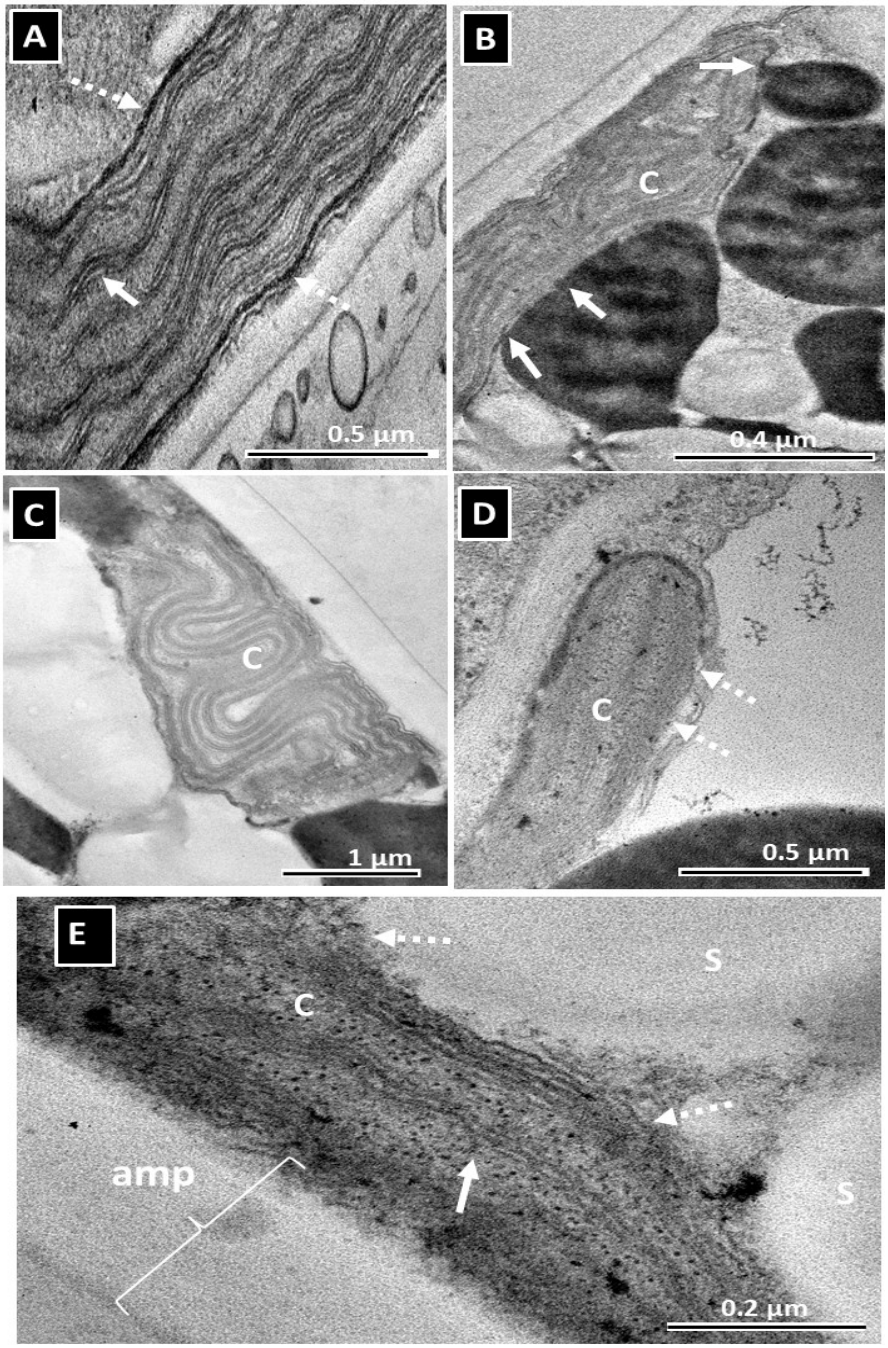


Figure 3. 24. **C**hloroplast structure in replete and N-deplete cells over 14 days

(A) Chloroplast structure in a replete cell, showing normal three thylakoid-stacking pattern (white arrow) and intact chloroplast envelope (black broken arrows).

(B) Chloroplast envelope and lipid bodies sites of contact (white arrows).
(C) Chloroplast profiles showing compression of thylakoid membranes resulting from accumulated starch and lipid reserves (black arrows) in N-deplete cells on day 7.
(D & E) Chloroplast profiles showing damage to the envelope (white broken arrows), and fragmented thylakoid membranes (white arrows) in N- deplete cells on day 14. *Abbrev: C=chloroplast; S=starch; V=vacuole.*

There were changes on chloroplasts of P-deplete when compared to those of replete cells, evidence as localized thylakoid lumen dilations on days 3 and 7 of treatment (e.g., Figs 3.25 B– D *cf* Fig. 3.25 A). The width of thylakoid membrane lumen was dilated and was significantly different ($p > 0.05$) relative to that of replete and N-deplete chloroplasts (Table 3.4).

There was damage to the chloroplast envelope and thylakoid membrane fragmentation and chloroplasts were amorphous on day-14 of treatment (Figs 3.25 E & F).

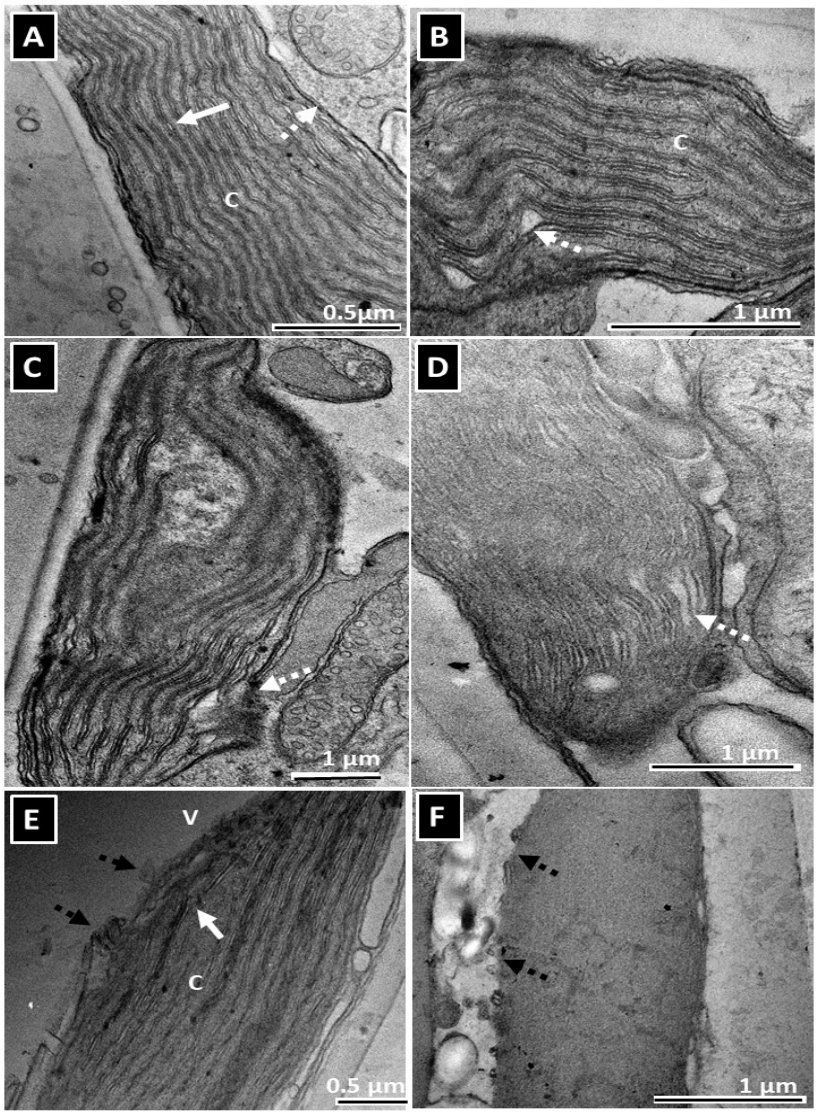


Figure 3.25 **C**hloroplast structure in P-deplete cells on days 3, 7 and 14.

(A) Chloroplast profile in P-replete cell showing no damage to envelope (broken white arrows) and thylakoid membranes (white arrows) on days 3 and 7 of treatment.

(B-C) Chloroplast envelope and lipid body site of contact (white arrows).

(D) Chloroplast profile in P-deplete cells showing damage to the envelope (broken arrow heads) while the thylakoid membranes are not damaged (white arrow). *Abbrev: C=chloroplast; S=starch; V=vacuole.*

3.3.3 Morphometric measurements of ultrastructure

Table 3.1. Proportion of vacuolated cell surface

Treatment	Total surface area of cell Mean ± SD (μm^2)	Vacuolated area of cell Mean ± SD (μm^2)	Proportion of vacuolated cell surface (%)	ANOVA, Tukey HSD; ($p \leq 0.05$) (n=25)
Replete	123.82± 50.79	7.50 ± 3.94	6	Replete vs N-deplete ($p < 0.01$)
N-deplete	161.15 ± 49.1	40.51±20.79	27	N-deplete vs P-deplete ($p > 0.05$)
P-deplete	128.44±51.29	23.71±16.66	24	P-deplete vs Replete ($p < 0.05$)

Table 3.2. Measurements of endomembrane organelles in Replete, N-& P-deplete cells

Treatments	ER lumen width Mean ± SD (µm) ANOVA, Tukey HSD ($p \leq 0.05$)	Number of MVBs per cell (n=25) Day3; Day14	Number of lytic vacuoles per cell (n=25) Day3; Day14	Surface area of lytic vacuoles Mean ± SD (μm^2)
Replete	0.06 ± 0.02 (p> 0.05)	1; 3	0; 3	1.17 ± 0.98
N-deplete	0.09 ± 0.13 (p> 0.05)	3; 8	2; 6	1.76 ±1.96
P-deplete	0.09 ± 0.16 (p> 0.05)	2; 5	2; 3	1.63 ± 1.16

Table 3.3. Structures associated with autophagy in cells after 14 days of nutrient depletion

Treatment	Total number of multilamellar bodies (n=25)	Total number of membranous clumps (n=25)	Total number of double membrane structures (n=25)
Replete	8	0	4
N-deplete	35	18	8
		0	5
P-deplete	10		

Table 3.4. Thylakoid width after 7 days of nutrient depletion

Treatment	Thylakoid width Mean ± SD (μm)	ANOVA, Tukey HSD ($p \leq 0.05$)
Replete	0.00966 ± 0.004	Replete vs N - deplete ($p < 0.05$)
N-deplete	0.00762 ± 0.003	N-deplete vs P-deplete ($p < 0.05$) P-deplete vs Replete ($p < 0.05$)
P-deplete	0.02176 ± 0.009	

3.3.4 DEVDase activity assay

A transfer of cultures to N-deplete medium resulted in a significant increase in relative fluorescence over replete cultures after only a day ($p < 0.05$; n=4) (Fig. 3.26). The observed increase in relative fluorescence observed in deplete cultures indicated that there was an increase in DEVDase activity in these cultures. However, the addition of a DEVDase inhibitor specific to DEVDase activity, was found to have no significant effect on the level of fluorescence, thus nullifying the assumption of DEVDase activity in the deplete cultures. The increase in fluorescence observed in deplete cultures after a day of treatment was not sustained and fluorescence levels decreased below the levels obtained in replete cultures on days 3 and 7 after treatment (Figs. 3.26). Again, the addition of a DEVDase inhibitor did not have a significant effect.

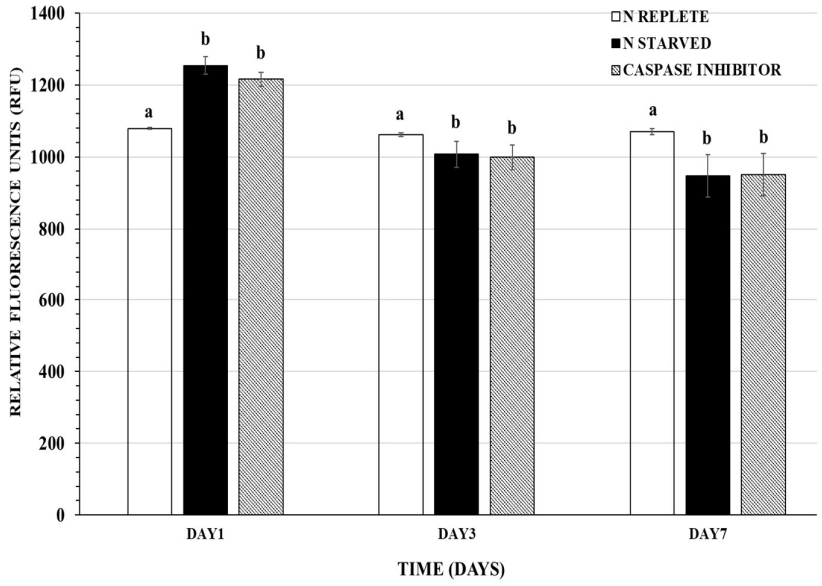


Figure 3.26 DEVDase activity on days 1, 3 and 7 following N starvation., Bars represent mean ± SE, n=6. Different letters represent significant differences at $p < 0.05$ using ANOVA and the Tukey Honest Significant Difference (HSD) post-test.

The DEVDase activity response of the P-deplete cells was similar to that observed in the N-deplete cells (Fig. 3.27 *cf* Fig. 3.26). An increase in relative fluorescence over

replete cultures was observed only on day 1 of treatment ($p < 0.05$; n=4) (Fig. 3.27), however the increase in fluorescence was not silenced by a DEVDase inhibitor.

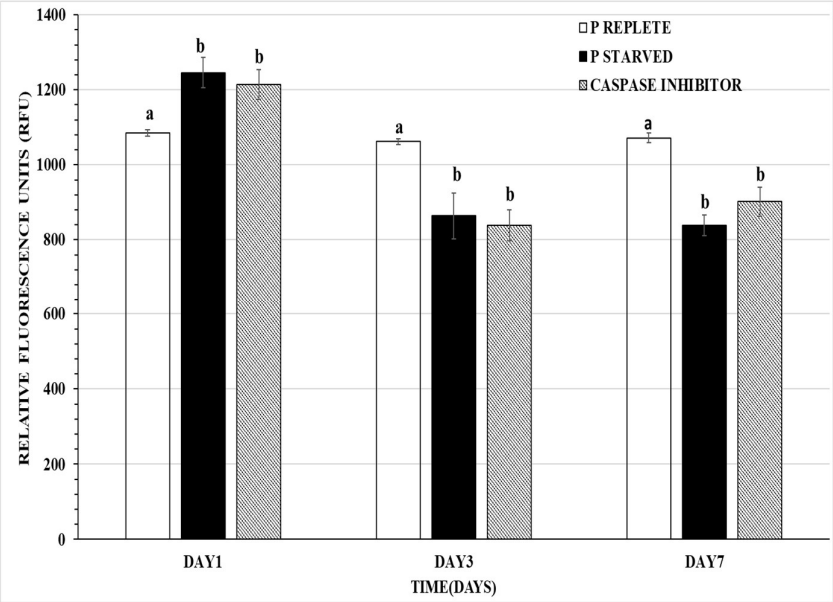


Figure 3.27 DEVDase activity on days 1, 3 and 7 following P starvation. Bars represent mean ± SE, n=6. Different letters represent significant differences at $p < 0.05$ using ANOVA and the Tukey Honest Significant Difference (HSD) post-test.

3.3.5 Reactive Oxygen Species (ROS)

3.3.5.1 Staining of N-deplete cells with DHR 123 fluorogenic probe

Both N-deplete and replete cells stained positively for the dihydrorhodamine (DHR) 123 fluorogenic probe. About 13 % of cells in the N-deplete treatment had higher fluorescence levels than the replete cells (Fig. 3. 28 A). The higher levels of green fluorescence translate to an increase in ROS.

After seven days of N starvation 55 % of N-deplete cells had higher ROS levels than replete cells (Fig. 3.28 B). The levels of ROS in N-deplete cells were higher on day 7 than those recorded on day 3.

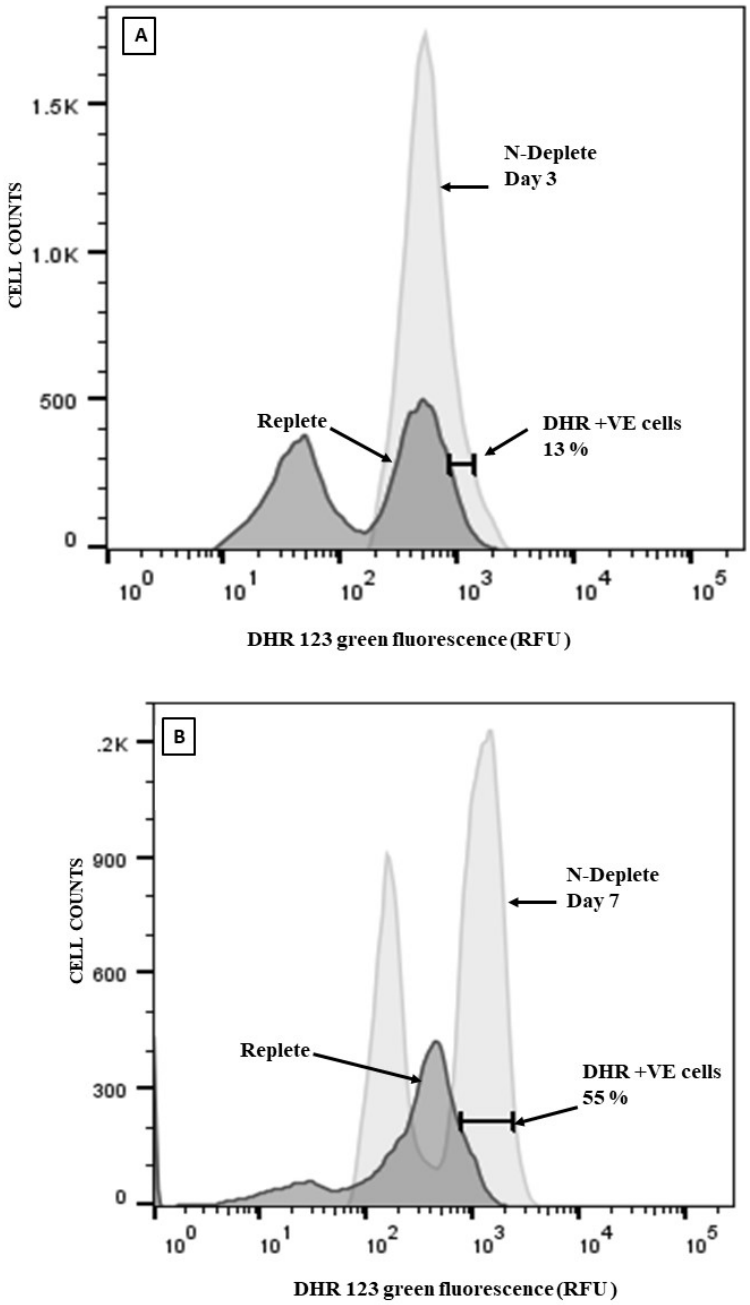


Figure 3.28 Green fluorescence emission in N-deplete and-replete cells, after staining with DHR 123 fluorescent probe on days 3 and 7 of N starvation. The X- axis represents green fluorescence (DHR 123 probe); Y - axis represents cell counts; gates represent the percentage of the populations of -N-deplete cells.

(A) Histogram of N starvation showing peaks of unstained replete, stained replete and stained N- deplete (DHR +VE) cells on day 3.
(B) Histogram of N starvation showing similar peaks as in (A). On day 7.

3.3.5.2 Staining of N- deplete cells with PI fluorogenic probe

A low percentage (13 %) of N-deplete cells stained positively for PI on day 3 (Fig. 3.29 A), indicating that they were dead. There was no change in the number of PI positive cells on day 7 (Fig. 3.29 B).

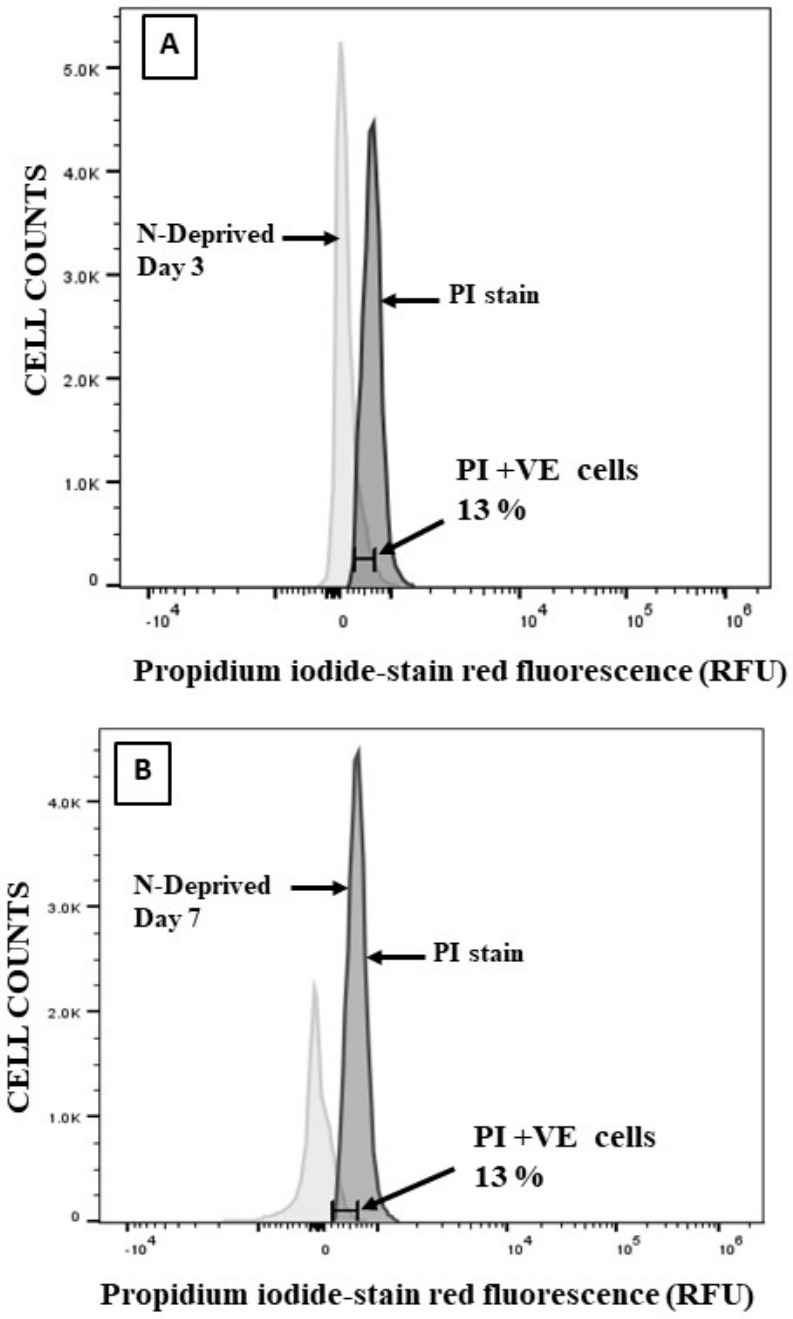


Figure 3.29 Red fluorescence emission in N-deplete and-replete cells, after staining with PI fluorescent probe on days 3 and 7 of N starvation. The X - axis represents PI probe red fluorescence.

(A) Histogram overlays on day 3 of N starvation showing peaks of the PI stain and PI +VE cells in the N- deplete population.

(B) Histogram overlays on day-7 of N starvation showing similar peaks as in (A).

3.3.5.3 Staining of P-deplete cells with DHR 123 fluorogenic probe

P-deplete cells stained positively for DHR 123 fluorogenic probe and 59 % of cells had higher ROS levels than the replete cells (Fig. 3. 30A).

On day 7 about 72 % of cells in the P-deplete treatment had higher ROS levels relative to those of the replete cells (Fig. 3.30B). The fluorescence levels in the P-deplete cells were higher than those recorded in the N-deplete cells (Figs 3.30 A & B *cf* Figs 3.28 A & B).

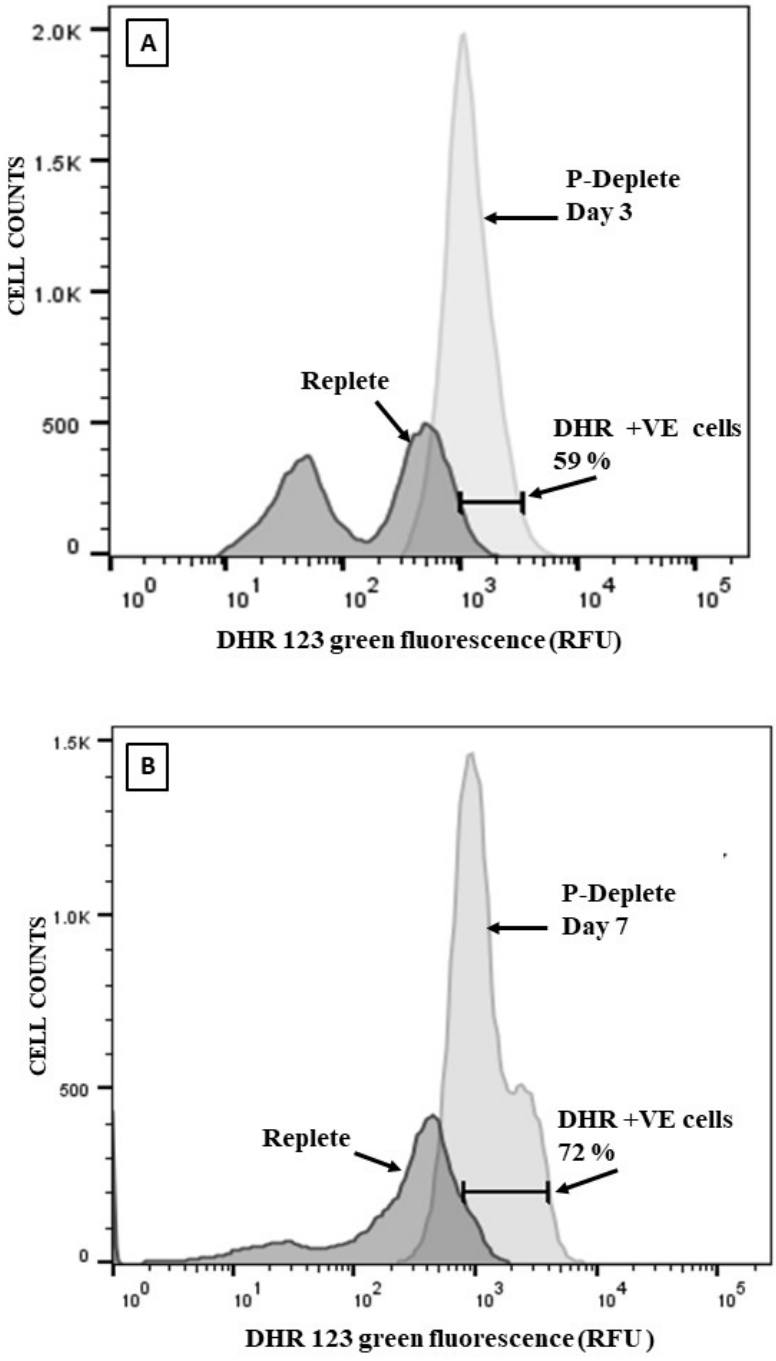


Figure 3.30 Green fluorescence emission in P-deplete and -replete cells, after staining with DHR 123 fluorescent probe on days 3 and 7 of P starvation. The X- axis represents DHR 123 probe green fluorescence; Y -axis represents cell counts; gates represent the percentage of the populations of P -deplete cells.

(A) Histogram on day 3 of P starvation showing peaks of unstained replete (DHR -VE) cells, stained replete and stained P- deplete (DHR +VE) cells.

(B) Histogram on day 7 of P starvation showing similar peaks as in (A). Note the peak shoulder showing cells with higher levels of green fluorescence in the P-deplete cells (red dotted arrow).

3.3.5.4 Staining of P-deplete cells with PI fluorogenic probe

A population of 31 % of P-deplete cells stained positively for PI on day 3 (Fig. 3.31 A). There was a decrease in the number of PI positive cells on day 7 when 42 % of PI positive cells was recorded (Fig. 3.31 B).

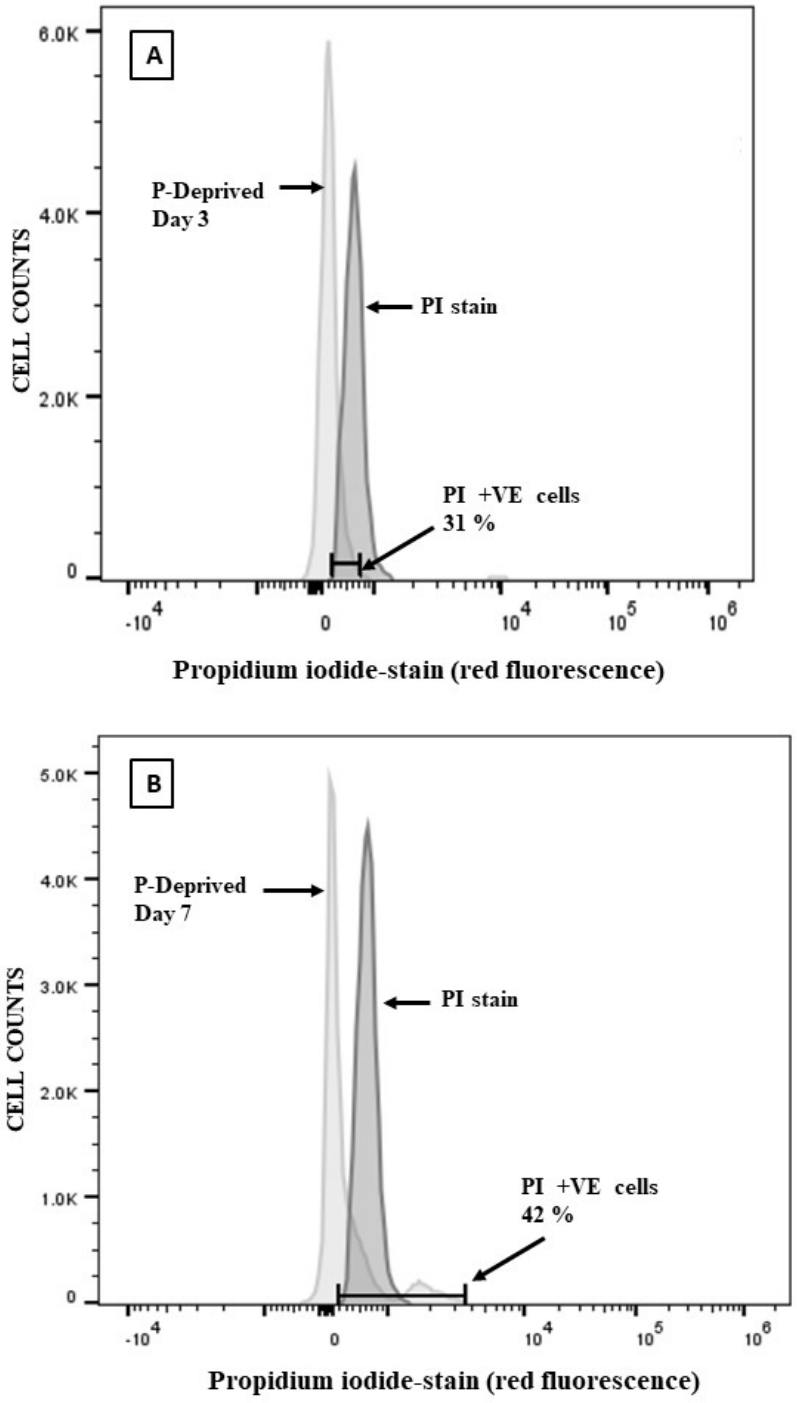


Figure 3.31 Red fluorescence emission in P-deplete and -replete cells, after staining with PI fluorescent probe on days 3 and 7 of P starvation. The X - axis represents PI probe red fluorescence

(A) Histogram overlays on day 3 of P starvation showing peaks of the PI stain and PI +VE cells in the P- deplete population.

(B) Histogram overlays on day 7 of P starvation showing similar peaks as in (A).

3.3.6 DNA Laddering assay in N- and P-deplete cells

The quantity of DNA extracted from the N- and P-deplete samples was less than the replete samples (Table 3.5). No ladders were detected in any samples run in an agarose electrophoresis gel (Fig. 3. 31).

Table 3.5. Quantification of extracted DNA in Replete, N-and P-deplete samples on day 7 of treatment.

Treatment	**DNA measurement*(ng/µL)***
Replete	211
N-deplete	**165.8**
P-deplete	**168**

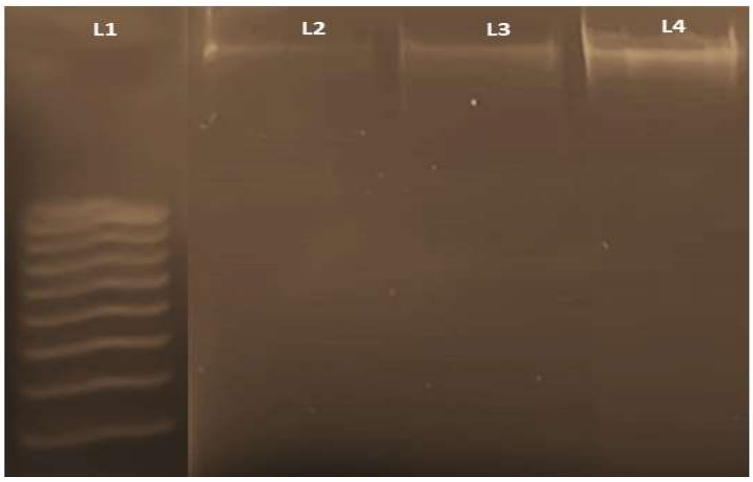


Figure 3.32 Agarose gel electrophoresis of N- and P -deplete samples.

L1=DNA marker (100bp); L2=N-deplete; L3=P-deplete; L4=Replete.

3.3.7 Summary of results that show evidence for PCD

The table below summarises the TEM and biochemical assay results as evidence for PCD *in P. redfieldii*.

Table 3.6. Summary of TEM and biochemical assay results as evidence for PCD

Treatment	TEM-alterations to cells	DEVDase	Excessive ROS	DNA Laddering	PI positive cells
N-deplete	✓	X	X	X	X
P-deplete	✓	X	✓	X	✓

3.4 DISCUSSION

The study aimed to deprive *P. redfieldii* cultures of two essential nutrients i.e., nitrates (N) and inorganic phosphates (P) to determine if they would induce PCD. Results obtained provide evidence for changes in the growth dynamics, ultrastructural morphology and biochemical activity of the stressed cells as a response to the stressors. PCD was induced in a portion of phosphate starved cells but not in those cells that were starved of nitrates.

3.4.1 Growth dynamics

The cell cycle arrest in *P. redfieldii c*ells as a response to macro-nutrient stress is expected because of the role that nitrates and phosphates play in cell cycle progression. A lack of inorganic phosphates negatively affects the phosphorylation of proteins involved in cell cycle progression, i.e., the cyclin -cyclin dependent kinases complex and its target proteins (Pokrzywinski et al., 2017c). While a lack of nitrates affects the synthesis of enzymes and other proteins required to facilitate cell cycle progression. Cell cycle arrest observed in *P. redfieldii* also occurred in the dinoflagellates *Amphidinium carterae* and *Prorocentrum cordatum* in response to N starvation (Kalinina *et al.*, 2023; Olson and Chisholm, 1986) and *Prorocentrum donghaiense* in response to P starvation (Li *et al*., 2021, 2015; Meizhen *et al.*, 2016). Cell cycle arrest in *P. redfieldii* must have occurred in the first growth stage of the cell cycle (G1) because both N- and P- deplete cells did not show logarithmic growth, a similar trend was observed in nitrogen starved cells of *P. donghainse* (Li *et al*., 2021).

In N-deplete cells of *P. redfieldii*, cell cycle arrest was an acclimation strategy while in P-deplete cells it preceded PCD. The latter observation corresponds with previous findings on dinoflagellates where cell cycle arrest was associated with PCD in *Prorocentrum minimum* and *Karlodinium veneficum* when they were subjected to a bacterial algicide (Pokrzywinski *et al.*, 2017c).

Generally, under stressful conditions microalgae develop various strategies that switch off their cell cycle, these include cell cycle arrest, formation of cysts and change from asexual to sexual reproduction (Franklin *et al.*, 2006).

3.4.2 Ultrastructure

Prorocentrum redfieldii cells exhibited various ultrastructural alterations in response to N and P starvation. Ultrastructural changes included an overaccumulation of reserves, extensive vacuolation, alterations to the nucleus, endomembrane system (including an upregulation of MVBs), mitochondria and chloroplasts. There was also structural evidence for autophagy.

Overaccumulation of reserves

An overaccumulation of reserves in N-deplete *P. redfieldii* cells is expected and indicates a disturbance in the C:N ratio inside the stressed cells. Nitrogen and carbon assimilation are interdependent, about half of carbon skeletons in phytoplankton are utilized during N assimilation for the synthesis of organic molecules like chlorophylls and proteins (Turpin, 1991). The overaccumulation of reserves in nutrient starved *P. redfieldii* cells is consistent with the behaviour of the field bloom cells.

Overaccumulation of reserves combined with diminished growth exhibited by *P. redfieldii* cells as a response to N and P starvation indicate that these cells were stressed and they often precede PCD in dinoflagellates (Li *et al.*, 2015; Meizhen *et al.*, 2016; Weng *et al*., 2014) and other algae (Sathe *et al*., 2019).

Vacuolation and autophagy

Increased vacuolation was exhibited by both N- and P-deplete cells. Observed changes in cell ultrastructure revealed that excessive vacuolation included the upregulation of MVBs and autophagy.

The upregulation of MVBs in nutrient starved *P. redfieldii* cells would facilitate transport of non-essential membrane macromolecules to the vacuoles to be recycled

so as to boost the levels of amino acids that would be used in the synthesis of essential proteins. The upregulation of MVBs as a response to nutrient stress observed in *P. redfieldii* cells also occurred in *Emiliania huxleyi* during P starvation (Shemi *et al.*, 2016).

The interplay between autophagy and upregulation of MVBs in the nutrient starved *P. redfieldii* cells was also witnessed in the field bloom cells and must have ensured an effective replenishing of critical amino acids by recycling proteins during the nutrient deplete conditions as reported in nutrient starved yeast cells (Müller *et al.*, 2015).

In *P. redfieldii* multilamellar bodies were observed at the interface and inside of vacuoles. Their contents were reminiscent of disintegrating chloroplasts. Such a condition was found in nitrogen starved *Nannochloropsis oceanica* (Heterokontophyta) and these bodies later transformed into lipid bodies (Roncaglia *et al*., 2021). Multilamellar bodies in *P. redfieldii* were also observed around degenerating organelles reminiscent of mitochondria both in the cytoplasm and within the confines of vacuoles which lends support to the idea that they were involved in the degradation of mitochondria. Information about multilamellar bodies and their role in plants and microalgae is limited. They have been associated with autophagy in higher plants e.g., during petal development in *Tillandsia albida* when they were involved in thylakoid membrane degradation (van Doorn and Papini, 2016). Multilamellar bodies in *P. redfieldii* were also observed around degenerating organelles that were most likely reminiscent of mitochondria both in the cytoplasm and within the confines of vacuoles which lends support to the idea that they were involved in the degradation of mitochondria.

The nucleus

The chromosome structure in nuclei of N-deplete cells remained intact in most of cells throughout the treatment period. Contrastingly, the intact structure of the liquid crystalline chromosome was unravelled in all cells of the P-deplete treatment. This difference is surprising because both P and N are constituents of nucleic acids, but it could be that the *P. redfieldii* cells were less efficient at recycling intracellular

resources of P relative to those of N. A lack of P would impact the structural integrity of DNA because phosphates form covalent bonds with deoxyribose sugar and together constitute the backbone of the DNA helix (Santos, 1999), or the lack of inorganic phosphate negatively impacted on the phosphorylation of the histone-like-proteins (HLPs) that are involved in the structural compaction of the liquid crystalline chromosomes of dinoflagellates (Gornik *et al.*, 2019).

The fact that all chromosomes in the P-deplete treatment were affected makes this alteration to be less likely a marker of PCD but could rather be directly linked to a lack of intracellular P. The unravelling of chromosomes of P-deplete cell nuclei were not observed in nuclei of bloom cells, which supports the fact that the unravelling of the chromosomes was specific to a lack of inorganic phosphates in these cells. However, the formation of chromatin clumps that was also present in the altered chromosomes could indicate fragmentation of DNA in these cells.

Piecemeal autophagy of the nucleus observed in field cells nuclei was also present in the nuclei of P-and N-deplete cells, and this demonstrates that although this affected a small portion of nuclei it could be an intrinsic feature in *P. redfieldii* stressed cells.

The endomembrane system

The interplay between MVBs and autophagy has already been discussed in the previous sections. Membranes derived from the ER were incorporated in the process of autophagy in nutrient deplete cells. The endoplasmic reticulum has been reported to be a membrane source for the formation of the double membraned structure that surrounds and engulfs parts of the cytoplasm and organelles during autophagy (Uemura *et al.*, 2014; van Doorn and Papini, 2013). Alterations to the Golgi cisternae occurred in all treatments including the replete cells during all sampling times and are therefore considered to be a normal occurrence, because they were also present in the replete cells at all stages of sampling.

The Mitochondria

The herniated mitochondria in both the N-and P-deplete cells of *P. redfieldii* can be associated with the opening of the mitochondrial permeability transition (MPT) pore caused by high levels of ROS that were detected in these cells. Similar mitochondrial alterations were observed in the field bloom cells and it can thus be assumed that the field bloom cells were also exposed to high ROS levels. Mitochondrial herniation coincided with autophagy of the damaged mitochondrial profiles in both N- and P-deplete cells and again mirrors what was observed in the field cells.

Another observation in the mitochondria of only the P-deplete cells was the swelling and ballooning of mitochondrial profiles as a result of the high ROS levels that were detected in this treatment.

The chloroplasts

Morphological changes to chloroplasts were observed in both N- and P-deplete cells. A lack of nitrogen in *P. redfieldii* must have negatively affected the turnover of macromolecules like chlorophylls and photosynthetic proteins of which nitrogen is a structural component. As a result, the proper functioning of photosynthetic reactions like the electron transport chain reactions would be disturbed and trigger the overproduction of ROS. The increased levels of ROS beyond the antioxidant activity of the cells would lead to oxidative stress (Liefer et al., 2018).

The ultrastructural changes that were observed in the thylakoid membranes of N-deplete cells like the reduction of the width of thylakoid lumen is expected because the thylakoid membranes are the primary production sites of ROS inside the chloroplasts and would be the most affected by oxidative damage. The accumulation of ROS species like the radical singlet oxygen occurs in the lumen of the thylakoid (Sharma *et al*., 2012) and therefore the luminal proteins would be the first targets of oxidative damage.

The dismantling of thylakoids and their subsequent degradation in vacuoles was more prevalent in the N-deplete than in the P-deplete cells and it is plausible that

this process was primarily used by *P. redfieldii* cells to remobilize intracellular resources of nitrogen than it being a means to alleviate the impact of high levels of ROS. The degradation of chloroplasts in lytic vacuoles in the form of multilamellar structures as a stress response occurs in other microalgae (Papini *et al.*, 2018; Roncaglia *et al.*, 2021).

The alterations in the chloroplasts in P-deplete can also be associated with the overproduction of ROS. Phosphate plays an important role in photosynthesis through phosphorylation of proteins, also during the conversion of the energy molecules ATP from ADP and NADP to NADPH.

3.4.3 Biochemical activity

The failure to detect DEVDase activity and its unsuccessful silencing by a DEVDase activity inhibitor in the N-deplete cells of *P. redfieldii* is expected because there were no major cell deaths in this treatment.

Although substantial numbers of cell deaths were recorded in the P-deplete cells, the failure to detect DEVDase activity in these cells is still acceptable because some phenotypes of PCD like autophagic PCD can occur without caspase / DEVDase activity (Affenzeller *et al.*, 2009; Sperandio *et al*., 2000). Caspase activity was not detected in the dinoflagellate, *A. cartarae* undergoing paraptotic cell death (Franklin and Berges, 2004) and the green algae *Micrasterias denticulata* undergoing autophagic cell death (Affenzeller *et al*., 2009). However, caspase activity was detected in *Dunaliella viridis* cells undergoing paraptotic and those undergoing autophagic cell death (Jimenez *et al*., 2009). In *P. donghaiense*, caspase activity was detected in cell undergoing mitochondrial apoptosis (Ji *et al.*, 2021), in the same species caspase activity was detected but it was not accompanied with cell death (Huang *et al*., 2016). A recent study on *Karenia brevis* has shown that caspase activity was present throughout the growth cycle of these cells which indicates that it has other roles that are not associated with cell death (Y Gao and Erdner, 2022).

All the above show the complexities associated with caspase-like activity in phytoplankton. Nevertheless, caspase-like activity is often associated with cell death in microalgae and in 94 % of experiments where it was assayed it gave a positive result (Barreto Filho *et al.*, 2023).

Both treatments of nutrient deplete cells of *P. redfieldii* experienced an overproduction of ROS. The effects of the increased levels of ROS in the stressed cells can be linked with the damage observed in mitochondrial and chloroplasts membranes of N-and P-deplete cells. Programmed cell death facilitated by the overproduction of ROS is a widely reported in phytoplankton PCD and results in oxidative stress (Barreto Filho *et al*., 2023; Bidle, 2016; Rzymski *et al*., 2020; Vardi *et al.,* 1999; Zhao *et al.,* 2020).

The fact that the overproduction of ROS did not translate to cell death in N-deplete cells of *P. redfieldii* cells indicates that these cells had developed better coping mechanisms to a lack of N than to a lack of P. A similar trend was demonstrated in *P. triestinum* (= epithet of the study organism), when subjected to N and P stress, the cells could acclimatize to N but not to P deprivation because of effective scavenging for intracellular nitrogen (Chan *et al.*, 2004).

The unrelatedness between the numbers of cells with high levels of ROS and cell deaths in the N-deplete cells shows that ROS could have been involved in other physiological processes like ROS mediated signalling from the chloroplasts and mitochondria to the nucleus. Some of these processes initiate the transcription of new genes and translation of proteins that function in stress acclimation (Suzuki *et al*., 2012). The role that ROS plays in other physiological processes other than mediating cell death has also been shown in other dinoflagellates (Y Gao and Erdner, 2022; Huang et al., 2016; Jauzein and Erdner, 2013).

The failure to recover oligo-nucleosomal ladders in the DNA of nutrient deprived *P. redfieldii* cells is unsurprising as dinoflagellates lack nucleosomes and true histones in the structural makeup of their chromosomes (Gornik *et al.*, 2012), failure to detect DNA ladders has been previously reported in other dinoflagellates (e.g. Vardi *et al.*, 1999).

The DNA laddering technique was chosen because it is highly specific to PCD than the other techniques like the TUNEL (Terminal deoxynucleotidyl transferase-mediated dUTP nick-end labelling) assay and it was important for this study to establish if nuclear fragmentation was an outcome of PCD and not necrosis. Alternative assays kits like TUNEL simply reveal that the DNA is fragmented, which also occurs in cells dying of necrosis.

3.4.4 Is there any evidence that PCD was induced by nutrient deprivation in *P. redfieldii?*

Both N- and P- deplete cells of *P. redfieldii* exhibited signs of stress acclimation, including cell-cycle arrest, the overaccumulation of carbon reserves and an enhanced catabolic activity. The negligible numbers of cell deaths in N-deplete *P. redfieldii* cells are evidence that these cells maintained their acclimation to N starvation throughout the experimental period, therefore N starvation did not successfully induce PCD. In contrast P starvation resulted in a programmed cell death in a substantial number of cells. There was also morphological evidence for secondary necrosis exhibited in P -deplete cells.

Morphological and biochemical markers associated with PCD in the P-deplete cells included extensive vacuolation by autophagy, alterations to mitochondrial and chloroplast membranes, an increase in ROS and loss of viability to a substantial number of cells. In a small portion of extensively vacuolated cells the amphiesmal membranes were retracted from the thecal plates.

The extensive vacuolation by autophagy in the P-deplete cells which is a marker of autophagic cell death (Kroemer *et al*., 2009) was also observed in the bloom cells. Other ultrastructural markers that accompany autophagic cell death like lytic vacuoles and double membraned structures engulfing organelles and parts of the cytoplasm were also observed in these cells.

Although alterations to the nucleus during PCD are normally associated with the activity of endonucleases which cleave the phosphodiester bonds of DNA (Kroemer *et al.,* 2009), in the P-deplete cells of *P. redfieldii* the unravelling of chromosomes

in not a marker of PCD and must have been directly related to a lack of organic phosphates which compromised the structural stability of the phosphodiester bonds in the DNA. However, the chromatin clumps that were observed in the later stages of the treatment are indicative of damaged DNA. Chromatin clumps were also observed in the bloom cells and conform to what has been observed in other dinoflagellates undergoing PCD (Ji *et al.*, 2021; Pokrzywinski *et al.*, 2017a).

The alterations observed in the mitochondrial and chloroplast membranes of P-deplete cells correlate to the high levels of ROS detected in these cells and have been previously associated with oxidative stress (Gorelova *et al.*, 2019; Rakhmatullina *et al.*, 2016). This has also been shown in other dinoflagellates where an overproduction of ROS resulted in oxidative stress which later induced programmed cell death (Ji *et al*., 2021; Pokrzywinski, 2014; Vardi *et al*., 1999). The swollen mitochondrial cristae in the P-deplete cells which are sites where oxidative phosphorylation (OXPHOS) takes place are a confirmation of the structural damage caused by the high levels of ROS which would have inevitably disturbed the OXPHOS reactions. When the overproduction of ROS is associated with an acute depletion of energy pools it results in an unprogrammed cell death as it occurs in symbiotic dinoflagellates *Symbiodinium sp.* exposed to heat stress (Dunn *et al.*, 2004).

Caspase-like activity is a biochemical marker associated with apoptotic-like cell death (Kerr *et al*., 1972; Kroemer *et al*., 2009; Saraste and Pulkki, 2000). It was not detected with the collapse of cell numbers (death) in P-deplete cells. However, the failure to detect caspase activity in these cells is still acceptable because the ultrastructural characteristics of the dying cells point to an autophagic cell death, which can occur without the activation of caspases as shown in *A. cartarae* (Franklin and Berges, 2004) and *Micrasterias denticulata* (Affenzeller *et al*., 2009).

The failure of the DNA laddering essay was attributed to the lack of nucleosomes and true histones in dinoflagellates (Gornik *et al.*, 2012).

Taken together, the above morphological and biochemical observations point to P starvation successfully inducing a programmed cell death in *P. redfieldii* cells. The

ultrastructural and biochemical markers point to an autophagic cell death that was exacerbated by oxidative stress. It can thus be said yes, P starvation was able to induce a programmed cell death in *P. redfieldii* whose morphotype corresponds with that of cells sampled from a collapsing bloom. The retraction of the amphiesmal membranes can also be regarded as the onset of secondary necrosis as witnessed in the bloom cells.

3.4.5 Similarities in structural elements of the laboratory nutrient deplete cells with those from a collapsing bloom

Similarities in ultrastructure of cells dying from P starvation and those cells dying from a collapsing bloom were excessive vacuolation by autophagy and the presence of autophagy related structures like lytic vacuoles and ER derived double membranes, upregulation of MVBs, herniated mitochondria and dilated chloroplast thylakoid lumina. High levels of ROS were detected in the P-deplete cells and based on the structural similarities with the alterations to mitochondria and chloroplast in the bloom cells it can be inferred that the bloom cells were also experiencing an oxidative stress. Both N and P starvation did not culminate in the massive cell deaths witnessed in a dying bloom. It is highly likely that the field bloom cells were affected by a combination of environmental stresses as shown in another collapsing bloom that cells were simultaneously subjected to low P and N; and to low levels of dissolved oxygen (Pitcher and Probyn, 2016a).

3.5 CONCLUDING REMARKS

This study investigated if depriving *P. redfieldii* cells of two essential macro-nutrients independently, i.e., nitrates (N) and organic phosphates (P), would induce a programmed cell death. The findings were used to determine whether the PCD associated morphological elements of cells in the laboratory based nutrient deprivation experiment reflected those of cells sampled during the collapsing bloom:

Nitrogen starvation did not successfully induce programmed cell death in *P. redfieldii* cells, instead the cells successfully acclimatized to the stress by initiating strategies like cell-cycle arrest, overaccumulation of reserves and upregulating

catabolic processes. This is a common response in microalgae subjected to biotic and abiotic stress (Borowitzka, 2018). Contrarily, phosphorus starvation successfully induced an autophagy associated programmed cell death in these cells which was exacerbated by oxidative stress.

The autophagic cell death phenotype in P-deplete cells was defined by the excessive vacuolation of cells by autophagy, lytic vacuoles and ER derived double-membraned structures (Kroemer and Levine, 2008). Biochemical assays in the P-deplete cells revealed that there was an overproduction of ROS.

There were similarities between cells dying from nutrient deprivation and those in a collapsing bloom and therefore from the high levels of ROS detected it nutrient deprived cells it can be concluded that the bloom collapse was mediated by oxidative stress. These findings are similar to previous findings where PCD mediated by oxidative stress was involved in a dinoflagellate bloom collapse (Vardi *et al.,* 1999).

The response of *P. redfieldii* to nutrient stress showed how these cells behave when nutrients become limiting and give insight to how *P. redfieldii* cells behave in the late stages of a bloom collapse. It shows that these cells can rapidly acclimatize to nutrient starvation through various strategies. It also showed that a lack of inorganic phosphates was more limiting in these cells than a lack of nitrates.

In the next chapter heat- shock which is an acute stress was used to induce PCD in *P. redfieldii* cells and to observe how the cells respond to an acute stress.

CHAPTER4- THE ULTRASTRUCTURE AND BIOCHEMICAL ACTIVITY OF *PROROCENTRUM REDFIELDII* CELLS SUBJECTED TO HEAT- SHOCK STRESS TO INDUCE CELL DEATH

4.1 INTRODUCTION

4.1.1 Background

The important role of phytoplankton as primary producers (Chapter 1, section 1.1), depends on many factors and temperature is one of them (Eppley, 1972;Falkowski and Raven, 2007; Grimaud *et al.*, 2015). The relationship between temperature and phytoplankton is explained using various study models. In the first model, an increase in the maximum growth rate of a species is linked to optimal growth temperature (Eppley, 1972; Raven and Geider, 1988; Regaudie-de-Gioux and Duarte, 2012; Sherman *et al*., 2016). The second model is of an evolutionary nature, and portrays the thermal adaptation of species to variations in temperature (Grimaud *et al.*, 2015; Thomas *et al*., 2012)

In view of the above, the consequence of global warming and climate change on the phytoplankton dynamics in the ocean cannot be ignored. It has been suggested that global warming will result in the increase of sea surface water temperatures (Houghton, 2001; Levitus *et al*., 2005; Regaudie-de-Gioux and Duarte, 2012). Increased temperatures result in thermal stratification of the water column (Guinder and Molinero, 2013). During downwelling and increase in thermal stratification is associated with nutrient depletion in the euphotic zone. Blooms that are dominated by dinoflagellates are prevalent in thermal stratified waters, as dinoflagellates can periodically migrate down to get nutrients at lower levels which are thus unavailable to the other non-motile groups *e.g.* diatoms (Pitcher *et al*., 2010; Guinder and Molinero, 2013).

Elevated temperatures put dinoflagellates at a competitive advantage over other organisms as they can form their blooms in thermal stratified waters. However, it would be of interest to establish the tolerance limit for *P. redfieldii* to elevated temperatures, i.e., the point at which elevated temperatures become a stress and induce cell death. It is important to note that the heat shock stimulus used in this study has been amplified to overcome the tolerance threshold of the organism but is not a reflection of what the organism would be exposed to in its natural habitat.

A study on average sea surface temperatures in St Helena Bay, which is the current study site, revealed a range of 12-25º C (Crichton *et al*., 2013). Recorded sea surface temperatures during sampling for the current study recorded sea surface temperatures that ranged between 20-22º C (Ndhlovu *et al*., 2017).

4.1.2 Heat shock proteins

Living organisms can mitigate stress by the upregulation of existing proteins or transcription and translation of new genes which are converted to proteins. The proteins counteract the adverse effects of the stress and acclimate the organisms to the new stress (Lindquist and Craig, 1988). Heat shock proteins (HSPs) are expressed as a defence response to a variety of environmental stresses e.g. heat-shock, heavy metals, UV light and hypoxia (Guo *et al*., 2012; Kobiyama *et al*., 2010; Lindquist and Craig, 1988). They are conserved in prokaryotes and eukaryotes (Guo *et al.*, 2015), and prevent denatured protein aggregation (Kobiyama *et al.*, 2010) by binding to the damaged regions of the proteins and altering the misfolded structure to a functional one (Lindquist and Craig, 1988).

Some bloom forming dinoflagellates have tolerance for temperature fluctuations (Deng *et al.*, 2018; Guang *et al*., 2004). The ability to tolerate broad temperature variations in dinoflagellates is attributed to the presence of HSPs (Guo and Ki, 2012). HSPs are identified across different classes in dinoflagellates but in this study only a summary of those that have been identified in bloom forming and symbiotic dinoflagellates are illustrated (see table 4.1).

Table 4.1. A summary of HSPs identified in bloom forming and symbiotic dinoflagellates

Dinoflagellate	Type of HSP	References
Prorocentrum minimum	HSP 70 & 90	(Guo *et al*., 2012)
Prorocentrum donghaiense	HSP 90	(Zhang et al., 2019a)
Alexandrium tamarense	HSP 70	(Kobiyama *et al.,* 2010)
Cochlodinium polykrikoides	HSP 70 & 90	(Guo *et al*., 2015)
Amphidinium cartarae	HSP 70 & 90	(Lauritano *et al*., 2017)
Karlodinium micrum	HSP 70 & 90	(Guo *et al*., 2015)
Symbiodinium sp.	HSP 70 & 90	(Rosic *et al*., 2011)

4.1.3 Heat stress as an inducer of programmed cell death in unicellular organisms

Studies where heat-shock was used to induce PCD in microalgae are summarized in a table below (Table 4.2).

A natural phenomenon where heat-shock induces PCD, occurs during the bleaching of the symbiotic dinoflagellates (*Symbiodinium sp*.) from their hosts the sea anemones in the phenomenon of coral bleaching (Segovia, 2008a)

Table 4.2. A summary of heat-shock induced programmed cell death in microalgae

Organism	PCD response	References
Symbiodinium **(Dinoflagellate)**	Necrotic-like cell death, swelling of the cell,	(Franklin et al., 2004a)
Dunaliella viridis **Chlorophyte**	Chromatin clusters and DNA strand breaks	(Jimenez *et al.*, 2009)
Heterosigma akashiwo **(Raphidophyte)**	externalization of phosphatidylserine and DNA fragmentation	Dingman and Lawrence, 20
Chlorella saccharophila **(Chlorophyte)**	DNA fragmentation chromatin condensation	(Zuppini *et al.*, 2007)
Volvox carteri **(Chlorophyte)**	DNA fragmentation accompanied by an increase in caspase3-like activity	Nedelcu, 2006
Chlamydomonas reinhardtti **(Chlorophyte)**	Increase in reactive oxygen species, protoplast shrinkage & DNA laddering and increased ROS	(Durand *et al.*, 2011)

The aim of this study was to investigate if subjecting *P. redfieldii* cells to heat- shock at 32 and 37º C would induce a programmed cell death.

The aim was addressed by the following objectives:

1) To determine if the ultrastructure of the cells is modified under heat-shock: This was achieved by subjecting the cultures to heat-shock at two temperatures (viz., 32 and 37º C). Samples were characterised by a detailed analysis of the ultrastructure of the control and heat-shocked cells by transmission electron microscopy. Alterations to the ultrastructure of heat-shocked cells were compared with those observed in control cells. The focus was on alterations to the nucleus, endomembrane system (Golgi bodies, endoplasmic reticulum and associated vesicles); mitochondria; chloroplasts; vacuolation and alterations to amphiesmal membranes.

2) To carry out concurrent PCD assays on the heat-shocked material including:
i) Caspase-like activity assay,

ii) DNA laddering assay, and

iii) ROS assay

3) To test whether the heat-shocked cells reflected those elements witnessed in the nutrient deprivation experiment:

This was achieved by assessing the impact of heat-shock on the ultrastructure and biochemical activity of the cells and these were then compared with those cells that were starved of nitrates and organic phosphates to detect similarities.

4.2 METHODS:

4.2.1 Growth conditions

Cultures of *P. redfieldii* with a concentration of about 3 x 10^5 cells ml^{-1} were grown up to the exponential growth stage in F/2 medium. Cultures were grown in eight Erlenmeyer flasks, whereby four replicates were subjected to heat-shock and the

remaining four were used as controls. To induce heat-shock four Erlenmeyer flasks with cultures were immersed in a water-bath at 32º C for 1 HR. The flasks were gently swirled at 20 minutes intervals. They were then removed from the bath and returned to the growth room and allowed to stand for 1 HR. The same procedure was repeated for the 37º C treatment. All flasks were then taken to a laminar flow unit where sampling was done for transmission electron microscopy, caspase and DNA laddering assays. This treatment was noted as 1 HR after heat -shock, further sampling was done at 48 HRS after being heat-shocked. Sampling for the 37º C heat-shock was only taken at 1 HR after the stress treatment.

4.2.2 Transmission electron microscopy

4.2.2.1 Fixation and embedding

About 5 ml of culture from the 4 replications of treated cells and 4 replications from the untreated cells were poured into glass centrifuge tubes. Cells were prepared for transmission electron microscopy as detailed previously (see chapter 2 section 2.2.3).

4.2.2.2 Microtomy and Viewing

Resin blocks of heat-shocked and control samples were cut into ultrathin sections of 60 nm using a RMC Boeckler Cryo-microtome (RMC Boeckler CR-X, PT-PC, PowerTome; AZ, USA). Sections were viewed on the FEI Tecnai T12 120Kv transmission electron microscope (FEI Tecnai T12 Spirit 120kv; Oregon, USA). The viewing was done at 80KV.

The ultrastructure from the first 25 cells encountered in linear, non-overlapping transects per treatment was captured and analysed. Viewing focus was on alterations to organelles, changes in the integrity of the amphiesmal membranes, vacuolation, subcellular structures and vesicles not observed in control cells.

4.2.3 DEVDase activity assay

4.2.3.1 Preparation of lysates

The DEVDase activity assay analysis assay in cells heat-shocked at 32º C and 37º C versus control cells was carried out at 1- and 48-hours post-treatment. A concentration of 5 X 10^5 cells ml^{-1} from each of the 3 replications of treated cells and 3 replications of untreated cells were poured into glass centrifuge tubes at 1 and 48 hours after treatment. Cells were prepared for DEVDase activity assay analyses as detailed in chapter 3.

4.2.4 Reactive oxygen species assay

The ROS analysis assay in heat-shocked cells at 32º C and 37º C versus control cultures was carried out at 1- and 48-hours post-treatment. A concentration of 3 x 10^5 cells ml^{-1} from each of the replications of the heat-shocked and control cells were poured into 50 ml Falcon centrifuge tubes and were analysed for ROS using a flow cytometer. The detailed preparation of samples for flow cytometry measures was detailed in chapter 3, section 3.2.5.

4.2.5 Gating strategies

The gating strategies that were used are like those that were detailed in chapter 3, section 3.3.2.3.1.

4.2.6 DNA Laddering assay

Cultures with a cell concentration of 3 X 10^5 cells mL^{-1} from the heat-shocked and control treatments were sampled for DNA extraction as detailed in chapter 3, section 3.2.6.

4.3 RESULTS

4.3.1 Cell ultrastructure

4.3.1.1 Carbon reserves and vacuolation

An increase in lipid bodies was observed in cells of *P. redfieldii* after 1 HR of heat-shock at 32º C when compared with the controls (e.g., Fig. 4.1 B *cf* Fig. 4.1 A). After 1 HR of heat-shock at 32º C there was no change in vacuolation in heat-shocked cells and it was similar to that observed in the controls (e.g., Fig. 4.1 B). After 48 HRS of heat- shock vacuolation was apparent in heat-shocked cells (e.g., Fig. 4.1 C & D). The average proportion of cell surface area occupied by vacuoles in the exposed profile of each cell (n=25) was about 15 % (e.g., Figs 4.1 C).

In a population of 20 % cells the amphiesmal membranes had retracted from the thecal plates at 48 HRS after heat-shock (e.g., Fig. 4.D). These cells were also vacuolated but to a lesser extent when compared with vacuolation observed in the nutrient deplete cells.

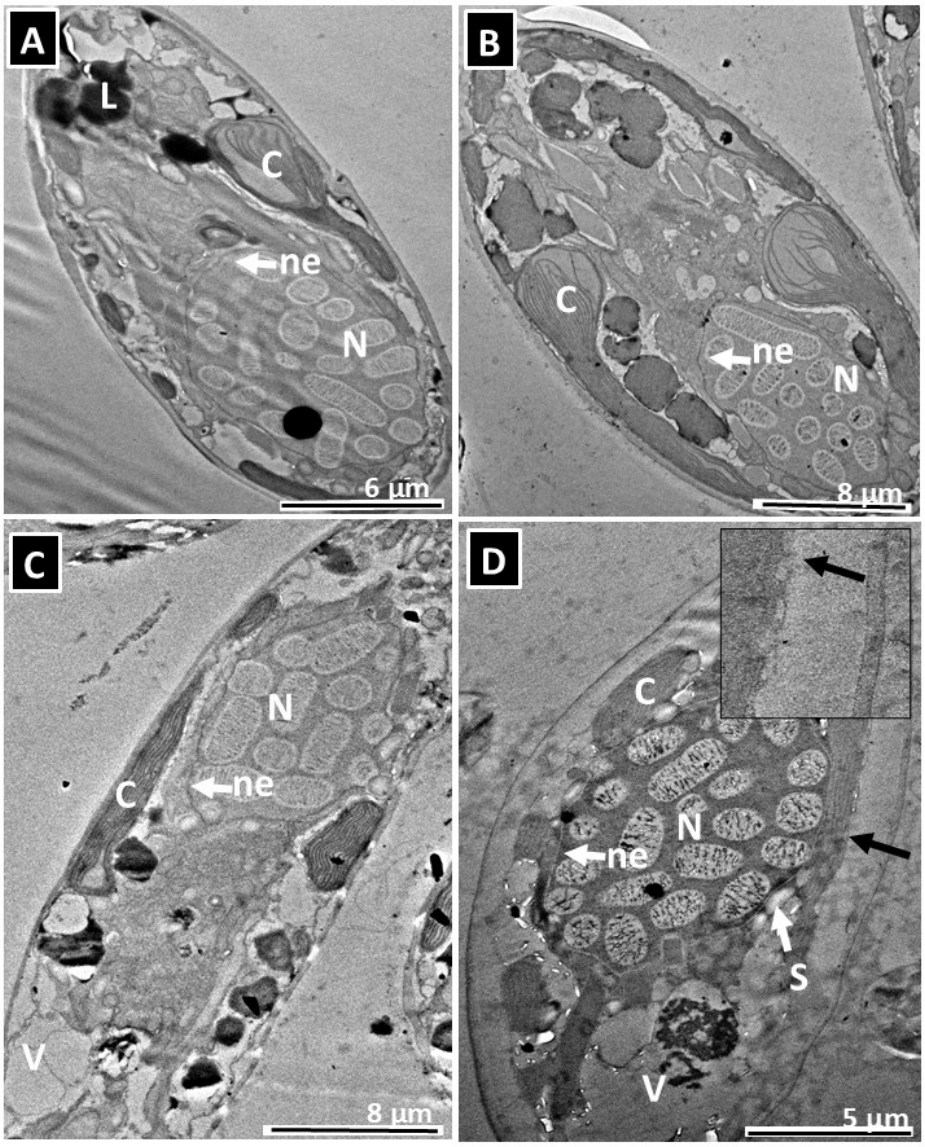


Figure 4.1 Overview of *P redfieldii* cells before and after exposure to heat-shock at 32 ºC.

(A) Control cell showing amphiesmal membranes abutted to thecal plates.
(B) Heat shocked cells at 32º C after 1 HR showing increase in lipid bodies.
(C & D) Heat shocked cells at 32º C after 48 HRS, cells show vacuolation and retraction of amphiesmal membranes (black arrows). Insert in (D) is a magnified area showing retracted amphiesmal membranes. *Abbrev: C=Chloroplast; L=Lipid; N=nucleus; ne =nuclear envelope; V=Vacuole.*

At 37º C after 1 HR of heat-shock, the amphiesmal membranes were retracted and damaged in some areas, in these cells the ultrastructure was mostly amorphous and not easily distinguishable (e.g., Fig. 4.2 A & B). The only organelles that could be identified were dismantled chloroplasts, lipid bodies and trichocysts.

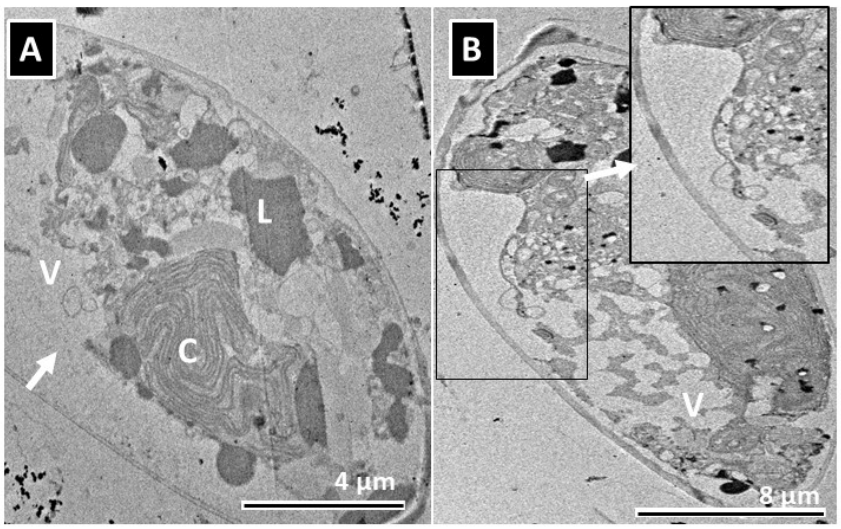


Figure 4.2 Overview of *P redfieldii* cells before and after exposure to heat-shock at 37 ºC.

(A & B) Heat shocked cells at 37º C, cells show retracted and damaged cytoplasmic membranes (black arrows). Insert in (B) shows a magnified area of damaged cytoplasmic membranes. *Abbrev: C=Chloroplast; L=Lipid; V=Vacuole*

4.3.1.2 The nucleus

The nuclei of viewed cells (n = 25) after 1 HR at 32º C of heat-shock treatment showed intact chromosomes and nuclear envelopes like those of the control cells (e.g., Fig. 4.3 A). Occasionally, there were invaginations of the nuclear envelope forming contact sites with adjacent lytic vacuoles which contained electron dense materials in 27 % of viewed cells (e.g., Figs 4.3 B & C). These invaginations to the

nuclear envelope were similar to those observed in the nuclei of nutrient deplete and bloom cells.

After 48 HRS of heat-shock at 32º C, the nuclear envelope membranes were dilated and areas of chromatin clumping were observed in the cells with retracted amphiesmal membranes (e.g., Fig. 4.2 D). Nuclei were not discernible in cells that were heat-shocked at 37º C.

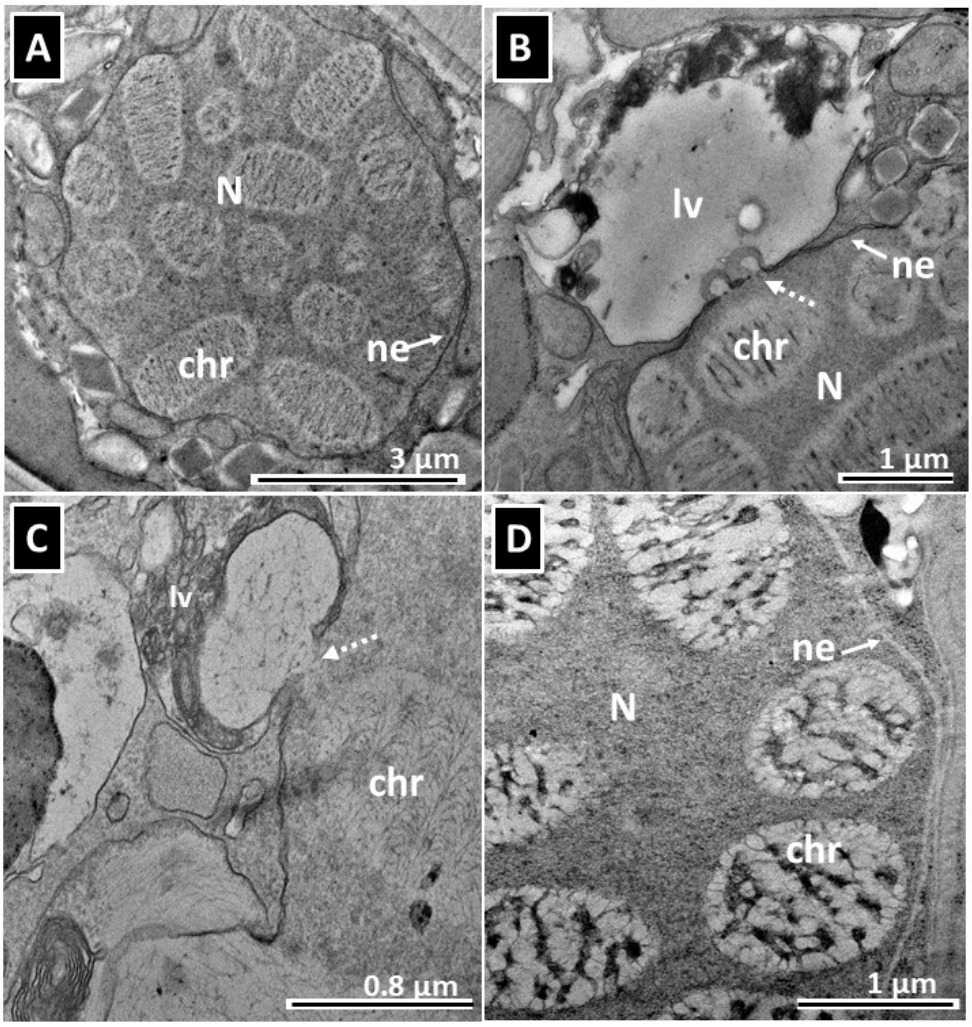


Figure 4.3 Nuclei of control and heat-shocked cells at 32º C after 1 & 48-HRS.

(A) Control cell nucleus showing an intact nuclear envelope and chromosomes.

(B & C) Nuclei of cells heat-shocked at 32º C after 1 HR showing intact nuclear envelope and chromosome structure, note invaginations of the nuclear envelope into adjacent vacuoles (broken arrow).
(D) Nucleus of cells heat-shocked at 32º C after 48 HRS showing a dilated nuclear envelope and areas of chromatin in the chromosomes. *Abbrev: chr=chromosome; lv=lytic vacuole; N = nucleus; ne= nuclear envelope.*

4.3.1.3 The endomembrane system

Control cells showed Golgi cisternae, rough and smooth ER ribosomes and multivesicular bodies (MVBs, e.g., Fig. 4.4 A). Golgi and ER cisternae were not altered after1HR of heat-shock at 32º C (e.g., Fig. 4.4 B). Multivesicular bodies were present on the trans-side of the Golgi after 1 HR of heat-shock (e.g., Fig. 4.4 B). After 48 HRS of heat-shock there was an abundance of ribosomes on the cytoplasm and also attached to ER cisternae (e.g., Fig. 4.4 C).

Endomembrane organelles were not discernible in cells that were heat-shocked at 37º C.

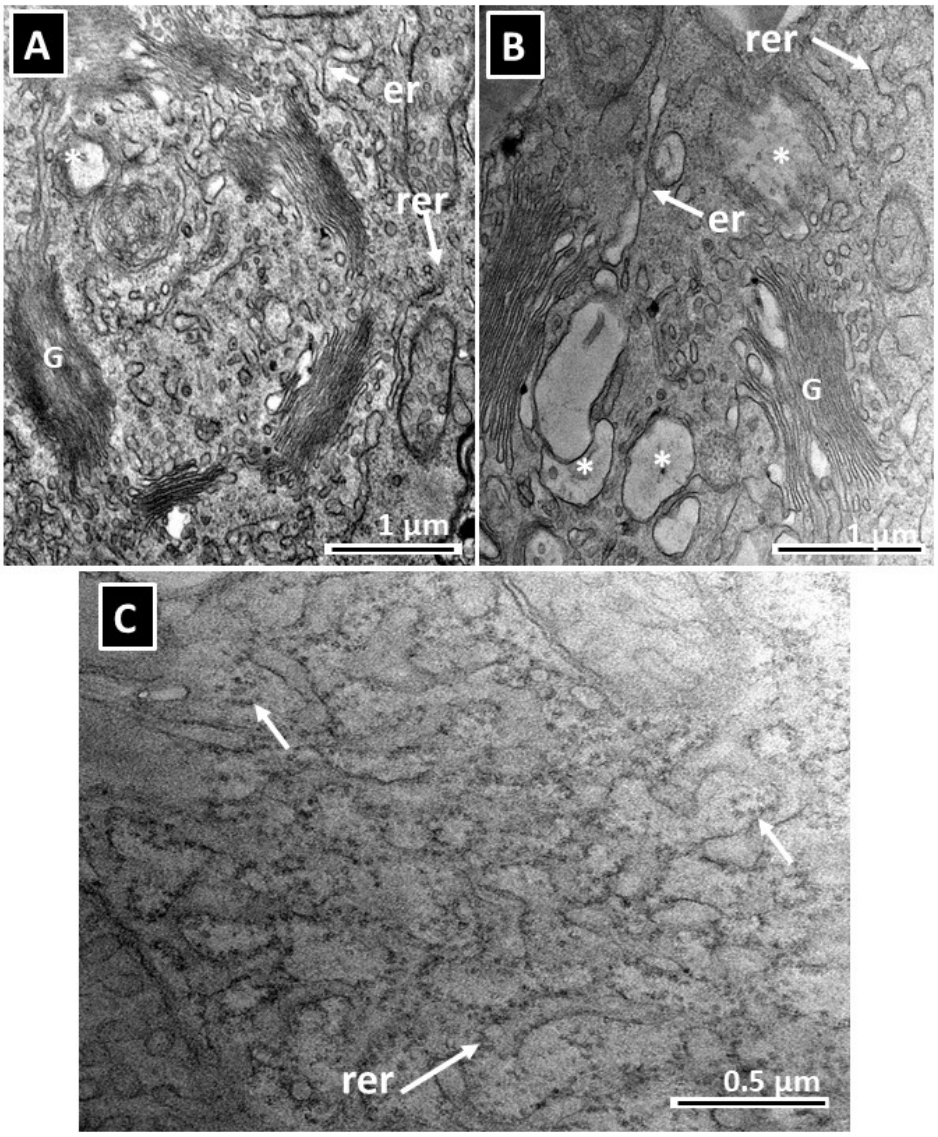


Figure 4.4 The Golgi cisternae and ER in control and cells after 1 and 48 HRS of being heat-shocked at 32º C.

(A) Control cell showing ER, Golgi cisternae and ribosomes.

(B) Heat-shocked cells at 32º C after 1 HR showing MVBs (white asterisks) and no alterations to Golgi and ER cisternae.

(C) Heat-shocked cells at 32º C after 48 HRS showing abundant ribosomes. *Abbrev: er = endoplasmic reticulum; G=Golgi bodies; rer=rough endoplasmic reticulum.*

4.3.1.4 Upregulation of multivesicular bodies and lytic vacuoles

There was an upregulation of MVBs and lytic vacuoles after 1 HR of 32º C heat-shock treatment. The MVBs merged with lytic vacuoles, which contained membranous material, damaged organelles and double-membraned structures (e.g., Figs 4.5 A & B). The lytic vacuoles coalesced to form larger structures (e.g., Figs 4. 5 A & B). The upregulation of the endocytic pathway is like that evidenced in the field and nutrient-deplete cells.

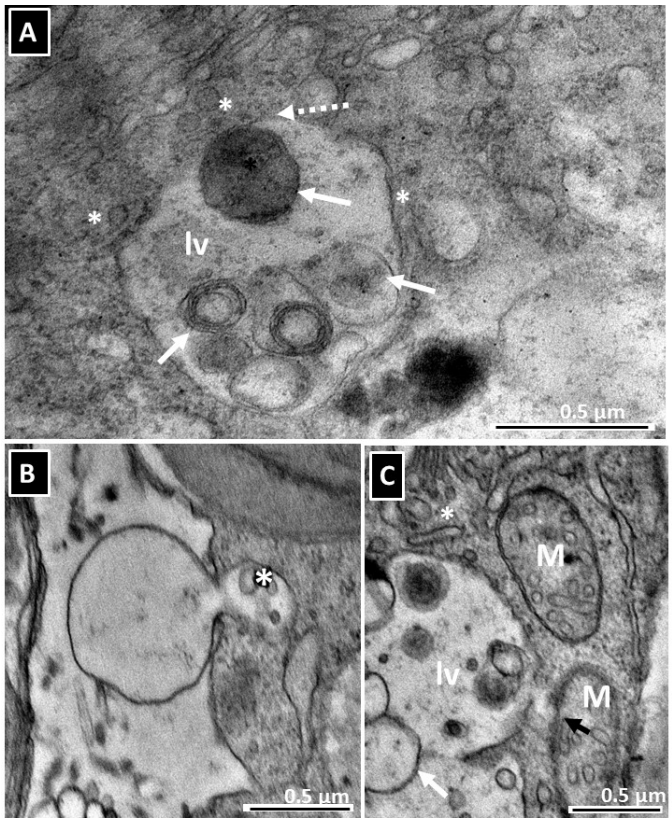


Figure 4. 5 Multivesicular bodies and lytic vacuoles in 32º C heat -shocked cells at 1 HR after treatment.

(A - C) MVBs (white asterisks) merge with lytic vacuoles (black asterisks) containing membranous materials, double membraned-structures in the 32º C heat-shocked treatment, 1-HR posttreatment. Note coalescence of MVBSs to form larger structures (broken white arrows) and in (C) a connection in between a mitochondrion and lytic vacuole (black arrow). *Abbrev. lv=lytic vacuoles; M=mitochondrion*.

4.3.1.5Multilamellar structures

Multilamellar structures formed by concentric membrane whorls were observed in the cytoplasm of cells after 1 HR of heat-shock (e.g., Fig. 4.6 A-D). The concentric membranes occasionally formed contact sites with chloroplasts (e.g., Figs 4.6 A). The multilamellar structures were also observed inside vacuoles (e.g., Figs 4.6 B-D).

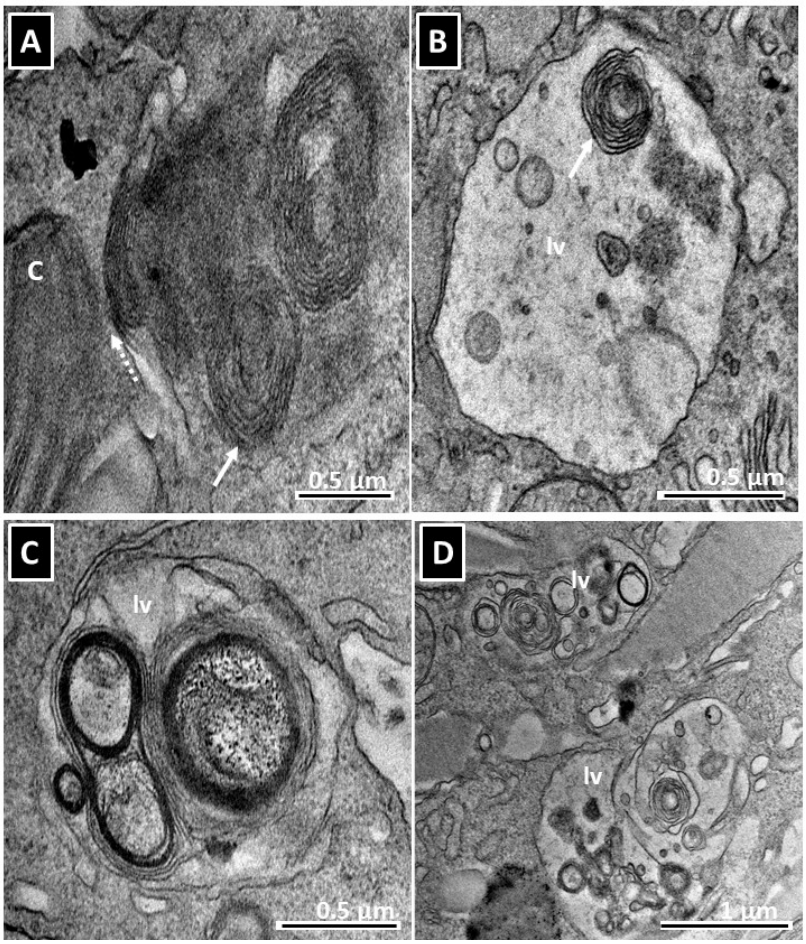


Figure 4.6 Multilamellar bodies in heat-shocked cells at 32º C after 1 HR of treatment.

(A) Membrane stacks connected to multilamellar bodies
(B) Multilamellar bodies connected to the chloroplast (broken arrow)

(C-E) Multilamellar bodies inside lytic vacuoles. *Abbrev. C-chloroplast; lv=lytic vacuoles*.

4.3.1.6 Microautophagy

The vacuolar membrane was often observed wrapping around vesicles at the interface of vacuoles (Figs 4.7 A-C). Organelles and parts of the cytoplasm were internalized by the vacuoles (Figs 4.7 A-C). The internalization of cytoplasmic vesicles and organelles with parts of the cytoplasm by invagination of tonoplast resembled micro-autophagy.

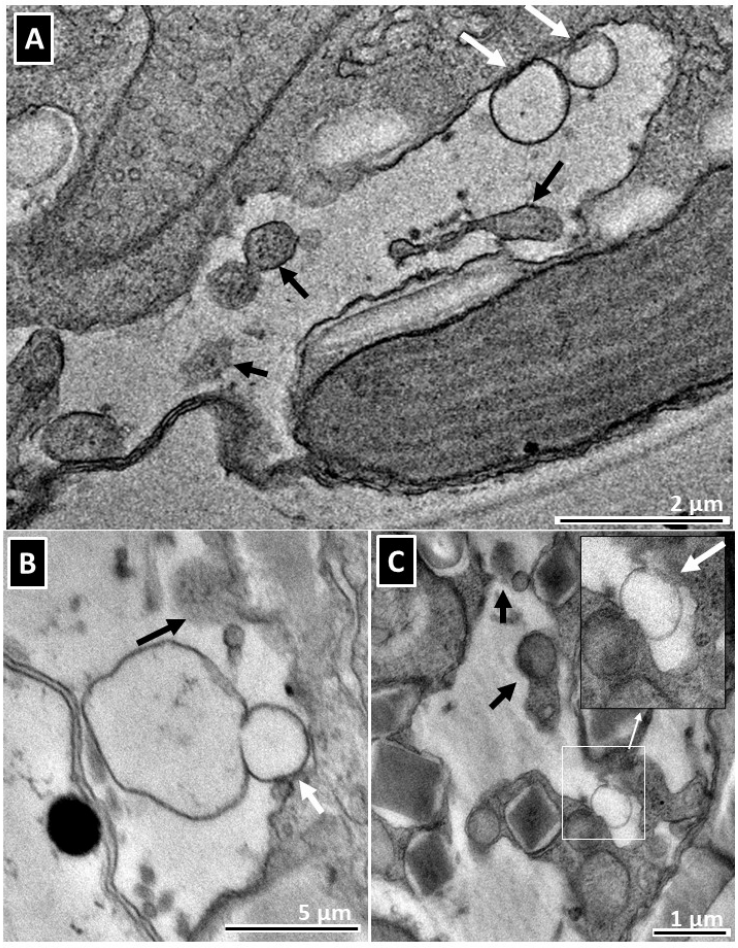


Figure 4.7 Evidence for microautophagy in heat-shocked cells at 32º C after 1 and 48 HRS of treatment.

(A-C) Evidence for microautophagy, note vesicles being internalized at the interface of vacuoles (white arrows) and organelles and cytoplasm internalized by vacuole (black arrows).

4.3.1.7 Mitochondria

The mitochondrial membranes including the cristae remained intact in 66 % of mitochondria from the viewed heat-shocked cells and were like those in the control after 1 HR of treatment (n=25). The remaining percentage consisted of herniated mitochondria (e.g., Figs 4.8 A-D).

Mitochondria surrounded by multilamellar structures were observed at the interface of lytic vacuoles (e.g., Figs 4.8 E). Occasionally, it was observed that mitochondria profiles were observed inside lytic vacuoles (e.g., Figs 4.8 F).

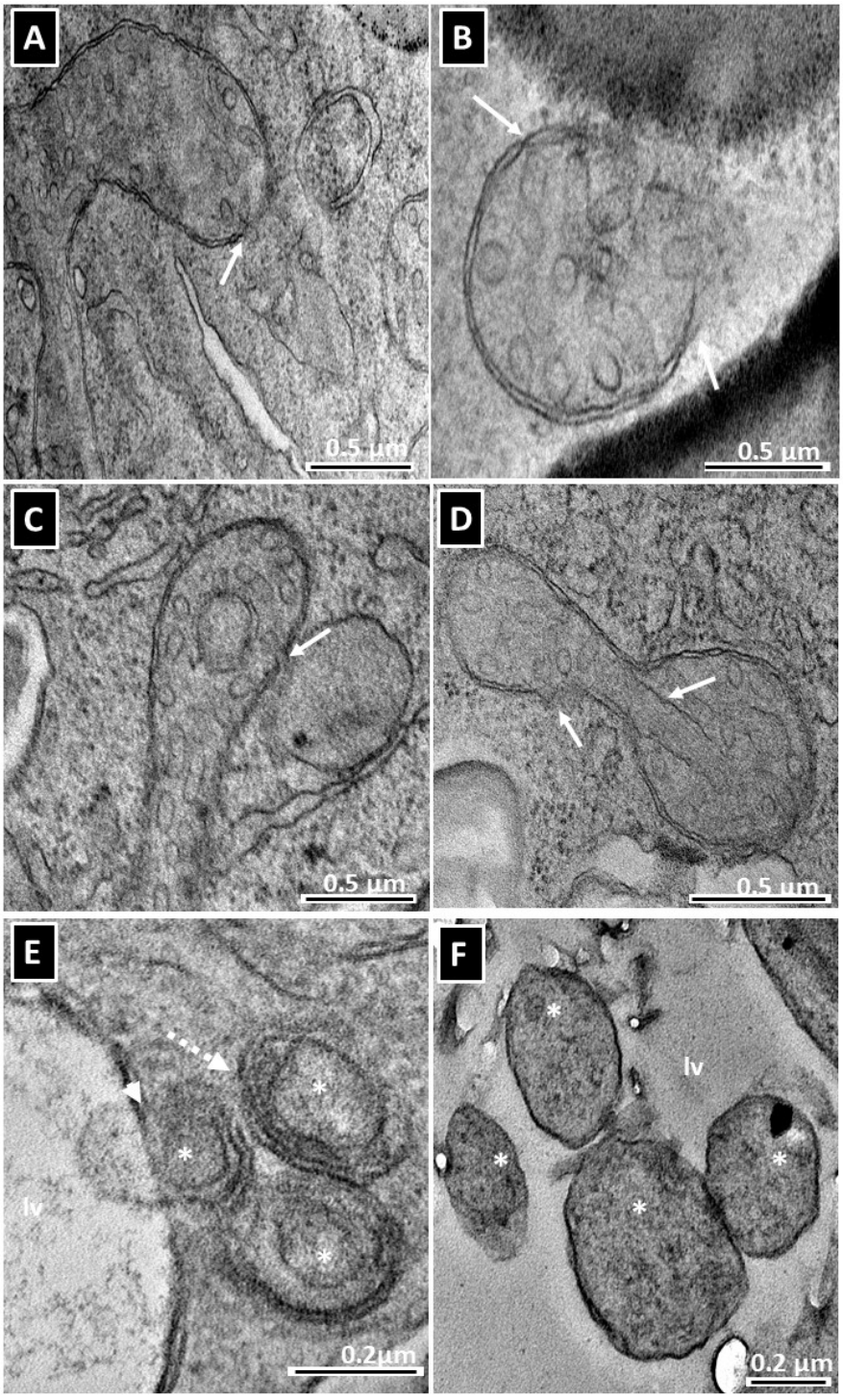


Figure 4.8 Alterations to mitochondria of heat shocked cells at 32º C after 1 and 48 HRS of treatment.

(A-D) Mitochondria profiles with ruptured outer membranes and herniated inner membranes (white arrows).
(E & F) Damaged mitochondria at the interface and inside lytic vacuoles (white asterisks). Note multiple membranes around profiles (broken white arrows)
Abbrev: lv=lytic vacuoles.

4.3.1.8 Chloroplasts

The chloroplast envelope and thylakoid membranes remained intact in most cells (n=25) subjected to 32º C heat-shock after 1 HR of the treatment and were similar to those of control chloroplasts (Fig. 4.9 A). Occasionally multilamellar structures were associated with the chloroplast envelope in 6 % of chloroplasts of heat-shocked cells after 1 HR of treatment (Fig. 4.9 B). After 48 HRS of heat-shock there was damage to the chloroplast envelope and the thylakoids were amorphous (Fig. 4.9 C & D).

The chloroplasts in cells heat-shocked at 37º C had degenerated with disorganized thylakoid membranes (Fig. 4.9 E).

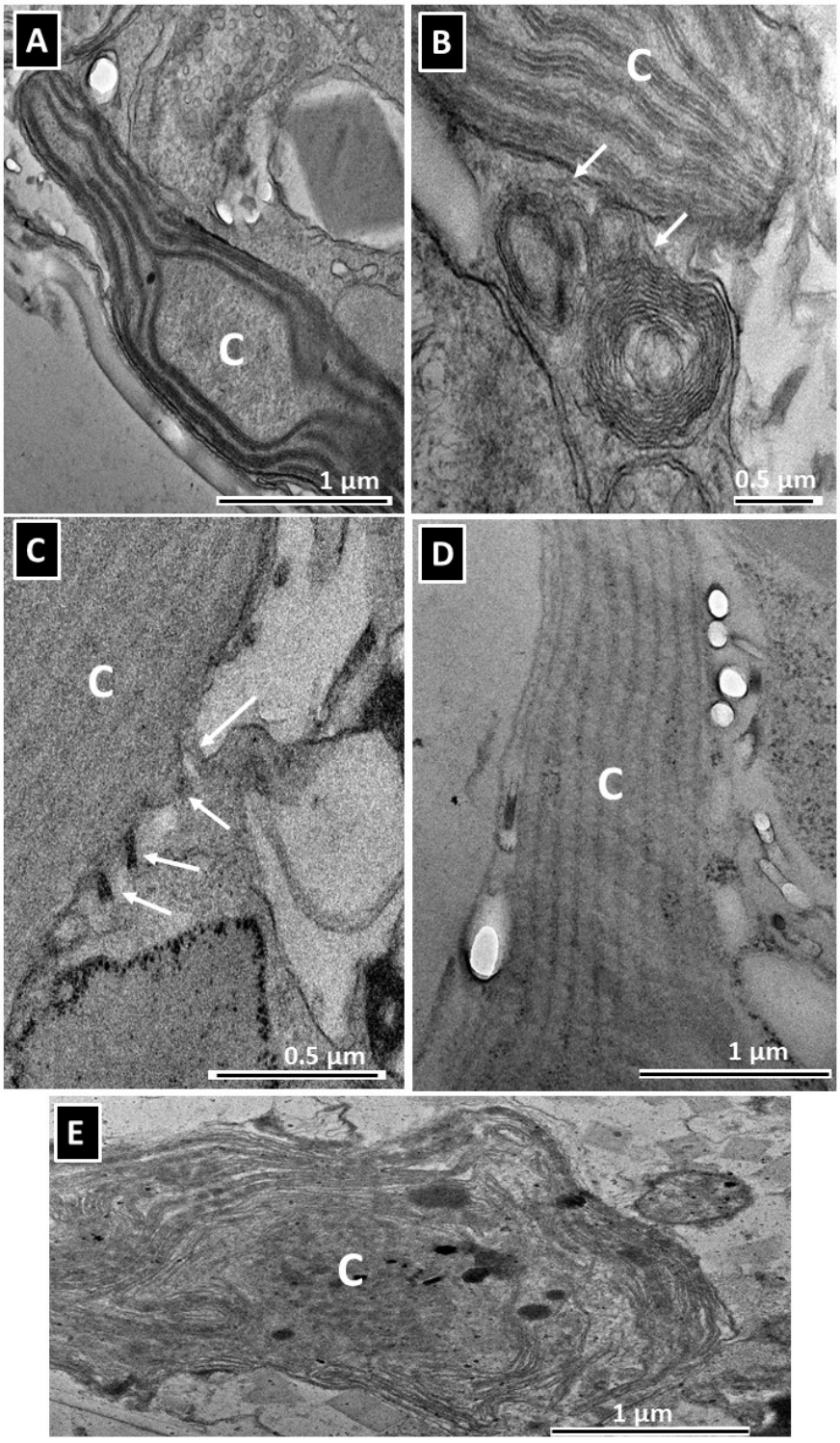


Figure 4.9 Chloroplasts in control cells and those heat-shocked at 32 and 37 ºC.

(A) Intact envelope (white arrow) and thylakoid membranes in chloroplasts of control cells.

(B) Contact sites between chloroplast envelope and multilamellar structures (white arrows) at 32º C after 1 HR of heat-shock.

(C & D) Amorphous chloroplasts and damaged chloroplast envelope in cells heat-shocked at 32º C after 48h HRS

(F) Disorganized thylakoids in cells heat-shocked at 37º C after 1 HR. *Abbrev: C-=chloroplast.*

4.3.2 DEVDase activity assay analysis assay

When cells were heat-shocked at 32º C there was a significant increase ($p < 0.05$; $n = 6$) in relative fluorescence when compared with that of unheated cells 1-HR post-treatment (Fig. 4.10 A). However, the addition of a DEVDase activity inhibitor specific to caspase-3 activity, was found to have no significant effect on the level of fluorescence, thus nullifying the assumption of DEVDase activity in the heat-shocked cells. Relative fluorescence was higher in heat-shocked cells than the control cells at 48- hours post-treatment ($p < 0.05$; $n = 6$) (Fig. 4.10A). However, the addition of a DEVDase activity inhibitor did not reduce DEVDase activity.

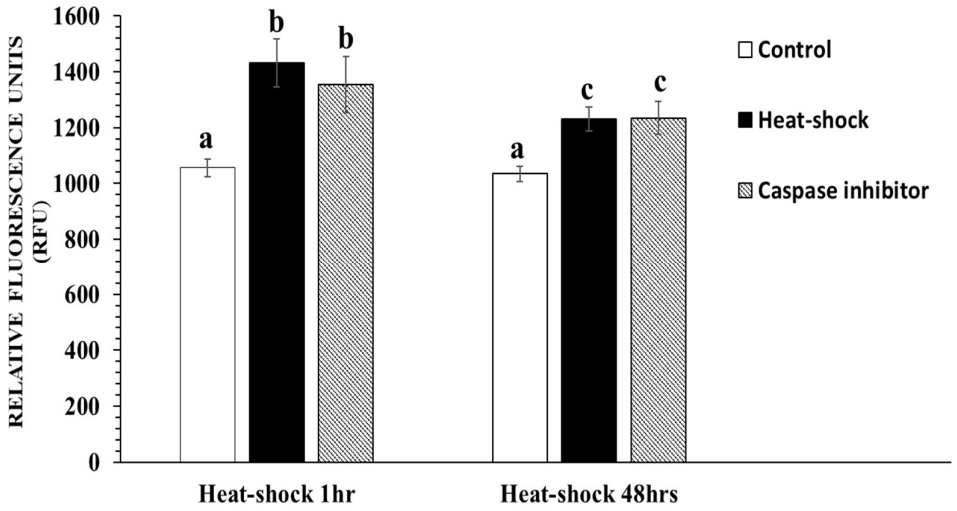


Figure 4.10 DEVDase activity in heat-shocked cells at 32º C, 1- and 48- HRS post-treatment. Bars represent mean ± SE, n=6. Different letters represent significant differences at $p < 0.05$ using ANOVA and the Tukey Honest Significant Difference (HSD) post-test.

4.3.3 Reactive Oxygen Species (ROS)

4.3.3.1 Staining of heat-shocked cells with DHR 123 fluorogenic probe

Both heat-shocked and control cells stained positively for the dihydrorhodamine (DHR) 123 fluorogenic probe. About 34 % of cells 1-HR after the heat-shock treatment had higher fluorescence levels than the control cells (e.g., Fig. 4. 11 A). The higher levels of green fluorescence translate to an increase in ROS.

After 48-HRS of heat-shock 31 % of heat-shocked cells had higher ROS levels than control cells (e.g., Fig. 4.11 B). The levels of ROS in heat-shocked cells were lower after 48 HRS than those recorded at 1 HR post treatment.

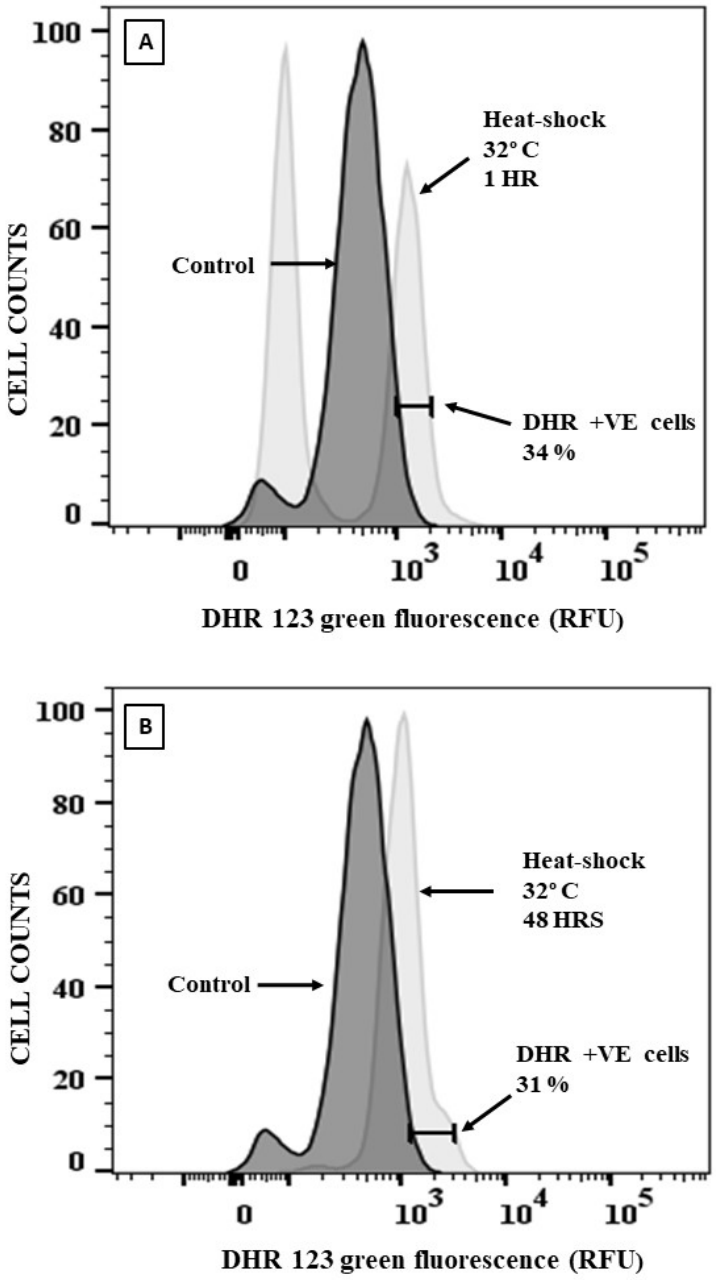


Figure 4.11 DHR 123 fluorescent probe showing green fluorescence emission in control and 32º C heat-shocked cells, after 1 and 48 HRS of heat stress. The X- axis represents green fluorescence (DHR 123 probe); Y- axis represents cell counts; gates represent the percentage of the population of heat-shocked cells.

At 37º C the fluorescence levels were all lower than those of the control cells and were therefore considered to be negative for the DHR 123 probe probe (Fig. 4. 12A).

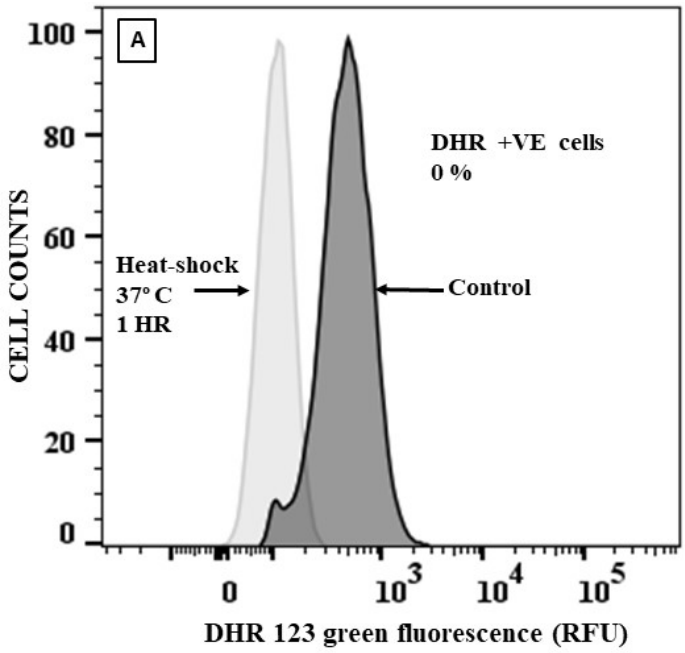


Figure 4.12 DHR 123 fluorescent probe showing green fluorescence emission in control and 37º C heat-shocked cells, after 1HR of heat stress. The X- axis represents green fluorescence (DHR 123); Y - axis represents cell counts; gates represent the percentage of the populations of heat-shocked cells.

4.3.3.2 Single-staining of heat-shocked cells with PI fluorescent probe

Approximately 19 % of cells heat shocked at 32º C were positively stained with PI, 1 HR posttreatment (Fig. 4.13 A). The number of PI positive cells increased to 23 % at 48 HRs posttreatment (Fig. 4.13 B).

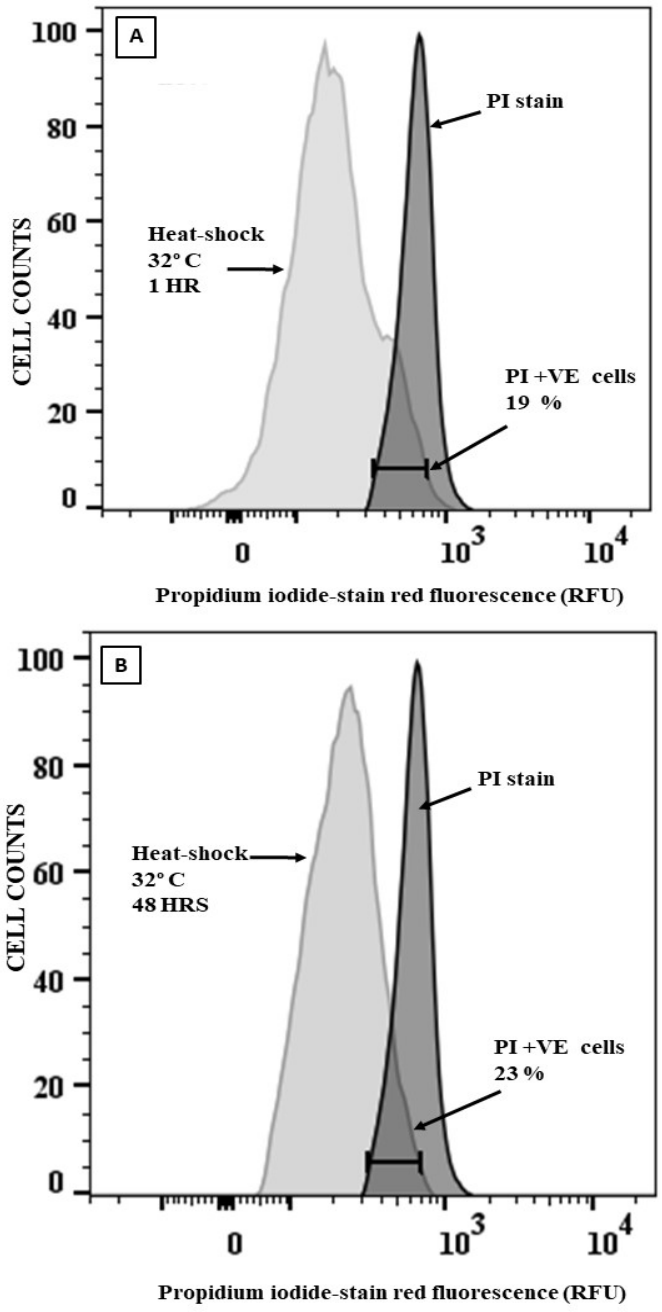


Figure 4.13 PI probe showing red fluorescence emission in heat-shocked cells at 32º C 1- and 48- HRS after treatment. The X- axis represents relative red fluorescence (PI); Y - axis represents cell counts; gates represent the percentage of the populations of PI positive cells.

About 92 % of cells heat-shocked at 37º C stained positively for PI at 1 HR posttreatment, indicating that they were dead (Fig. 4.14 A).

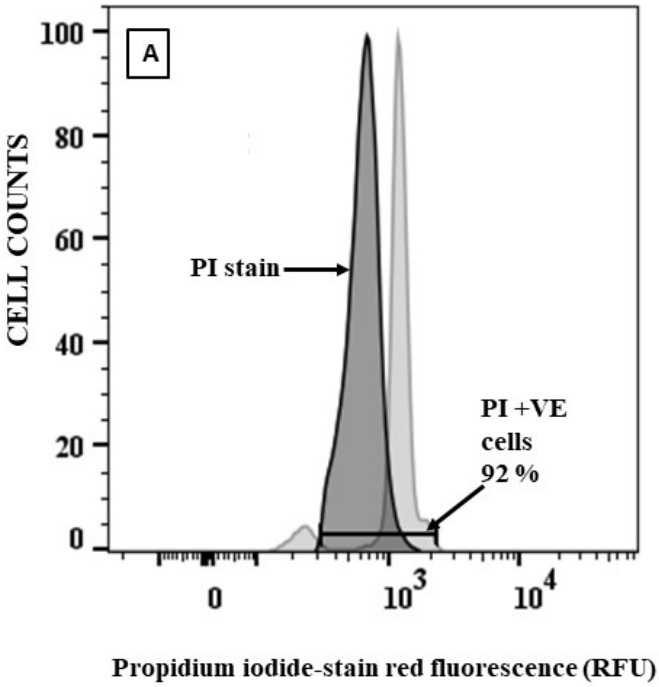


Figure 4.14 PI probe showing red fluorescence emission in heat-shocked cells at 37º C 1- HR after treatment. X- axis represents relative red fluorescence (PI); Y - axis represents cell counts; gates represent the percentage of the populations of heat-shocked cells

4.4 DISCUSSION

This study subjected *P. redfieldii* cells to varying levels of heat-shock to determine if heat stress would induce PCD and to establish if the response of these cells to an acute stress like heat-shock would be different from that of cells deprived of essential nutrients like nitrates and organic phosphates. The response of *P. redfieldii* to heat-shock at 32 ºC was unexpected as the majority of cells showed stress tolerance. Programmed cell death was however induced to a small population of cells and there were similarities in the morphology and biochemical activity of cells dying of heat-shock to those dying from nutrient deprivation. It was also established that increasing the temperature to 37 ºC was lethal to the cells and the majority of cells died in an unprogrammed manner.

4.4.1 Ultrastructural morphology

Ultrastructural changes in heat-shocked cells at 32 ºC of *P. redfieldii* included moderate vacuolation, alteration of nuclei, the upregulation of ribosomes and MVBs, alterations to mitochondria and chloroplasts and the retraction and damage of the amphiesmal membranes. These changes were also observed in the field and nutrient deprived cells. Cells that were heat-shocked at 37 ºC were lysed and only disintegrated chloroplasts and lipid bodies could be discerned.

Vacuolation and autophagy

The activation of a catabolic process in cells that were heat-shocked at 32 ºC revealed that the impact of thermal stress was within the coping limits of *P. redfieldii*. It is possible that the heat-shock stress activated an upregulation of heat-shock proteins in *P. redfieldii* that mitigated the impact of the thermal shock. An upregulated expression of heat-shock proteins has been shown in other species of Prorocentrum like *P. minimum* and *P. cordatum* (Dougan *et al*., 2023; Guo and Ki, 2012), and other dinoflagellates like *Symbiodinium sp*. when exposed to heat-shock treatment (Rosic *et al.*, 2011). It is also possible that the thecal plates offered a layer of protection against the heat and therefore dampened the effects of the 32 ºC heat-shock in *P. redfieldii* cells.

It was also noted that the catabolic processes in the heat-shocked cells constituted of microautophagy, MVBs and multilamellar structures but lacked the ER derived double membraned structures that were observed in nutrient and bloom cells. It is possible that the catabolic process in these cells was involved in the degradation of damaged and folded proteins as a result of the heat-shock. The activation of autophagy in response to heat-shock has previously occurred in *Arabidopsis thaliana* (Sedaghatmehr *et al*., 2019; Zhou *et al*., 2013).

The upregulation of catabolic processes in heat-shocked cells which was also observed in the bloom and nutrient deprived cells indicates that it is an inherent coping mechanism against various stress types in *P. redfieldii*.

The nucleus

The chromatin clumps and dilated nuclear envelopes observed in the nuclei of heat-shocked cells after 48 HRS of treatment reveal damage that could be associated with secondary necrosis in these cells.

Piecemeal autophagy of the nucleus observed in the nuclei of heat-shocked cells agrees with what has been observed in the nutrient deprived and bloom cells. It can also be suggested that this phenomenon is an inherent response of *P. redfieldii* nuclei against various types of stress.

The endomembrane system

An abundance of ribosomes after 48 HRS of the 32º C heat-shock treatment in *P. redfieldii* cells points to an upregulated synthesis of proteins that would be involved in stress acclimation, like heat shock proteins as it has been shown in other dinoflagellates (Dougan et al., 2023; Guo and Ki, 2012; Zhang et al., 2019a). The upregulation of MVBs in the heat-shocked cells agrees with what has been observed in the nutrient deprived and bloom cells and highlights the interplay between the endocytic and the autophagic pathways in these organisms.

The Mitochondria

The phenomenon of herniated mitochondria in cells that were heat-shocked at 32 ºC is consistent with what was observed in mitochondria of nutrient deprived and bloom cells. These mitochondria could also have been experiencing increased levels of ROS that could no longer be counteracted by antioxidants as it was established for those cells that were deprived of nutrients. Changes in mitochondrial membranes when exposed to thermal stress have been reported in the dinoflagellate host *Aiptasia pulchella* during coral bleaching (Dunn *et al.*, 2012). Mitochondrial depolarization was determined as a marker of PCD in heat-shocked *Plasmodium falciparum* undergoing autophagy-like PCD (Engelbrecht and Coetzer, 2013). *Plasmodium* and *Prorocentrum* belong to the supergroup Alveolata in the eukaryotic tree and therefore they could share some similarities in the manner which they undergo PCD.

The removal of damaged mitochondria in heat-shocked cells did not involve the engulfment by ER derived double membranes that were witnessed in the field and nutrient deprived cells but were observed inside multilamellar structures. Their elimination is viewed as a way of mitigating high levels of ROS and is consistent with what was observed in the nutrient deprived and bloom cells.

The chloroplasts

Alterations of chloroplasts subjected to heat-shock at 32º C in *P. redfieldii* are consistent with the response observed in other phytoplankton chloroplasts exposed to heat stress in various studies (Zuppini *et al*., 2009, 2007).

The damage to the chloroplast was gradual because changes to the chloroplast membranes were only evident after 48HRS of heat-shock treatment. Contrastingly, chloroplast thylakoids were completely dismantled in cells that were exposed to the 37º C heat-shock treatment. This phenomenon is associated with necrotic cell death (Dunn *et al.*, 2004).

4.4.2 Biochemical activity

The failure of DEVDase activity in the heat-shocked cells at 32º C in. *P. redfieldii* is consistent with the response observed in the nutrient deprived cells. It is acceptable because other PCD phenotypes like autophagic cell death and paraptosis can occur without the activation of caspase-activity (Affenzeller *et al.*, 2009; Sperandio *et al*., 2000).

An accumulation of ROS was indicative of oxidative stress in the heat-shocked cells. The levels of oxidative stress were not changed but instead were reduced after 48 HRS and this response of the heat-shocked cells differed from that of the P-deplete cells. The difference in the behaviour of *P. redfieldii* to the two stressors is likely to be a result of an upregulation of heat-shock proteins. Although, the activity of heat-shock proteins was not carried out in this study, in other dinoflagellates an upregulation of heat-shock proteins resulted in thermal stress tolerance (Kobiyama *et al*., 2010; Zhang *et al*., 2019b).

Contrastingly cells that were heated at 37 ºC had low levels of ROS that were even lower than those in the control cells and shows that the heat-shock in these cells was lethal and they died by necrosis. It is likely that in these cells the heat shock proteins were not activated. This agrees with the view that heat-shock proteins are activated under mild heat-stress conditions (Lindquist and Craig, 1988).

The majority of cells that were heated at 32º C were viable at 1- and 48-HRS after heat-shock, while most cells that were heat-shocked at 37º C were not viable 1-HR post-treatment. The viability of the heat-shocked cells corresponds with the levels of ROS in these cells indicating that oxidative stress mediated cell death in these cells.

4.4.3 Is there any evidence that PCD was induced by heat-shock in *P. redfieldii?*

The ultrastructure of cells subjected to a 32º C heat-shock revealed that the stress was not acute and did not induce a rapid PCD in these cells. Catabolic pathways like the upregulation of MBVs were upregulated. The 32º C heat-shock treatment can be considered to be a mild heat-stressor for cells of *P. redfieldii*, an outcome that was unexpected for an organism that grows at much lower

temperatures (± 19º C) in its natural habitat. The outer covering (theca) of *P. redfieldii* could have minimized the effect of the stress on these organisms. Also, the presence of HSPs in some bloom forming dinoflagellates provides them the ability to have tolerance for temperature fluctuations (Deng *et al.*, 2018; Guang *et al*., 2004).

However, a minority of cells exhibited ultrastructural characteristics that were similar to those observed in the P-deplete and bloom cells. Morphological and biochemical markers associated with PCD in the minority of heat-shocked cells included extensive vacuolation by autophagy, alterations to mitochondrial and chloroplast membranes, an increase in ROS and loss of viability. In these cells the amphiesmal membranes were retracted from the thecal plates. It can thus be said yes, heat-shock was able to induce a programmed cell death in a minority of *P. redfieldii* whose morphotype corresponds with that of cells sampled from the P-deplete and those from a collapsing bloom. The retraction of the amphiesmal membranes can be regarded as the onset of secondary necrosis as witnessed in the bloom cells. Heat-shock has successfully induced PCD in several microalgae (Franklin *et al*., 2004; Jimenez *et al.*, 2009; Dingman and Lawrence, 2012; Zuppini *et al.*, 2007; Nedelcu, 2006; Durand *et al.*, 2011).

Contrastingly, subjecting the cells to 37º C heat-shock revealed that the stress was acute a necrotic cell death. This was revealed by the complete lysis of most organelles except for chloroplast membranes which were highly dismantled and damaged. The low levels of ROS in the PI positive cells indicate that the impact of the heat stimulus on the cells was immediate.

4.5 CONCLUDING REMARKS

This study elucidated the morphological and biochemical response of *P. redfieldii* when it is subjected to heat-shock. Heat-shock stress at 32º C was not an acute stressor and consequently induced autophagic cell death in a minority of *P. redfieldii* cells a phenotype which was similar to what was exhibited in the dying nutrient deplete and bloom cells. The ability to mitigate stress could have resulted from the upregulation of heat-shock proteins and also the protective covering

of the theca. However, the elevation of temperature to 37º C, resulted in an uncontrolled degradation of the cells which resulted in a necrotic cell death.

CHAPTER 5- GENERAL DISCUSSION & CONCLUDING REMARKS

This study determined, for the first time, ultrastructural changes that occur in cells sampled from a collapsing harmful algal bloom of *P. redfieldii* and established whether there was structural evidence of PCD as a driver of the bloom collapse. The ultrastructural responses were then compared with those of cultures grown in replete conditions deprived of two essential macronutrients in the form of nitrates (NO^{3-}) and inorganic phosphates (PO_4^{3-}), and heat stress. For each stressor tested, biochemical assays known to associate with PCD, such as the expression of DEVDase activity, accumulation of ROS as well as DNA laddering, were used to corroborate that the ultrastructural responses were linked with the induction of PCD.

Programmed cell death is a broad concept, which has been given many definitions over the years. However, these definitions have been conceptualized recently into five concepts, namely, the mechanistic, evolutionary, developmental, ecological and immunological concepts (Durand and Ramsey, 2023). The current study has adopted to define PCD in *P. redfieldii* by using the mechanistic concept, which gives insight of the structural and biochemical pathway in a cell undergoing PCD. Therefore, the mechanistic definition which is adopted by Durand and Ramsey (2023) that PCD is "an active, genetically controlled, cellular self-destruction driven by a series of complex biochemical events and specialized cellular machinery" (Berman-Frank *et al.,* 2004, pg 997) was used to determine if PCD occurred in dying cells of *P. redfieldii*.

The findings of this study established that cells dying from a collapsing bloom exhibited morphological characteristics like extensive vacuolation, ER derived double membrane structures and lytic vacuoles, which resemble the process of autophagy. There was an upregulation of the endomembrane system and interaction between the endomembrane and autophagic system. There were also structural alterations in the mitochondria and chloroplasts which are organelles known to be sources of ROS. Similar morphological characteristics were revealed in those cells dying from a lack of inorganic phosphates and those dying from a mild heat-shock (32 ºC). Biochemical activity further revealed an overproduction of ROS in the nutrient and the mild heat-shocked

deprived cells.

In view of the mechanistic definition of PCD, the morphological and biochemical characteristics exhibited by *P. redfieldii* cells dying from the collapsing bloom and those dying from nutrient deprivation and mild heat-shock, partially satisfy the mechanistic definition of PCD by Berman-Frank *et al.* (2004). This is because the absence of DEVDase activity in the dying *P. redfieldii* cells does not agree with the "active, genetically controlled" part of the definition. However, the dying cells at ultrastructure level revealed an integrated response between the autophagic and endomembrane machinery which ensured a controlled self-destruction of the cells in response to stress and an accumulation of ROS at a biochemical level which mediated the cell death, and their behaviour agrees with the second part of the definition, a "cellular self-destruction driven by a series of complex biochemical events and specialized cellular machinery". In the current study, PCD in the *P. redfieldii* cells can therefore be defined as a mechanistic, DEVDase-independent cell death driven by an integrated response between the autophagic and endomembrane machinery mediated by excessive levels of ROS. In contrast, the cells that were heat-shock at 37 ºC died an uncontrolled cell death and do not satisfy the mechanistic definition.

The morphological characteristics revealed by the dying cells of *P. redfieldii* fit the phenotype of autophagic cell death. Autophagic cell death is defined as cell death that occurs with autophagy (Kroemer and Levine, 2008). Based on the evolutionary concept of PCD, which defines PCD as either and adaptation or non-adaptation (Durand and Ramsey, 2018), autophagic cell death is regarded to be a non-adaptation. However, it is postulated that at an ecological level an autophagic cell death in *P. redfieldii* could offer some benefits to this organism. This is because dinoflagellate blooms occur during the downwelling period when the water is initially nutrient rich but because there are no upwelling winds the nutrients are not replenished (Smayda and Trainer, 2010). Dinoflagellates use this downwelling window to proliferate and form blooms. A prolonged form of cell death like an autophagic cell death would give these organisms an advantage to fully utilise this window before the next upwelling cycle begins. Secondary necrosis as the oxidative stress levels increase is also not ruled out in these cells.

Through a detailed ultrastructural investigation of *P. redfieldii* cells collected from a collapsing bloom, this study has answered the main aim by revealing the nature of cell death of this organism. This is the first account of an ultrastructural study relating to cell death mechanisms of *P. redfieldii* dying in a bloom event in an upwelling region and will contribute to our understanding of the process of bloom collapse. It will also add to the fundamental knowledge that is required to alleviate the problem of anaerobic HABs caused by dinoflagellates which affect the population dynamics in the Benguela region. For an example the findings that inorganic phosphates are more limiting than nitrates in *P. redfieldii* would be useful especially to the small-scale aquaculture farmers in the region.

Some of the limitations that were experienced during this study were in the methodology. Measurements of chlorophyll fluorescence in the laboratory would have contributed to the knowledge about the physiological state of the nutrient deprived cells but the inability to access an aquatic chlorophyll fluorescence meter hindered this method. The traditional centrifugation technique to collect and concentrate the algal cells was used in the current study, however in hindsight a gentle suction of cells onto pore filters could have been a better method of collection.

The ultrastructural study on *P. redfieldii* revealed some interesting facts about the autophagic flux that was upregulated as a response to stress in these cells. In future, a detailed analysis on the molecular aspects of autophagy in stressed *P. redfieldii* cells would bring more insight about autophagy mechanisms in this organism. For an example a molecular study can reveal if the process that resembled piecemeal autophagy of the nucleus (PMN) is executed by ATG genes because there are no existing reports of its occurrence in dinoflagellates.

In conclusion, this study using detailed ultrastructure has shown the nature of cell death in *P. redfieldii* and has proved the existence of PCD in a collapsing bloom.

REFERENCES

Abadie, E., Kaci, L., Berteaux, T., Hess, P., Sechet, V., Masseret, E., Rolland, J., Laabir, M. 2015. Effect of Nitrate, Ammonium and Urea on Growth and Pinnatoxin G Production of Vulcanodinium rugosum. Marine Drugs 13(9), 5642–5656. doi.org/10.3390/md13095642

Affenzeller, M. J., Darehshouri, A., Andosch, A., Lutz, C., Lutz-Meindl, U. 2009. Salt stress-induced cell death in the unicellular green alga Micrasterias denticulata. Journal of Experimental Botany 60 (3), 939–954. doi.org/10.1093/jxb/ern348

Affenzeller, Matthias Josef, Darehshouri, A., Andosch, A., Lütz, C., Lütz-Meindl, U. 2009. PCD and autophagy in the unicellular green alga Micrasterias denticulata. Autophagy 5(6), 854–855.

Allen, R.T., Hunter, W.J., Agrawal, D.K. 1997. Morphological and biochemical characterization and analysis of apoptosis. Journal of Pharmacological Toxicology Methods 37(4), 215–228. doi.org/10.1016/S1056-8719(97)00033-6

Ameisen, J.C. 2009. The Origin and Evolution of Programmed Cell Death, in: John Wiley & Sons, Ltd (Ed.), Encyclopedia of Life Sciences. John Wiley & Sons, Ltd, Chichester, UK, p. a0021988. doi.org/10.1002/9780470015902.a0021988

Ameisen, J.C. 1996. The Origin of Programmed Cell Death. Science 272, 1278–1279. doi.org/10.1126/science.272.5266.1278

Ameisen, J.C., Idziorek, T., Billaut-Mulot, O., Loyens, M., Tissier, J.P., Potentier, A., Ouaissi, A. 1995. Apoptosis in a unicellular eukaryote (Trypanosoma cruzi): implications for the evolutionary origin and role of programmed cell death in the control of cell proliferation, differentiation and survival. Cell Death Differentiation2(4), 285–300.

Anderson, D.M. 1989. Toxic Algal Blooms and Red Tides: A Global Perspective, in: Okaichi, T., Nemoto, T. (Eds.), Red Tides: Biology, Environmental Science, and Toxicology. Elsevier, New York.

Anderson, D.M., Cembella, A.D., Hallegraeff, G.M. 2012. Progress in understanding harmful algal blooms (HABs): Paradigm shifts and new technologies for research, monitoring and management. Annual Review of Marine Science 4, 143–176. doi.org/10.1146/annurev-marine-120308-081121

Anderson, D.M., Glibert, P.M., Burkholder, J.M. 2002. Harmful algal blooms and eutrophication: Nutrient sources, composition, and consequences. Estuaries 25(4), 704–726. doi.org/10.1007/BF02804901

Aoki, K., Satoi, S., Harada, S., Uchida, S., Iwasa, Y., Ikenouchi, J. 2020. Coordinated changes in cell membrane and cytoplasm during maturation of apoptotic bleb. Molecular Biologyof the Cell31(8), 833–844. doi.org/10.1091/mbc.E19-12-0691

Ashford, T.P., Porter, K.R. 1962. Cytoplasmic componentsin hepatic cell lysosomes. Journal of Cell Biology 12(1), 198–202.

Azam, F. 1998. Microbial Control of Oceanic Carbon Flux: The Plot Thickens. Science280, 694–696. doi.org/10.1126/science.280.5364.694

Backer, L.A.C., Mcgillicuddy, D.J. 2006. At the interface between coastal oceanography and human health. Oceanography 19 (2), 13.

Bakun, A., Agostini, V.N. 2001. Seasonal patterns of wind-induced upwelling/downwelling in the Mediterranean Sea. Scientia Marina 65(3), 243–257. doi.org/10.3989/scimar.2001.65n3243

Barreto Filho, M.M., Bagatini, I.L., Durand, P.M. 2023. How shall we measure programmed cell death in eukaryotic microalgae? European Journal of Phycology58 (1), 13-34. doi.org/10.1080/09670262.22.2041731

Barreto Filho, M.M., Durand, P.M., Andolfato, N.E., Jordaan, A., Sarmento, H., Bagatini, I.L. 2022b. Programmed cell death in the coccoid green microalga Ankistrodesmus densus Korshikov (Sphaeropleales, Selenastraceae). European Journal of Phycology57 (2), 193–206. doi.org/10.1080/09670262.2021.1938240

Barsanti, L., Gualtieri, P.2005. Algae: Anatomy, Biochemistry, and Biotechnology (1st ed.). Florida: CRC Press.

Bar-Zeev, E., Avishay, I., Bidle, K.D., Berman-Frank, I.2013. Programmed cell death in the marine cyanobacterium Trichodesmium mediates carbon and nitrogen export. The ISME Journal7 (12), 2340–2348. doi.org/10.1038/ismej.2013.121

Bassham, D.C., Crespo, J.L. 2014. Autophagy in plants and algae. Frontiers in Plant Science5, 679. doi.org/10.3389/fpls.2014.00679

Bekker, A., Holland, H.D., Wang, P.-L., Rumble, D., Stein, H.J., Hannah, J.L., Coetzee, L.L., Beukes, N.J. 2004. Dating the rise of atmospheric oxygen. Nature 427, 117–120. doi.org/10.1038/nature02260

Benitez-nelson, C.R. 1999. The biogeochemical cycling of phosphorus in marine systems. Earth-Science Reviews 51, 109-135. doi.org/10.1016/S0012-8252(00)00018-0

Berges, J.A., Falkowski, P.G. 1998. Physiological stress and cell death in marine phytoplankton: Induction of proteases in response to nitrogen or light limitation. Limnology & Oceanography 43 (1), 129–135. doi.org/10.4319/lo.1998.43.1.0129

Berman-Frank, I., Bidle, K.D., Haramaty, L., Falkowski, P.G. 2004. The demise of the marine cyanobacterium, Trichodesmium spp., via an autocatalyzed cell death pathway. Limnology & Oceanography 49 (4), 997–1005. doi.org/10.4319/lo.2004.49.4.0997

Bidle, K.D., 2016. Programmed Cell Death in Unicellular Phytoplankton. Current Biology 26 (13), R594–R607. doi.org/10.1016/j.cub.2016.05.056

Bidle, K.D., Bender, S.J. 2008. Iron Starvation and Culture Age Activate Metacaspases and Programmed Cell Death in the Marine Diatom Thalassiosira pseudonana. Eukaryotic Cell 7(2), 223–236. doi.org/10.1128/EC.00296-07

Bidle, K.D., Falkowski, P.G., 2004. Cell death in planktonic, photosynthetic microorganisms. National Reviews in Microbiology 2, 643–655. doi.org/10.1038/nrmicro956

Bidle, K. D., Haramaty, L., Barcelos e Ramos, J., Falkowski, P. 2007. Viral activation and recruitment of metacaspases in the unicellular coccolithophore, Emiliania huxleyi. Proceedings of the National Academy of Sciences104 (14), 6049–6054. doi.org/10.1073/pnas.0701240104

Bišová, K., Zachleder, V. 2014. Cell-cycle regulation in green algae dividing by multiple fission. Journal of Experimental Botany 65, 2585–2602. doi.org/10.1093/jxb/ert466

Borowitzka, M.A. 2018. The 'stress' concept in microalgal biology—homeostasis, acclimation and adaptation. Journal of Applied Phycology, 30(5), 2815–2825. doi.org/10.1007/s10811-018-1399-0

Bortner, C.D., Oldenburg, N.B., Cidlowski, J.A. 1995. The role of DNA fragmentation in apoptosis. Trends in Cell Biology 5(1), 21–26. doi.org/10.1016/s0962-8924(00)88932-1

Boss, E., Behrenfeld, M. 2010. In situ evaluation of the initiation of the North Atlantic phytoplankton bloom. Geophysical Research Letter 37 (18). doi.org/10.1029/2010GL044174

Bramucci, A.R., Case, R.J. 2019. Phaeobacter inhibens induces apoptosis-like programmed cell death in calcifying Emiliania huxleyi. Scientific Reports 9(1), 5215. doi.org/10.1038/s41598-018-36847-6

Brussaard, C., Riegman, R., Noordeloos, A., Cadee, G., Witte, H., Kop, A.J., Nieuwland, G., Duyl, F., Bak, R.P.M. 1995. Effects of grazing, sedimentation and phytoplankton cell lysis on the structure of a coastal pelagic food web. Marine Ecology Progress Series, 123, 259–271. doi.org/10.3354/meps123259

Burki, F., Roger, A.J., Brown, M.W., Simpson, A.G.B. 2020. The New Tree of Eukaryotes. Trends in Ecology and Evolution 35(1), 43–55. doi.org/10.1016/j.tree.2019.08.008

Bursa, A. 1959. The genus Prorocentrum Ehrenberg. Morphodynamics, protoplasmatic structures, and taxonomy. Canadian Journal of Botany 37 (1), 1–31.

Burson, A., Matthijs, H.C.P., de Bruijne, W., Talens, R., Hoogenboom, R., Gerssen, A., et al. 2014. Termination of a toxic Alexandrium bloom with hydrogen peroxide. Harmful Algae 31, 125–135. doi.org/10.1016/j.hal.2013.10.017

Cape Nature, 2015. Warning: Red tide along the West Coast. CapeNature. URL https://www.capenature.co.za/warning-red-tide-along-west-coast/ (accessed 5.17.19).

Carmona-Gutierrez, D., Bauer, M.A., Zimmermann, A., Aguilera, A., Austriaco, N., Ayscough, K., et al. 2018. Guidelines and recommendations on yeast cell death nomenclature. Microbial Cell 5, 4–31. doi.org/10.15698/mic2018.01.607

Chan, L.L., Hodgkiss, I.J., Wan, J.M.-F., Lum, J.H.-K., Mak, A.S.-C., Sit, W.-H., Lo, S.C.-L. 2004. Proteomic study of a model causative agent of harmful algal blooms, Prorocentrum triestinum II: The use of differentially expressed protein profiles under different growth phases and growth conditions for bloom prediction. Proteomics 4, 3214–3226. doi.org/10.1002/pmic.200300838

Chan, Y.-H., Wong, J.T.Y. 2007. Concentration-dependent organization of DNA by the dinoflagellate histone-like protein HCc3. Nucleic Acids Research 35(8), 2573–2583. doi.org/10.1093/nar/gkm165

Choi, C.J., Berges, J.A. 2013. New types of metacaspases in phytoplankton reveal diverse origins of cell death proteases. Cell Death & Disease, (2), 490. doi.org/10.1038/cddis.2013.21

Choi, C.J., Brosnahan, M.L., Sehein, T.R., Anderson, D.M., Erdner, D.L. 2017. Insights into the loss factors of phytoplankton blooms: The role of cell mortality in the decline of two inshore Alexandrium blooms. Limnology &Oceanography 62(4), 1742–1753. doi.org/10.1002/lno.10530

Chow, M.H., Yan, K.T.H., Bennett, M.J., Wong, J.T.Y. 2010. Birefringence and DNA Condensation of Liquid Crystalline Chromosomes. Eukaryotic Cell 9, 1577–1587. doi.org/10.1128/EC.00026-10

Clarke, P.G., Clarke, S. 1996. Nineteenth century research on naturally occurring cell death and related phenomena. Anatomy & Embryology 193(2), 81–99. doi.org/10.1007/BF00214700

Cohen, G.M. 1997. Caspases: the executioners of apoptosis. Biochemical Journal 326 (1), 1–16. doi.org/10.1042/bj3260001

Coleman, M.L., Chisholm, S.W. 2010. Ecosystem-specific selection pressures revealed through comparative population genomics. Proceedings of the National Academy of Science 107(43), 18634–18639. doi.org/10.1073/pnas.1009480107

Collins, A.R. 2004. The comet assay for DNA damage and repair. Molecular Biotechnology 26(3), 249. doi.org/10.1385/MB:26:3:249

Connolly, P.F., Jäger, R., Fearnhead, H.O.2014. New roles for old enzymes: killer caspases as the engine of cell behavior changes. Frontiers in Physiology 5, 1-10. doi.org/10.3389/fphys.2014.00149

Crawford, R.M. 1981. The Siliceous Components of the Diatom Cell Wall and Their Morphological Variation, in: Simpson, T.L., Volcani, B.E. (Eds.), Silicon and Siliceous Structures in Biological Systems. Springer, New York, pp. 129–156. doi.org/10.1007/978-1-4612-5944-2_6

Crichton, M., Hutchings, L., Lamont, T., Jarre, A. 2013. From physics to phytoplankton: Prediction of dominant cell size in St Helena Bay in the Southern Benguela. Journal of Plankton Research35, 526–541. doi.org/10.1093/plankt/fbt012

Csanady, G. T. 1982. On the Structure of Transient Upwelling Events. Journal of Physical Oceanography12,84-96.

Cui, Y., He, Y., Cao, W., Gao, J., Jiang, L. 2018. The Multivesicular Body and Autophagosome Pathways in Plants. Frontiers in Plant Science9, 1837. doi.org/10.3389/fpls.2018.01837

Dagenais-Bellefeuille, S., Morse, D. 2013. Putting the N in dinoflagellates. Frontiers of Microbiology 4, 369. doi.org/10.3389/fmicb.2013.00369

Darehshouri, A., Affenzeller, M., Lütz-Meindl, U.2008. Cell death in the unicellular green alga Micrasterias upon H_2O_2 induction. Plant Biology10 (6), 732–745. https://doi.org/10.1111/j.1438-8677.2008.00078.x

Das, K., Roychoudhury, A. 2014. Reactive oxygen species (ROS) and response of antioxidants as ROS-scavengers during environmental stress in plants. Frontiers in Environmental Science 2. doi.org/10.3389/fenvs.2014.00053

Debrabant, A., Lee, N., Bertholet, S., Duncan, R., Nakhasi, H.L. 2003. Programmed cell death in trypanosomatids and other unicellular organisms. International Journal of Parasitology33 (3), 257–267. doi.org/10.1016/S0020-7519(03)00008-0

Deng, Y., Hu, Z., Chai, Z., Tang, Y.Z. 2018. Molecular cloning of heat shock protein 60 (Hsp60) and 10 (Hsp10) genes from the cosmopolitan and harmful dinoflagellate Scrippsiella trochoidea and their differential transcriptions responding to temperature stress and alteration of life cycle. Marine Biology166 (1), 7. doi.org/10.1007/s00227-018-3455-3

Deponte, M. 2008. Programmed cell death in protists. Biochima et Biophysica Acta (BBA) - Molecular Cell Research 1783(7), 1396–1405.doi.org/10.1016/j.bbamcr.2008.01.018

Dingman, J.E., Lawrence, J.E. 2012. Heat-stress-induced programmed cell death in Heterosigma akashiwo (Raphidophyceae). Harmful Algae 16, 108–116. doi.org/10.1016/j.hal.2012.02.003

Dodge, J. 1965. Chromosome structure in the dinoflagellates and the problem of the mesokaryotic cell. Excerpta Medica International Congress Series 91, 264–265.

Dodge, J.D. 1975. The Prorocentrales (Dinophyceae). II. Revision of the taxonomy within the genus Prorocentrum. Botanical Journal of the Linnean Society 71(2), 103–125. doi.org/10.1111/j.1095-8339.1975.tb02449.x

Dodge, J.D. 1973. The Fine Structure of Algal Cells. London, Academic Press.

Dodge, J.D. 1972. The ultrastructure of the dinoflagellate pusule: A unique osmo-regulatory organelle. Protoplasma 75(3), 285–302. doi.org/10.1007/BF01279820

Dodge, J.D. 1968. The fine structure of chloroplasts and pyrenoids in some marine dinoflagellates. Journal of Cell Science 3, 41–48.

Dodge, J.D., Bibby, B.T. 1973. The Prorocentrales (Dinophyceae): I. A comparative account of fine structure in the genera Prorocentrum and Exuviaella. Botanical Journal of the Linnean Society 67(2), 175–187. doi.org/10.1111/j.1095-8339.1973.tb01737.x

Dou-ding, L., Goebel, J. 2001. Five red tide species in genus Prorocentrum including the description of Prorocentrum donghaiense Lu SP. nov. from the East China Sea. Chinese Journal of Oceanology & Limnology 19, 337–344. doi.org/10.1007/BF02850738

Dougan, K.E., Deng, Z.-L., Wöhlbrand, L., Reuse, C., Bunk, B., Chen, Y., et al. 2023. Multi-omics analysis reveals the molecular response to heat stress in a "red tide" dinoflagellate. Genome Biology 24 (1), 1–32. doi.org/10.1186/s13059-023-03107-4

Dunn, S.R., Pernice, M., Green, K., Hoegh-Guldberg, O., Dove, S.G. 2012. Thermal stress promotes host mitochondrial degradation in symbiotic cnidarians: are the batteries of the reef going to run out? PLOS ONE 7(7), e39024. doi.org/10.1371/journal.pone.0039024

Dunn, S.R., Schnitzler, C.E., Weis, V.M. 2007. Apoptosis and autophagy as mechanisms of dinoflagellate symbiont release during cnidarian bleaching: every which way you lose. Proceedings of the Royal Society of Biological Science 274(1629), 3079–3085. doi.org/10.1098/rspb.2007.0711

Dunn, S.R., Thomason, J.C., Le Tissier, M.D.A., Bythell, J.C. 2004. Heat stress induces different forms of cell death in sea anemones and their endosymbiotic algae depending on temperature and duration. Cell Death & Differentiation 11(11), 1213–1222. doi.org/10.1038/sj.cdd.4401484

Durand, P.M. 2020. The Evolutionary Origins of Life and Death. University of Chicago Press.

Durand, P.M., Choudhury, R., Rashidi, A., Michod, R.E. 2014. Programmed death in a unicellular organism has species-specific fitness effects. Biology Letters 10, 1088. doi.org/10.1098/rsbl.2013.1088

Durand, P.M., Ramsey, G. 2023. The concepts and origins of cell mortality. History & Philosophies of the Life Sciences 45(2), 23. doi.org/10.1007/s40656-023-00581-8

Durand, P.M., Ramsey, G. 2018. The Nature of Programmed Cell Death. Biological Theory. doi.org/10.1007/s13752-018-0311-0

Durand, P.M., Rashidi, A., Michod, R.E. 2011. How an Organism Dies Affects the Fitness of Its Neighbors. The American Naturalist 177 (2), 224–232. doi.org/10.1086/657686

Durand, P.M., Sym, S., & Michod, R.E. 2016. Programmed Cell Death and Complexity in Microbial Systems. Current Biology 26 (13), R587-R593. doi.org/10.1016/j.cub.2016.05.057

Duve, C. 1959. Lysosomes, a new group of cytoplasmic particle.

Dyhrman, S.T. 2016. Nutrients and Their Acquisition: Phosphorus Physiology in Microalgae, in: Borowitzka, M.A., Beardall, J., Raven, J.A. (Eds.), The Physiology of Microalgae. Springer International Publishing, Cham, pp. 155–183. doi.org/10.1007/978-3-319-24945-2_8

Ebrahimi, M., Habernig, L., Broeskamp, F., Aufschnaiter, A., Diessl, J., Atienza, I., et al.2021. Phosphate restriction promotes longevity via activation of autophagy and the multivesicular body pathway. Cells 10 (11), 3161.

Ekert, P., Silke, J., Vaux, D. 1999. Caspase inhibitors. Cell Death & Differentiation6(11), 1081–1086.doi.org/10.1038/sj.cdd.4400594

Elmore, S. 2007. Apoptosis: A Review of Programmed Cell Death. Toxicologic Pathology 35(4), 495–516. doi.org/10.1080/01926230701320337

Engelbrecht, D., Coetzer, T.L. 2013. Turning up the heat: heat stress induces markers of programmed cell death in Plasmodium falciparum in vitro. Cell Death & Disease4(12), e971–e971. doi.org/10.1038/cddis.2013.505

Eppley, R.W. 1972. Temperature and phytoplankton growth in the sea. Fisheries Bulletin 10, 1063-1085.

Erdner, D., Choi, C.J., Brosnahan, M., Sehein, T., Anderson, D.M. 2016. Contribution of Cell Mortality to the Decline of a Toxic Dinoflagellate Bloom. Proceedings in American Geophysical Union. PP24A-0547.

Fader, C.M., Colombo, M.I. 2009. Autophagy and multivesicular bodies: two closely related partners. Cell Death & Differentiation 16, 70–78. doi.org/10.1038/cdd.2008.168

Falkowski, P.G. 1994. The role of phytoplankton photosynthesis in global biogeochemical cycles. Photosynthesis Research 39 (3), 235–258. doi.org/10.1007/BF00014586

Falkowski, P.G. Raven, J.A. 2007. Aquatic Photosynthesis. Massachusetts, Blackwell Science.

Faust, M.A., Gulledge, R.A. 2002. Identifying Harmful Marine Dinoflagellates. Contributions from the United States National Herbarium 42, 1–144.

Fawcett, A., Bernard, S., Pitcher, G., Probyn, T., du Randt, A. 2006. Real-time monitoring of harmful algal blooms in the southern Benguela. African Journal of Marine Science 28, 257–260. doi.org/10.2989/18142320609504158

Feldmann, G., Haouzi, D., Moreau, A., Durand-Schneider, A., Bringuier, A., Berson, A., Mansouri, A., Fau, D., Pessayre, D. 2000. Opening of the mitochondrial permeability transition pore causes matrix expansion and outer membrane rupture in Fas-mediated hepatic apoptosis in mice. Hepatology 31, 674–683.

Fisher, R.M., Cornwallis, C.K., West, S.A. 2013. Group Formation, Relatedness, and the Evolution of Multicellularity. Current Biology 23, 1120–1125. doi.org/10.1016/j.cub.2013.05.004

Forde, B.G. 2000. Nitrate transporters in plants: structure, function and regulation. Biochimica et Biophysica Acta BBA - Biomembranes1465, 219–235. doi.org/10.1016/S0005-2736(00)00140-1

Foyer, C.H., Ferrario-Méry, S., Noctor, G. 2001. Interactions Between Carbon and Nitrogen Metabolism, in: Lea, P.J., Morot-Gaudry, J.-F. (Eds.), Plant Nitrogen. Berlin, Springer, , pp. 237–254. doi.org/10.1007/978-3-662-04064-5_9

Foyer, C.H., Hanke, G. 2022. ROS production and signalling in chloroplasts: cornerstones and evolving concepts. The Plant Journal 111, 642–661. doi.org/10.1111/tpj.15856

Franklin, D., Hoegh-Guldberg, O., Jones, R., Berges, J. 2004a. Cell death and degeneration in the symbiotic dinoflagellates of the coral Stylophora pistillata during bleaching. Marine Ecology Progress Series 272, 117–130. doi.org/10.3354/meps272117

Franklin, D.J., Berges, J.A. 2004. Mortality in cultures of the dinoflagellate Amphidinium carterae during culture senescence and darkness. Proceedings of the Royal Society of London 271, 2099–2107. doi.org/10.1098/rspb.2004.2810

Franklin, D.J., Brussaard, C.P.D., Berges, J.A. 2006. What is the role and nature of programmed cell death in phytoplankton ecology? European Journal of Phycology 41, 1–14. doi.org/10.1080/09670260500505433

Fuchs, Y., Steller, H. 2011. Programmed Cell Death in Animal Development and Disease. Cell147, 742–758. doi.org/10.1016/j.cell.2011.10.033

Gagat, P., Bodyl, A., Mackiewicz, P., Stiller, J.W. 2014. Tertiary plastid endosymbiosis in Dinoflagellates, in: Loffelhardt, W. (Ed.), Endosymbiosis. Springer-verlag.

Galluzzi, L., Vitale, I., Aaronson, S.A., Abrams, J.M., Adam, D., Agostinis, P., et al. 2018. Molecular mechanisms of cell death: recommendations of the Nomenclature Committee on Cell Death (2018). Cell Death & Differentiation 25, 486–541. doi.org/10.1038/s41418-017-0012-4

Gao, Y, Erdner, D. 2022. Dynamics of cell death across growth stages and the diel cycle in the dinoflagellate Karenia brevis. The Journal of Eukaryotic Microbiology 69(1). doi.org/10.1111/jeu.12874

Gao, Y. , Erdner, D.L. 2022. Insights into Stress-Induced Death Processes during Aging in the Marine Bloom-Forming Dinoflagellate Karenia brevis. Journal of Marine Science & Engineering 10 (12), 1993. doi.org/10.3390/jmse10121993

Glibert, P.M., Burkholder, J.M., Parrow, M.W., Lewitus, A.J., Gustafson, D.E. 2006. Direct uptake of nitrogen by Pfiesteria piscicida and Pfiesteria shumwayae, and nitrogen nutritional preferences. Harmful Algae 5(4), 380–394. doi.org/10.1016/j.hal.2006.04.009

Glibert, P.M., Wilkerson, F.P., Dugdale, R.C., Raven, J.A., Dupont, C.L., Leavitt, P.R., Parker, A.E., Burkholder, J.M., Kana, T.M.2016. Pluses and minuses of ammonium and nitrate uptake and assimilation by phytoplankton and implications for productivity and community composition, with emphasis on nitrogen-enriched conditions. Limnology & Oceanography 61(1), 165–197. doi.org/10.1002/lno.10203

Glücksmann, A. 1951. Cell Deaths in Normal Vertebrate Ontogeny. Biological Reviews 26(1), 59–86. doi.org/10.1111/j.1469-185X.1951.tb00774.x

Goncalves, E.C., Koh, J., Zhu, N., Yoo, M.-J., Chen, S., Matsuo, T., et al. 2016. Nitrogen starvation-induced accumulation of triacylglycerol in the green algae: evidence for a role for ROC40, a transcription factor involved in circadian rhythm. The Plant Journal 85(6), 743–757. doi.org/10.1111/tpj.13144

Gorelova, O., Baulina, O., Ismagulova, T., Kokabi, K., Lobakova, E., Selyakh, I., et al. 2019. Stress-induced changes in the ultrastructure of the photosynthetic apparatus of green microalgae. Protoplasma 256(1), 261–277. doi.org/10.1007/s00709-018-1294-1

Gornik, S.G., Ford, K.L., Mulhern, T.D., Bacic, A., McFadden, G.I. Waller, R.F. 2012. Loss of Nucleosomal DNA Condensation Coincides with Appearance of a Novel Nuclear Protein in Dinoflagellates. Current Biology 22(24), 2303–2312. doi.org/10.1016/j.cub.2012.10.036

Gornik, S.G., Hu, I., Lassadi, I., Waller, R.F., 2019. The Biochemistry and Evolution of the Dinoflagellate nucleus. Microorganisms 7(8). doi.org/10.3390/microorganisms7080245

Grimaud, G.M., Le guennec, V., Ayata, S.-D., Mairet, F., Sciandra, A., Bernard, O. 2015. Modelling the effect of temperature on phytoplankton growth across the global ocean. Proceedings of the8th Vienna International Conference on Mathematical Modelling 48, 228–233. doi.org/10.1016/j.ifacol.2015.05.059

Guang, D., Yeguang, L., Hongjun, H., Yuzao, Q., Yahong, G., Zhongkui, L. 2004. Effects of temperature, light and pH on photosynthesis, and of light--dark cycle on growth rate and biomass of Scrippsiella trochoidea and Alexandrium tamarense. Wuhan Botanical research, 22(2), 129–135.

Guillard, R.R.L., Ryther, J.H. 1962. Studies of marine planktonic diatoms: Cyclotella nana Hustedt, and Detonula Confervacea (Cleve) Gran. Canadian Journal of Microbiology8(2), 229–239. doi.org/10.1139/m62-029

Guinder, V., Molinero, J.C. 2013. Climate Change Effects on Marine Phytoplankton, in: Marine Ecology in a Changing World (1st ed.). Florida, CRC press. doi.org/10.1201/b16334-4

Guo, R., Ebenezer, V., Ki, J.-S. 2012. Transcriptional responses of heat shock protein 70 (Hsp70) to thermal, bisphenol A, and copper stresses in the dinoflagellate Prorocentrum minimum. Chemosphere 89, 512–520. doi.org/10.1016/j.chemosphere.2012.05.014

Guo, R., Ki, J.-S. 2012. Differential transcription of heat shock protein 90 (HSP90) in the dinoflagellate Prorocentrum minimum by copper and endocrine-disrupting chemicals. Ecotoxicology, 21(5), 1448–1457. doi.org/10.1007/s10646-012-0898-z

Guo, R., Youn, S.H., Ki, J.-S. 2015. Heat Shock Protein 70 and 90 Genes in the Harmful Dinoflagellate Cochlodinium polykrikoides: Genomic Structures and Transcriptional Responses to Environmental Stresses. International Journal of Genomics. doi.org/10.1155/2015/484626

Hallegraeff, G.M. 1993. A review of harmful algal blooms and their apparent global increase. Phycologia 32(2), 79–99. doi.org/10.2216/i0031-8884-32-2-79.1

Hariri, M., Millane, G., Guimond, M.-P., Guay, G., Dennis, J.W., Nabi, I.R. 2000. Biogenesis of Multilamellar Bodies via Autophagy. Molecular Biology of the Cell 11(1), 255–268. doi.org/10.1091/mbc.11.1.255

Hasanzadeh, M., Shadjou, N., de la Guardia, M. 2017. Early-stage diagnosis of programmed cell death (apoptosis) using electroanalysis: Nanomaterial and methods overview. TrAC Trends in Analytical Chemistry 93, 199–211. doi.org/10.1016/j.trac.2017.06.007

Hatsugai, N., Kuroyanagi, M., Yamada, K., Meshi, T., Tsuda, S., Kondo, M., Nishimura, M., Hara-Nishimura, I. 2004. A Plant Vacuolar Protease, VPE, Mediates Virus-Induced Hypersensitive Cell Death. Science 305 (5685), 855–858. doi.org/10.1126/science.1099859

Heil, C.A., Glibert, P.M., Fan, C. 2005. *Prorocentrum minimum* (Pavillard) Schiller: A review of a harmful algal bloom species of growing worldwide importance. Harmful Algae 4, 449–470. doi.org/10.1016/j.hal.2004.08.003

Hoppenrath, M., Leander, B.S. 2008. Morphology and Molecular Phylogeny of a new marine sand-dwelling *Prorocentrum* species, *P. Tsawwassenense* (Dinophyceae, Prorocentrales), From British Columbia, Canada. Journal of Phycology 44(2), 451–466. doi.org/10.1111/j.1529-8817.2008.00483.x

Houghton, J. 2001. The science of global warming. Interdisciplinary Science Reviews 26(4), 247–257. doi.org/10.1179/isr.2001.26.4.247

Huang, X., Huang, B., Chen, J., Liu, X. 2016. Cellular responses of the dinoflagellate Prorocentrum donghaiense Lu to phosphate limitation and chronological ageing. Journal of Plankton Research 38, 83–93. doi.org/10.1093/plankt/fbv112

Hutchings, L., Pitcher, G., Probyn, T.A., Bailey, G.W. 1995. The chemical and biological consequences of coastal upwelling. pp. 65–81. In: Upwelling in oceans: modern processes and ancient records (1st ed.), John Wiley & Sons Ltd.

Iglesias-Guimarais, V., Gil-Guiñon, E., Gabernet, G., García-Belinchón, M., Sánchez-Osuna, M., Casanelles, E., et al. 2012. Apoptotic DNA Degradation into Oligonucleosomal Fragments, but Not Apoptotic Nuclear Morphology, Relies on a Cytosolic Pool of DFF40/CAD Endonuclease. The Journal of Biological Chemistry 287(10), 7766–7779. doi.org/10.1074/jbc.M111.290718

Janouškovec, J., Gavelis, G.S., Burki, F., Dinh, D., Bachvaroff, T.R., Gornik, S.G., et al. 2017. Major transitions in dinoflagellate evolution unveiled by phylotranscriptomics. Proceedings of the National Academy of Science 114, E171–E180. doi.org/10.1073/pnas.1614842114

Jauzein, C., Erdner, D.L. 2013. Stress-related Responses in Alexandrium tamarense Cells Exposed to Environmental Changes. Journal of Eukaryotic Microbiology 60 (5), 526–538. doi.org/10.1111/jeu.12065

Ji, H., Yu, Z., He, L., Zhu, J., Cao, X., Song, X. 2021. Programmed cell death induced by modified clay in controlling Prorocentrum donghaiense bloom. Journal of Environmental Sciences 109, 123–134. doi.org/10.1016/j.jes.2021.03.039

Jiang, P. L., Pasaribu, B., Chen, C. S. 2014. Nitrogen-Deprivation Elevates Lipid Levels in Symbiodinium spp. by Lipid Droplet Accumulation: Morphological and Compositional Analyses. PLOS ONE 9(1). doi.org/10.1371/journal.pone.0087416

Jimenez, C., Capasso, J.M., Edelstein, C.L., Rivard, C.J., Lucia, S., Breusegem, S., Berl, T., Segovia, M. 2009. Different ways to die: cell death modes of the unicellular chlorophyte Dunaliella viridis exposed to various environmental stresses are mediated by the caspase-like activity DEVDase. Journal of Experimental Botany 60, 815–828. doi.org/10.1093/jxb/ern330

Jing, X., Lin, S., Zhang, H., Koerting, C., Yu, Z. 2017. Utilization of urea and expression profiles of related genes in the dinoflagellate Prorocentrum donghaiense. PLOS ONE 12, e0187837. doi.org/10.1371/journal.pone.0187837

Johnson, J.G., Janech, M.G., Van Dolah, F.M. 2014. Caspase-like activity during aging and cell death in the toxic dinoflagellate Karenia brevis. Harmful Algae 31, 41–53. doi.org/10.1016/j.hal.2013.08.005

Julien, O., Wells, J.A. 2017. Caspases and their substrates. Cell Death & Differentiation 24, 1380–1389. doi.org/10.1038/cdd.2017.44

Kalinina, V., Berdieva, M., Aksenov, N., Skarlato, S. 2023. Phosphorus deficiency induces sexual reproduction in the dinoflagellate Prorocentrum cordatum Scientific Reports 13, 14191. doi.org/10.1038/s41598-023-41339-3

Karl, D.M. 2014. Microbially mediated transformations of phosphorus in the sea: new views of an old cycle. Annual Review of Marine Science 6, 279–337. doi.org/10.1146/annurev-marine-010213-135046

Kerr, J.F.R., Wyllie, A.H., Currie, A.R. 1972. Apoptosis: A Basic Biological Phenomenon with Wide-ranging Implications in Tissue Kinetics. British Journal of Cancer 26, 239–257.

Khalili, M., Radosevich, J.A. 2018. Paraptosis, in: Radosevich, J. (Ed.), Apoptosis and Beyond. John Wiley & Sons, Inc., Hoboken, NJ, USA, pp. 343–366. https://doi.org/10.1002/9781119432463.ch16

Kiel, J.A.K.W. 2010a. Autophagy in unicellular eukaryotes. Philosophical Transactions of the Royal Society of Biological Sciences 365, 819–830. doi.org/10.1098/rstb.2009.0237

Kinnally, K.W., Peixoto, P.M., Ryu, S.-Y., Dejean, L.M. 2011. Is mPTP the gatekeeper for necrosis, apoptosis, or both? Biochimica Biophysica Acta BBA - Molecular Cell Research 1813(4), 616–622. doi.org/10.1016/j.bbamcr.2010.09.013

Kirchman, D.L. 1999. Phytoplankton death in the sea. Nature 398 (6725), 293–294. doi.org/10.1038/18570

Klemenčič, M., Funk, C. 2018. Structural and functional diversity of caspase homologues in non-metazoan organisms. Protoplasma 255, 387–397. doi.org/10.1007/s00709-017-1145-5

Klut, M.E., Bisalputra, T., Antia, N.J. 1987. Some observations on the structure and function of the dinoflagellate pusule. Canadian Journal of Botany 65, 736–744. doi.org/10.1139/b87-098

Kobiyama, A., Tanaka, S., Kaneko, Y., Lim, P.-T., Ogata, T. 2010. Temperature tolerance and expression of heat shock protein 70 in the toxic dinoflagellate *Alexandrium tamarense* (Dinophyceae). Harmful Algae, 9 (2), 180–185. doi.org/10.1016/j.hal.2009.09.002

Kourtis, N., Tavernarakis, N. 2009. Autophagy and cell death in model organisms. Cell Death & Differentiation 16 (1), 21–30. doi.org/10.1038/cdd.2008.120

Kroemer, G., El-Deiry, W.S., Golstein, P., Peter, M.E., Vaux, D., Vandenabeele, P., et al.2005. Classification of cell death: recommendations of the Nomenclature Committee on Cell Death. Cell Death & Differentiation12, 1463–1467. doi.org/10.1038/sj.cdd.4401724

Kroemer, G., Galluzzi, L., Vandenabeele, P., Abrams, J., Alnemri, E.S., Baehrecke, E.H., et al. 2009. Classification of cell death: recommendations of the Nomenclature Committee on Cell Death 2009. Cell Death & Differentiation 16 (1), 3–11. https://doi.org/10.1038/cdd.2008.150

Kroemer, G., Levine, B. 2008. Autophagic cell death: the story of a misnomer. Nature Reviews Molecular Cell Biology 9 (12), 1004–1010.doi.org/10.1038/nrm2529

Kroemer, G., Petit, P., Zamzami, N., Vayssière, J.-L., Mignotte, B. 1995. The biochemistry of programmed cell death. The FASEB Journal9 (13), 1277–1287. https://doi.org/10.1096/fasebj.9.13.7557017

Kudela, R.M., Seeyave, S., Cochlan, W.P. 2010. The role of nutrients in regulation and promotion of harmful algal blooms in upwelling systems. Progress in Oceanography 85, 122–135. doi.org/10.1016/j.pocean.2010.02.008

Kuthanova, A., Opatrny, Z., Fischer, L. 2008. Is internucleosomal DNA fragmentation an indicator of programmed death in plant cells? Journal of Experimental Botany 59(8), 2233–2240. doi.org/10.1093/jxb/ern090

Kvam, E., Goldfarb, D. 2007. Nucleus-Vacuole Junctions and Piecemeal Microautophagy of the Nucleus in S. cerevisiae. Autophagy 3(2), 85–92. doi.org/10.4161/auto.3586

Kwon, S.I., Park, O.K. 2008. Autophagy in plants. Journal of Plant Biology 51(5), 313–320. doi.org/10.1007/BF03036132

Kyrylkova, K., Kyryachenko, S., Leid, M., Kioussi, C. 2012. Detection of Apoptosis by TUNEL Assay, in: Kioussi, C. (Ed.), Odontogenesis, Methods in Molecular Biology. Humana Press, Totowa, NJ, pp. 41–47. doi.org/10.1007/978-1-61779-860-3_5

La, S.R., Ndhlovu, A., Durand, P.M.2022. The Ancient Origins of Death Domains Support the 'Original Sin' Hypothesis for the Evolution of Programmed Cell Death. Journal of Molecular Evolution, 90 (1), 95–113. doi.org/10.1007/s00239-021-10044-y

Lau, R.K.L., Kwok, A.C.M., Chan, W.K., Zhang, T.Y., Wong, J.T.Y. 2007. Mechanical characterization of cellulosic thecal plates in dinoflagellates by nanoindentation. Journal of Nanoscience & Nanotechnology 7(2), 452–457.

Lauritano, C., De Luca, D., Ferrarini, A., Avanzato, C., Minio, A., Esposito, F., Ianora, A. 2017. De novo transcriptome of the cosmopolitan dinoflagellate Amphidinium carterae to identify enzymes with biotechnological potential. Scientific Reports7(1), 11701. doi.org/10.1038/s41598-017-12092-1

Lawrence, J.E., Chan, A.M., Suttle, C.A. 2001. A novel virus (HaNIV) cause lysis of the toxic bloom-forming alga Heterosima Aashiwo (Raphidophyceae). Journal of Phycology 37 (2), 216–222. doi.org/10.1046/j.1529-8817.2001.037002216.x

Le Borgne, R., Hoflack, B. 1998. Protein transport from the secretory to the endocytic pathway in mammalian cells. Biochimica et Biophysica Acta BBA - Molecular Cell Research 1404 (1), 195–209. doi.org/10.1016/S0167-4889(98)00057-3

Lee, P.Y., Costumbrado, J., Hsu, C.-Y., Kim, Y.H. 2012. Agarose Gel Electrophoresis for the Separation of DNA Fragments. Journal of Visualized Experiments20 (62). doi.org/10.3791/3923

Lemasters, J.J., Nieminen, A.-L., Qian, T., Trost, L.C., Elmore, S.P., Nishimura, Y., et al.1998. The mitochondrial permeability transition in cell death: a common mechanism in necrosis, apoptosis and autophagy. Biochimica et Biophysica Acta BBA - Molecular Cell Research Bioenergetics1366 (1), 177–196. doi.org/10.1016/S0005-2728(98)00112-1

Levitus, S., Antonov, J., Boyer, T. 2005. Warming of the world ocean, 1955–2003. Geophysical Research Letter 32 (2). doi.org/10.1029/2004GL021592

Li, D.-W., Tan, J.-Z., Li, Z.-F., Ou, L.-J. 2024. Membrane lipid remodeling and autophagy to cope with phosphorus deficiency in the dinoflagellate *Prorocentrum shikokuense*. Chemosphere 349, 140844.

Li, H., Li, L., Yu, L., Yang, X., Shi, X., Wang, J., Li, J., Lin, S. 2021. Transcriptome profiling reveals versatile dissolved organic nitrogen utilization, mixotrophy, and N conservation in

the dinoflagellate Prorocentrum shikokuense under N deficiency. Science of the Total Environment 763, 143013. doi.org/10.1016/j.scitotenv.2020.143013

Li, M., Li, L., Shi, X., Lin, L., Lin, S. 2015. Effects of phosphorus deficiency and adenosine 5′-triphosphate (ATP) on growth and cell cycle of the dinoflagellate *Prorocentrum donghaiense*. Harmful Algae 45, 35-41. doi.org/10.1016/j.hal.2015.05.013.

Li, W., Li, J., Bao, J. 2012. Microautophagy: lesser-known self-eating. Cellular & Molecular Life Science 69, 1125–1136. doi.org/10.1007/s00018-011-0865-5

Liefer, J.D., Garg, A., Campbell, D.A., Irwin, A.J., Finkel, Z.V. 2018. Nitrogen starvation induces distinct photosynthetic responses and recovery dynamics in diatoms and prasinophytes. PLOS ONE 13, e0195705. doi.org/10.1371/journal.pone.0195705

Lin, S., Litaker, R.W., Sunda, W.G. 2016. Phosphorus physiological ecology and molecular mechanisms in marine phytoplankton. Journal of Phycology 52 (1), 10–36. doi.org/10.1111/jpy.12365

Lindquist, S., Craig, E.A.1988. The Heat-Shock Proteins. Annual Review of Genetics 22, 631–677.

Lockshin, R.A., Williams, C.M., 1964. Programmed cell death—II. Endocrine potentiation of the breakdown of the intersegmental muscles of silk moths., Journal of Insect Physiology 10 (4), 643–649. doi.org/10.1016/0022-1910(64)90034-4

Loeblich, A.R., III, Sherley, J.L., Schmidt, R.J. 1979. The correct position of flagellar insertion in *Prorocentrum* and description of *Prorocentrum rhathymum* sp. nov. (Pyrrhophyta). Journal of Plankton Research 1, 113–120. doi.org/10.1093/plankt/1.2.113

Lorenzo, Y., Costa, S., Collins, A.R., Azqueta, A. 2013. The comet assay, DNA damage, DNA repair and cytotoxicity: hedgehogs are not always dead. Mutagenesis 28, 427–432. doi.org/10.1093/mutage/get018

Lu, S., Hodgkiss, I.J. 2004. Harmful algal bloom causative collected from Hong Kong waters, in: Ang, P.O. (Ed.), Asian Pacific Phycology in the 21st Century: Prospects and Challenges, Developments in Hydrobiology. Springer Netherlands, Dordrecht, pp. 231–238. doi.org/10.1007/978-94-007-0944-7_30

MacKenzie, S.H., Clark, A.C. 2012. Death by Caspase Dimerization, in: Matthews, J.M. (Ed.), Protein Dimerization and Oligomerization in Biology, Advances in Experimental Medicine and Biology. Springer, New York, NY, pp. 55–73. doi.org/10.1007/978-1-4614-3229-6_4

Margalef, R. 1978. Phytoplankton communities in upwelling areas. The example of NW Africa. Comunidades fitoplanctónicas en áreas de afloramiento. El ejemplo del NW de África,3.

McCall, K. 2010. Genetic control of necrosis – another type of programmed cell death. Current Opinion in Cell Biology 22, 882–888. doi.org/10.1016/j.ceb.2010.09.002

McLuskey, K., Mottram, J.C. 2015. Comparative structural analysis of the caspase family with other clan CD cysteine peptidases. Biochemical Journal466, 219–232. doi.org/10.1042/BJ20141324

Meizhen, L., Xingou, S., Chentao, G., Senjie, L. 2016 Phosphorus Deficiency Inhibits Cell Division but Not Growth in the Dinoflagellate Amphidinium carterae. Frontiers in Microbiology7, 826.

Mínguez, A., Franca, S. 1994 Dinoflagellates have a eukaryotic nuclear matrix with lamin-like proteins and topoisomerase II 13. Journal of Cell Science 107, 2861-73. doi.org/ 10.1242/jcs.107.10.2861.

Minina, E.A., Coll, N.S., Tuominen, H., Bozhkov, P.V. 2017. Metacaspases versus caspases in development and cell fate regulation. Cell Death & Differentiation 24, 1314–1325. doi.org/10.1038/cdd.2017.18

Minina, E.A., Smertenko, A.P., Bozhkov, P.V. 2014. Vacuolar cell death in plants: Metacaspase releases the brakes on autophagy. Autophagy 10, 928–929. doi.org/10.4161/auto.28236

Mizushima, N. 2004. Methods for monitoring autophagy. The International Journal of Biochemistry &Cell Biology36,2491–2502. doi.org/10.1016/j.biocel.2004.02.005

Moharikar, S., D'Souza, J.S., Kulkarni, A.B., Rao, B.J. 2006. Apoptotic-Like Cell Death Pathway Is Induced in Unicellular Chlorophyte Chlamydomonas Reinhardtii (chlorophyceae) Cells Following Uv Irradiation: Detection and Functional Analyses1. Journal of Phycology 42, 423–433. doi.org/10.1111/j.1529-8817.2006.00207.x

Monier, A., Welsh, R.M., Gentemann, C., Weinstock, G., Sodergren, E., Armbrust, E.V., Eisen, J.A., Worden, A.Z. 2012. Phosphate transporters in marine phytoplankton and their

viruses: cross-domain commonalities in viral-host gene exchanges. Environmental Microbiology 14, 162–176. doi.org/10.1111/j.1462-2920.2011.02576.x

Morel, E. 2020. Endoplasmic Reticulum Membrane and Contact Site Dynamics in Autophagy Regulation and Stress Response. Frontiers in Cell & DevelopmentalBiology8, 343. doi.org/10.3389/fcell.2020.00343

Müller, M., Schmidt, O., Angelova, M., Faserl, K., Weys, S., Kremser, L., Pfaffenwimmer, T., Dalik, T., Kraft, C., Trajanoski, Z., Lindner, H., Teis, D. 2015. The coordinated action of the MVB pathway and autophagy ensures cell survival during starvation. eLife 4. doi.org/10.7554/eLife.07736

Mullineaux, P.M., Exposito-Rodriguez, M., Laissue, P.P., Smirnoff, N. 2018. ROS-dependent signalling pathways in plants and algae exposed to high light: Comparisons with other eukaryotes. Free Radical Biology & Medicine 122, 52–64. doi.org/10.1016/j.freeradbiomed.2018.01.033

Nagata, S., Nagase, H., Kawane, K., Mukae, N., Fukuyama, H. 2003. Degradation of chromosomal DNA during apoptosis. Cell Death & Differentiation 10, 108–116. doi.org/10.1038/sj.cdd.4401161

Ndhlovu, A., Dhar, N., Garg, N., Xuma, T., Pitcher, G.C., Sym, S.D., Durand, P.M. 2017. A red tide forming dinoflagellate Prorocentrum triestinum: identification, phylogeny and impacts on St Helena Bay, South Africa. Phycologia 56 (6), 649–665. doi.org/10.2216/16-114.1

Ndhlovu, A., Durand, P., Ramsey, G. 2020. Programmed cell death as a black queen in microbial communities. Molecular Ecology 30(5),1110-1119 doi.org/10.1111/mec.15757

Nedelcu, A.M. 2009. Comparative Genomics of Phylogenetically Diverse Unicellular Eukaryotes Provide New Insights into the Genetic Basis for the Evolution of the Programmed Cell Death Machinery. Journal of Molecular Evolution 68 (3), 256-268. doi: 10.1007/s00239-009-9201-1.

Nedelcu, A.M. 2006 . Evidence for p53-like-mediated stress responses in green algae. FEBS Letters. 580, 3013–3017. doi.org/10.1016/j.febslet.2006.04.044

Nedelcu, A.M., Driscoll, W.W., Durand, P.M., Herron, M.D., Rashidi, A. 2011. On the paradigm of altruistic suicide in the unicellular world. Evolution 65 (1), 3–20. doi.org/10.1111/j.1558-5646.2010.01103.x

Nicotera, P., Melino, G. 2004. Regulation of the apoptosis-necrosis switch. Oncogene,23, 2757–2765. doi.org/10.1038/sj.onc.1207559

Ohtsuka, S., Suzaki, T., Horiguchi, T., Suzuki, N.2015. Marine Protists: Diversity and Dynamics. Springer link, Japan.

Olive, P.L., Banáth, J.P. 2006. The comet assay: a method to measure DNA damage in individual cells. Nature Protocols 1, 23–29. doi.org/10.1038/nprot.2006.5

Olson, R.J., Chisholm, S.W. 1986. Effects of light and nitrogen limitation on the cell cycle of the dinoflagellate Amphidinium carteri. Journal of Plankton Research, 8(4), 785–793. doi.org/10.1093/plankt/8.4.785

Orchard, E.D., Webb, E.A., Dyhrman, S.T. 2009. Molecular analysis of the phosphorus starvation response in Trichodesmium spp. Environmental Microbiology 11(9), 2400–2411. doi.org/10.1111/j.1462-2920.2009.01968.x

Orellana, M.V., Pang, W.L., Durand, P.M., Whitehead, K., Baliga, N.S. 2013. A Role for Programmed Cell Death in the Microbial Loop. PLOS ONE 8(5), e62595. doi.org/10.1371/journal.pone.0062595

Pacini, E., Jacquard, C., Clément, C. 2011. Pollen vacuoles and their significance. Planta 234(2), 217–227. doi.org/10.1007/s00425-011-1462-4

Papini, A., Gonnelli, C., Tani, C., Falco, P.D., Wolswijk, G., Santosuosso, U., Nuccio, C., Schiff, S., Lazzara, L., Menicucci, F., Belli, M., Karssa, T.H., Ballini, R. 2018. Autophagy Induced by Heavy Metal and Starvation Stress in Microalgae. Phytomorphology: An International Journal of Plant Morphology 68, 7–12.

Patel, D., Witt, S.N. 2017. Ethanolamine and Phosphatidylethanolamine: Partners in Health and Disease. Oxidative Medicine and Cellular Longevity e4829180. https://doi.org/10.1155/2017/4829180

Patel, R., Rinker, L., Peng, J., Chilian, W.M. 2017. Reactive Oxygen Species: The Good and the Bad, In: Reactive Oxygen Species (ROS) in Living Cells, Filip, C., & Albu, E. (Eds.), IntecOpen.

Petrov, V., Hille, J., Mueller-Roeber, B., Gechev, T.S. 2015. ROS-mediated abiotic stress-induced programmed cell death in plants. Frontiers in Plant Science 6. doi.org/10.3389/fpls.2015.00069

Pitcher, G., Moita, T., Trainer, V., Kudela, R., Figueiras, P., Probyn, T. 2005. Global Ecology and Oceanography of Harmful Algal Blooms, GEOHAB Core Research Project: HABs in Upwelling Systems. IOC and SCOR, Paris and Baltimore, 82.

Pitcher, G.C. 1988. Mesoscale heterogeneities of the phytoplankton distribution in St Helena Bay, South Africa, following an upwelling event. South African Journal of Marine Science7, 9 –23. doi.org/10.2989/025776188784379170

Pitcher, G.C., Calder, D. 2000. Harmful algal blooms of the southern Benguela Current: a review and appraisal of monitoring from 1989 to 1997. South African Journal of Marine Science 22, 255–271. doi.org/10.2989/025776100784125681

Pitcher, G.C., Figueiras, F.G., Hickey, B.M., Moita, M.T. 2010. The physical oceanography of upwelling systems and the development of harmful algal blooms. Progress in Oceanography 85, 5–32. doi.org/10.1016/j.pocean.2010.02.002

Pitcher, G.C., Jacinto, G.S. 2020. Ocean deoxygenation links to harmful algal blooms. In: Oceans deoxygenation, everyone's problem-causes, impacts, consequences & solutions, D. Laffoley and J.M. Baxter (Eds.), IUCN, Gland, Switzerland.

Pitcher, G.C., Louw, D.C. 2021. Harmful algal blooms of the Benguela eastern boundary upwelling system. Harmful Algae 102, 101898. doi.org/10.1016/j.hal.2020.101898

Pitcher, G.C., Probyn, T.A. 2016a. Suffocating Phytoplankton, Suffocating Waters—Red Tides and Anoxia. Frontiers in Marine Science 3. doi.org/10.3389/fmars.2016.00186

Pitcher, G.C., Probyn, T.A. 2011. Anoxia in southern Benguela during the autumn of 2009 and its linkage to a bloom of the dinoflagellate Ceratium balechii. Harmful Algae 11, 23–32. doi.org/10.1016/j.hal.2011.07.001

Pitcher, G.C., Probyn, T.A., du Randt, A., Lucas, Andrew.J., Bernard, S., Evers-King, H., Lamont, T., Hutchings, L. 2014. Dynamics of oxygen depletion in the nearshore of a coastal embayment of the southern Benguela upwelling system. Journal of Geophysical Research: Oceans 119, 2183–2200. doi.org/10.1002/2013JC009443

Pitcher, G.C., Walker, D.R., Mitchell-Innes, B.A., Moloney, C.L. 1991. Short-term variability during an anchor station study in the southern Benguela upwelling system: Phytoplankton dynamics. Progress in Oceanography 28, 39–64. doi.org/10.1016/0079-6611(91)90020-M

Pokrzywinski, K. 2014. Characterization of bacterial algicide IRI-160AA: insights on programmed death pathways and organelle impacts in harmful dinoflagellates (Thesis). University of Delaware.

Pokrzywinski, K.L., Tilney, C.L., Modla, S., Caplan, J.L., Ross, J., Warner, M.E., Coyne, K.J. 2017a. Effects of the bacterial algicide IRI-160AA on cellular morphology of harmful dinoflagellates. Harmful Algae 62, 127–135. doi.org/10.1016/j.hal.2016.12.004

Pokrzywinski, K.L., Tilney, C.L., Warner, M.E., Coyne, K.J. 2017b. Cell cycle arrest and biochemical changes accompanying cell death in harmful dinoflagellates following exposure to bacterial algicide IRI-160AA. Scientific Reports7(1), 1-13. doi.org/10.1038/srep45102

Pop, C., Salvesen, G.S. 2009. Human Caspases: Activation, Specificity, and Regulation. Journal of Biological Chemistry284, 21777–21781. doi.org/10.1074/jbc. r800084200

Probyn, T.A., Pitcher, G.C., Monteiro, P.M.S., Boyd, A.J., Nelson, G. 2000. Physical processes contributing to harmful algal blooms in Saldanha Bay, South Africa. Journal of Marine Science 22, 285–297. doi.org/10.2989/025776100784125807

Prokhorova, E.A., Zamaraev, A.V., Kopeina, G.S., Zhivotovsky, B., Lavrik, I.N. 2015. Role of the nucleus in apoptosis: signaling and execution. Cellular & Molecular Life Sciences, 72 (23), 4593–4612. doi.org/10.1007/s00018-015-2031-y

Pulkkanen, K.J., Laukkanen, M.O., Naarala, J., Yla-Herttuala, S. 2000. False-positive apoptosis signal in mouse kidney and liver detected with TUNEL assay. Apoptosis 5, 329–333. doi.org/10.1023/A:1009631424351

Qi, R., Liu, X.Y.2006. New Advance in Caspase-Independent Programmed Cell Death and its Potential in Cancer Therapy. International Journal of Biomedical Science 2(3), 211–216.

Rabinowitz, J.D., White, E. 2010. Autophagy and Metabolism. Science 330 (6009), 1344–1348. doi.org/10.1126/science.1193497

Rakhmatullina, D., Ponomareva, A., Gazizova, N., Minibayeva, F. 2016. Mitochondrial morphology and dynamics in Triticum aestivum roots in response to rotenone and antimycin A. Protoplasma 253 (5), 1299–1308. doi.org/10.1007/s00709-015-0888-0

Raven, J.A., Geider, R.J. 1988. Temperature and algal growth. New Phytologist 110 (4), 441–461. doi.org/10.1111/j.1469-8137. 1988.tb00282.x

Rawlings, N.D., Barrett, A.J., Finn, R. 2016. Twenty years of the MEROPS database of proteolytic enzymes, their substrates and inhibitors. Nucleic Acids Research, 44, D343–D350. doi.org/10.1093/nar/gkv1118

Ray, P.D., Huang, B.-W., Tsuji, Y. 2012. Reactive oxygen species (ROS) homeostasis and redox regulation in cellular signalling. Cellular Signalling24(5), 981–990. doi.org/10.1016/j.cellsig.2012.01.008

Regaudie-de-Gioux, A., Duarte, C.M. 2012. Temperature dependence of planktonic metabolism in the ocean. Global Biogeochemical Cycles26(1), 1-10. doi.org/10.1029/2010GB003907

Riaz, S., Sui, Z., Niaz, Z., Khan, S., Liu, Y., Liu, H. 2018. Distinctive Nuclear Features of Dinoflagellates with A Particular Focus on Histone and Histone-Replacement Proteins. Microorganisms 6(4),128. doi.org/10.3390/microorganisms6040128

Rodriguez-Enriquez, S., He, L., Lemasters, J.J. 2004. Role of mitochondrial permeability transition pores in mitochondrial autophagy. The International Journal of Biochemistry & Cell Biology: Autophagy and Cell Fate 36(12), 2463–2472. doi.org/10.1016/j.biocel.2004.04.009

Rojo, E., Martín, R., Carter, C., Zouhar, J., Pan, S., Plotnikova, J., Jin, H., Paneque, M., Sánchez-Serrano, J.J., Baker, B., Ausubel, F.M., Raikhel, N.V. 2004. VPEγ Exhibits a Caspase-like Activity that Contributes to Defense against Pathogens. Current Biology14(21), 1897–1906. doi.org/10.1016/j.cub.2004.09.056

Roncaglia, B., Papini, A., Chini Zittelli, G., Rodolfi, L., Tredici, M.R. 2021. Cell wall and organelle modifications during nitrogen starvation in Nannochloropsis oceanica F&M-M24. Journal of Applied Phycology 33(4), 2069–2080. doi.org/10.1007/s10811-021-02416-0

Rosic, N.N., Pernice, M., Dove, S., Dunn, S., Hoegh-Guldberg, O. 2011. Gene expression profiles of cytosolic heat shock proteins Hsp70 and Hsp90 from symbiotic dinoflagellates in

response to thermal stress: possible implications for coral bleaching. Cell Stress Chaperones 16 (1), 69–80. doi.org/10.1007/s12192-010-0222-x

Roy, S.S., Hajnóczky, G. 2008. Calcium, mitochondria and apoptosis studied by fluorescence measurements. Methods 46 (3), 213–223. doi.org/10.1016/j.ymeth.2008.09.024

Rynearson, T.A., Newton, J.A., Armbrust, E.V. 2006. Spring Bloom Development, Genetic Variation, and Population Succession in the Planktonic Diatom Ditylum brightwellii. Limnology & Oceanography51(3), 1249–1261.

Rzymski, P., Klimaszyk, P., Jurczak, T., Poniedziałek, B. 2020. Oxidative Stress, Programmed Cell Death and Microcystin Release in Microcystis aeruginosa in Response to Daphnia Grazers. Frontiers in Microbiology 11. doi.org/10.3389/fmicb.2020.01201

Salmaso, N., Buzzi, F., Garibaldi, L., Morabito, G., Simona, M. 2012. Effects of nutrient availability and temperature on phytoplankton development: a case study from large lakes south of the Alps. Aquatic Sciences74, 555–570. doi.org/10.1007/s00027-012-0248-5

Salvesen, G.S., Hempel, A., Coll, N.S. 2016. Protease signaling in animal and plant-regulated cell death. The FEBS Journal283, 2577–2598. doi.org/10.1111/febs.13616

Santos, C. 1999. Probing DNA Structure by NMR Spectroscopy, in: Barton, S.D., Nakanishi, K., Meth-Cohn, O. (Eds.), Comprehensive Natural Products Chemistry. Pergamon, Oxford, pp. 55–80. doi.org/10.1016/B978-0-08-091283-7.00154-5

Saraste, A., Pulkki, K. 2000. Morphologic and biochemical hallmarks of apoptosis. Cardiovascular Research 45(3), 528–537. doi.org/10.1016/S0008-6363(99)00384-3

Sathe, S., Orellana, M.V., Baliga, N.S., Durand, P.M. 2019. Temporal and metabolic overlap between lipid accumulation and programmed cell death due to nitrogen starvation in the unicellular chlorophyte Chlamydomonas reinhardtii. Phycological Research 67 (3), 173-183.doi.org/10.1111/pre.12368

Saunders, T.L., Windley, S.P., Gervinskas, G., Balka, K.R., Rowe, C., Lane, R., et al. 2024. Exposure of the inner mitochondrial membrane triggers apoptotic mitophagy. Cell Death & Differentiation 31(3), 335–347. doi.org/10.1038/s41418-024-01260-2

Scheuring, D., Viotti, C., Krüger, F., Künzl, F., Sturm, S., Bubeck, J., et al. 2011. Multivesicular Bodies Mature from the Trans-Golgi Network/Early Endosome in Arabidopsis. The Plant Cell 23(9), 3463–3481. doi.org/10.1105/tpc.111.086918

Schindler, D.W. 1977. Evolution of Phosphorus Limitation in Lakes. Science 195(4275), 260–262. doi.org/10.1126/science.195.4275.260

Schweichel, J.-U., Merker, H.-J. 1973. The morphology of various types of cell death in prenatal tissues. Teratology 7(3), 253–266. doi.org/10.1002/tera.1420070306

Sedaghatmehr, M., Thirumalaikumar, V.P., Kamranfar, I., Marmagne, A., Masclaux-Daubresse, C., Balazadeh, S. 2019. A regulatory role of autophagy for resetting the memory of heat stress in plants. Plant Cell & Environment42 (3), 1054–1064. doi.org/10.1111/pce.13426

Segovia, M. 2008a. Programmed Cell Death in Dinoflagellates, in: Programmed Cell Death in Protozoa. Springer New York, New York, NY, pp. 126–142. doi.org/10.1007/978-0-387-76717-8_11

Segovia, M. 2003. Cell Death in the Unicellular Chlorophyte *Dunaliella tertiolecta*. A Hypothesis on the Evolution of Apoptosis in Higher Plants and Metazoans. Plant Physiology 132(1), 99–105. doi.org/10.1104/pp.102.017129

Segovia, M. Berges, J.A. 2009. Inhibition of Caspase-like Activities Prevents the Appearance of Reactive Oxygen Species and Dark-induced Apoptosis in the Unicellular Chlorophyte *Dunaliella Tertiolecta*. Journal of Phycology 45(5), 1116–1126. doi.org/10.1111/j.1529-8817.2009.00733.x

Sellner, K.G., Doucette, G.J., Kirkpatrick, G.J. 2003. Harmful algal blooms: causes, impacts and detection. Journal of Industrial Microbiology & Biotechnology 30 (7), 383–406. doi.org/10.1007/s10295-003-0074-9

Send, U., Beardsley, R.C., Winant, C.D. 1987. Relaxation from upwelling in the Coastal Ocean Dynamics Experiment. Journal of Geophysical Research92(C2), 1683. doi.org/10.1029/JC092iC02p01683

Sesso, A., Belizário, J.E., Marques, M.M., Higuchi, M.L., Schumacher, R.I., Colquhoun, A., Ito, E., Kawakami, J. 2012. Mitochondrial Swelling and Incipient Outer Membrane Rupture in Preapoptotic and Apoptotic Cells. The Anatomical Record: Advances in Integrative Anatomy & Evolutionary Biology 295 (10), 1647–1659. doi.org/10.1002/ar.22553

Sharma, P., Jha, A.B., Dubey, R.S., Pessarakli, M. 2012. Reactive Oxygen Species, Oxidative Damage, and Antioxidative Defense Mechanism in Plants under Stressful Conditions. Journal of Botany 2012 (1), 1-69. doi.org/10.1155/2012/217037

Shemi, A., Ben-Dor, S., Vardi, A., 2015. Elucidating the composition and conservation of the autophagy pathway in photosynthetic eukaryotes. Autophagy 11(4), 701–715. doi.org/10.1080/15548627.2015.1034407

Shemi, A., Schatz, D., Fredricks, H.F., Mooy, B.A.S.V., Porat, Z., Vardi, A. 2016. Phosphorus starvation induces membrane remodeling and recycling in Emiliania huxleyi., New Phytologist 211(3), 886–898. doi.org/10.1111/nph.13940

Shen, J., Tower, J. 2009. Programmed cell death and apoptosis in aging and life span regulation. Discovery Medicine 8 (43), 223–226.

Sherman, E., Moore, J.K., Primeau, F., Tanouye, D. 2016. Temperature influence on phytoplankton community growth rates. Global Biogeochemical Cycles 30 (4), 550–559. doi.org/10.1002/2015GB005272

Shrestha, S., Clark, A.C.2021. Evolution of the folding landscape of effector caspases. Journal of Biological Chemistry 297 (5). doi.org/10.1016/j.jbc.2021.101249

Siano, R., Montresor, M., 2005. Morphology, ultrastructure and feeding behaviour of Protoperidinium vorax sp. nov. (Dinophyceae, Peridiniales). European Journal of Phycology, 40 (2), 221–232. doi.org/10.1080/09670260500128293

Silva, M.T. 2010. Secondary necrosis: The natural outcome of the complete apoptotic program. FEBS Letters 584 (22), 4491–4499. doi.org/10.1016/j.febslet.2010.10.046

Simeonova, E., Schikora, A., Charzyńska, M., Mostowska, A. 2000. Aspects of programmed cell death during leaf senescence of mono- and dicotyledonous plants. Protoplasma 214, 93–101. doi.org/10.1007/BF02524266

Simon, B., Fletcher, J.A., Doebeli, M. 2013. Towards a General Theory of Group Selection. Evolution 67, 1561–1572. doi.org/10.1111/j.1558-5646.2012.01835.x

Skarlato, S., Filatova, N., Knyazev, N., Berdieva, M., Telesh, I. 2018. Salinity stress response of the invasive dinoflagellate Prorocentrum minimum. Estuarine, Coastal & Shelf Science 211, 199–207. doi.org/10.1016/j.ecss.2017.07.007

Smayda, T.J. 2002. Adaptive Ecology, Growth Strategies and the Global Bloom Expansion of Dinoflagellates. Journal of Oceanography 58, 281–294. https://doi.org/10.1023/A:1015861725470

Smayda, T.J. 1997. What is a bloom? A commentary. Limnology & Oceanography 42, 1132–1136. doi.org/10.4319/lo.1997.42.5_part_2.1132

Smayda, T. J., Trainer, V.L. 2010. Dinoflagellate blooms in upwelling systems: Seeding, variability, and contrasts with diatom bloom behaviour. Progress in Oceanography, Special Issue on Harmful Algal Blooms in Upwelling Systems 85, 92–107. doi.org/10.1016/j.pocean.2010.02.006

Sogin, M.L. 1991. Early evolution and the origin of eukaryotes. Current Opinion in Genetics & Development 1, 457–463. doi.org/10.1016/S0959-437X(05)80192-3

Solovchenko, A., Baulina, O., Ptushenko, O., Gorelova, O. 2019. Ultrastructural patterns of photoacclimation and photodamage to photosynthetic algae cell under environmental stress. Physiologia Plantarum166, 251–263. doi.org/10.1111/ppl.12912

Solymosi, K. 2012. Plastid Structure, Diversification and Interconversions I. Algae. Current Chemical Biology6, 167–186. doi.org/10.2174/2212796811206030002

Soyer-Gobillard, M.O. 2017. Dinoflagellates, in: Reference Module in Life Sciences. Elsevier. doi.org/10.1016/B978-0-12-809633-8.13034-1

Spector, D.L., 1984. Dinoflagellates. Academic Press.

Sperandio, S., Belle, I. Bredesen, D.E. 2000. An alternative, nonapoptotic form of programmed cell death. Proceedings of the National Academy of Science. 97, 14376–14381. doi.org/10.1073/pnas.97.26.14376

Sperandio, S., Poksay, K., de Belle, I., Lafuente, M.J., Liu, B., Nasir, J., Bredesen, D.E. 2004. Paraptosis: mediation by MAP kinases and inhibition by AIP-1/Alix. Cell Death & Differentiation 11, 1066–1075. doi.org/10.1038/sj.cdd.4401465

Spitzer, C., Li, F., Buono, R., Roschzttardtz, H., Chung, T., Zhang, M., Osteryoung, K.W., Vierstra, R.D., Otegui, M.S. 2015. The Endosomal Protein Charged Multivesicular body protein 1 Regulates the Autophagic Turnover of Plastids in Arabidopsis. The Plant Cell 27, 391–402. doi.org/10.1105/tpc.114.135939

Spungin, D., Berman-Frank, I. 2019. Assessment of Metacaspase Activity in Phytoplankton. BIO-Protocol 9(16). doi.org/10.21769/BioProtoc.3341

Spurr, A.R. 1969. A low-viscosity epoxy resin embedding medium for electron microscopy. Journal of Ultrastructure Research 26, 31–43. doi.org/10.1016/S0022-5320(69)90033-1

Stearns, F.W. 2010. One Hundred Years of Pleiotropy: A Retrospective. Genetics 186, 767–773. doi.org/10.1534/genetics.110.122549

Stephen, V.C., Hockey, P.A.R. 2007. Evidence for an increasing incidence and severity of Harmful Algal Blooms in the southern Benguela region. South African Journal of Science 103, 223–231.

Suzuki, N., Koussevitzky, S., Mittler, R., Miller, G. 2012. ROS and redox signalling in the response of plants to abiotic stress. Plant Cell & Environment 35, 259–270.

Talbert, P.B., Henikoff, S. 2012. Chromatin: Packaging without Nucleosomes. Current Biology 22, R1040–R1043. doi.org/10.1016/j.cub.2012.10.052

Taylor, D.L. 1968. In situ studies on the cytochemistry and ultrastructure of a symbiotic marine dinoflagellate. Journal of Marine Biological Association of the United Kingdom 48, 349–366. doi.org/10.1017/S0025315400034548

Taylor, F.J.R. (Ed). 1991. The Biology of Dinoflagellates, 1st edition. ed. Wiley-Blackwell, Oxford; Boston.

Taylor, F.J.R. 1987. The Biology of dinoflagellates. Blackwell Scientific Publications, Oxford; Boston.

Thomas, M., Kremer, C., Klausmeier, C., Litchman, E. 2012. A Global Pattern of Thermal Adaptation in Marine Phytoplankton. Science 338. doi.org/10.1126/science.1224836

Tinari, A., Giammarioli, A.M., Manganelli, V., Ciarlo, L., Malorni, W. 2008. Analyzing Morphological and Ultrastructural Features in Cell Death, in: Methods in Enzymology. Elsevier, pp. 1–26. doi.org/10.1016/S0076-6879(08)01401-8

Trainer, V.L., Pitcher, G.C., Reguera, B., Smayda, T.J. 2010. The distribution and impacts of harmful algal bloom species in eastern boundary upwelling systems. Progress in Oceanography 85, 33–52. doi.org/10.1016/j.pocean.2010.02.003

Tsiatsiani, L., Van Breusegem, F., Gallois, P., Zavialov, A., Lam, E., Bozhkov, P.V. 2011. Metacaspases. Cell Death & Differentiation 18, 1279–1288. doi.org/10.1038/cdd.2011.66

Tsukada, M., Ohsumi, Y. 1993. Isolation and characterization of autophagy-defective mutants of *Saccharomyces cerevisiae*. FEBS Letters 333, 169–174. doi.org/10.1016/0014-5793(93)80398-E

Turpin, D.H. 1991. Effects of Inorganic N Availability on Algal Photosynthesis and Carbon Metabolism. Journal of Phycology 27, 14–20. doi.org/10.1111/j.0022-3646.1991.00014.x

Uemura, T., Yamamoto, M., Kametaka, A., Sou, Y., Yabashi, A., Yamada, A., et al. 2014. A Cluster of Thin Tubular Structures Mediates Transformation of the Endoplasmic Reticulum to Autophagic Isolation Membrane. Molecular Cell Biology 34, 1695–1706. doi.org/10.1128/MCB.01327-13

Uren, A.G., O'Rourke, K., Aravind, L.A., Pisabarro, M.T., Seshagiri, S., Koonin, E.V., Dixit, V.M. 2000. Identification of paracaspases and metacaspases: two ancient families of caspase-like proteins, one of which plays a key role in MALT lymphoma. Molecular Cell 6, 961–967.

Van den Eijnde, S.M., Boshart, L., Baehrecke, E.H., De Zeeuw, C.I., Reutelingsperger, C.P.M., Vermeij-Keers, C. 1998. Cell surface exposure of phosphatidylserine during apoptosis is phylogenetically conserved. Apoptosis 3, 9–16. doi.org/10.1023/A:1009650917818

Van Doorn, W.G., Beers, E.P., Dangl, J.L., Franklin-Tong, V.E., Gallois, P., Hara-Nishimura, I., et al. 2011. Morphological classification of plant cell deaths. Cell Death & Differentiation 18, 1241–1246. doi.org/10.1038/cdd.2011.36

Van Doorn, W.G., Papini, A. 2016. Plastid degeneration in *Tillandsia* (Bromeliaceae) provides evidence about the origin of multilamellar bodies in plants. doi.org/10.1101/038158

Van Doorn, W.G., Papini, A. 2013. Ultrastructure of autophagy in plant cells. Autophagy 9, 1922–1936. doi.org/10.4161/auto.26275

Vardi, A., Berman-Frank, I., Rozenberg, T., Hadas, O., Kaplan, A., Levine, A. 1999. Programmed cell death of the dinoflagellate *Peridinium gatunense* is mediated by CO_2 limitation and oxidative stress. Current Biology 9, 1061–1064. doi.org/10.1016/S0960-9822(99)80459-X

Vardi, A., Eisenstadt, D., Murik, O., Berman-Frank, I., Zohary, T., Levine, A., Kaplan, A. 2007. Synchronization of cell death in a dinoflagellate population is mediated by an excreted thiol protease. Environmental Microbiology 9, 360–369. doi.org/10.1111/j.1462-2920.2006.01146.x

Vardi, A., Mooy, B.A.S.V., Fredricks, H.F., Popendorf, K.J., Ossolinski, J.E., Haramaty, L., Bidle, K.D. 2009. Viral Glycosphingolipids Induce Lytic Infection and Cell Death in Marine Phytoplankton. Science 326, 861–865. doi.org/10.1126/science.1177322

Veldhuis, M., Brussaard, C., 2006. Harmful Algae and Cell Death, in: Ecology of Harmful Algae. Ecological Studies: Analysis and Synthesis. pp. 153–162. doi.org/10.1007/978-3-540-32210-8_12

Vercammen, D., van de Cotte, B., De Jaeger, G., Eeckhout, D., Casteels, P., Vandepoele, K., Vandenberghe, I., Van Beeumen, J., Inzé, D., Van Breusegem, F. 2004. Type II Metacaspases Atmc4 and Atmc9 of Arabidopsis thaliana Cleave Substrates after Arginine and Lysine. Journal of Biological Chemistry 279, 45329–45336. doi.org/10.1074/jbc.M406329200

Viotti, C. 2014. ER and vacuoles never been closer. Frontiers in Plant Science 5, 20. doi.org/10.3389/fpls.2014.00020

Vitale, A., Denecke, J. 1999. The Endoplasmic Reticulum-Gateway of the Secretory Pathway. Plant Cell 11, 615–628. doi.org/10.1105/tpc.11.4.615

Vostinar, A.E., Goldsby, H.J., Ofria, C. 2019. Suicidal selection: Programmed cell death can evolve in unicellular organisms due solely to kin selection. Ecology & Evolution 9 (16), 9129–9136. doi.org/10.1002/ece3.5460

Walsh, J.J. 1983. Death in the sea: Enigmatic phytoplankton losses. Progress in Oceanography 12, 1–86. doi.org/10.1016/0079-6611(83)90006-X

Wang, D.-Z., Zhang, H., Zhang, Y., Zhang, S.-F. 2014. Marine dinoflagellate proteomics: Current status and future perspectives. Journal of Proteomics 105, 121–132. doi.org/10.1016/j.jprot.2014.01.026

Wang, H., Chen, F., Mi, T., Liu, Q., Yu, Z., Zhen, Y. 2020. Responses of Marine Diatom *Skeletonema marinoi* to Nutrient Deficiency: Programmed Cell Death. Applied & Environmental Microbiology 86. doi.org/10.1128/AEM.02460-19

Wang, H., Mi, T., Zhen, Y., Jing, X., Liu, Q., Yu, Z. 2017. Metacaspases and programmed cell death in S*keletonema marinoi* in response to silicate limitation. Journal of Plankton Research 39, 729–743. doi.org/10.1093/plankt/fbw090

Wang, L., Xiao, L., Yang, H., Chen, G., Zeng, H., Zhao, H., Zhu, Y. 2020. Genome-Wide Identification, Expression Profiling, and Evolution of Phosphate Transporter Gene Family in Green Algae. Frontiers in Genetics 11, 590947. doi.org/10.3389/fgene.2020.590947

Welburn, S.C., Barcinski, M.A., Williams, G.T. 1997. Programmed cell death in trypanosomatids. Parasitology Today13, 22–26.

Wells, M.L., Trainer, V.L., Smayda, T.J., Karlson, B.S.O., Trick, C.G., Kudela., et al. 2015. Harmful algal blooms and climate change: Learning from the past and present to forecast the future. Harmful Algae 49, 68. doi.org/10.1016/j.hal.2015.07.009

Weng, L.-C., Pasaribu, B., -Ping Lin, I., Tsai, C.-H., Chen, C.-S., Jiang, P.-L. 2014. Nitrogen Deprivation Induces Lipid Droplet Accumulation and Alters Fatty Acid Metabolism in Symbiotic Dinoflagellates Isolated from *Aiptasia pulchella*. Scientific Reports 4, 5777. doi.org/10.1038/srep05777

Wilken, S., Soares, M., Urrutia-Cordero, P., Ratcovich, J., Ekvall, M.K., Van Donk, E., Hansson, L.-A. 2018. Primary producers or consumers? Increasing phytoplankton bacterivory along a gradient of lake warming and browning. Limnology & Oceanography 63, S142–S155. doi.org/10.1002/lno.10728

Winter, J.G., DeSellas, A.M., Fletcher, R., Heintsch, L., Morley, A., Nakamoto, L. Utsumi, K. 2011 Algal blooms in Ontario, Canada: Increases in reports since 1994. Lake & Reservoir Management27, 107–114. doi.org/10.1080/07438141.2011.557765

Yan, G., Elbadawi, M., Efferth, T. 2020a. Multiple cell death modalities and their key features (Review). World Academy of Sciences Journal 2, 39–48. doi.org/10.3892/wasj.2020.40

Yang, Z., Klionsky, D.J. 2009. An Overview of the Molecular Mechanism of Autophagy. Current Topics in Microbiology & Immunology 335, 1–32. doi.org/10.1007/978-3-642-00302-8_1

Yasuhara, S., Zhu, Y., Matsui, T., Tipirneni, N., Yasuhara, Y., Kaneki, M., et al. (2003). Comparison of Comet Assay, Electron Microscopy, and Flow Cytometry for Detection of Apoptosis. Journal of Histochemistry & Cytochemistry 51, 873–885. doi.org/10.1177/002215540305100703

Yoon, M.J., Lee, A.R., Jeong, S.A., Kim, Y.-S., Kim, J.Y., Kwon, Y.-J., Choi, K.S. 2014. Release of Ca^{2+} from the endoplasmic reticulum and its subsequent influx into mitochondria trigger celastrol-induced paraptosis in cancer cells. Oncotarget 5, 6816–6831.

Yoshida, A., Pommier, Y., Ueda, T. 2006. Endonuclease activation and chromosomal DNA fragmentation during apoptosis in leukaemia cells. International Journal of Hematology 84, 31–37. doi.org/10.1007/BF03342699

Zhang, C.Y., Chen, G.F., Wang, Y.Y., Zhang, X.D., Li, C.H. 2019b. Molecular characterization of heat shock protein 90 from the dinoflagellate *Prorocentrum donghaiense* and its transcriptional response to thermal, copper and nutrient stresses. Marine Biology Research 15, 343–356. doi.org/10.1080/17451000.2019.1662445

Zhang, X., Tang, X., Wang, M., Zhang, W., Zhou, B., Wang, Y. 2017. ROS and calcium signaling mediated pathways involved in stress responses of the marine microalgae Dunaliella salina to enhanced UV-B radiation. Journal of Photochemistry & Photobiology, 173, 360–367. doi.org/10.1016/j.jphotobiol.2017.05.038

Zhao, C.-Q., Jiang, L.-S., Dai, L.-Y. 2006. Programmed cell death in intervertebral disc degeneration. Apoptosis 11, 2079–2088. doi.org/10.1007/s10495-006-0290-7

Zhao, Yirong, Tang, X., Qu, F., Liu, Q., Li, J., Li, L., Zhang, B. 2020. ROS-mediated programmed cell death (PCD) of Thalassiosira pseudonana under the stress of BDE-47. Environmental Pollution, 262,114342. doi.org/10.1016/j.envpol.2020.114342

Zhou, J., Fritz, L. (1994). The PAS/Accumulation bodies in *Prorocentrum Lima* and *Prorocentrum Maculosum* (Dinophyceae) are dinoflagellate lysososmes. Journal of Phycology. doi.org/10.1111/j.0022-3646.1994.00039.x

Zhou, J., Wang, J., Cheng, Y., Chi, Y.-J., Fan, B., Yu, J.-Q., Chen, Z. 2013. NBR1-Mediated Selective Autophagy Targets Insoluble Ubiquitinated Protein Aggregates in Plant Stress Responses. PLOS Genetics, 9, e1003196. doi.org/10.1371/journal.pgen.1003196

Zhou, T., Zheng, J., Cao, H., Wang, X., Lou, K., Zhang, X., Tao, Y. 2018. Growth suppression and apoptosis-like cell death in Microcystis aeruginosa by H_2O_2: A new insight into

extracellular and intracellular damage pathways. Chemosphere 211, 1098–1108. doi.org/10.1016/j.chemosphere.2018.08.042

Zhuang, X., Cui, Y., Gao, C., Jiang, L. 2015. Endocytic and autophagic pathways crosstalk in plants. Current Opinion in Plant Biology 28, 39–47. doi.org/10.1016/j.pbi.2015.08.010

Zorov, D.B., Juhaszova, M., Sollott, S.J. 2014. Mitochondrial Reactive Oxygen Species (ROS) and ROS-Induced ROS Release. Physiological Reviews 94(3), 909–950. doi.org/10.1152/physrev.00026.2013

Zuppini, A., Andreoli, C., Baldan, B. 2007. Heat Stress: an Inducer of Programmed Cell Death in Chlorella saccharophila. Plant Cell Physiology 48(7), 1000–1009. doi.org/10.1093/pcp/pcm070

Zuppini, A., Gerotto, C., Baldan, B. 2010. Programmed Cell Death and Adaptation: Two Different Types of Abiotic Stress Response in a Unicellular Chlorophyte. Plant Cell Physiology 51(6), 884–895. doi.org/10.1093/pcp/pcq069

Zuppini, A., Gerotto, C., Moscatiello, R., Bergantino, E., Baldan, B. 2009. Chlorella saccharophila cytochrome f and its involvement in the heat shock response. Journal of Experimental Botany 60(14), 4189–4200. doi.org/10.1093/jxb/erp264